Fracture of Aluminum Naval Structures

by

Konstantinos P. Galanis

Naval Engineer, Massachusetts Institute of Technology (2002)
MSc in Ocean Systems Management, Massachusetts Institute of Technology (2002)
BSc in Marine Engineering, Hellenic Naval Academy (1992)

Submitted to the Department of Mechanical Engineering
in partial fulfillment of the requirements for the degree of

Doctor of Philosophy
in Naval Architecture, Marine Engineering and Applied Mechanics

at the

MASSACHUSETTS INSTITUTE OF TECHNOLOGY

June 2007

Signature of Author .....
Department of Mechanical Engineering
15 May 2007

Certified by .....
Tomasz Wierzbicki
Professor of Applied Mechanics
Thesis Supervisor

Accepted by .....
Lallit Anand
Chairperson, Department Committee on Graduate Students

Fracture of Aluminum Naval Structures

by

Konstantinos P. Galanis

Submitted to the Department of Mechanical Engineering
on 15 May 2007, in partial fulfillment of the
requirements for the degree of
Doctor of Philosophy
in Naval Architecture, Marine Engineering and Applied Mechanics

Abstract

Structural catastrophic failure of naval vessels due to extreme loads such as underwater or air explosion, high velocity impact (torpedoes), or hydrodynamic loads (high speed vessels) is primarily caused by fracture. Traditionally, naval structures have been designed to resist yielding, buckling and fatigue, but not fracture. Consequently, adequate methods and procedures to design ships against fracture have not been developed.

The rapidly increasing application of lightweight materials, such as aluminum alloys, in the shipbuilding industry requires fundamental understanding of mechanisms and mechanics of fracture that govern naval stiffened panels. Therefore, a comprehensive tool consisting of application of advanced fracture models, material calibration, and validation through component testing is provided that will increase the survivability envelope and speed up the development process of new vessels.

Cracking is a major cause of structural degradation, which is a primary source of costly repair work on metal structures. This thesis studies the structural response of various stiffened plates and compares them with unstiffened plates represented by compact tension (CT) specimens. An extensive experimental program is presented that includes coupon testing and small and intermediate scale tests on naval aluminum structures including a variety of monolithic T-type extruded and flatbar welded specimens. Representative naval designs are selected and subjected to quasi-static loading and a number of key parameters, such as geometry, loading rate and structural configuration are evaluated with respect to fracture.

Numerical modeling and analyses of ductile fracture initiation and propagation on a precracked geometry using a commercial finite element code (ABAQUS), taking into account the behavior of simple uncracked material, has been performed showing a very good agreement with small and intermediate scale tests.

Two major contributions of this thesis are the mapping of crack patterns in stiffened plates and the development of a methodology which enables ship designers to evaluate critical areas within a structure with respect to crack initiation, propagation, optimum material usage, and computational cost.

Thesis Supervisor: Tomasz Wierzbicki
Title: Professor of Applied Mechanics

Contents

List of Figures

List of Tables

Acknowledgement - *Ειδική μνεία*

Ευχαριστώ τον Θεό και την Αγία Παρασκευή που με αξίωσαν να ολοκληρώσω με επιτυχία αυτό το εγχείρημα.

I have to state that pursuing and completing my graduate studies at the best Institute of Technology worldwide, MIT, is an honour for me and my family, and I promise to serve Philosophy and Science with all my efforts, as a commitment to my Greek ancestors.

Above all, I would like to express my deepest thanks to my academic advisor Professor of Applied Mechanics, **Tomasz Wierzbicki** for his continuous support, guidance and patience. He taught me, among other, how to apply the theoretical knowledge in order to solve real problems which can improve our lives.

I would also like to express my deepest appreciation to Professor **Vassilios Papazoglou** for offering the Shipbuilding Technology Laboratory facilities at the National Technical University of Athens, School of Naval Architecture and Marine Engineering. Beyond that, he provided an adequate academic environment, interminable support and superior advisory. His contribution in terms of planning the experiments and important implications for ship structural design could actually qualify him to be a co-advisor of this thesis.

I would also like to pay respect to Kawasaki Professor of Engineering, **Nicholaos Patrikalakis** for inspiring me to pursue graduate studies at a doctoral level and for his endless support. This dream would not have been true without him.

In addition, I would like to thank my thesis committee members Professor of the Practice of Naval Construction and Engineering, Captain **Patrick Keenan** USN and Senior Lecturer, Dr. **David Burke** for providing in-depth academic assistance and expertise.

I would also like to thank the Hellenic Navy, MIT, USN Office of Naval Research, Greek and American taxpayers for investing a considerable amount of money for my education and I hope that I have satisfied all of them with my performance.

The decision of the Hellenic Navy to honour my graduation with the presence of Admiral E. Mitrou HN and the Consul General of Boston accompanied with other high ranked officers enhances me to increase my efforts for exploiting new horizons. Special thanks belong to

Professor of Naval Architecture and Marine Engineering, Theodosios Boufounos of the Hellenic Naval Academy who encouraged me in every aspect, honouring me and Mr. Panagiotis Alourdas for advising me during this long academic adventure.

I would also like to thank Elefsis Shipyards, George Kokkalas, the personnel of the Naval Base of Salamis, Stefanos Michalopoulos, Athanasios Markoulis and Associate Professor Nikolaos Tsouvalis for assisting to the experimental program.

I have to acknowledge the crucial support of my MIT ICL labmates, JongMin Shim, Yuanli Bai, and Carey Walters, spending with me a lot of their time and this is highly-appreciated.

I would like to thank the MIT administrative staff Leslie Regan, Sheila McNary and Pete Beaulieu for providing instant solutions to all my requests proving that it requires all hands to succeed in every task!

Beyond the academic personnel, I would also like to thank my Greek friends for their support, Dr. Manos Chaniotakis, Liz Chaniotakis and their handsome children, Periklis Roukas, Apostolos Bastas, Dimitris Ayvatoglu, Spyros Anestis, George Constantinides, George Kokosalakis, Theodoros Konstantakopoulos, Anna Stefanidou, Christina Antonopoulos, Domniki Asimaki and Andreas Langousis.

I would also like to thank all my friends at US that created a very friendly environment, Jan Lammerding, Silva Krause, Manfred Kraus, Michelle Zanolin, James Seo and my Euroclub volleyball mates.

The fulfillment of my academic requirements as a student would not have taken place without the efforts of all my teachers, tutors and instructors throughout my whole academic career and I am happy that they saw that their efforts had satisfactory results.

I would also like to thank my sister Katerina and her husband Antonis for believing in me even at the most difficult moments. Special thanks belong to my parents-in-law, Savvas and Maria for their support with every means. Thank you!

I hope that this effort will be superseded in the near future, from our loved descendants, my son **Panagiotis**, my goddaughter Georgia, my niece Christina, my godson Karolos-Panagiotis and -I wish- the ones to come.

There are no words to describe my warmest love and appreciation to my spouse **Christina** for her continuous support, dedication and understanding. She is always there for me sacrificing

everything to keep me happy and relaxed. To her and our son, I decided to devote my life, therefore,...

...this dissertation is dedicated to my parents, my father Panagiotis and my mother Christina, for their daily support, sacrifices and offer of all the essentials needed to achieve all my life ambitions, dreams and goals, since I was a little child. I wish my child(ren) will love me the way I love them. This, will be my last life-goal.

May this achievement serve as an inspiration for everyone who believes that IMPOSSIBLE IS NOTHING, typical qualification of the Hellenes.

Στους γονείς μου,

Παναγιώτη και Χριστίνα

Nomenclature

Abbreviations

e.g.	for example [in Latin, exempli gratia]
et al.	and others [in Latin, et alia]
i.e.	that is [in Latin, id est]
vs.	with respect to [in Latin, versus]

Acronyms

ADH	Advanced Double Hull
CCT	Center Cracked Tension specimen
CT	Compact Tension specimen
CTE	Compact Tension specimen with T-type Extruded stiffener
CTEB	Compact Tension specimen with Extruded T-type stiffener (no rear plate)
CTEI	Compact Tension specimen with Extruded flatbar stiffener
CTOD	Crack Tip Opening Displacement
CTW	Compact Tension specimen with Welded flatbar stiffener
DENT	Double Edge Notched Tension specimen
FE	Finite Element
HAZ	Heat Affected Zone
SSDENT	Single Stiffened Double Edge Notched Tension specimen
TSCCT	Twin Stiffened Centre Cracked Tension specimen

Greek symbols

α	crack size
δ	displacement
δ_f	displacement to fracture
δ_R	relative elongation
Δ_l	mesh size
$\Delta l_{\min}$	smallest element dimension in the mesh

Δt	time step
$\overline{\varepsilon}$	plastic equivalent strain
ε_1, ε_3, ε_3	maximum, medium and minimum principal strain, respectively
ε_{eng}	engineering strain
$\overline{\varepsilon}_f$	plastic equivalent strain to fracture
ε_{true}	true strain
ε_y	yield strain
ν	Poisson's ratio
ρ	material density
$\overline{\sigma}$	von Mises equivalent stress
σ_1, σ_2, σ_3	maximum, medium and minimum principal stress, respectively
σ_{eng}	engineering stress
σ_o	flow stress
σ_{true}	true stress
σ_t	ultimate tensile stress
σ_y	yield stress

English symbols

A_o	initial area of the gauge section
B	minimum material thickness
c_d	dilatational wave speed
D	accumulative damage parameter
D_c	accumulative damage parameter to fracture
E	Young's modulus
h_w	height of the stiffener's web
K_I	mode I stress intensity factor
l	current gauge length
l_o	initial gauge length
n	knee factor
P	reaction force

t	thickness
t_w	thickness of the stiffener's web

Chapter 1

Introduction

1.1 Trends in the Shipbuilding Industry

The world shipbuilding industry has faced a significant rise in new ship orders and deliveries since the beginning of the century, driven both by economic globalization, energy needs, consequent increase in freight and finally by last-minute demand from purchasers trying to beat the implementation of new structural regulations set by classification societies. Unfortunately, global shipbuilding capacity has also continued to increase and experience have shown that this will eventually result in significant overcapacity and excess competition, with shipbuilders slashing prices to lure business.

Marine vessels are very complex structures compared with other types of structures. They are subject to a very wide range of loads in the harsh sea environment. Progress in technologies related to ship and submarine design and construction is being constantly developed. The ship designers strive to develop rational and optimal designs based on direct strength analysis methods using the latest technologies in order to realize the shipowner's requirements in the best possible way. Many shipbuilding programs around the world have faced and are facing problems in the transition from design to construction. In addition, several marine accidents bring more problems due to severe consequences to humans and/or the environment, Fig. 1-1.

The shipbuilding productivity in the United States is not considered to be competitive for several reasons. Some of the symptoms were the lack of product design, lack of production and process technology integration, lack of effective design for producibility, inadequate design,

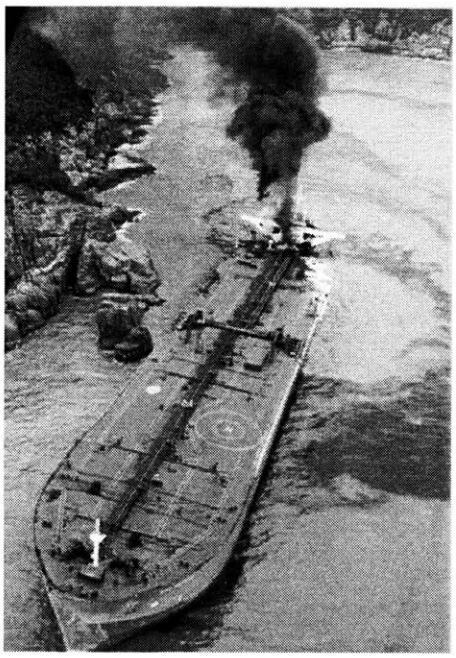

Figure 1-1: An oil tanker accident caused by grounding on a rock

product development capacity and production planning (Frankel [71]).

Shipbuilders are constantly looking for ways to reduce the weight of the structure in order to optimize the overall displacement and hence the cost of the vessel. The easiest option for the designer is to choose a lightweight material, such as composite materials and aluminum. Aluminum has become the adopted choice of material for high-speed vessels due to its high strength to weight characteristics. Comparing to steel, aluminum is more prone to fatigue cracking and has no fatigue limit (Mazzolani [174]).

In order to minimize the structural weight, the designer is using finite element methods to optimize the scantlings utilizing commercial or in-house developed codes. This can lead to a structure that has the empirical margins of safety reduced owing to the accuracy of mathematical modeling embedded in the software used. However, what is often overlooked is the effect that the manufacturing process has on the overall life of the fabricated structure. This aspect is excluded from the designer's calculations, which assist in reducing the scantlings. Currently, there is no guidance for overall life reduction for the designer that establishes good and bad workshop practice, other than experience, or the implications of basic shipyard fabrication.

Whenever strain-hardened alloys improve mechanical strength, they reduce ductility. This has consequences when forming the hull plate by potentially introducing crack-like flaws into the alloy matrix if the plater overrolls the plate. If there is misalignment or there is too much gap between the plates, the weld will create localized stress concentrations. If the welder has poor joint preparation or gas shielding, porosity can be introduced into the weld. Porosity has a significant effect on the fatigue life of the weldment.

Therefore, there is urge for developing sound strategies concerning the area of materials, structures and design to alleviate the amount of structural damage and reduce the number of casualties. This is a very complex and difficult problem and in-depth research is needed from academia and industry. The Aluminum Shipbuilding industry should leverage research and development to effect change across the non-nuclear surface shipbuilding, modernization and repair enterprise by coordinating with U.S. shipbuilders to adapt and implement "World Class" commercial best manufacturing practices. The U.S. shipbuilding industry lags behind the global shipbuilding market significantly in adapting new technologies due to long-standing inefficient manufacturing processes, and improvement in this area is key to closing this gap. Hopefully, the results of this research will enhance the abilities of the military and commercial shipbuilding audit and repair sectors.

1.2 The Naval Shipbuilding Industry

Warships are the most compelling image of a Navy. From the ancient Greek city states to the dawn of the 21st century, warships have evoked emotions of foreboding presence and commanding power. Nowadays, the Navy around the world is ushering in a new era in surface combatant and submarine design and naval warfare capabilities and all countries are focusing on applying smart and efficient technologies.

Modern national and military strategies and policies prescribe that forward-deployed naval forces move freely at the strategic level to support joint operations, to protect and maintain adequate access to strategic and operational sea lines of communication, ports, transit routes, and choke points. The inability of forward-deployed forces to manoeuvre freely diminishes their contributions to joint operations ashore and jeopardizes national interests. However, operating

in close proximity to shore increases the risk to which naval forces are exposed, through greater exposure to a more robust threat regime, where naval forces potentially face simultaneous shore, air, and sea based threats.

Naval vessels, including surface combatants and submarines, require high strength metallic plate in increasing portions of the hull structure for weight reduction, better stability, increased payload and mobility, and survivability. They are designed under naval engineering standards defined by the Navy. In the modern naval shipbuilding industry there is an increasing difficulty justifying expensive military standards for many aspects of the design. It is obvious that often the solution is not only to follow the best commercial practice, but also to comply with international safety legislation. Modern warship design and construction remains a very complex process and the recent trends make the designer's tasks even harder. Fortunately, modern design tools offer the potential for much deeper design investigations at earlier stages. This reduces risk in the design at the crucial early stages before the majority of budget cost becomes committed.

This thesis seeks innovative scientific and engineering solutions to inefficiencies in the long-standing destructive inspection methods for marine aluminum structures. The U.S. Navy has for many years limited the use of aluminum alloys in topside structures because of the potential for catastrophic damage due to fire and the frequency of fatigue cracks forming in these structures. Recently, there has been resurgence in the planned use of aluminum alloys in naval surface ships. As a result, naval shipbuilding and repair facilities will require improved methods of inspecting structures made from aluminum alloys. Portability, adaptability, precision and automation will be important attributes to consider in developing solutions.

1.3 Naval Structural Design

In service, naval structures are subjected to a complex spectrum of loads and environments, and the structural steels and welding materials used in hull fabrication must demonstrate high fracture toughness for these extreme conditions. The routine dynamic loads in service include wave loading, sea slap, slamming, vibration, thermal excursions in both tropical and arctic seas, cargo, buoyancy, aircraft/helicopter landing, and weapon reactions. The structural integrity of

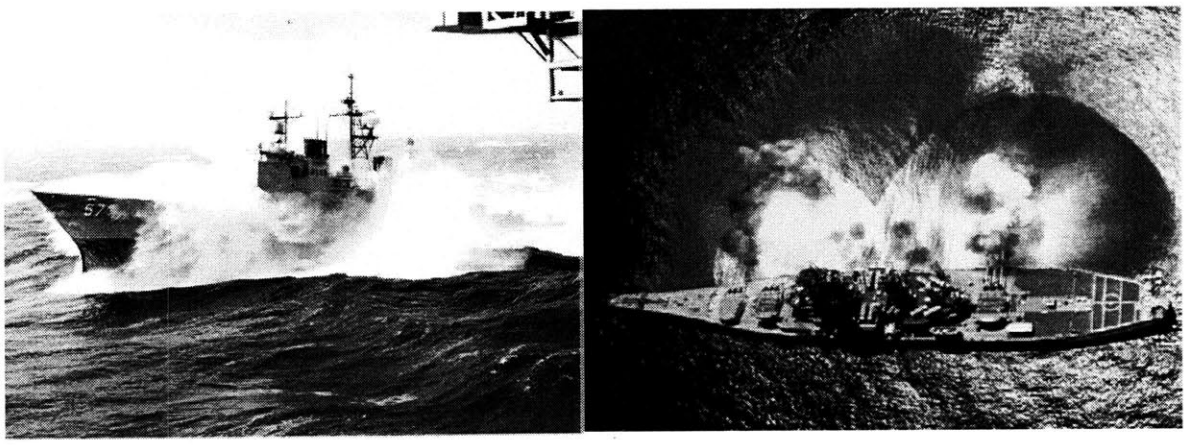

Figure 1-2: Naval vessels under extreme environmental and operational conditions

the hull must be assured for continuous seakeeping in these environments, as well as in response to weapon effects, Fig. 1-2.

Because the primary mission of a naval vessel is to prevail in combat, economic evaluation of building cost has been a secondary factor. Structural design of naval vessels is not subjected to class rules. Tentative rules for naval vessels and aluminum high speed craft were published by American classification societies [4] [5] [6] but the U.S. Navy is using its own standards in design of naval vessels due to long-standing experience and reliability. The specifications of the U.S. Navy define design loads for naval vessels and present strength criteria. Most class rules suggest basic formulae to determine component dimensions. However, U.S. Navy specifications emphasize strength criteria, and designers need to determine component dimensions while satisfying the strength criteria. The design process of naval vessels is closer to a direct strength analysis and design method. Recently, the U.S. Navy adopted ABS rules for the construction of a new naval aluminum vessel, Littoral Combat Ship (LCS).

Structural design is the oldest and most fundamental of the technical disciplines, which together comprise the art of naval architecture. Over the past decades, structural design as it is applied to naval vessels has diverged from and converged with that for commercial ships for a variety of reasons. In recent times, resource constraints have made it necessary for governments around the world to seek out alternatives to established practices in many areas including naval vessel acquisition. Fortunately, the convergence of commercial and naval design practices

has made it possible to look at commercial processes. One development arising from these conditions is that navies have increasingly turned to the application of classification society processes and resources to help them in establishing and applying technical criteria for naval ship design and construction including those related to the ship's structure.

Structural analysis and design are two words that are very often associated. Sometimes they are used indifferently one for the other even if there are some important differences between performing a design and completing an analysis. Structural analysis refers to stress and strength assessment of the structure and requires information on loads and needs an initial structural scantling design. Output of the structural analysis is the structural response defined in terms of stresses, deflections and strength. Then, the estimated response is compared to the design criteria. Structural design refers to the process followed to select the initial structural scantlings and to update these scantlings from the early design state to the detailed design stage. To perform structural analysis, initial design is needed and structural analysis is required to design. Ship structural analysis and design is a matter of compromises:

- compromise between accuracy and the available time to perform the design,
- to limit uncertainty and reduce conservatism in design while being accurate,
- compromise between weight and cost,
- compromise between least construction cost, and global owner life cycle cost, and
- builder optimum design may be different from the owner optimum design.

A naval structural design process consists of three levels, since it usually refers to large and complex systems: (i) concept design, which deals with the topology or overall geometry of the vessel, (ii) preliminary design, where the scantlings of all principal structural members are established, and (iii) the detailed design, concerned with local aspects. In the stage of the preliminary design, the naval engineer takes the most significant decisions based on the available options and optimizes the structure so that it fulfills the objectives and satisfies all of the various constraints and requirements.

Ship structure is composed almost entirely of orthogonally (longitudinally and transversely) stiffened plating, Fig. 1-3. Both the plating and stiffeners must be designed to sustain working

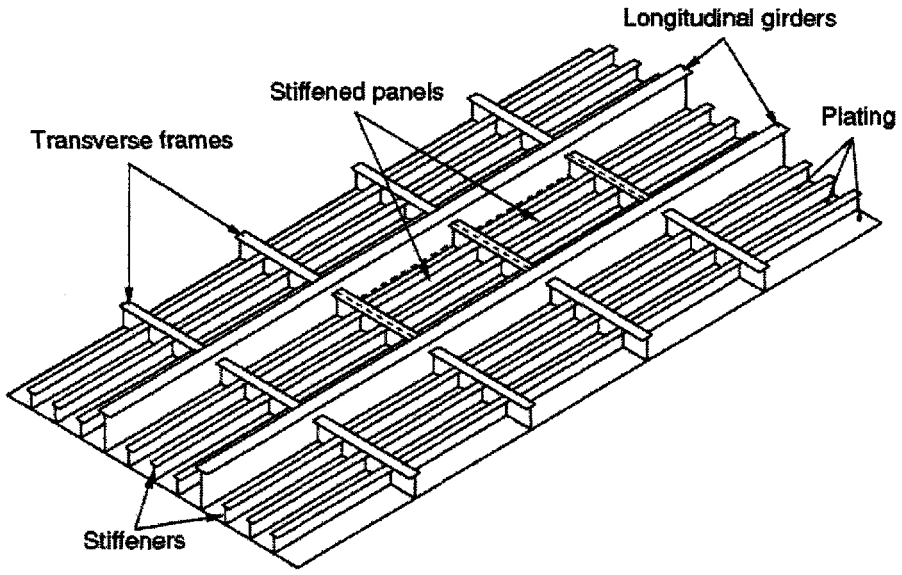

Figure 1-3: A typical stiffened panel for naval applications with longitudinal, transverse and orthogonal stiffeners

loads. Plate panels in the ship are welded around their periphery to stiffeners or adjacent panels. Fatigue tests are addressing the properties of local structural issues, such as capacity of plating between stiffeners, the proportions of the flange and web elements of stiffeners, and the fatigue strength of a welded detail. However, local structural issues like these must be understood before the larger, general structure can be designed. As the overall structure increases in size, the size, shape, and length of the members may be limited to control buckling of main load carrying members. Therefore, grillage structures, containing multiple longitudinal and transverse stiffeners, have to be evaluated for catastrophic modes of buckling failure and to define margins of safety for design against ultimate failure.

It is within the responsibilities of a naval engineer to ensure that the design process will lead to the optimum structurally designed vessel based on mainly empirically selected loading. The designer of a naval ship must anticipate the sort of mishandling and misfortune possible and the probable intent of any enemy, so that he may design the vessel to mitigate the effects and render counter action. He seeks to define the hazards in sufficiently precise terms and to describe the forms of protection required. Most of these forms are stated in international of

Figure 1-4: The wreck of the Russian nuclear submarine Kursk drydocked at the port of Roslyakovo, which sunk with 118 crew members on 8 August 2000 [courtecy of Russian NTV channel]

national regulations, but these regulations do not, however, remove the need to understand the problems. Despite all that anticipation and regulations can achieve, losses at sea continue, Fig. 1-4.

The structural designer is faced with the challenge to continuously strive for lighter and more efficient structures, while facing increased safety requirements and regulations. The weight saving potential through the use of new materials and sandwich structures is impressive in most applications and has been under examination for several decades.

1.3.1 Surface ship construction

Up to the 1950's, classification assessment of ship's strength was mainly based on past experience, static and quasi-static wave profile loads, as the natural forces and behavior of the sea were deemed at the time to be largely unpredictable. This rule and minimum standards framework ensured safety for existing ships but was more difficult to apply to new types of ships. Furthermore, the requirements referring to the ship's structure scantlings had tabular form and were not expressed in non-dimensional format, normally derived from the principles of structural mechanics. At the time the ship structure was appraised in terms of separate

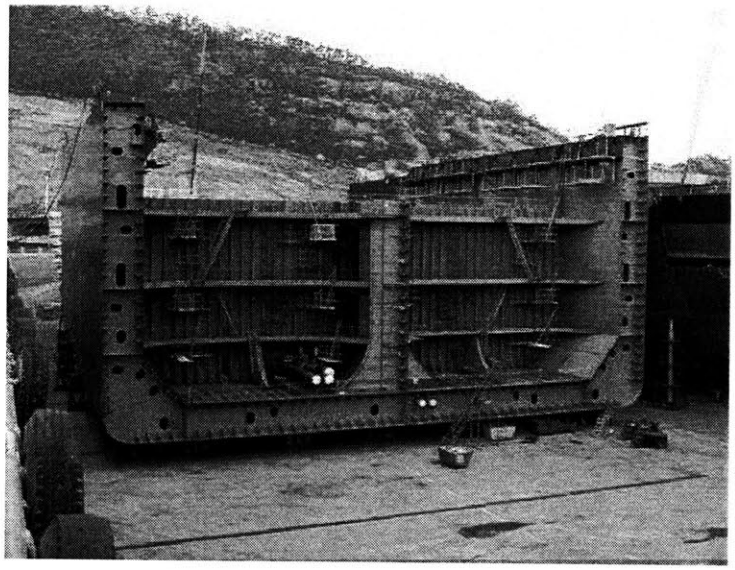

Figure 1-5: Midship section of a steel surface vessel

structure members, Fig. 1-5. It was conservatively assumed that if each structure member satisfied the minimum requirements then the whole hull structure would be safe. On larger ships, the verification of deck cross section was additionally required. Nevertheless, trends to optimize the fleet led to new ship types reflecting the diversity of carried cargo and means of loading and unloading. The safety standards applied at the time appeared to be inadequate to the new types of ships. Classification societies started to develop new safety standards in response to this new situation.

Safety standards in the present rules correspond to the division of the hull structure strength into hull girder, zone, and local problems, i.e. three problems in total. Theoretically four criteria, namely yielding of the structure material, buckling of the structure, fatigue of structure details and ultimate strength, have to be applied to each problem, effectively resulting in 12 problems. In practice, the ultimate strength criterion, in current rules, is only applied to certain structures (e.g. bulkheads) and the fatigue strength criterion is applied only to the design requirements of some structural connections (e.g. for connections of longitudinals); thus, reducing the number of problems. In the yield check the allowable stress is divided into components, i.e. the criterion for hull girder, zone and local strength components.

Excluding loading in excess of the reserve buoyancy, a ship can be sunk only by letting water

in. Water may be let in by collision, grounding, weapon effects or by operation of a system that can communicate with the water. Optimum design is often assumed to mean the minimum weight structure capable of performing the required mission. Usually, the designers are using methods for assessing the minimum requirements to provide against failure. The sea imposes on areas of the ship extreme loads which have not been yet extensively measured. Therefore, the definition of structural failure has been an area of several approaches from shipbuilders considering shipowners desires, classification societies rules, experience and type of the vessel.

From a ship structural view there are four possible ways of failing: (a) direct fracture caused mainly by a part of the structure reaching the ultimate tensile, compressive, shear or crushing strengths, (b) fatigue fracture for structures that operate in extreme environments with high-cycle loading, (c) instability, which includes buckling, wrinkling, tripping or shrinking and (d) unacceptable deformation mainly due to misalignments or vibrations. The whole ship girder provides the background and the boundaries for local structural design. There are four types of structure with which the ship designer must deal: (a) plating-stiffener combinations, (b) panels of plating, (c) frameworks, and (d) fittings. All of these parts have been thoroughly examined for the types of loading used in naval architecture, expect fracture, which is an area that seems to be examined only in modern ship designs.

1.3.2 Submarine pressure hull

Structural steel is used mostly for the construction of submarines. The fracture safety of submarines is addressed through the use of structural steels and welding materials for hull fabrication that demonstrate high fracture toughness and flaw tolerance for these extreme service conditions. Thus, the key requirements for naval shipbuilding steels used for submarines are not only strength, weldability, and toughness at low temperature under shock events, but also driven by economics, in order to keep an affordable vessel acquisition cost. Except for vessel protection plating, the use of higher strength steel in a naval structure is usually a means to reduce weight and is a cost versus benefit decision. Thinner plate and less weld metal are required for HY / HSLA-80 structure compared to HSS (DH / EH-36). However, buckling limits, requiring additional stiffening, may prevent optimum use of HSLA / HY-80 for weight reduction.

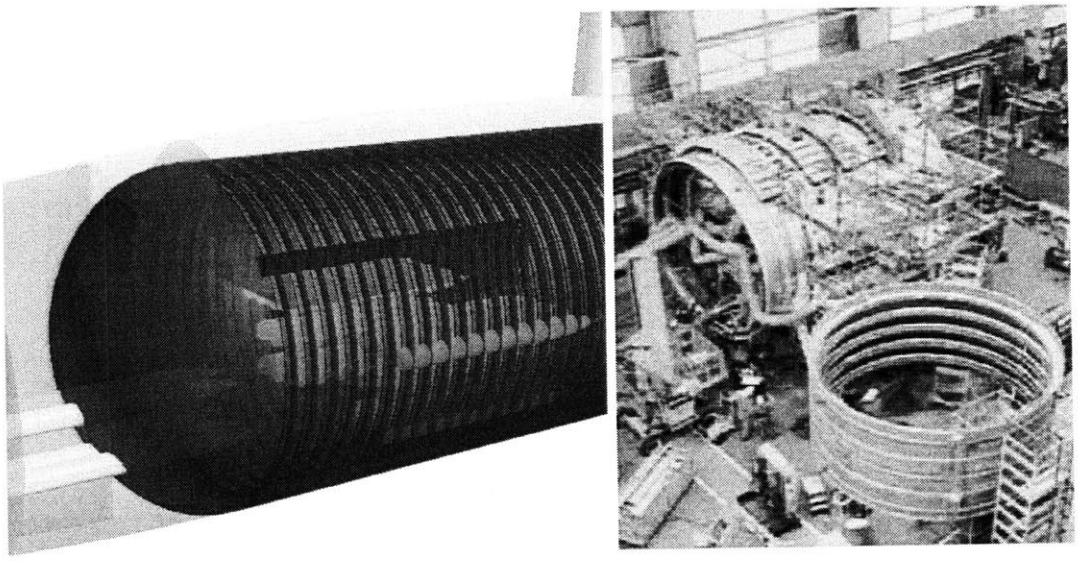

Figure 1-6: Computer model (left) and initial stage erection at a shipyard facility (right) of a submarine pressure hull

There have been limited publications about submarine structural strength concerning fatigue, fracture and corrosion, which are the main factors affecting operational capabilities. Usually, the response of a stiffened cylinder subjected to underwater explosion is examined in the literature (Cichocki [48]; Ramajeyathilagam [249]). Simple design formulae are developed by Park and Cho [223] for predicting the residual damage of unstiffened and stiffened plates under explosion loadings. A method for the evaluation of the fatigue operational life of submarine pressure hulls has been developed from Robles et al. [262], by applying linear elastic fracture mechanics.

A submarine pressure hull can be simulated as a ring-stiffened cylinder, which lends itself to an analytical and an experimental evaluation of structural behavior, Fig. 1-6. Over the years, the prediction of linear elastic response of ring-stiffened cylinder subjected to transversely exponentially decaying shock waves has been the area of research, and this work is summarized by Haxton and Haywood [97]. Additionally, Liang et al. [155] studied the nonlinear responses of a submersible pressure hull proposing their results (numerical simulations) to be implemented for future submarine design and maintenance.

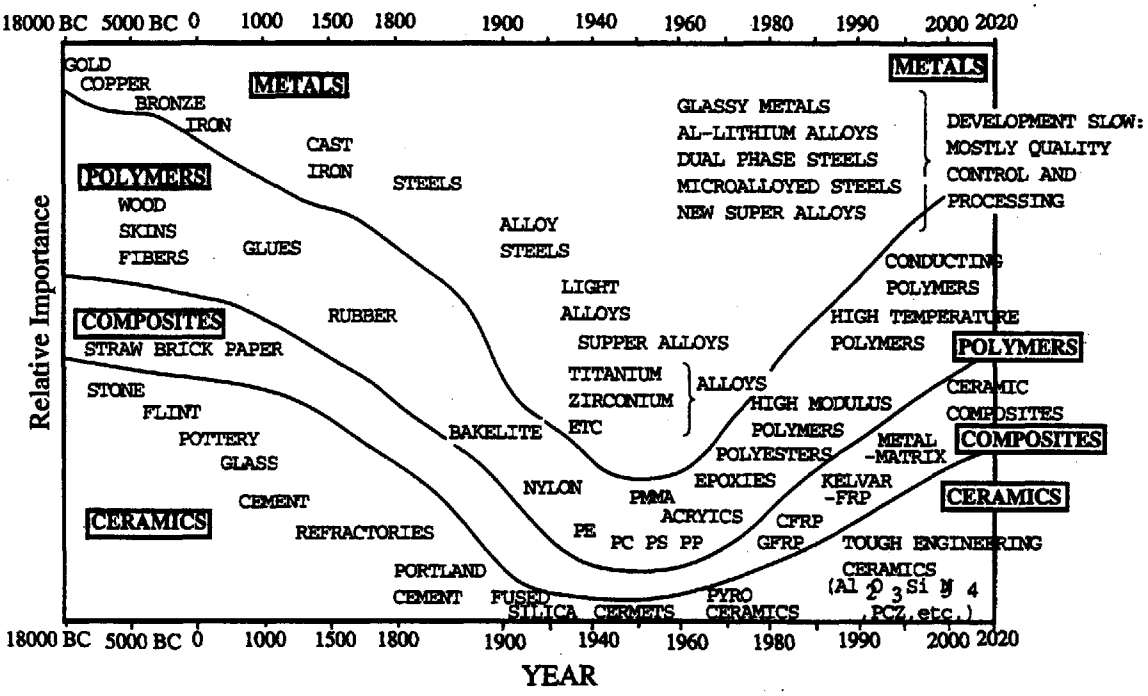

Figure 1-7: Evolution of materials for mechanical and civil engineering

1.4 Marine Applications of Aluminum Alloys

The current demand for fast sea transportation in both commercial and military applications has accentuated the need for lightweight materials that can provide a challenging combination of material property requirements. The use of materials in engineering have altered throughout history as shown in Fig. 1-7[1]. The high strength-to-weight characteristics of aluminum alloys are particularly attractive for use in these new high performance vessels.

Aluminum owes most of its applications to its low density (0.16 kg/ m^3) and to the relatively high strength of its alloys. Other uses depend upon its comparatively good corrosion resistance, good working properties, high electrical and thermal conductivity, reflectivity, and toughness at low temperatures. Designs utilizing aluminum take into account its relatively low modulus of elasticity (69×10^3 MPa) and high coefficient of thermal expansion ($2.3 \times 10^{-5}/°C$).

[1]Froese, F. H., Aerospace materials for the twenty-first century, *Materials Design*, originally prepared by Ashby, M. F. in 1987

Aluminum alloys, on the other hand, possess better casting and machining characteristics and better mechanical properties than the pure metal and, therefore, are used more extensively. Aluminum alloys are divided into two general classes: (i) wrought alloys and (ii) cast alloys, each with its own alloy designation system. Wrought alloys are available in a number of product forms. Extrusions, produced by pushing the heated metal through a die opening, are among the most useful. A great variety of custom shapes, as well as standard shapes such as I-beams, angles, channels, pipe, rectangular tube, and many others, are extruded.

Aluminum was used for boat construction as far back as 1891 in the first steam launch by Escher Wyss, followed in 1894 by the first torpedo boat by Yarrow & Co. In 1895, the alu-skinned "Defender" won the America's Cup. It was in the 1920's that aluminum shipping applications started to expand in both the civil and military domains, due to new alloys becoming available for marine applications. By 1960, aluminum was firmly established in all marine sectors around the globe. In 1962, the "France" was built using $1,600$ tonnes of aluminum for its superstructure. The first high-speed catamarans were produced in 1970's, Fig. 1-8.

Today, more than $1,000$ high-speed passenger ships are in service, most of which have a structure and superstructure made of aluminum. Cruise ship superstructures continue to be made of aluminum, while over half of all yachts have aluminum hulls.

Aluminum is used in hulls, deckhouses, and hatch covers of commercial ships, as well as in equipment items, such as ladders, railings, gratings, windows, and doors. The major incentive for employing aluminum is its weight saving compared to steel. Because it is common practice to use weldable aluminum alloys having strengths approaching or comparable to mild steel, equal-strength structures can be designed to a weight saving of $55 \sim 67\%$. However, to compensate for the lower modulus of elasticity of aluminum and to conform to normal deflection limitations, a somewhat lower, but substantial, reduction in weight is usually obtained.

Aluminum construction increases speed and size, enhances fuel economy, and lowers maintenance. Weight savings of $35 \sim 45\%$ in hulls, and $55 \sim 65\%$ in superstructures, can be achieved with aluminum compared to steel. Higher vessel speeds and load capacities, enabled by use of aluminum, attract extra traffic volume and profit for the ferry operator.

Aluminum is recognized by and complies with the requirements of the High Speed Code of the International Maritime Organization. for vessel design, safety, and control of fire risk. The

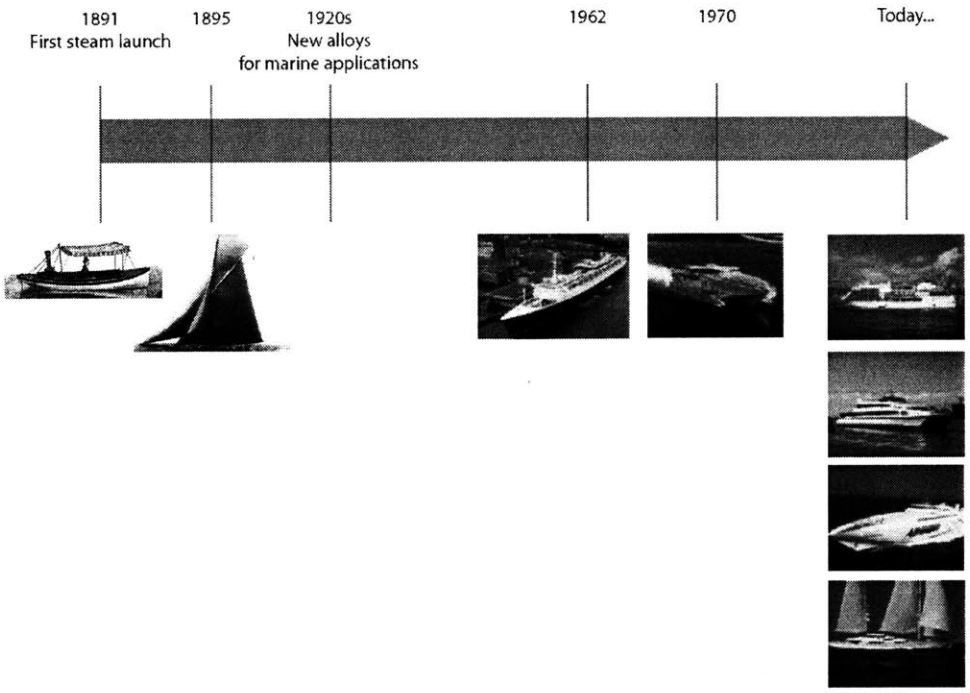

Figure 1-8: Historical application of aluminum at the shipbuilding industry

metal stands up to the torsional, flexural, compression and impact loads of high speed water travel as well or better than steel. Aluminum-intensive cargo ships with load capacities up to 3,000 metric tons are under design to operate at up to 60 knots, cross the Atlantic in under 60 hours, and handle Class 6 seas.

Military requirements seek smaller, more agile vessel designs with a lower radar cross section and capable of 60 to 80 knots or more - another excellent fit for aluminum given aluminum manufacturing advances, such as friction-stir welding and structural bonding.

Marine grade aluminum alloys are used for helicopter decks, telescoping bridges, accommodation modules, stair towers, cable ladders, fire walls, mud mats, gratings, and many other applications around the globe. Aluminum structures weigh $40-70$ % less than equivalent steel structures in these applications. Larger, lighter aluminum structures can be handled and lifted with smaller, less expensive equipment. In marine environments, properly selected aluminum alloys require no painting or protection against exposure, and require little or no maintenance.

Aluminum is widely used in cruise ships, pleasure boats, irrigation pipe, heat exchangers,

sewage treatment plants, and rain carrying equipment because of its durability in the natural environment. Installations of aluminum culvert sheeting and pipelines have shown its resistance to corrosion in many soils. Some aluminum drill pipes, for example, have been in use for more than 20 years.

Aluminum seawall shapes are extruded, achieving the most strength with the least material. Since aluminum is easy to extrude and fabricate, retrofitting offshore platforms and custom-tailoring is cost-effective. Designers can create either a single-piece component, bolted connections, or interlocking sections for fast and simple fit-up on site. Aluminum can be connected and secured using a wide variety of proven mechanical methods and is welded three times faster than steel, using inexpensive welding devices. Critical design of structural elements is required when lightweight, high-strength hull structures are constructed of aluminum. In modern shipbuilding these structures become more complex and in-depth analysis is applied (Latorre et al. [150]; Lee et al. [153]; Kennell et al. [135]).

1.4.1 Properties of aluminum alloys for marine applications

Compared to steel, the material characteristics of aluminum alloys can be focused on two issues: (i) stress-stain relationship and (ii) heat-affected zone (Wang et al. [324]).

Stress-strain law

A generalized law $\varepsilon = \varepsilon(\sigma)$ was proposed by Ramberg and Osgood [252] for aluminum alloys:

$$\varepsilon = \frac{\sigma}{E} + 0.002(\frac{\sigma}{\sigma_y})^n \tag{1.1}$$

where

n = knee factor, which can be determined by Mazzolani [174] as $n = \dfrac{\ln 2}{\ln(1 + k\chi)}$

$k = \dfrac{\sigma_t - \sigma_y}{10\varepsilon_t}\dfrac{\sigma_t}{\sigma_y}$

σ_t = ultimate tensile strength

σ_y = minimum yield strength (0.2% strain)

ε_t = fracture strain

Heat affected zone (HAZ)

In welded profiles, the heat input removes some of the beneficial effects from heat treatment or strain hardening and leads to a decrease in the elastic limit, which results in the strength redistribution along the cross section profile with the minimum at the welds.

The relationship between HAZ extent and plate thickness for fillet weld and butt weld in BS 8118 [35] can be expressed as:

$$z = \min\left\{3t_A, 20 + t_A/3\right\}, \text{ mm} \tag{1.2}$$

for fillet weld, excluding $7xxx$ series alloys

$$z = \min\left\{3t_B^2/t_A, 20 + t_A/3\right\}, \text{ mm} \tag{1.3}$$

for butt weld, excluding $7xxx$ series alloys

where t_A is the lesser of $0.5(t_B + t_C)$ and $1.5t_B$, t_B and t_C are the thickness of the thinnest and thickest elements connected by welding, respectively. The modified factors, α and n in BS 8118, are ignored in the analysis by Kristensen and Moan [143]. If all of the elements connected by welding have the same thickness, the above formula can be rewritten as:

$$z = \left\{ \begin{array}{c} 3t \text{ if } t \leq 7.5\,\text{mm} \\ 20 + t/3 \text{ if } t > 7.5\,\text{mm} \end{array} \right\}, \text{mm} \tag{1.4}$$

The $5xxx$ series alloys used for the majority of commercial marine applications have weld yield strengths of 100 to 200 MPa and good corrosion resistance. These aluminum-magnesium alloys retain good weld ductility without post weld heat treatment and they can be fabricated with normal shipyard techniques and equipment.

The weldable aluminum-magnesium-zinc alloys are also receiving attention in this field. Tensile strength reductions in 10-year sea-water corrosion tests of 1.62 mm thick bare sheet specimens are only 2 to 5%. The $6xxx$ series alloys, widely used for pleasure boats, show a 5 to 7% decrease in similar tests.

Alclad aluminum alloys are seldom required in construction of marine vessels. They are used, however, in a few applications, such as piping, for maximum assurance against excessive

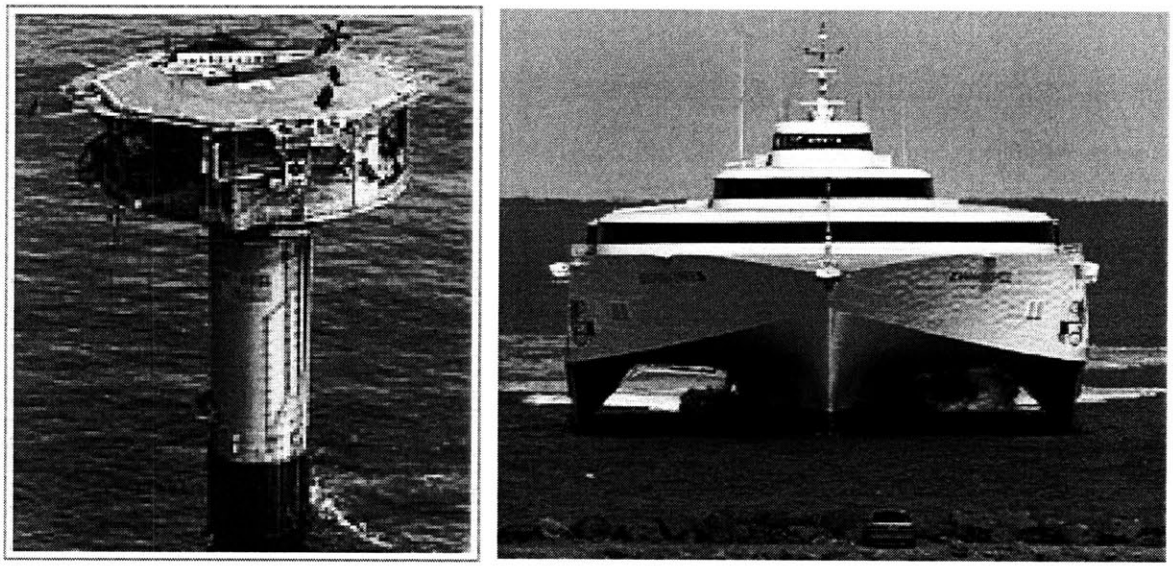

Figure 1-9: The first all-aluminum oil rig, which was installed in Venezuela in 1957 (left), and "Benchijigua Express" (right), which is currently the world's largest aluminum commercial ship, a trimaran hull type with 126.7 m length and speed of 40.5 knots, built and delivered in 2005 by Austal [courtecy of Austal]

depth of pitting. Also, alclad $2xxx$ and $7xxx$ series alloys are selected where tensile strengths of $480-550$ MPa are required, considerably higher than now available in the $5xxx$ series alloys.

The high-strength alloys are employed where welding is not required, and where their higher strengths can be used to advantage. Protective measures such as cladding, painting, or cathodic protection must be used for satisfactory life in marine service, because of their lower resistance to corrosion by sea water.

1.4.2 Commercial marine applications of aluminum

Aluminum and its alloys are widely used for numerous marine applications from offshore to shipbuilding industry, as shown in Fig. 1-9. The use of small boats has expanded rapidly since 1945. Early applications of aluminum were mainly in canoes and small fishing boats, in which aluminum is now the dominant material. Small craft and small outboard cruisers up to 6 m long generally are constructed either of aluminum or plastic. Styling often is more important than engineering superiority in these consumer products.

Small boats are fabricated from a wide range of aluminum sheet alloys, mainly in the $5xxx$ and $6xxx$ series. These have an optimum combination of strength, cost, ease of fabrication, and corrosion resistance. Generally, 5052−H32, 5052−H34, or 6061−T6 is used for small hulls that need no stretch forming. Where stretch forming is employed, 6061−T4 sheet, which may be subsequently artificially aged to the T6 temper, is utilized. Extrusions of 6061 or 6063 are used for structural and decorative sections, such as keels, chines, gunwales, and spray rails.

Larger inboard boats, 6 to 38 m long, are fabricated of aluminum alloys for reasons similar to those for small craft. Normally, these boats employ welded construction for hull, interior structure, and cabins. The most popular alloy for hulls is 5086−H32, in thicknesses of 4.5 to 12.7 mm. Bulkheads, fuel tanks, and cabins are usually of the same alloy as the hull, although 5052 or 6061 can be utilized. Structural members, either in special extrusions or standard structural shapes, can be of 6061−T6 or 5086−H112 in all-welded construction.

Sailing craft follow a pattern similar to that for power craft; the smaller boats using riveted construction of 5052 or 6061 alloy, and larger custom yachts using all-welded construction in 5086. The light weight of aluminum hulls in sailing craft allows the designer wide latitude in providing balance between sail area and ballast-displacement ratio.

Crew boats are normally of hard-chine, planing-hull type, using developable surfaces in the hull form. This results in an efficient hull that is economical to fabricate. The builder also benefits from the lighter weight of the material being lifted into place, since fewer workers and pieces of hoisting equipment are required.

The majority of aluminum personnel boats are fabricated of 5456−H321 sheet and plate 4.8 to 9.5 mm. thick, and 5456−H111 or 6061−T6 extruded shapes. Alloy 5086 is also widely used for hull plating.

Equipment aboard fishing vessels is often aluminum. The aluminum fishroom, common in Europe, is used in some vessels in the United States. Extruded or roll-formed aluminum hold sections in 6061−T6 or 6063−T6 result in fishroom systems that are nonabsorptive, sanitary, and easily rearranged by the crew.

Passenger vessels utilize large quantities of aluminum in superstructures and equipment. The 2,000 metric tons in the "SS United States", built in 1952, resulted in an 8,000-ton decrease in displacement. The lighter topside weight permitted a beam reduction, saving hull weight

and allowing reduced power capacity, while still providing the high service speeds necessary on modern ocean liners. Riveted 6061−T6 plate was employed for the deckhouse structure, superstructure decks, and bulk- heads. The remainder of the aluminum was utilized in furniture, equipment, ventilation ducts, ladders, stair treads, and railings.

Major European-built liners have used aluminum extensively in superstructures and equipment, ranging from 1,000 to 2,000 tons per ship. The "Oriana", "Canberra", and "France" employed welded construction, using sheet, plate and extrusions of aluminum-magnesium and aluminum-magnesium-manganese alloys. Since appearance is important in this class of ship, the structures are painted; aluminum allows at least 50% longer time until repainting is required.

Dry cargo ships have been affected by new design trends that emphasize a need for lower topside weight. Heavier cargo handling gear and related machinery, and more narrow, hydrodynamically contoured, high-speed hulls have increased stability problems. Thus, weight saving is required to permit more efficient hull designs. Aluminum structures normally weigh only 40 % as much as steel structures, using construction details similar to steel practice (welded plate and stiffeners bracketed at the decks). In some instances, additional weight is saved by application of special extrusions.

Bulk carriers normally can take direct advantage of any weight saving by carrying additional cargo. Six Canadian ore carriers utilized 150 to 250 tons aluminum in deckhouse structures, hatch covers, and equipment such as railings and lifeboats. Aluminum booms of riveted 2014−T6, 6061−T6, or 6070−T6 extruded or rolled shapes on self-unloading ore carriers enable operators to achieve economies in converting older ships to update their usefulness. In a typical installation, a 57.5 m steel boom on the "J. R. Sensibar" was replaced with a 77.5 m aluminum boom, increasing the dockside unloading area available to the ship without having to alter the existing boom support structure.

Passenger ferries use aluminum superstructures to maintain safe stability while carrying more passengers. In 1939, New York City's Staten Island ferries initiated this application of aluminum with three riveted superstructures, involving a total of 100 tons of 6061−T6 plates and shapes. This resulted in a reduction in fuel consumption of 220 gal per round trip for each ferry and an annual operating cost that was $107,000 less than for a similar ferry with an all-steel superstructure. A group of three ships, built in 1964, used 100 tons of welded 5086

plates and extrusions for the topside structure. Smaller ferries in operation off the Pacific Coast and in the St. Lawrence River have hulls of welded 5086−H32 plate, 3/16 or 1/4 in thick.

Hydrofoils are high-speed craft used for commuter and excursion service. Although their use in Europe has been an economic reality for decades, the availability of competing forms of transportation has restricted application in the U.S. Early European applications dictated minimum hull weight to utilize practical power sources. This led to the exclusive use of a 6061 type alloy and riveted construction for the hull, cabin, and bulkheads. Craft built recently in the United States have employed welded construction with the $5xxx$ series alloys.

The 90 ton, 105 ft long hydrofoil "H.S. Denison" was built in 1961 for the Maritime Administration. A combination of riveting and welding was used in fabricating the hull, cabin, and bulkheads of 5456 sheet, plate, and extrusions. Alloy 7079−T6 forgings formed part of the steel foil structure. Piping systems were of aluminum or plastics, following aircraft practice.

Smaller hydrofoil craft have also been constructed of aluminum. Two 45 ft long craft of welded 5456 were built, with 10 more planned for similar construction. Welded 5086 sheet, plate, and extrusions were used to build the 34 ft "Albatross", which can carry 24 passengers at speeds up to 40 *mph*.

Aluminum is not only the accepted material for hydrofoil hull structure, but is used also in small foil systems in the form of alloy 356−T6 castings and 6061−T6 extrusions. However, in large craft, such as the "Denison" and the Navy's PCB and AGEH, high-strength steels are employed for the foil structures. Although many questions remain concerning the relative importance of the various factors in material selection, it has been established that the strength and stiffness provided by the high-yield-strength steels (150,000 to 200,000 psi) are necessary in the large craft.

1.4.3 Naval aluminum vessels

About 6,000 tons of aluminum per year, is used on U.S. Navy destroyers. During the 1930's, extensive application of aluminum in destroyers was developed, and design practices were refined. During World War II, construction reverted to steel because of the shortage of aluminum. Following the war, with growing emphasis on electronic equipment, deckhouse structure weight became a critical factor, and aluminum was reinstated to combat this problem.

Alloy development in the past decade has resulted in an almost standard application of 5456 plate and extrusions in the welded deckhouse structures of destroyers. Quantities now used range from 100 to 350 tons per ship, depending on the type of destroyer. The weight savings in the aluminum deckhouse structure, normally about $40 \sim 45\%$, are utilized to maintain sufficient ship stability while employing the narrow hull necessary for high service speeds. Additional equipment installations also are permitted topside.

Over half the aluminum used is in the deckhouse structure, the remainder being employed in a variety of equipment applications. These include lockers, desks, chairs, bunks, doors, windows, ladders, gratings, and galley equipment. A wide range of the more corrosion-resistant wrought and cast alloys is found in these items, including 5052, 5086, 6061 and 356.

Aluminum applications totaled over 1,750 tons on the aircraft carrier "Enterprise" (CVA-65) completed in 1961. The largest single item was the four deck-edge elevators. The first such elevator platforms, employing welded 6061−T6 members in a tubular-truss structure, had been installed on the carrier "Shangri-La" (CVA-38). Later, alloy 5154−H36 was used for the welded elevators on CVA-61. Alloy and welding developments led to application of alloy 5456 plate and extrusions in the elevators on the "Enterprise". These were designed with an open grillwork structure; the deep girders were fabricated from 19 to 51 mm thick. The 15.7 by 25.7 m structures weighted 105 tons each, 35 tons less than similar steel units. Reduced inertia, during operation between the flight and hangar decks, permitted reductions in operating machinery.

Sea Fighter, launched in February, 9^{th}, 2005 is an experimental littoral combat ship of the U.S. Navy. Sea Fighter's hull is of a SWATH design, constructed out of aluminum. The basic design has a displacement of 1,100 tons while measuring 73 m long and 22 m broad. The littoral combat ship (LCS) is the first of the U.S. Navy's next-generation surface combatants. Intended as a relatively small surface combatant for operations in the littoral region close to shore, the LCS is smaller than the Navy's guided missile frigates, and they have been compared to the corvette of international usage. On 27 May 2004, the U.S. Department of Defense announced that General Dynamics - Bath Iron Works, Bath, Maine ($78,798,188) was awarded contract options for final system design with options for detail design and construction of up to two Flight 0 Littoral Combat Ships (LCS). The design, is a slender, stabilized monohull, more commonly known as a trimaran. The estimated design sprint speed is over 40 knots as well as

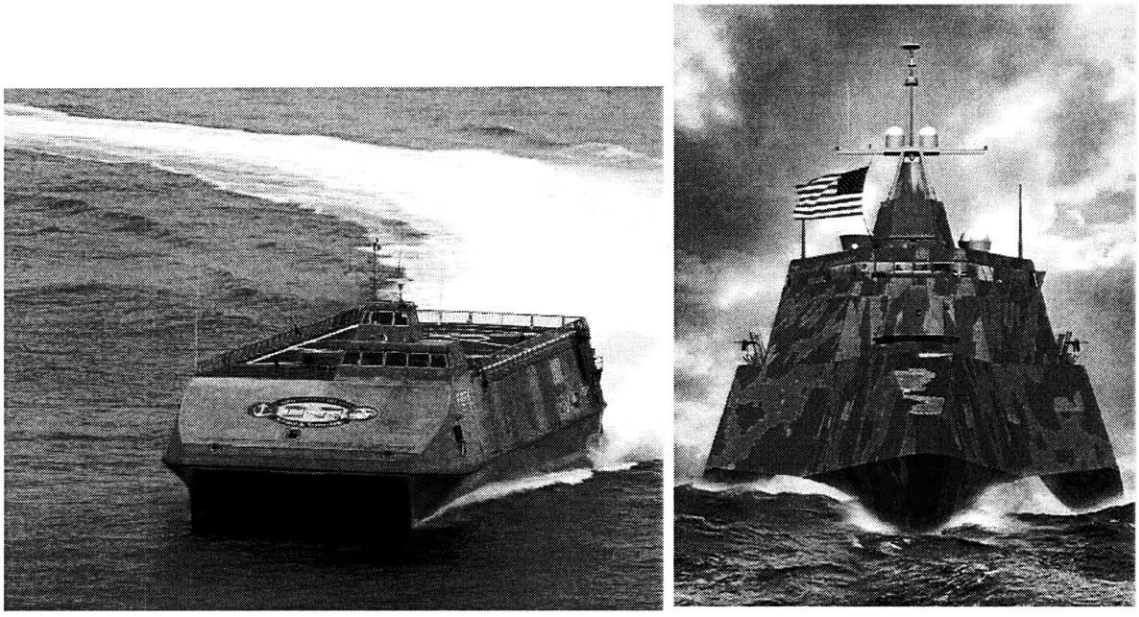

Figure 1-10: Sea fighter (left) is currently the largest aluminum vessel of the U.S. Navy, with a catamaran hull type, displacement of 450 tons, length of 79.9 m and speed of 50 knots, and Littoral Combat Ship (LCS) (right) will be the near future largest aluminum vessel of the US Navy, with a trimaran hull type, displacement of 2,637 tons, length of 127.8 m and speed over 40 knots [courtecy of U.S. Navy]

long-range transit distances of over 3,500 miles. On 19 January 2006, the keel for the General Dynamics trimaran, USS Independence (LCS-2), was laid at the Austal USA shipyards in Mobile, Alabama, Fig. 1-10[2].

1.4.4 Aluminum ship construction

The Navy is aggressively pursuing improved structures and novel construction methods that could serve to dramatically revolutionize future vessels. They will have significantly different hull forms, be fabricated increasingly by automated methods, and will utilize even more light-weight metal, hybrid, and aluminum structures than we currently envision,

The ultimate compressive strength of stiffeners modelled by plate elements supported along one edge was investigated by Xiao and Menzemer [340]. A comparison between the analytical results and available experimental data showed that current design for compressive strength

[2] www.naval-technology.com

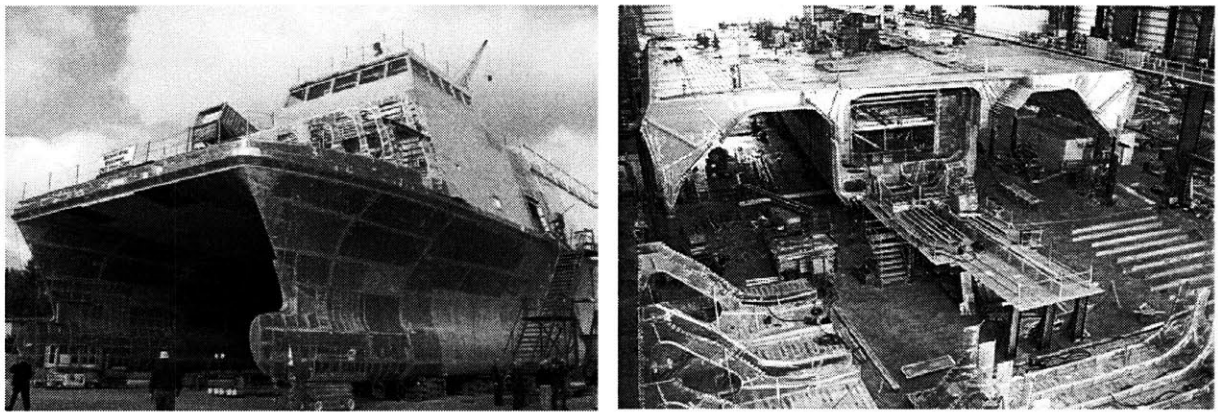

Figure 1-11: Sea Fighter under construction (left), November 2004, and Littoral Combat Ship's construction progress (right) as of July 2006 [courtecy of U.S. Navy]

of outstanding elements is conservative. It is suggested that the differences are related to the establishment of the boundary conditions. The behavior of the same type of elements has been analyzed numerically and experimentally by Zha and Moan [353].

The development of Eurocode 9 for aluminium structures lead Tryland et al. [308], to study numerically the behavior of I beams and deck profiles under concentrated loading in the beam's transverse direction. The results were validated against data obtained from an experimental program. Comparisons have shown that design formulae developed for steel beams (Eurocode 3) should be adjusted to account for the difference in material properties when applied to aluminium beams.

Failure of a device or structure to function properly might be brought about by any one or a combination of many different responses to loads and environments while in service. For example, too much or too little elastic deformation might produce failure. A fractured load-carrying structural member or a shear pin that does not shear under overload conditions each would constitute failure. Progression of a crack due to fluctuating loads or aggressive environment might lead to failure after a period of time if resulting excessive deflection or fracture interferes with proper machine function.

A primary responsibility of a naval engineer is to ensure that his or her design functions as intended for the prescribed design lifetime and, at the same time, that it be competitive in the marketplace. Success in designing competitive products while averting premature mechanical

failures can be achieved consistently only by recognizing and evaluating all potential modes of failure that might govern the design. To recognize potential failure modes a designer must be acquainted with the array of failure modes observed in practice, and with the conditions leading to these failures. Section 2.4 in next chapter summarizes the mechanical failure modes most commonly observed in practice, followed by a brief description of each one.

1.5 Milestones in the Shipbuilding Industry

Growing concern for the serious consequences for human lives and environment, due to major accidents of ships in the recent years and the growing knowledge of dynamic behavior of structures under impact load, have made it a challenge for researchers and product developers to use improved construction for ships to withstand impact loads caused by collisions and groundings. In certain fields of marine transport, improvement of structural safety can even lead to commercial profit as it allows increased cargo loads at a decreased risk level.

Fatigue and fracture are engineering disciplines that have been studied for more than 150 years but are still developing and of large contemporary interest, not only for ship and offshore structures, but for virtually all engineering structures.

Although crack growth in plates and riveted stiffened panels (for airframes) has been studied extensively, few investigations of crack propagation in a panel with multiple welded stiffeners were found. Welded stiffeners affect crack growth in a unique way because of residual stresses present from the welding process (Dexter and Pilarski [55]; Dexter et al. [56]). Furthermore, in contrast to riveted stiffeners, cracks may propagate into, and sever, integral welded stiffeners. Llopart et al. [158] performed experiments and numerical analyses concerning the fatigue crack growth and crack turning on integral stiffened structures used for aircraft under mode I loading. They observed that for small crack lengths in the fuselage sheet, the influence of the stringer geometry is small.

Prior to 1940, steel ships were riveted. Riveted construction was good for structural integrity because a crack in one structural element could not propagate into adjoining structural elements. If a crack propagated in the shell, the intact structural elements, such as stiffeners, limited the crack opening and often arrested the crack growth. A corresponding increase in the

amount of force carried by the stiffeners resulted from providing displacement control to the crack opening. This effect is known as load shedding.

During World War II, all-welded construction was introduced, perhaps most noted in the construction of Liberty Ships. A combination of steel with low notch toughness, poor weld processes, and high stress concentrating details contributed to brittle fracture in many of these ships. In addition, welding creates tensile residual stresses near stiffeners, which tend to accelerate crack growth. Early investigations led to notch toughness requirements for ship steel, as well as improved welding methods and design details. The adoption of these provisions substantially reduced the incidence of brittle fracture.

The advent of high-strength steel **in the 1970's** allowed ship designers to design for a higher allowable stress. Unfortunately, the stress ranges increase in magnitude if the allowable stress is increased, because the scantlings are typically reduced relative to what they would be if low strength steel were used. Although the yield and ultimate tensile strength of the steel had increased, the resistance to fatigue cracking of welded details is independent of the strength level and the type of steel. Therefore, the higher stress ranges have translated to an increase in the incidence of cracking. Fortunately, the notch toughness of the steel and weld metal allows the cracks to grow in a stable manner.

The failure of MV Kurdistan, Fig. 1-12, demonstrated the classic combination of high stress, low toughness and defect which are required to cause initiation of a brittle fracture. The ship suffered a catastrophic brittle fracture initiating in the port bilge keel weld, which propagated into the ship's structure, causing her to break in two. All materials tested met the required standards. However, the weld in the ground bar of the port bilge keel was incorrectly made, inducing a large weld defect, and reducing the local toughness. The formal investigation into the MV Kurdistan, as presented in details by Garwood [80], involved the use of elastic-plastic fracture mechanics (for the first time in a U.K. court) to help ascertain the circumstances leading to the failure.

There is a need to estimate the time before any crack can grow to a critical length, or length at which the ship's integrity is susceptible. Such estimates severely affect the profitability of ship transport, as any time out of service represents a substantial loss in revenue.

There have been several incidents involving naval structures that changed completely the

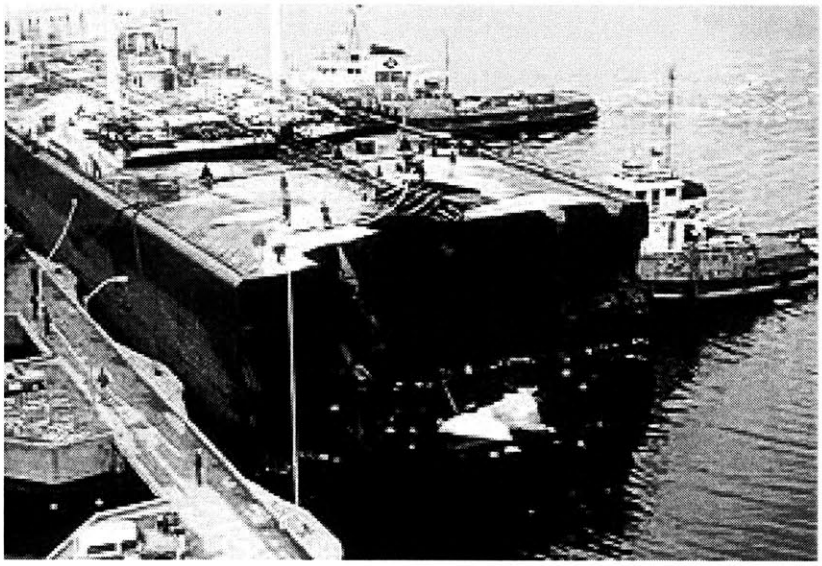

Figure 1-12: MV Kurdistan after experiencing a catastrophic accident

way that the shipbuilding industry handled ship and submarine construction. Most of the cases included either the severe damage of the structure or even human losses. Many challenges facing prediction of explosive damage of naval vessels can be identified in the photographs of a hole driven in the port side of USS Cole and the collision damage of USS San Francisco. Clearly seen in Fig. 1-13 are hard point fracture, weldment fracture, radial cracks leading to holing and petalling.

Recent years have revealed a continuous increase of the interest in risks associated with collision and grounding accidents. The driving force is an ever-rising public concern about the safety of shipping, with regard to protection of the environment, human lives, and economic values in a direct or indirect sense. It is equally important in a formal risk assessment to focus on the active and passive safety, that is, on both the probability of an accident occurring and the consequences of the accident.

In prediction of the consequences of a collision or grounding accident, it is crucial to be able to predict the structural damage involved in the accident. The development in software and computer power in recent years has made it possible to obtain accurate and detailed solutions for the very complex, highly nonlinear structural behavior involved in the crash process (Kitamura [140]). In this field of crashworthiness, there has been a significant technology transfer from

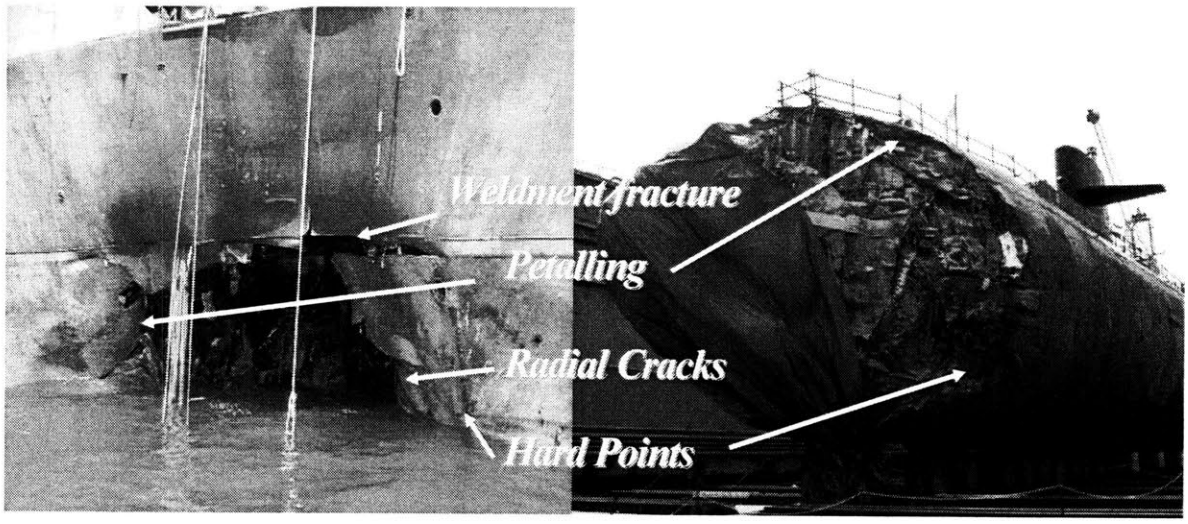

Figure 1-13: Damage caused from weapons effect to the starboard side of USS Cole on October 2000 (left) and the bow of the USS San Francisco submarine docked after collision in January 2005 (right). Various features of tearing fractured plates are clearly visible on the photographs [courtecy of U.S. Navy]

the automotive industry, where full-scale compliance tests have been mandatory for more than 20 years. The obligatory compliance tests of passenger cars are limited in number and have rigorously defined test scenarios. Consequently, finite element modeling, although quite costly, has proved to be a cost-effective tool for structural crashworthiness optimization of a large-scale production car body.

In the maritime sector several authors have demonstrated how ship-to-ship collisions or ship grounding on hard rock can be modeled with general-purpose, nonlinear finite element programs. Unlike the automotive engineer, however, the ship designer is not given a well-defined set of impact scenarios for which the structure should be optimized. When existing collision and grounding accident records are considered, it is quite clear that, in order to capture an actual range of possible impact loads on a structure, a risk analysis has to include a large number of accident scenarios. It would be convenient to assume that if the structure is designed to efficiently withstand a few of these scenarios, it is generally safe. Still the problem remains, which scenarios are representative of a majority of ship collisions. In the transportation sector it will almost always prove highly irrational to select worst-case scenarios, because

the probability of these scenarios is so small that their contribution to the total risk is negligible. A comprehensive risk analysis therefore has to consider thousands of impact scenarios and weigh the probability of each scenario with potential consequences.

Typically, the probability of each investigated scenario is known only at a limited level of accuracy, so it may not be worthwhile to predict the consequences with a significantly higher accuracy. For this reason, it turns out that simplified and fast modeling tools are very useful in certain types of risk analysis.

1.6 Problem Statement

The use of aluminum in the shipbuilding industry is highly related to the understanding of the fracture mechanics that govern naval aluminum panels, because the vessels operate in extreme environmental and functional conditions that can lead to the loss of the entire structure.

The maritime industry is facing nowadays a huge demand for ship availability, which results in full time activities for the shipyards worldwide either for new ship construction or for fast repair and maintenance. There is also desire for the production of naval vessels (both surface and underwater) with new types of materials, such as high strength steels which usually present a reduction in the fracture toughness with an increase of the mechanical strength. This reduction can imply a decrease of the estimated fatigue lifetime for the structure, considering the process of crack propagation under cyclic loading stresses or impact loading. The operational envelope of all these vessels has to be extended by minimizing the need for intervals due to damage or maintenance. The extremely high costs related with vessel repair and maintenance due to fracture of critical structural components and/or the hull and the requirements for top level standards and quality for these structures have brought the shipbuilding industry to investigate in depth the phenomenon of crack propagation and arrest due to fracture, fatigue or flaw.

There is a significant amount of work on cracks in riveted aircraft panels, some studies on crack growth in panels with welded stiffeners and few studies on crack growth in plates with welded stiffeners which are axially loaded. On the other hand, there are no research published on the effect of the type and design of stiffeners in the crack propagation and arrest phenomena improving the fracture toughness of a construction, except from cutting stiffened panels parallel

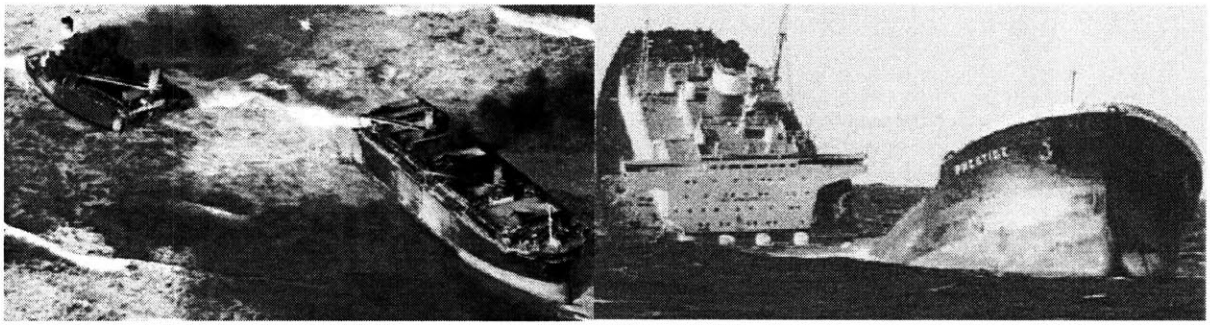

Figure 1-14: Hull rupture due to unstable crack propagation

with the stiffeners by Simonsen and Ocakli [288].

Structural elements subjected to dynamic loads of significant amplitude are susceptible to extensive cracking. The primary variables influencing the possibility of fatigue cracking in welded steel structural elements are the severity of the stress concentration of the particular design detail and the nominal stress range.

There have been some serious accidents or damages to steel vessels, which brought up the question of creating criteria for evaluating the hull strength, by assessing the fatigue life due to crack existence, loss corrosion or damage (collision or grounding), Fig. 1-14.

The definition of the term "failure", when applied to naval structures, is subject to many interpretations. A seemingly insignificant crack under the right circumstances could propagate across the entire hull, leading to the loss of the vessel. Such an event could be a catastrophic failure that resulted from an initially minor failure. In other circumstances, a similar crack may never propagate, but, because it is part of the cargo envelope of the hull, i.e. fuel oil, can lead to pollution of the sea so that the structurally minor failure becomes an environmentally major failure.

1.7 Research Objective

The overall objective of this study has been to understand the mechanics of fracture that govern the structural response of naval structures. The work has primarily been focused on high-speed craft built in lightweight materials such as naval aluminum. Experiments conducted

on small and intermediate scale aluminum plates and panels reveal that the crack propagation and arrest phenomena are highly depended on the presence of stiffeners, the type of stiffener and the stiffening configuration.

Survivability should be improved by providing superior damage tolerance. Ship affordability is enhanced by allowing greater automation in hull fabrication and by integrating distributive systems within hull configuration. This dual use technology should have a profound influence on both naval and commercial applications. The development areas selected are:

a. Structural integrity: investigates the strength and stress behavior of the structure to determine if there is any critical weakness, and

b. Survivability: investigates the benefits to be derived from this application by performance enhancement.

Fracture is a multifaceted problem that spans lengths covering six orders of magnitude. As shown in Fig. 1-15, it starts at a microscale length with the formation, growth and linkage of microvoids from which a unit material volume is composed, and then continues to the thickness of the structure and the widths of a typical stiffening element. Cracks initiated in this way propagate over the widths of a typical panel and even further across bulkheads and decks separating adjacent bays. In order to cover this broad range of failure mechanisms and length scales, a system approach is necessary because structural failure must be dealt with all the way from the initiation site to the damaged state of a hull girder. Different methods must be used to control and predict fracture at each of the above levels of complexities. Furthermore, fracture must be included in the whole design cycle, because controlling fracture will depend on the choice of materials, detailed structural design (secondary and tertiary scantlings), overall hull design concept (single versus double hulls), etc. Major advances in fracture research would bring immediate payoffs for the Navy and the shipbuilding industry.

Aluminum alloys are generally more promising materials than steel for construction of weight critical transportation systems such as high speed vessels because of the excellent strength to weight ratio. They also exhibit good characteristics related to corrosion resistance and toughness. This does not infer, however, that aluminum alloys does not exhibit some disadvantages when they are used as strength members, which include low stiffness and difficulty of welding resulting in minor and major failures, Fig. 1-16. It is therefore of crucial importance to better

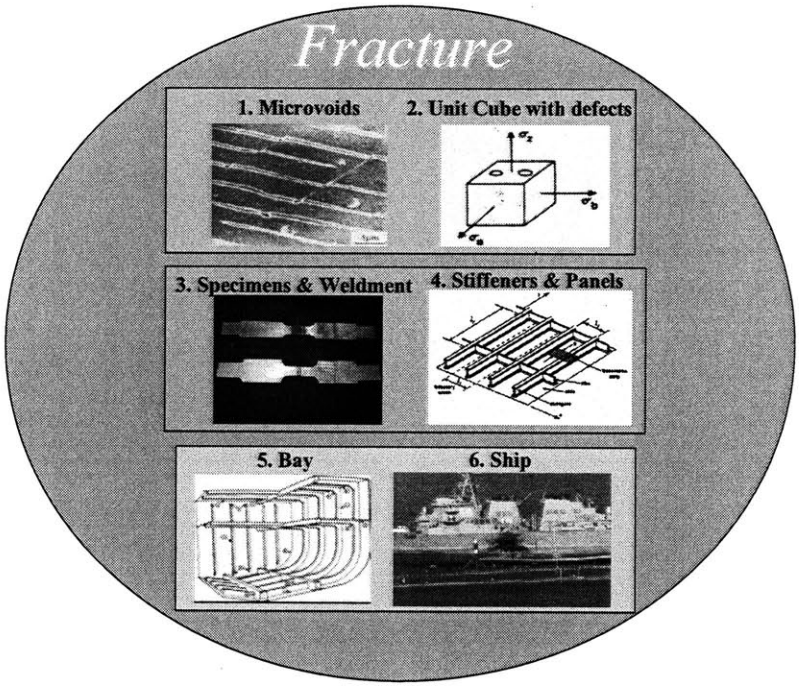

Figure 1-15: Fracture at six orders of magnitude of lengths

understand the mechanical characteristics of aluminum alloy base metal and its welding effects so that aluminum alloys can be used effectively for design and construction of light weight structures.

The present study investigates the characteristics of tensile strength of aluminum alloy base metal and fillet welded stiffeners for naval applications, concerning welded configurations. A series of tensile tests in a quasi-static condition are carried out on base metal and fillet welded stiffeners of aluminum alloys, varying the type of stiffener. The results and insights developed in this study will be useful for designing naval aluminum structures. These results are compared with T-type extruded aluminum stiffened panels to evaluate the effect of different manufacturing and design methods. As a last step, comparisons between stiffened and unstiffened structural configurations representing naval structures are performed. Additionally, the effect of stiffener dimensions on the crack propagation and arrest is examined. A series of experiments is performed, by changing the length and height of the web of a flatbar stiffener and then the classical T-type stiffener is examined.

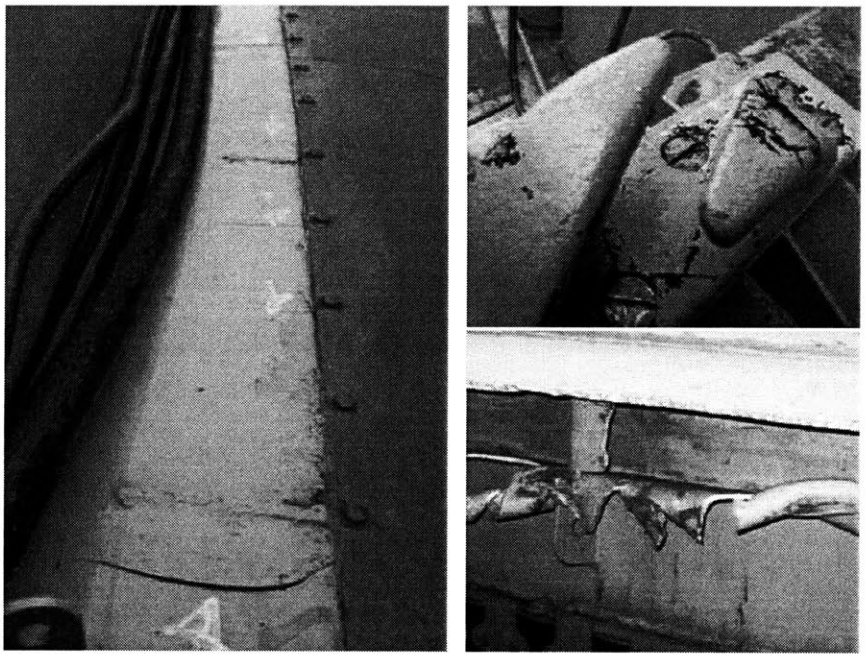

Figure 1-16: Numerous cracks alongside the main deck of a naval vessel (left) and catastrophic fracture caused at structural components due to operational or accidental loading (right) [courtecy of Hellenic Navy]

The ultimate goal of this dissertation is to develop design concepts for naval combatants, submarines and other protective structures, to increase their damage tolerance by enhancing their damage survivability envelope against various extreme loads, most notably explosions, but also low and high velocity impacts, and their operational life concerning fatigue or corrosion. Specifically, fracture analyses for structural-scale response of stiffened (welded and extruded) panels are examined, analyzed and presented. The operational life of a naval vessel will be better estimated applying the existing knowledge.

The results of this study will offer a significant contribution to the overall examination of the behavior, design and optimization of naval structures subjected to normal and/or extreme loads such as explosive loading. A history of research and a review of the developments of engineering structures subjected to explosive loading are well presented by Bulson [36].

The major objective of this thesis is to develop means for improving reliability of stiffened structures by thoroughly analyzing a series of problems that can occur during fabrication of welded or extruded aluminum structures so that these problems can be minimized or even eliminated. As the strength of the material increases it becomes more difficult to maintain good fracture toughness. The results will help to minimize hull collapse or rupture while plastic energy dissipation capacity is maximized.

Many studies have been conducted, but the continuing occurrence of structural failure problems indicate that more emphasis is needed on transferring the results of research into design, construction, inspection, and repair of ships. This research tries to make ends meet between research and shipbuilding industry.

1.8 Outline of Thesis

This thesis consists of four major parts. The first part, which is described in Chapters 1 and 2, provides information about the current trends in the shipbuilding industry and the marine applications of aluminum in naval structures and presents a historical review of the fracture aspects related to unstiffened and stiffened structures. Emphasis is given on failure modes that are related to the use of this material, especially for vessels that operate under extreme environmental and operational conditions.

The second part, that is included in Chapter 3, is the core of this thesis, and describes all the experimental tests performed in order to map the crack pattern. It is divided into the methodology followed in order to approach this aspect, the design of experiments, explanation of the selection of the specimens and experimental setups and, finally, the experiments. They include test of uniaxial tensile ("dogbone") specimens to analyze the material property and to calibrate the fracture criteria, small-scale testing of unstiffened and stiffened Compact Tension (CT) specimens, and finally, intermediate-scale testing of two pairs of specimens, comparing the crack propagation between unstiffened and stiffened extruded panels.

The third part, that is related to Chapter 4, describes the numerical simulations performed to examine the relationship between the experimental results and the theoretical background included in the widely used commercial codes. The valid model resulted can then be used to examine various designs and find the optimum one that satisfies the existing criteria set from naval architecture and increase damage tolerance envelope.

The fourth part, namely Chapter 5, concludes the research and recommends areas that should be examined for improving the contributions of this dissertation.

Chapter 2

Background

2.1 Loading of Naval Structures

It is necessary for the designer to clarify the strength that the hull structure should have with respect to each of the various steps taken in the analysis process, from load estimation through to strength evaluation when carrying out direct strength analysis in order to verify the equivalence of structural strength with the requirements. Loads acting on a ship structure are quite varied and peculiar, in comparison to static structures and other vehicles.

Structural design of a vessel's hull is an iterative process in which five steps are followed:

1. to *decide* which are the most important loads on the structure for its expected operational life, and the equivalent critical modes of failure;

2. to *propose* and develop a structural configuration and to make a preliminary estimate of weight and centre of gravity;

3. to *create* a model (or mathematical idealization) of the proposed structure which is sufficiently representative of the real structure in all important aspects;

4. to *analyze* the model and compare its performance against specified design criteria for the agreed failure modes;

5. to *modify* the structural configuration to achieve adequate performance while at the same time avoiding the use of superfluous material and unnecessary cost.

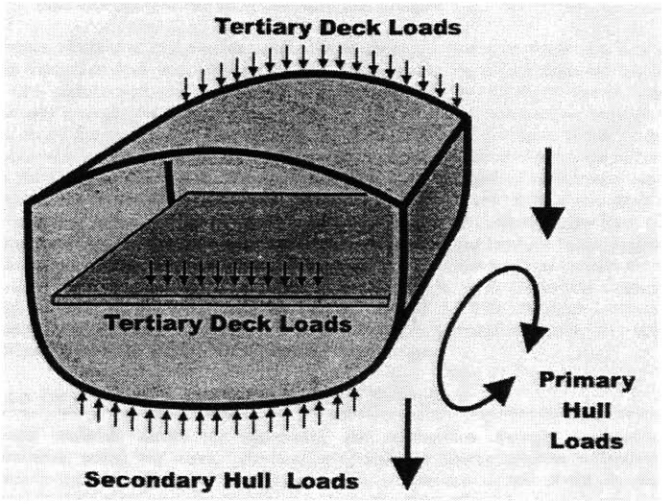

Figure 2-1: Schematic of a ship midsection subjected to various scales of loading

Naval structures are subjected to various types of loading during the service life that may cause cracking, Fig. 2-1. The propagation of these cracks will affect eventually the structural integrity and water-tightness of the naval structures. The existing method of repairing severe fabrication flaws and cracks detected during the service life can lead to prohibitive through-life maintenance costs. A detailed damage tolerance analysis can offer the ship designer a useful tool in order to optimize these structures and improve their reliability. Fracture mechanics offer quantitative access to the residual strength and residual life of a cracked structural member.

The loads applied on ships can be classified as follows:

1. static loads: the ones experienced by the ship in still water that act with time duration well above the range of sea waves periods (weight of the ship, static buoyancy, thermal loads and concentrated loads such as dry-docking or grounding),

2. quasi-static loads: a second class includes those with a period corresponding to wave actions ($\sim$ 3 to 15 s) (wave-induced hull pressure variations, hull pressure variations from oscillatory ship motions, inertial reactions),

3. dynamic loads: when studying responses with frequency components close to the first structural resonance modes, the dynamic properties of the structure have to be considered

(periodic loads such as springing and mechanical excitation or transient impulsive loads such as slamming or even sloshing),

4. high frequency loads: at frequencies higher than the first resonance modes ($> 10 - 20$ Hz) also are present on ships (hydrodynamic loads induced by propulsive devices on hull or appendages, loads imparted to the hull by reciprocating or unbalanced rotating machinery, hydro-elastic loads resulting from interaction of appendages with the flow past the ship, wave-induced loads due primarily to short waves - springing),

5. impact loads: whipping, and

6. other loads: for example thermal or accidental (ice loads, collision, sloshing, landing of aircraft or helicopters, impact from other vessels, piers or other obstacles).

A ship structure is subjected to significant stress ranges from wave loading in rough seas as well as vibration from slamming or impact of waves, and therefore fatigue cracking is a potential problem for vessels.

Therefore, for assessment of existing ships, submarines and other structures, particularly if there are existing through-thickness cracks, a method is needed for predicting the safe propagation life of long, through-thickness cracks. The research involved in this thesis is focused on developing crack propagation models for predicting worst-case crack growth rates in welded and extruded aluminum stiffened panels, common structural elements in naval structures.

2.2 Structural Configurations

Future naval ships and submarines must be designed to survive exposure to extreme loading conditions from impact and explosions. Various structural failure modes contribute to the loss of integrity of naval vessels subject to blast loading; these being dependent on material selection and structural configuration. Modeling vessel response encompasses material constitutive equations, fracture and damage mechanics, non-linear dynamics simulation codes and structural finite element analyses. The advancement and integration of these disciplines are necessary in order to provide a design framework for developing optimum structural configurations and energy absorbing materials. Naval vessels are designed so as to fulfil their mission in scenarios

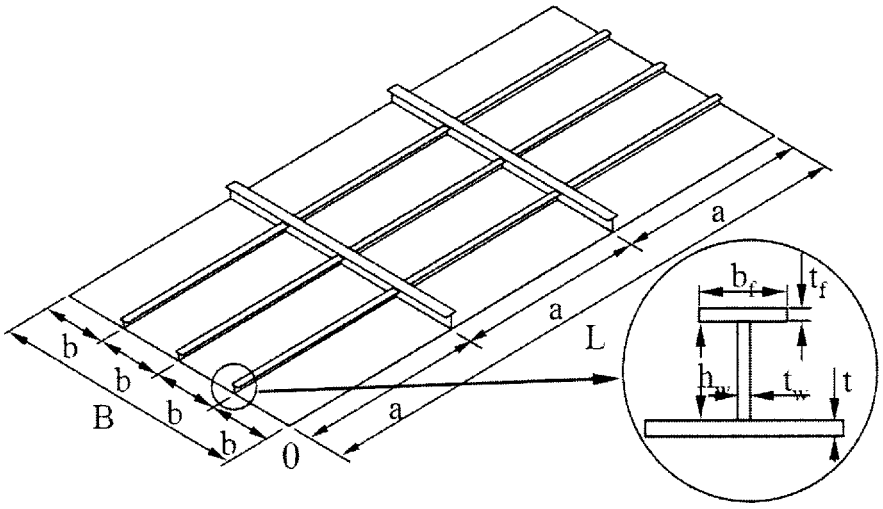

Figure 2-2: Typical structural configuration for naval structures (B is the panel width, b is the effective width between the stiffeners, L is the panel length, a is the distance between the girders, t is the plate thickness, t_w, h_w, t_f, and b_f are the stiffener dimensions, web thickness and height, flange thickness and width, respectively)

where there are high threat levels.

A ship structure can be regarded as an assemblage of continuous stiffened plates with equally spaced longitudinal stiffeners of approximately the same size, Fig. 2-2. The main load component for the deck structure, the bottom structure and longitudinal bulkheads close to the deck and bottom is axial compression or tension. Therefore, in standard design analyses of the ultimate hull girder bending moments, the only load components considered are longitudinal stresses. However, the external bottom plating and the lower parts of the side shells can in addition be subjected to relatively high external lateral pressure and the inner bottom and inner longitudinal bulkheads to lateral pressure loads from explosives (mines, torpedoes, missiles) (Cole [50] [51]; Smith and Hetherington [292]), Figs. 2-3 and 2-4.

The ultimate strength of ship plates is very important from the design and safety viewpoint because the collapse loads of plates can often act as an indicator of the ultimate strength of the whole stiffened panel in ship structures (Hughes [109]). The problem has been addressed for years for the general plated structures and for several decades even with regard to ship structures. The methods which have been proposed can be divided into: (i) finite element

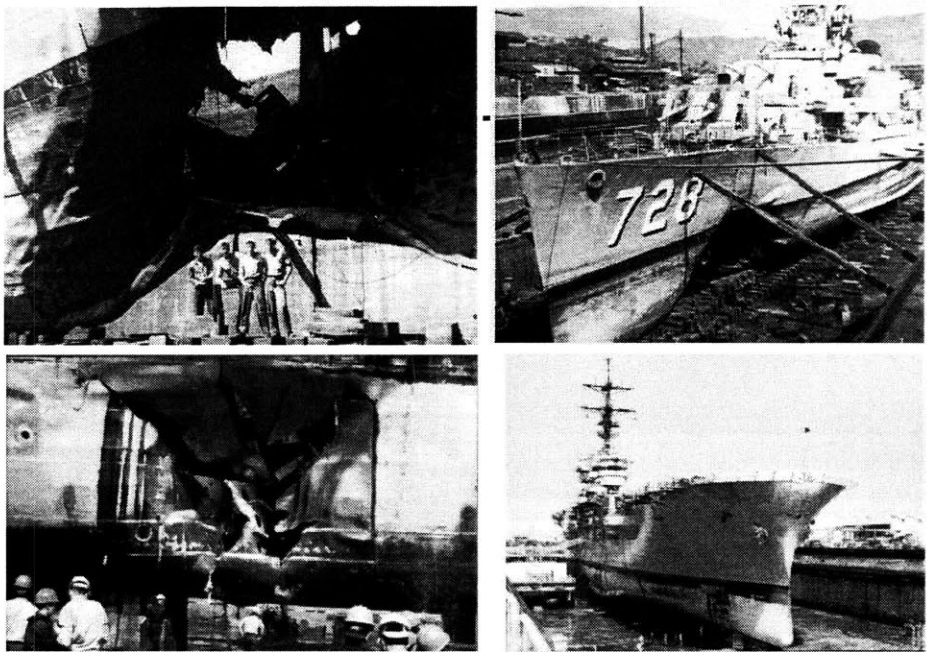

Figure 2-3: Damage caused to naval vessels, USS Mansfield, 1950 (top) and USS Tripoli, 1991 (bottom), due to mine strike [courtecy of U.S. Navy]

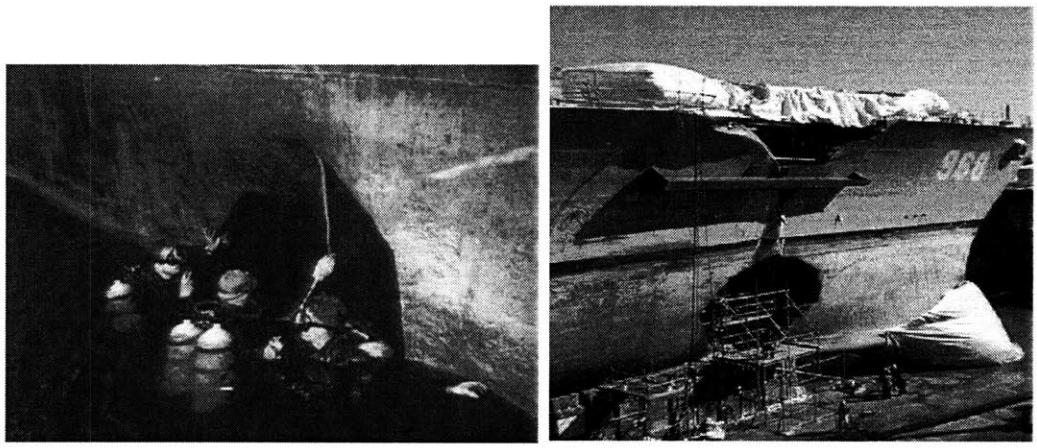

Figure 2-4: Torpedo damage to USS Liberty, June 8, 1967 (left) and collision damage to USS Radford (right), February 5, 1999 [courtecy of U.S. Navy]

methods, (ii) experiments, (iii) empirical formulae which are based either on numerical or experimental results and, (iv) analytical or semi-analytical approaches.

Cracks in ship structure must always be a matter of concern. Because plating is continuously welded, a crack, if not arrested, can grow for a considerable distance. Cracks may propagate in ship hull structure in a stable manner with a length exceeding the stiffener spacing. This is particularly dangerous in the naval structure, where unchecked crack growth could lead to the loss of the ship. Therefore, crack arrest has always been an important area for researchers, even for aluminum naval applications (Sielski [277]). The key to survival is understanding that survivability has three major elements, namely: damage tolerance, damage repair and damage avoidance. The first one of these factors will be examined during this research.

Exploding concentrated underwater charges to damage underwater structures such as ship hulls is a part of naval warfare strategies. Careful design of structures to withstand the shock loads still remains a challenge to structural designers. Hence, there is a continuing need to understand the structural behavior of hull panels due to non-contact underwater explosion, both for vulnerability assessment and for providing rational shock hardening to the hull against such threats. The structural analysis is quite complex involving large deformation, high strain rates, material non-linearity and fluid-structure interaction. The propagation and arrest of cracks is an important issue when evaluating structural integrity. The methodology developed within this dissertation can be used as a tool for the designers in order to face this problem.

The advances in computational mechanics and the increase in computing power have recently allowed for further investigation of physical phenomena in failure analysis. The finite element method has established itself as a primary solution technique and is routinely used for solving complex engineering problems.

Several structural configurations exist, such as the Advanced Double Hull (ADH) initially presented by Beach [19], which consists of a unidirectionally - stiffened structural system where the main structural elements are arranged longitudinally, and a possible crack will propagate parallel to the stiffeners, Fig. 2-5.

The most important features of a ship's survivability are its subdivision design, to limit damage spread, and construction practices, to ensure design integrity. The primary strength members of a ship are the keel and main deck regions that run the length of the ship. Its girders,

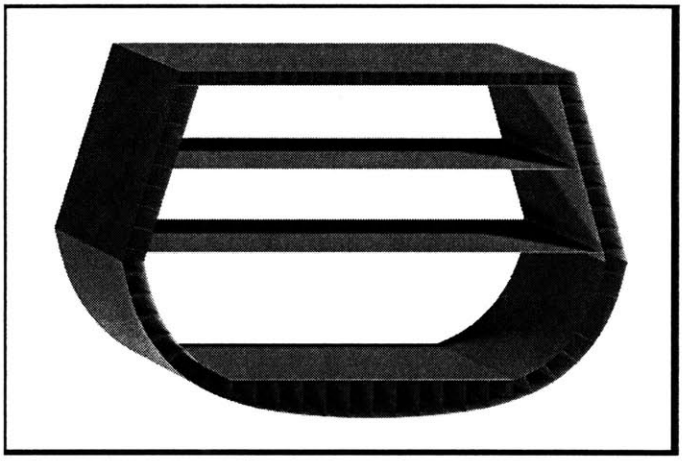

Figure 2-5: Stainless steel ADH mid-body section

frames and stringers connect and support the keel and main deck. A shell of steel plating supported by a web of longitudinal and transverse stiffeners serves to stiffen the structure. It is important to the strength of the structure that the members be unbroken. The structure of all ships must carry loads imposed by the sea; warships must also be able to accept damage that can destroy a portion of the structure and its continuity.

To strengthen the stiffened shell, ships are divided horizontally by decks and vertically by bulkheads. Decks and bulkheads contribute to the overall strength of the ship and divide the hull into watertight compartments. In all ships the main deck, shell and their web of stiffeners, along with the decks and bulkheads, give the ship the strength it needs plus a margin that allows it to resist damage without failure. Increased survivability, reduced weight, and reduced total ownership costs (including maintenance and repairability) have been targeted as a priority of the Navy. Nevertheless, the behavior of stiffeners towards fracture has never been examined in depth since it was taken for granted that the stiffener acts by default as a crack arrestor.

Naval vessels are usually constructed with complex stiffening systems. Figure 2-6 shows a typical panel, which represents the basis on which most of the current applications are designed. Additionally, several other stiffening types exist in naval structures and depend on the loading, material and component, Fig. 2-7. Llopart et al. [158] performed tests on different types of stringer configurations used for aircraft (blade, hat and $J-$type) and they found that the hat

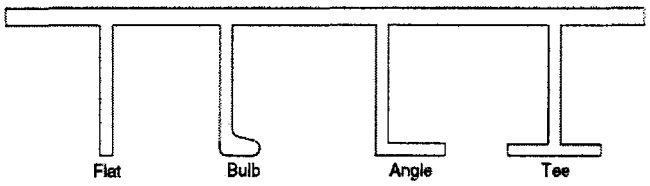

Figure 2-6: Various types of beam members (stiffeners)

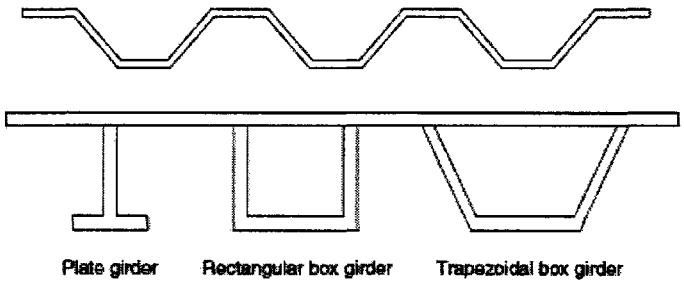

Figure 2-7: A self-stiffened plate – corrugated panel (top) and various types of strong main support members (bottom).

stringer presents the worst crack growth over almost all zones examined.

In addition to the most common types of stiffeners described above, there are special designs of aluminum hull structures for high speed craft which are more complex. One design is the floating frame, where the bottom hull panel has alternating "floating" transverse frames that are welded on top of longitudinal stiffeners (Herrington and Latorre [99]). This structure has been experimentally and numerically examined and an optimization analysis showed that by proper selection of the panel components and the selection of available extrusions, the weight of the original panel design could be reduced by approximately 15%. An investigation performed by Latorre et al. [150] on the suitability of using hull panels with alternating fixed and floating frames for a $30 - 40$ knot aluminum catamaran ferry has already been analyzed numerically and physically tested meeting the American Bureau of Shipping (ABS) High Speed Graft rules [6].

2.3 Survivability

Naval vessels are required to retain a high standard of operational effectiveness when under attack. Since a naval vessel needs to withstand combat conditions, an additional factor beyond normal design requirements must be considered in its architecture. This factor is the ship's ability to survive weapons effects. The effects that need to be taken into account are: above water attack, primarily internal and external blast; underwater explosions, shock and whipping; fragmentation and residual strength.

In order to minimize the platforms vulnerability special measures must be taken, such as incorporation of protective or hardened structures and equipment. Structural and systems arrangements must be configured in such a way that the highest probability of survival during combat is assured. The role of the ship will define the minimum acceptable standards of vulnerability to attack.

Also of importance when considering the design of a warship is the subdivision policy adopted. The extent and standard of subdivision has a major impact upon ship safety and resistance to damage from weapon effects. Subdivision policy should address aspects of ship design from the point of view of resistance to spread of fire, smoke and flooding.

Layout and strength considerations are addressed only to the extent that they influence the disposition and construction standards of watertight and smoke-tight subdivision. A warship, like a frigate, can be exposed to a vast variety of weapon systems from above (e.g. missiles, bombs, shells and nuclear detonations) and below water (e.g. torpedoes and mines) and the effects of each are markedly different. In either case the weapon can detonate on or following impact, or at a standoff using a proximity fuse.

In the underwater case, penetration following impact but before detonation is likely to be very limited as the velocity of the weapon is low, and damage will therefore be restricted to the vicinity of the impact point. Frequently, greater damage can be done underwater from a standoff explosion which can cause extensive shock damage over a large part of the vessel, and may also damage the primary structure through whipping (Geers [84]; Keil [133]). Conversely, above water attacks can be at high velocity and the weapon may penetrate far into the hull before detonating, causing a very large volume of damage, while a stand-off weapon in air will only generally shower the target with fragments (except in the case of fuel-air explosives). To

perform the vulnerability reduction satisfactorily the effects of all these weapon systems have to be taken into account in the ship design process. The history of underwater explosion research was described in a paper published in 1961, by Keil [134].

Underwater weapons consist of torpedoes and mines, although near miss bombs exploding underwater may produce similar effects. Both mines and torpedoes can be activated by ship signatures to seek out a target and explode in close proximity. Underwater weapons usually explode close to the hull, producing damage by shock and whipping. The shock may damage equipment, machinery and personnel or cause distortion or rupture of the hull if sufficiently severe.

Survivability is defined as the capacity of a ship to absorb damage and maintain mission integrity. In general, the goal of surface ship survivability is to enhance operational readiness and warfighting sustainability for each surface unit by:

1. reducing the probability that surface ships will be detected,
2. increasing the ability of those ships to withstand damage, and
3. improving the capabilities and skills of personnel to enable them to expeditiously handle recovery from combat scenarios or accidents and promptly restore vital ship systems.

As was demonstrated during the Falkland Islands engagement, a hit from a single modern high-explosion weapon is capable of severely damaging a ship or rendering entire combat systems inoperable. The Navy should continue to give high priority to the identification of new technology applications through research and testing programs.

Survivability is one of the most important attributes of surface ships. It is especially critical in these days, as the public becomes ever more sensitive to the deaths and injury of naval personnel, while naval vessels become more expensive. Total Ship Survivability (TSS), a systems-engineering approach to survivability, ensures a more efficient incorporation of survivability into new ship designs and acquisitions.

A ship can survive combat either by avoiding damage or by continuing to function after damage. Damage can be avoided by preventing attack, by a "softkill" employing electronic warfare or jamming of an attacking weapon, or by destroying the attacker. If damaged by

attack, the ship continues to function by minimizing vulnerability and providing safe, efficient, and rapid recoverability of both the ship and its functions. If all else fails, the ship must provide safe abandonment by the crew.

The ship survivability timeline is commonly divided into two phases. The first phase is the "Kill Chain", which emphasizes hit avoidance. The second phase is "Damage Tolerance", which limits damage from a successful attack and recovers from it. If an attack is successful, the next phase is to limit the extent and severity of damage. The provisions for limiting damage are a function of the ship's design. Compartmentation, redundancy, distribution of systems, selection of materials, and armor contribute to this. Then, the crew prevents further damage, such as from fire and flooding, to save the ship, and recovers functions, including maneuverability, crew support, and even combat capability. As crew sizes diminish, the ship must be more self-contained in damage prevention and function recovery because human-intensive methods will not be possible.

It is important to recognize that not all attacks are made by launching a weapon from a platform. Some small boat or terrorist attacks, for example, are quite different because the timeline may be compressed, and the ranges quite close. Mines present a special case, lying in wait for an unsuspecting ship and following an abbreviated Kill Chain. Influence mines, in particular, detect and activate, may identify, and engage a ship in a short period of time. Contact mines do not follow a Kill Chain. Submarines, on the other hand, may be directed from another source, and so may follow the pattern described, but may also perform the entire Kill Chain independently.

The survivability and reliability of damaged ships after collision and grounding was studied by Fang and Das [68]. Based on the Monte Carlo simulation technique, the failure probability of a damaged ship varies with different damage types, damage position, damage extent and sea conditions. Their analysis also indicated that the risk (failure probability) caused by grounding is far less than those caused by collision. This may be attributed to the fact that the residual ultimate strength of ship hull girder after grounding reduces more slowly than that in the case of a collision.

2.4 Basic Types of Structural Failure for Ships

Ship structural failure may occur as a result of a variety of causes, and the degree or severity of the failure may vary from a minor esthetic degradation to catastrophic failure resulting in total loss of the ship. Three major failure modes are defined in naval architecture:

1. tensile or compressive yield of the material (plasticity),
2. compressive instability (buckling), and
3. fracture that includes ductile tensile rupture, low-cycle fatigue and brittle fracture.

Yield occurs when the stress in a structural member exceeds a level that results in a permanent plastic deformation of the material of which the member is constructed. This stress level is termed the material yield stress. At a somewhat higher stress, termed the ultimate stress, fracture of the material occurs. While many structural design criteria are based upon the prevention of any yield whatsoever, it should be observed that localized yield in some portions of a structure is acceptable. Yield must be considered as a serviceability limit state.

Instability and buckling failure of a structural member loaded in compression may occur at a stress level that is substantially lower than the material yield stress. The load at which instability or buckling occurs is a function of member geometry and material elasticity modulus, that is, slenderness, rather than material strength. The most common example of an instability failure is the buckling of a simple column under a compressive load that equals or exceeds the Euler critical load. A plate in compression also will have a critical buckling load whose value depends on the plate thickness, lateral dimensions, edge support conditions and material elasticity modulus.

In contrast to the column, however, exceeding this load by a small margin will not necessarily result in complete collapse of the plate but only in an elastic deflection of the central portion of the plate away from its initial plane. After removal of the load, the plate may return to its original un-deformed configuration (for elastic buckling). The ultimate load that may be carried by a buckled plate is determined by the onset of yielding at some point in the plate material or in the stiffeners, in the case of a stiffened panel. Once begun, yield may propagate rapidly throughout the entire plate or stiffened panel with further increase in load.

Fatigue failure occurs as a result of a cumulative effect in a structural member that is exposed to a stress pattern alternating from tension to compression through many cycles. Conceptually,

each cycle of stress causes some small but irreversible damage within the material and, after the accumulation of enough such damage, the ability of the member to withstand loading is reduced below the level of the applied load. Two categories of fatigue damage are generally recognized and they are termed high-cycle and low-cycle fatigue. In high-cycle fatigue, failure is initiated in the form of small cracks, which grow slowly and which may often be detected and repaired before the structure is endangered. High-cycle fatigue involves several millions of cycles of relatively low stress (less than yield) and is typically encountered in machine parts rotating at high speed or in structural components exposed to severe and prolonged vibration. Low-cycle fatigue involves higher stress levels, up to and beyond yield, which may result in cracks being initiated after several thousand cycles.

The loading environment that is typical of ships and ocean structures is of such a nature that the cyclical stresses may be of a relatively low level during the greater part of the time, with occasional periods of very high stress levels caused by storms. Exposure to such load conditions may result in the occurrence of low-cycle fatigue cracks after an interval of a few years. These cracks may grow to serious size if they are not detected and repaired.

Concerning brittle fracture, small cracks suddenly begin to grow and travel almost explosively through a major portion of the structure. The term brittle fracture refers to the fact that below a certain temperature, the ultimate tensile strength of steel diminishes sharply (lower impact energy). The originating crack is usually found to have started as a result of poor design or manufacturing practice. Fatigue is often found to play an important role in the initiation and early growth of such originating cracks.

The prevention of brittle fracture is largely a matter of material selection and proper attention to the design of structural details in order to avoid stress concentrations. The control of brittle fracture involves a combination of design and inspection standards aimed toward the prevention of stress concentrations, and the selection of steels having a high degree of notch toughness, especially at low temperatures. Quality control during construction and in-service inspection form key elements in a program of fracture control.

Damage can be reduced by the use of new materials, novel structural configurations, different design and manufacturing methods and improved computational techniques. It is clear that this cannot be accomplished by a single improvement but rather a combination of various measures.

Figure 2-8: Various types of failure for marine vessels: collision, grounding, and stranding

Furthermore, a major leap forward can only be achieved by developing new technologies rather than by integrating existing tools. It is obvious, that fracture should be at the forefront of research for naval vessel designs since accidents occur, unfortunately, during their operation, Fig. 2-8.

Parallel analytical and numerical solutions should be obtained and, by a thorough comparison with experimental results and suitable scaling, loads to full-size ship plating developed. The importance of the research is to provide a bridge between the results obtained at the scale of a material element to the scale of typical panels of bays of the ship hull. The intermediate stage is necessary in the system approach to fracture prediction because it is impossible to jump over two or three orders of magnitude without calibration and validation. In addition to exclusively military applications, this technology could be used in the commercial sector for predicting effects of collision, grounding, onboard gas explosion, etc. as well as damage of aluminum and even steel structures.

Over the past years the personnel of the Impact and Crashworthiness Laboratory at Massachusetts Institute of Technology (MIT), under the leadership of its Director, Professor Tomasz

Wierzbicki, have been actively involved in research concerning fracture. Initially, under the Tank Safety project, vast experience from a comprehensive problem of deformation and fracture of small-scale (1:50) longitudinally stiffened single and double hulls was gained. The main knowledge and experience can be summarized in research including the following areas:

- *Ship grounding, stranding and collision*, (**1990**: [328], **1991**: [329], [181], [226], **1992**: [300], [239],**1993**: [321], [180], [173], [11], **1994**: [138], [25], [156], [157], [89], [225], [242], [342], **1995**: [46], [13], [168], [237], [281], [243], [282], [310], [290], [291], **1996**: [169], [283], [284])
- *Crushing* (**1983**: [326], [327], **1992**: [60], **1994**: [88], [2], [44], **1995**: [45])
- *Fracture of plates and stiffened panels* (**1991**: [301], [299], **1992**: [330], **1993**: [331], [332], [177], [305] **1994**: [333], [10], [92], [178], [302], [306], [360], **1995**: [334], [183], [32], [236], [337], [356], **1997**: [26])

The most representative examples of such successful tests are shown in Fig. 2-9 tearing fracture of longitudinally stiffened single hull and also longitudinally stiffened double hull, which dished and fractured under spherical punch.

Within further research with other related projects, the ICL members succeeded in developing a practical and accurate criterion for fracture initiation in various aluminum alloys.

Traditionally, ship design practice was mainly based on yield and buckling considerations of structures subjected to a great variety of design loads. There has been some explicit consideration of failure due to fracture as a product of collision, grounding, and explosions (internal, contact and stand-off). Experience, especially with naval vessels has shown numerous cracks caused from collisions, contact and stand-off explosions. The bigger the cracks the more dangerous for the structural integrity of the ship. The high toughness of modern ship steels generally prevented sudden brittle fracture, so cracks could grow to considerable lengths before they posed serious structural problems. Much research is conducted to predict the initiation and development of such cracks in order to determine rules that require explicit consideration of failure due to fracture, which is discussed in later parts.

Classical fracture mechanics offers methods to predict initiation and growth of fatigue cracks in homogenous plating. Real ship structures are complicated by the presence of stiffeners, and

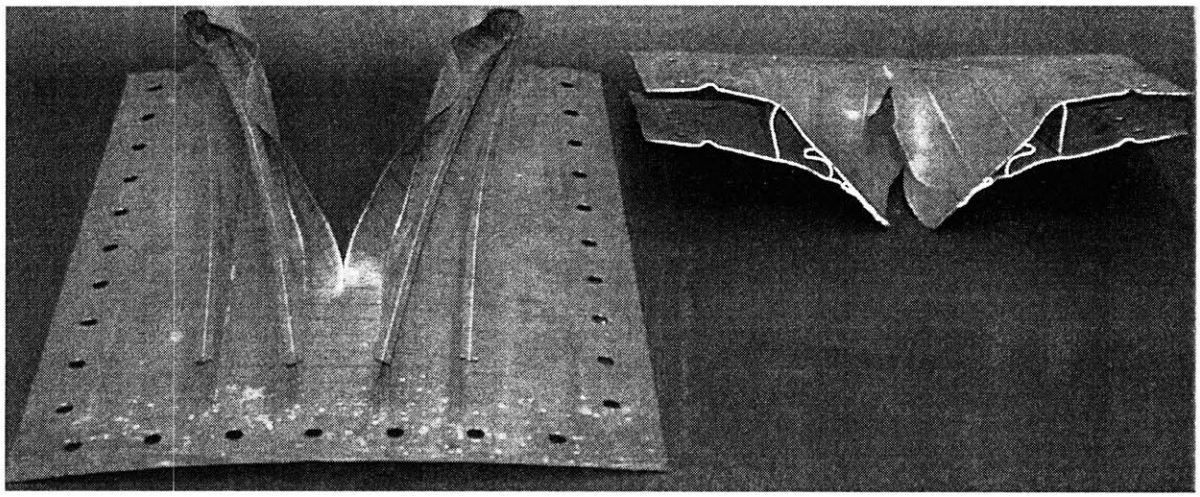

Figure 2-9: Existing work on damaged and fractured small-scale structural models subjected to localized transverse loading showing the crack propagation between and parallel to the stiffeners of stiffened panels for single (left) and double (right) plate structural configurations

complex residual stress fields caused by welding of these stiffeners. The purpose of the current research is to assess methods to predict the growth of large cracks in realistic stiffened ship plating. This work presents the results of a series of experiments with large cracks propagating across stiffened panels (extruded and welded).

Naval structures require deep consideration during the design stage of their behavior and resistance to dynamic loading, such as explosions (underwater and air) and limited publications exist, which usually describe general guidelines (Rajendran et al. [247]; Park and Cho [223]), based on fundamentals of explosions, Fig. 2-10.

Underwater explosion damage can impair the strength of a ship in two ways; structural strength members may rupture or buckle and compartment flooding can occur, increasing load on the damaged ship girder. An underwater explosion frequently opens a larger hole in the shell of a large ship than it does in a small one. The large ship is better able to survive the loss of structural strength because a smaller portion of the main structural members, heavier and more numerous than in small ships, will be damaged. The chances of structural failure in a large ship because of the underwater explosion or bomb hit are small.

Underwater explosions in the midships region of a small ship may rupture a large portion of

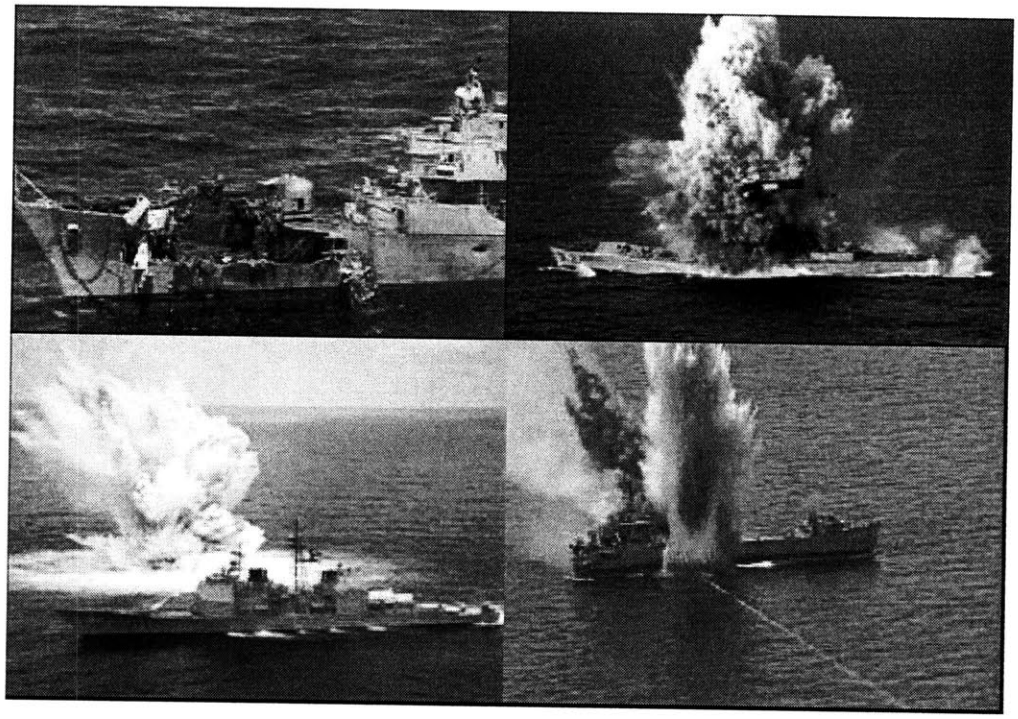

Figure 2-10: Explosion loading of naval vessels: internal, stand-off and weapons effect

the main strength members. With extensive damage to the main strength members, the ship may break up unless the strength of the fractured members can be replaced before the ship is subject to the action of heavy seas.

An explosion at either the bow or stern of a small ship usually causes intense local destruction but does not seriously threaten combat capability or ship loss. The effect of such an explosion is to shake the ship like a whip. Waves of flexural vibration pass down the length of the hull, producing stresses like those in hogging and sagging, of shorter duration but greater intensity. The result, although not usually obvious, can be structurally damaging. It consists mainly of compression failures in the midships region, evidenced by wrinkled deck plating, wrinkled shell plating, buckled longitudinal girders, and buckling, laying over the flanges, wrinkling, or other failure of members in the midships portion of the ship that contribute to longitudinal strength. It is a feature of compression members that, once buckled, they can never again develop even a fraction of their original strength. Attempted straightening is useless; the only answer is immediate reinforcing by shoring and later replacement. Stiffeners should be spaced no more

than 100 times the plating thickness or stiffener thickness, whichever is smaller.

The effect of the shock pulse of non-contact explosion on submerged exposed structures is generally critical. Severe acceleration peaks of hundreds of gravity accelerations (g's) are induced in the structure within a few milliseconds and can lead to structural failure and damage the equipment fitted inside the hull. Even neglecting local cavitation, the correct evaluation of the structural response of submerged structures to shock pulse must account for the fluid-structure interaction problem. This means that the actual stiffness of the target structure cannot be neglected in the actual load evaluation.

Fatigue damage of structures is mainly a two-stage process consisting of a crack nucleation and a sub-critical crack propagation phase (Petinov [234]). Fatigue fracture of marine structures has been thoroughly examined and several rules by the International Association of Classification Societies (IACS) [112] have been applied , while areas that face most often the possibility of being damaged have been statistically allocated.

2.5 Fracture Mechanics

Fracture mechanics has been applied throughout the world in the design of any structure where sudden, catastrophic failure would cause loss of life or other serious consequences. Examples are nuclear-reactor pressure vessels, submarines, aircraft, missiles, and tanks for storage of toxic or flammable materials.

The use of stress analysis in modern design procedures ensures that in normal service very few engineering components fail because they are overloaded. However, weakening of the component by such mechanisms as corrosion or fatigue-cracking may produce a catastrophic fracture and in some instances, such as in the design of a naval structure, the fracture properties of the components are the most important consideration. The study of how materials fracture is known as fracture mechanics and the resistance of a material to fracture is colloquially known as its "toughness".

Three basic types of stress fields can be defined for crack-tip stress analysis, each one associated with a distinct mode of crack deformation, as illustrated in Fig. 2-11. The opening mode, mode I, is associated with local displacement in which the crack surfaces move directly

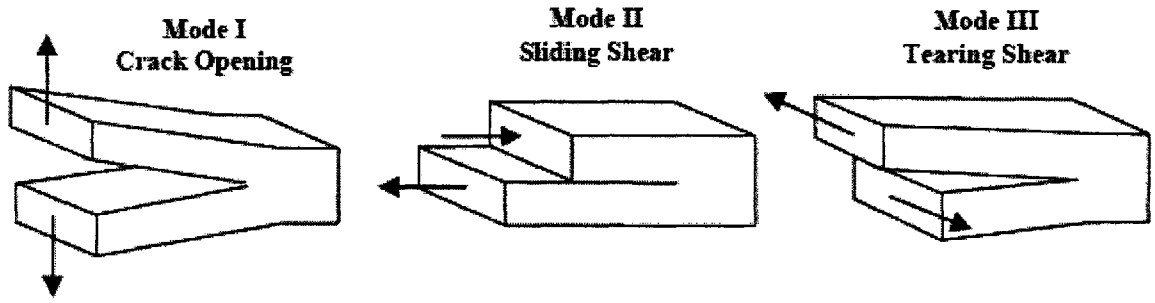

Figure 2-11: The three independent opening modes, associated with crack growth: mode I-tensile; mode II-in-plane shear; mode III-anti-plane shear

apart. The sliding mode, mode II, is developed when crack surfaces slide over each other in a direction perpendicular to the leading edge of the crack. The tearing mode, mode III, is characterized by crack surfaces sliding with respect to each other in a direction parallel to the leading edge of the crack. Superposition of these three modes will fully describe the most general three-dimensional case of local crack-tip deformation and stress field. The most commonly found failures are due to cracks propagating predominantly in mode I, and for this reason materials are generally characterized by their resistance to fracture in that mode. The theories examined in the following sections will therefore consider mode I only but many of the conclusions will also apply to modes II and III.

Fracture mechanics concerns the design and analysis of structures which contain cracks or flaws. On some size-scale all materials contain flaws either microscopic, due to cracked inclusions, debonded fibres etc., or macroscopic, due to corrosion, fatigue, welding flaws etc. Thus fracture mechanics is involved in any detailed design or safety assessment of a structure. As cracks can grow during service due to e.g. fatigue, fracture mechanics assessments are required throughout the life of a structure or component, not just at start of life. Fracture mechanics answers the questions: What is the largest sized crack that a structure can contain or the largest load the structure can bear for failure to be avoided? How long before a crack which was safe becomes unsafe? What material should be used in a certain application to ensure safety?

Studies in the US in the 1970's by the US National Bureau of Standards estimated that "cost

of fracture" due to accidents, overdesign of structures, inspection costs, repair and replacement was on the order of 120 billion dollars a year. While fracture cannot of course be avoided, this study estimated that, if best fracture control technology at the time was applied, 35 billion dollars could be saved annually. This indicates the importance of fracture mechanics to modern industrialized society.

With the appearance of large monolithic structures such as the ship hull, fully dynamic aspects of crack propagation and arrest were treated by Pellini and colleagues [227] [228] [229] [230]. Prior to **1940**, in the naval industry, metal structures were generally fabricated by riveting and bolting. The failure of a component part of such structures was generally an isolated event which rarely led to total collapse. The integrity of such structures with their ductile performance was ensured by the elongation and reduction-of-area ductility parameters of the conventional tensile test.

But **during the World War II**, welded fabrication gave monolithic structures of C-Mn steels with thickness less than 75 mm, such as the Liberty ships, in which the initiation of fracture in an element was often followed by nearly instantaneous fracture of the entire ship. Thus, the problem of initiation, propagation and arrest was elevated. At that time, the only test with notched specimens leading to a transition region (including the temperature field) of ship fractures was the Charpy V-notch impact test, which was developed about 1905 and then has been used for qualitative assessments of the transition temperature range.

By 1950, correlations were developed disclosing that the fracture initiation, propagation and arrest plates featured distinctly different maximum values of impact energy (KV) at the temperature corresponding to the service fracture. But **by 1953**, it was demonstrated that the critical transition temperature references moved to higher absorbed energy (CV) indices for many improved ship plate steels, and other types of steels that differed from the original ship fracture type and required specific calibrations for different steels.

Thereafter, Pellini [227], at the Naval Research Laboratory, introduced the notion of the NDT (nil ductility transition) temperature, defined as the temperature at which the "small flaw" initiation curve falls to nominal yield-strength stress levels with decreasing temperature. Pellini promoted new types of tests, both fracture-initiation and fracture-arrest tests, as correlated with the NDT temperature established by the drop-weight test. Validation of the NDT concept has

been documented by correlations with numerous service failures encountered in ship, pressure-vessel, machinery-component, forged- and cast-steel applications.

Experience has shown that the onset of stable tearing establishes an important material property termed fracture toughness. The fracture toughness may be used as a design criterion in fracture prevention, just as the yield strength is used as a design criterion in prevention of yielding of a ductile material under static loading. It should be noted that not all materials and or specimen types exhibit stable tearing. Many materials and or specimen configurations exhibit rapid crack propagation without any evidence of prior stable tearing.

No structure is entirely free of defects and even on a microscopic scale these defects act as stress-raisers which initiate the growth of cracks. The theory of fracture mechanics therefore assumes the pre-existence of cracks and develops criteria for the catastrophic growth of these cracks. The designer must then ensure that no such criteria can be met in the structure.

2.5.1 Fracture theory

Griffith (1921) postulated that for unit crack extension to occur under the influence of the applied stress, the decrease in potential energy of the system, by virtue of the displacement of the outer boundaries and the change in the stored elastic energy, must equal the increase in surface energy due to crack extension. One of the most important and key concepts in the entire field of Materials Science and Engineering is fracture. In its simplest form, fracture can be described as a single body being separated into pieces by an imposed stress.

For engineering materials there are only two possible modes of fracture, ductile and brittle. In general, the main difference between brittle and ductile fracture can be attributed to the amount of plastic deformation that the material undergoes before fracture occurs. Ductile materials demonstrate large amounts of plastic deformation while brittle materials show little or no plastic deformation before fracture. Figure 2-12, a tensile stress-strain curve, represents the degree of plastic deformation exhibited by both brittle and ductile materials before fracture.

More than any other single factor, the large number of sudden and catastrophic fractures that occurred in ships during and following World War II gave the impetus for the development of fracture mechanics. Of approximately 5,000 welded ships constructed during the war, over 1,000 suffered structural damage, with 150 of these being seriously damaged, and 10 frac-

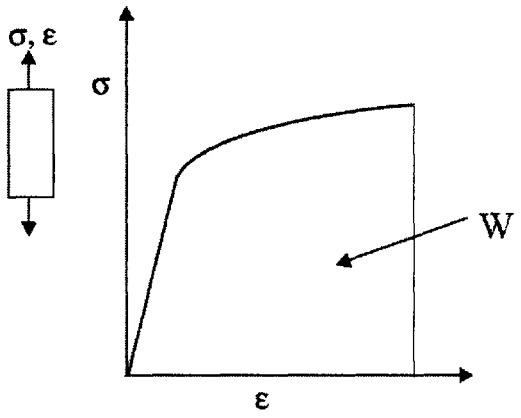

Figure 2-12: Typical stress strain curve for a material

tured into two parts. After the war, George Irwin [114] who was at the U.S. Naval Research Laboratory, made use of Griffith's idea, and thus set the foundations of fracture mechanics.

Fracture mechanics is a field that recognizes that all structures are manufactured with, or will ultimately contain, flaws that govern the eventual failure of the structure. The study of the stresses caused by the flaws and the material's resistance to failure from them forms the basis for the field of fracture mechanics. Irwin's work permitted, for the first time, the capability to calculate the strength of structures containing defects. The net result of these new design principles increased the reliability of structures due to improved design capability and an improved predictive capability of in-service damage.

Irwin developed the scientific principles for understanding the relationships between applied stresses and cracks or other defects in metallic materials. He formulated the concept that fracture toughness should be measured in terms of resistance to crack propagation. Critical values of stress intensity describing the onset of fracture, the onset of environmental cracking, and the rate of fatigue crack growth were established later.

Irwin made three major contributions:

(a) He (and independently Orowan) extended Griffith's original theory to metals by accounting for yielding at the crack tip. This resulted in what is sometimes called the modified Griffith's theory.

(b) He altered Westergaard's general solution by introducing the concept of the stress in-

tensity factor (SIF).

(c) He introduced the concept of energy release rate G.

Crack initiation and propagation are essential to fracture. The manner through which the crack propagates through the material gives great insight into the mode of fracture. In ductile materials (ductile fracture), the crack moves slowly and is accompanied by a large amount of plastic deformation. The crack will usually not extend unless an increased stress is applied. On the other hand, in dealing with brittle fracture, cracks spread very rapidly with little or no plastic deformation. The cracks that propagate in a brittle material will continue to grow and increase in magnitude once they are initiated. Another important mannerism of crack propagation is the way in which the advancing crack travels through the material. A crack that passes through the grains within the material is undergoing transgranular fracture. However, a crack that propagates along the grain boundaries is termed an intergranular fracture.

The failure of many ductile materials can be attributed to cup and cone fracture. This form of ductile fracture occurs in stages that initiate after necking begins. First, small microvoids form in the interior of the material. Next, deformation continues and the microvoids enlarge to form a crack. The crack continues to grow and it spreads laterally towards the edges of the specimen. Finally, crack propagation is rapid along a surface that makes about a 45 degree angle with the tensile stress axis. The new fracture surface has a very irregular appearance. The final shearing of the specimen produces a cup type shape on one fracture surface and a cone shape on the adjacent connecting fracture surface, hence the name, cup and cone fracture.

In most design situations a material that demonstrates ductile fracture is usually preferred for several reasons. First and foremost, brittle fracture occurs very rapidly and catastrophically without any warning. Ductile materials plastically deform, thereby slowing the process of fracture and giving ample time for the problem to be corrected. Second, because of the plastic deformation, more strain energy is needed to cause ductile fracture. Next, ductile materials are considered to be "forgiving" materials, because of their toughness you can make a mistake in the use or design of a ductile material and still the material will probably not fail. Also, the properties of a ductile material can be enhanced through the use of one of the strengthening mechanisms. Strain hardening is a perfect example, as the ductile material is deformed more and more its strength and hardness increase because of the generation of more

and more dislocations. Therefore, in engineering applications, especially those that have safety concerns involved, ductile materials are the obvious choice. Safety and dependability are the main concerns in material design, but in order to attain these goals there has to be a thorough understanding of fracture, both brittle and ductile. Understanding fracture and failure of materials will lead the materials engineer to develop safer and more dependable materials and products.

The simplest useful model for the stresses near the tip of a crack is based on the assumptions of linear elastic material behavior and a two-dimensional analysis; thus, the procedure is often referred to as linear elastic fracture mechanics.

Although the validity of the linear elastic assumption may be questioned in view of plastic zone formation at the tip of a crack in any real engineering material, as long as small-scale yielding occurs, that is, as long as the plastic zone size remains small compared to the dimensions of the crack, the linear elastic model gives good engineering results. Thus, the small-scale yielding concept implies that the small plastic zone is confined within a linear elastic field surrounding the crack tip. If the material properties, section size, loading conditions, and environment combine in such a way that large-scale plastic zones are formed, the basic assumptions of linear elastic fracture mechanics are violated, and elastic-plastic fracture mechanics methods must be employed.

When the material behavior is brittle rather than ductile, the mechanics of the failure process are much different. Instead of the slow coalescence of voids associated with ductile rupture, brittle fracture proceeds by the high-velocity propagation of a crack across the loaded member. If the material behavior is clearly brittle, fracture may be predicted with reasonable accuracy through use of the maximum normal stress theory of failure. In words, the maximum normal stress theory may be expressed as follows: *Failure is predicted to occur in the multiaxial state of stress when the maximum principal normal stress becomes equal to or exceeds the maximum normal stress at the time of failure in a simple uniaxial stress test using a specimen of the same material.*

Mathematically, the maximum normal stress theory becomes: *Failure is predicted by the maximum normal stress theory to occur if*

$$\sigma_1 \geqslant \sigma_t \quad | \sigma_3 | \geqslant \sigma_c \tag{2.1}$$

where σ_1, σ_2, and σ_3 are the principal stresses at a point, ordered such that $\sigma_1 \geqslant \sigma_2 \geqslant \sigma_3$, σ_t is the uniaxial failure strength in tension, and σ_c is the uniaxial failure strength in compression.

On the other hand, more recent experience has led to the understanding that nominally ductile materials may also fail by a brittle fracture response in the presence of cracks or flaws if the combination of crack size, geometry of the part, temperature, and/or loading rate lies within certain critical regions. Furthermore, the development of higher-strength structural alloys, the wider use of welding, and the use of thicker sections in some cases have combined their influence to reduce toward a critical level the capacity of some structural members to accommodate local plastic strain without fracture. At the same time, fabrication by welding, residual stresses due to machining, and assembly mismatch in production have increased the need for accommodating local plastic strain to prevent failure. Fluctuating service loads of greater severity and more aggressive environments have also contributed to unexpected fractures.

An important observation in studying fracture behavior is that the magnitude of the nominal applied stress that causes fracture is related to the size of the crack or cracklike flaw within the structure (Anderson [8]). For example, observations of the behavior of central through-the-thickness cracks, oriented normal to the applied tensile stress in steel and aluminum plates [1], showed that as the tensile loading on the precracked plates was slowly increased, the crack initially extended slowly for a time and then abruptly extended to failure by rapid crack propagation. The slow stable crack growth or tearing was characterized by speeds of the order of fractions of an inch per minute. The rapid crack propagation was characterized by speeds of the order of hundreds of feet per second. For the aluminum alloy the fracture stress was less than the yield strength for cracks longer than about 0.75 in. For the steel alloy the fracture stress was less than the yield strength for cracks longer than about 0.5 in. In both cases, for shorter cracks the fracture stress approaches the ultimate strength of the material determined from a conventional uniaxial tension test.

Experience has shown that the onset of stable tearing establishes an important material

[1] American Society for Testing and Materials. "Progress in Measuring Fracture Toughness and Using Fracture Mechanics". *Materials Research and Standards*, March, 103-119, 1964.

property termed fracture toughness. The fracture toughness may be used as a design criterion in fracture prevention, just as the yield strength is used as a design criterion in prevention of yielding of a ductile material under static loading. It should be noted that not all materials and or specimen types exhibit stable tearing. Many materials and or specimen configurations exhibit rapid crack propagation without any evidence of prior stable tearing.

In many cases slow crack propagation occurs by means other than stable tearing, especially under conditions of fluctuating loads and/or aggressive environments. In analyses and predictions involving fatigue failure phenomena, characterization of the rate of slow crack extension and the initial flaw size, together with critical crack size, are used to determine the useful life of a component or structure subjected to fluctuating loads.

The simplest useful model for the stresses near the tip of a crack is based on the assumptions of linear elastic material behavior and a two-dimensional analysis; thus, the procedure is often referred to as linear elastic fracture mechanics.

Although the validity of the linear elastic assumption may be questioned in view of plastic zone formation at the tip of a crack in any real engineering material, as long as small-scale yielding occurs, that is, as long as the plastic zone size remains small compared to the dimensions of the crack, the linear elastic model gives good engineering results. Thus, the small-scale yielding concept implies that the small plastic zone is confined within a linear elastic field surrounding the crack tip. If the material properties, section size, loading conditions, and environment combine in such a way that large-scale plastic zones are formed, the basic assumptions of linear elastic fracture mechanics are violated, and elastic-plastic fracture mechanics methods must be employed.

In terms of the coordinates shown in Fig. 2-13, the stresses near the crack tip for mode I loading may be written as

$$\sigma_x = \frac{K_I}{\sqrt{2\pi r}} \cos\frac{\theta}{2}\left[1 - \sin\frac{\theta}{2}\sin\frac{3\theta}{2}\right] \tag{2.2}$$

$$\sigma_y = \frac{K_I}{\sqrt{2\pi r}} \cos\frac{\theta}{2}\left[1 + \sin\frac{\theta}{2}\sin\frac{3\theta}{2}\right] \tag{2.3}$$

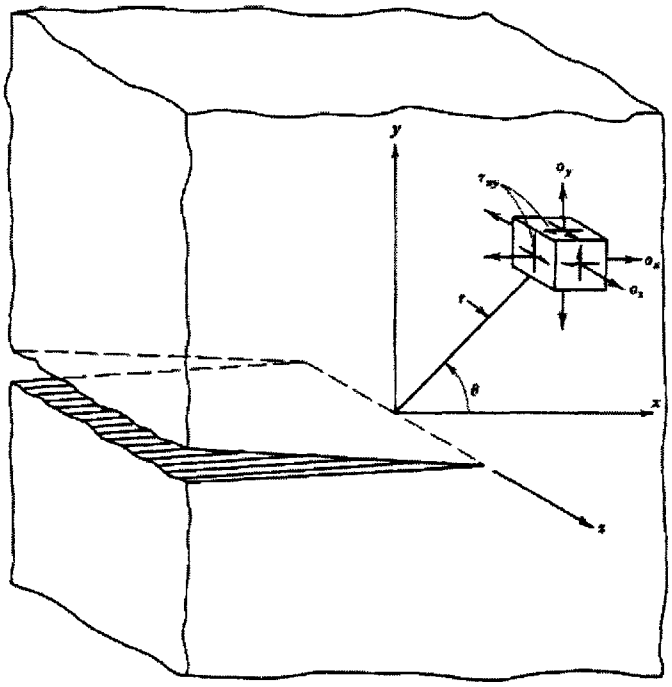

Figure 2-13: Coordinates measured from the leading edge of a crack

$$\tau_{xy} = \frac{K_I}{\sqrt{2\pi r}} \sin\frac{\theta}{2} \cos\frac{\theta}{2} \cos\frac{3\theta}{2} \tag{2.4}$$

The parameter K_I is known as the mode I stress intensity factor. This parameter represents the strength of the stress field surrounding the tip of the crack. Since fracture is induced by the crack-tip stress field, the stress intensity factor is the primary correlation parameter used in current practice.

In general, the expressions for the stress intensity factor are of the form

$$K_I = C\sigma\sqrt{\pi\alpha} \tag{2.5}$$

where α is the crack size, σ is the gross-section stress, and C is dependent on the type of loading and the geometry away from the crack. Much work has been completed in determining values of C for a wide variety of conditions.

Many commercial finite-element analysis software packages possess special crack-tip ele-

ments allowing the numerical computation of stress intensity factors. A discussion of some of the techniques employed within these software packages is given by Anderson [8]. Through the use of weight functions, stress intensity factors may also be computed easily using numerical integration and the stresses that would exist in the uncracked body. From Eq. (2.5), the stress intensity factor increases proportionally with gross nominal stress and also is a function of the crack length α. The value of K_I associated with the onset of fracture has been designated the critical stress intensity factor, K_C. As noted earlier, the fracture of specimens with different crack lengths occurs at different values of gross-section stress, but at a constant value of K_C. Thus, K_C provides a single-parameter fracture criterion that allows the prediction of fracture based on Eq. (2.5). That is, fracture is predicted to occur if

$$K_I \geqq K_C \tag{2.6}$$

In studying material behavior, one finds that for a given material, as the specimen thickness is increased, the critical stress intensity K_C decreases to a lower limiting value. This lower limiting value defines a basic material property K_{IC}, the plane-strain fracture toughness for the material. Standard test methods have been established for the determination of K_{IC} values. For the plane-strain fracture toughness K_{IC} to be a valid failure prediction criterion for a specimen or a machine part, plane-strain conditions must exist at the crack tip; that is, the material must be thick enough to ensure plane-strain conditions. It has been estimated empirically that for plane-strain conditions the minimum material thickness B must be

$$B \geqslant 2.5 \left(\frac{K_{IC}}{\sigma_y} \right)^2 \tag{2.7}$$

where σ_y is the material yield strength.

If the material is not thick enough to meet the criterion of Eq. (2.7), plane stress is a more likely state of stress at the crack tip; and K_C, the critical stress intensity factor for failure prediction under plane stress conditions, may be estimated using a semi-empirical relationship [8]:

$$K_C = K_{IC} \left[1 + \frac{1.4}{B^2} \left(\frac{K_{IC}}{\sigma_y} \right)^4 \right]^{1/2} \tag{2.8}$$

As long as the crack-tip plastic zone remains in the regime of small-scale yielding, this estimation procedure provides a good design approach. For conditions that result in large crack-tip plastic zones (large applied stresses, large crack lengths), performing a failure assessment using linear elastic fracture mechanics (LEFM) is invalid and potentially non-conservative. A better design approach would involve the implementation of an appropriate elastic-plastic fracture mechanics (EPFM) procedure when large-scale yielding is generated at the crack tip.

2.6 Crack Initiation, Propagation and Arrest

Recently, the operational environment for naval and commercial vessels is changing rapidly due to terrorism, and as a result, the demand for a cost effective structural design especially for naval vessels needs to be re-examined. Most of these structures are required to operate in a dynamic environment. The field of Impact Dynamics covers an extremely wide range of situations and is of interest to engineers from a number of different disciplines. Structural impact is known as a complex problem, from an analytical, experimental and numerical point of view. One reason is the great variety of physical parameters involved that may cause highly non-linear and sometimes unexpected structural behavior when varied.

Over the last few years, there has been a significant amount of experimental research into a wide range of blast loaded stiffened panels for examination of the damage tolerance of various structures (Houlston et al. [102]; Houlston and Slater [103]; Cichocki and Ruchwa [49]). Crack initiation, propagation and arrest has been an area of research for several years (Broberg [30]). Even though the main obstacle of the crack propagation in a steel plate is the welded stiffener, there has not been any significant work published on this area with the exception of Dexter and Pilarski [55] and Dexter et al. [56]. The presence of stiffeners on the crack propagation path can be a significant parameter for the crack arrest phenomenon, as initially observed by Rodd [263], adding value to the fracture toughness of the material, which has been thoroughly investigated by Sielski [278] and Khan at al. [137]. Therefore, numerical and experimental work is performed in this dissertation for the evaluation and assessment of the stiffener dimensions and design, concerning the direction of the crack. The comparison between theoretical predictions and experimental results will ultimately lead to the design of an alternative more efficient structure.

A scaled model of an existing naval structure will be used to obtain a more realistic view and examine structural components that are already designed to resist all naval loading excluding fracture in combination with the usage of naval steels.

Additionally, there has been recently some serious demand for aluminium vessels, which brought up the question of examination of the fracture of stiffened panels constructed from steel or aluminum. The comparison between these two different types of materials is very critical in developing optimized structures for the shipbuilding industry with respect to the design of stiffened panels with increased damage tolerance.

The objective of this dissertation is to develop and implement new, innovative approaches and techniques for the destructive inspection of marine aluminum structures.

The crack arrest phenomena in cylindrical containers and pipes have been extensively studied in relation to the pressure vessel technology, Parks and Freund [224]; Freund et al. [72]; and Zhuang and O'Donoghue [363]. No parallel analysis is readily available in the case of splitting fracture in plates. The mechanics of the crack arrest process must then be well understood. The webs or girders in the Advanced Double Hull (ADH) structure offer a formidable obstacle for a propagating crack in the transverse direction, Sikora et al. [280]. Tearing fracture will be arrested for a while at the foot of the stiffener, then will be re-initiated on the other side of the stiffener, and eventually the longitudinal stiffener will be broken as well. A test on a quarter model of splitting damage of the longitudinally stiffened, double hull, which was performed by Rodd et al. [263] and numerically examined by Kee et al. [131] gives only a glimpse of this important phenomenon. It is still unknown, however, what aspect of the design (strength of the filet weld, relative thickness of the bare plate and stiffener, height of the stiffener or hull separation) will stop the crack, re-direct it or overcome the obstacle, Fig. 2-14.

In the "conventional" ADH design, there is no mechanism to stop tearing fracture in the longitudinal direction. The concept of welded (or even hot rolled) buffer strips must be investigated, as illustrated in the Fig. 2-15. Finally, the process of plate tearing in the diagonal direction with respect to the longitudinal stiffener must be fully understood. It is expected that cracks will run in a "zig-zag" pattern. For the purpose of designing optimum blast resistant structures, the ultimate intellectual challenge will be to develop a general concept of crack resistant core of sandwich structures. It is unknown at this point which design will offer better

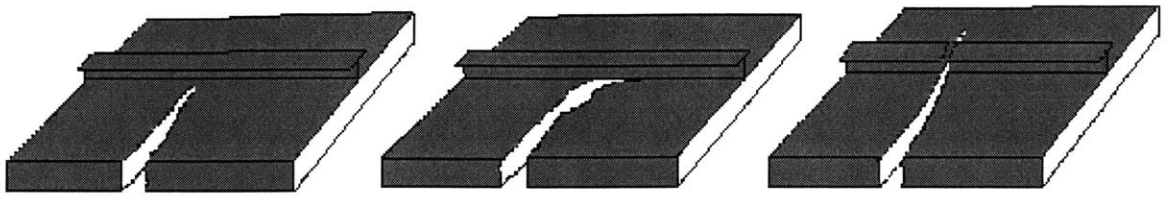

Figure 2-14: A conceptual sketch of a stiffener serving as a crack arrestor: (i) stopping the crack (left), (ii) redirecting (center), and (iii) passing through (right)

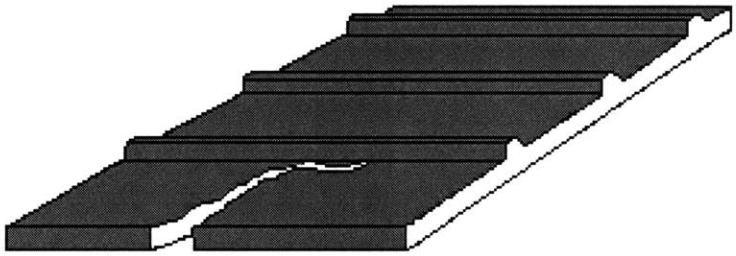

Figure 2-15: An example of a hot-rolled ribbed plate with integrated crack arrestors

resistance to tearing; a uniform plate or a slightly thinner plate with integrated ribs of the same weight, Fig. 2-15.

In-depth research is being performed under the auspices of the Ship Structure Committee [119] [238] [86] [41] [87] [54] [58] [57], which over the years are examining the crack propagation due to fatigue in stiffened panels.

Drilling a hole ahead of the crack, either to arrest or delay the crack propagation, has proven to be an effective and simple technique (Sielski [277]; Goto et al. [90]). A method of crack patching is realized with adhesively bonded fiber composite to reinforce the cracked parts (Bell et al. [20]; Bernard et al. [21]). Ghfiri et al. [85], observing the micro-structure at the failure section of cracked aluminum alloys with expanded or non-expanded holes at the tip of a crack, indicated that the hole expansion process modifies the condition and properties of the surface layer and affects significantly the length of the nucleation stage of the fatigue process. It is worth mentioning that Forsyth in 1976 [70], while examining crack growth in aluminum alloys, observed that fatigue fractures frequently exhibit evidence of macroscopic tensile crack jumps interspersed between periods of fatigue crack growth.

Priest [240] utilized the data from temperature gradient double tension tests and dynamic small scale tests on two steels having different toughness levels in a quasi-static crack arrest analysis. An energy balance approach using the total initial elastic energy progressively depleted by the absorbed fracture propagation energy predicted arrest temperatures to within 7 °C of the values measured at the arrested crack tip in double tension tests. Also, Priest [241] used again the energy balance for the prediction of toughness values required to ensure arrest in double tension crack arrest tests. The analysis required calculation of the total energy that depended on the force applied to the main plate and the effective length of the structure including the test frame. Theoretical calculations indicated that the energy release rate at crack arrest was governed by both the width and the length of the structure, examined the influence of structural dimensions on crack arrest and developed an energy balance in crack propagation and arrest.

2.7 Existing Work on Structures

Stiffened plates and panels are extensively used in steel and aluminum marine structures such as ships, submarines and offshore installations. The behavior of such structures are of crucial importance for the overall structural strength. Aluminum is gaining acceptance in load-carrying structures, where a high strength/weight ratio and durability are an advantage. Stiffened panels in aluminum are extensively used in a variety of marine structures as basic elements. These stiffened panels are required to resist extreme loading conditions, e.g. in terms of axial compressive and tensile loads. As aluminum is a relatively new structural material compared to steel, especially in marine applications, most of the existing design codes for plates and stiffened panels are mainly based on experience with steel structures. Because material properties of aluminum are quite different compared to steel, such approaches are uncertain.

Several experimental and numerical studies on the response of unstiffened and stiffened plates subjected to blast loading have been conducted by Yuen and Nurick [349]; Langdon et al. [149]; Louca and Pan [159]; Rudrapatna et al. [266] [267]; Guruprasad and Mukherjee [93] [94]; Wang [323]. For the purpose of this dissertation, several tensile tests of stiffened panels from naval aluminum are performed in combination with iterative finite element analyses by modeling a scaled portion of the ship.

The tearing process of flat plates has been formulated and solved in an approximate way in a series of papers by Wierzbicki, and his follower Simonsen [285] [287]. This analysis included the distinction of the phases a plate is following when deformed subject to explosive and impact loading, which are dishing, discing, and petalling (Wierzbicki [336]).

Ultimate strength of structural members and systems is a real measure in strength assessment in a sense that the ultimate strength is the maximum capacity that they can have. No additional load can be carried beyond the ultimate strength. Under general combined loads, buckling and yielding dominate the ultimate strength when compressive stress is dominant, whereas only yielding dominates the ultimate strength when tensile stress is dominant.

It is now common to design structural members and systems so that they do not collapse by buckling or yielding. However, until the middle of the 19^{th} century, the design criterion was the breaking strength of the material. This was partly because wrought iron used for ship structures at that time was a brittle material and was week against tensile load, just like concrete. Another reason was that the buckling phenomenon and its consequences were not well understood, although it had been known that a structure may collapse by buckling in the compression side of bending through Fairbairn's famous collapse test on box girder bridge models in 1845 (Timoshenko [303]). It was after Bryan [34] that the panel buckling was theoretically understood and calculated, and that the buckling strength was used as a criterion for determining panel thickness.

Series of experiments and computational models for global buckling and postbuckling analyses of aluminum stiffened panels for naval structures have already been performed (Byklum [38] [39]). The applied loads are biaxial in-plane compression or tension, shear, and lateral pressure. The lateral pressure is accounted for by assuming the deflection to be a combination of a clamped and a simply supported deflection modes. Prior to that, the large deflection response of unstiffened plates have been studied analytically by Ueda et al. [312] and Paik et al. [207] [208]. As a result, the buckling and ultimate strength of aluminum plates and stiffened panels of marine structures can be well estimated [324]. The behavior of different types of stiffeners has also been investigated under torsional buckling and collapse, with emphasis on the effect of the heat-affected zones (HAZ) for aluminum panels used for marine structures [353]. Various features, such as material thickness, welding process, weld condition, and distance from the weld,

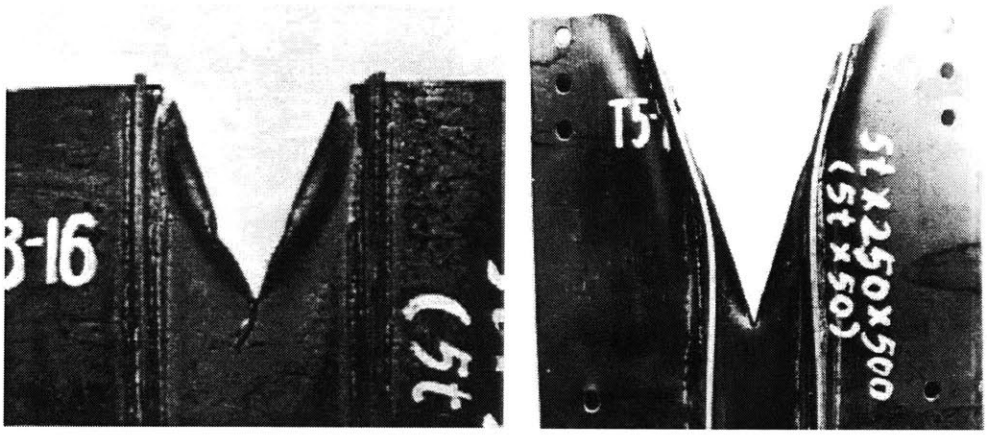

Figure 2-16: Existing work on crack propagation between and parallel to the stiffeners on stiffened panels for single plates structural configurations (left) and photographs of a longitudinally stiffened plate cut by a wedge (right) [courtecy of Ship Structural Mechanics Laboratory, Pusan University]

affect the properties of the HAZ. Shaw and Huang [276] analyzed the buckling characteristics of cracked plates subjected to uniaxial tensile loads using the finite element method.

Additionally, extensive work has been done on the collision and grounding of ships. This work included analytical approaches (Minorsky [184]; Woisin [338]; Wierzbicki [327]) and detailed finite element simulations [140].

There has been some experimental and numerical work by Yuen and Nurick [349] on the response of built-in mild steel quadrangular plates with different stiffener configurations (unstiffened, single, double, cross and double cross) subjected to blast loading.

Continuous stiffened plates under combined thrust and lateral pressure have three collapse modes, which are stiffener-induced failure caused by stiffener yielding, plate-induced failure by local plate collapse and hinge-induced failure by the formation of plastic hinges predominantly in bending. Yanagihara et al. [344] developed a simplified method to estimate the ultimate strength of the stiffened plates based on the collapse behavior observed by the finite element method. Yanagihara et al. [345] extended the method so as to consider the lateral pressure on the stiffener side as well as on the plate side. Since the lateral pressure on the stiffener side causes compression at the stiffener top at mid-span, the so called stiffener-induced failure takes place until it changes to the hinge-induced failure mode under a high lateral pressure.

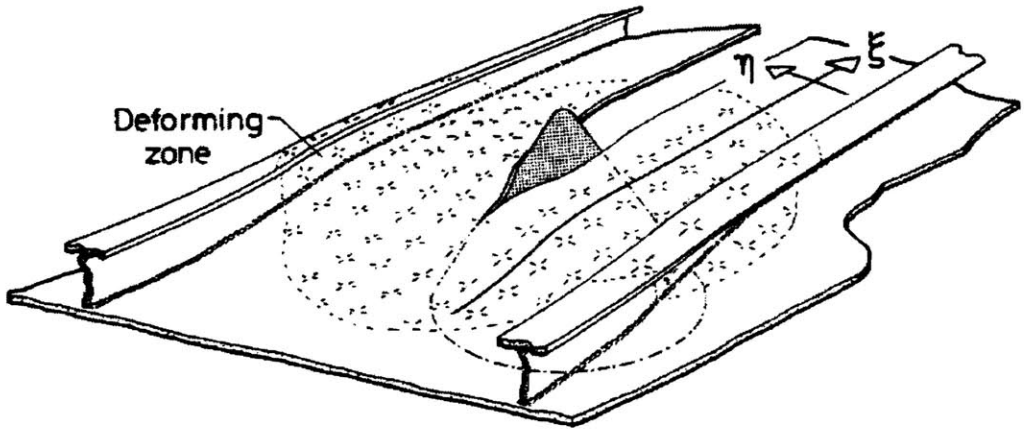

Figure 2-17: Sketch of the idea of a moving deformation zone, Simonsen, [286]

Furthermore, Harada et al. [95] extended the application of the formulae to biaxial thrust condition based on a series of elastoplastic large deflection FE analyses.

As part of a project to develop guidelines for reducing cracks in aluminum ship structures, Latorre et al. [151] performed experiments showing that the stress levels developed depend strongly on the welded connection details. This investigation summarizes the analysis of a common structural detail, one that results in a transversely loaded weldment and links to two sets of experimental test results. The first is the stress concentration observed at the intersection of the longitudinal and transverse members in a 1.5 m $\times$ 3 m aluminum bottom panel tested under uniform pressure loading. The second is the reduction in fatigue life due to weld geometry variations between manually welded and machine-welded aluminum specimens. In order to clarify these two observations, the authors completed a detailed finite element analysis of a welded aluminum T-stiffener. The results showed a significant stress concentration in the weld toe area. This stress concentration was shown to be strongly dependent on the weld toe geometry.

Sumi et al. [295] investigated the characteristics of fatigue crack propagation and the remaining life assessment of ship structures by focusing attention on curved crack paths, the effects of weld, complicated stress distributions at three-dimensional structural joints, and structural redundancy. They developed an advanced numerical simulation system to predict realistic phenomena of fatigue crack propagation. The presented method may offer an efficient

simulation-based tool for the fatigue crack management of critical details.

Simonsen and Törnqvist [289] presented a combined experimental–numerical procedure for the development and calibration of macroscopic crack propagation criteria in large-scale shell structures. A novel experiment was set-up in which a mode-I crack can be driven 400 mm through a 20(+) mm thick plate under fully plastic and controlled conditions. The test specimen can be deformed either in combined in-plane bending and extension or in pure extension. Experimental results were described for 5 and 10 mm thick aluminium and steel plates. By performing an inverse finite-element analysis of the experimental results, where the simulated crack growth is forced to correspond to the experimental observations, empirical criteria for ductile crack propagation emerged very clearly. Using the experiments with edge crack specimens (ECS) in combined in-plane bending and extension, crack propagation criteria were developed for steel and aluminium plates, mainly as curves showing the critical element deformation versus the shell element size. These derived crack propagation criteria were then validated against a separate set of experiments considering centre crack specimens (CCS) which have a different crack-tip constraint. The applicability of the often-used equivalent strain criterion was discussed versus a more rationally based criterion which takes into account the stress triaxiality. A large-scale grounding experiment was also simulated showing very good agreement with measurements. Also, Abramowicz and Simonsen [3] proved that theories and experiments demonstrate that the effect of fracture may be very significant for the loads and energy absorption in axial crushing of typical ship structural components.

Byklum et al. [39] derived a computational model for global buckling and post buckling analysis of stiffened panels. The loads considered were biaxial in-plane compression or tension, shear, and lateral pressure. Deflections were assumed in the form of trigonometric function series, and the principle of stationary potential energy was used for deriving the equilibrium equations. Lateral pressure was accounted for by taking the deflection as a combination of a clamped and a simply supported deflection mode. The global buckling model was based on Marguerre's nonlinear plate theory, by deriving a set of anisotropic stiffness coefficients to account for the plate stiffening. Local buckling was treated in a separate local model developed previously. The anisotropic stiffness coefficients used in the global model were derived from the local analysis. Together, the two models provide a tool for buckling assessment of stiffened

panels. Implemented in the computer code PULS, developed at Det Norske Veritas, local and global stresses were combined in an incremental procedure. Ultimate limit state estimates for design were obtained by calculating the stresses at certain critical points, and using the onset of yielding due to membrane stress as the limiting criterion.

Paik et al. [212] compared some useful ultimate limit state (ULS) methods adopted for the design of aerospace, marine and land-based aluminium structures. A common practice for aerospace, marine and civil engineering welded stiffened panel applications was discussed.

Paik et al. [213] measured some typical plate initial deflection shapes for merchant ship plating between stiffeners. The influence of such initial deflection shapes on the ultimate strength behavior of steel plates subjected to biaxial compression as well as uniaxial thrust was then investigated applying nonlinear finite element analyses.

Paik and Pedersen [204] developed a method for analyzing the structural damage due to ship collision within the framework of the idealized structural unit method (ISUM), which was proposed by Ueda and Rashed [311]. Fujikubo and Kaeding [73] developed a new simplified model for collapse analysis of stiffened plates, also based on ISUM. Both local buckling of the plate panel and overall buckling of the stiffener could be analyzed by combining the plate and beam-column elements of ISUM. The application of this method to a time-domain collapse analysis of a pontoon-type Very Large Floating Structure (VLFS) in regular waves was presented by Fujikubo et al. [74] [75]. The ISUM plate element was extended by Kaeding et al. [124] so that lateral loads could be directly applied to the plate element. Moreover, Fujikubo and Pei [76] demonstrated the application of ISUM to analyze the progressive collapse behavior of a ship's hull girder in longitudinal bending. Continuing his work, Fujikubo et al. [77] [78] developed a simplified method to estimate the ultimate strength of a continuous plate, typical in ship bottom plating, subjected to combined transverse thrust and lateral pressure. They performed a series of elastic/elastoplastic large deflection finite element analyses of a continuous plate supported along the lines of longitudinal stiffeners and transverse frames.

The weight function method was originally derived for crack problems to calculate stress intensity factors for arbitrary loading conditions. Sumi et al. [296] extended this to formulate the structural response analyses of two-dimensional elasticity, plate bending, and three dimensional plate structures by using the finite element method. The solution procedure was based on

the well-known Maxwell–Betti reciprocal theorem. The method is very useful for the analysis of structures subjected to a vast range of loading conditions, because structural responses can simply be calculated by the inner product of the universal weight function and load vectors. The validity and convergence characteristics of the method were investigated by two dimensional elastic and plate bending problems, respectively. Finally, the method was applied to the calculation of the response amplitude operator (RAOs) of a stress component at a critical structural detail of a double-hull tanker.

Zhang, S. et al. [355] developed semi-analytical methods for the analysis of plate crushing and ship bow damage in head-on collisions. Existing experimental and theoretical studies for crushing analysis of plated structures were reviewed and compared. Simple formulae for determining the crushing force, force-deformation curve and damage extent of a ship bow, expressed in terms of ship principal particulars, were derived for longitudinally stiffened oil tankers and bulk carriers with length of 150 m and above. It was suggested that the approach developed can be used easily to determine the crushing resistance and damage extent of the ship bow when ship length and collision speed are known. The method can be used in the probabilistic analyses of damage extents in ship collisions where a large number of calculations are generally required.

Analytical methods are still welcomed by structural engineers, because of their soundness and physical meaning. Many kinds of analytical formulations have been proposed to predict their structural behavior for unstiffened and stiffened plates, even beyond the ultimate state. Hu and Cui [104] developed a simplified analytical method to predict the ultimate strength of unstiffened and stiffened plates based on the combination of elastic large deflection analysis and rigid plastic mechanism analysis. The predictions by the developed method were compared with test data and the design equations of classification society rules. The influences of various factors, such as welding residual stress, transverse stress and lateral pressure were also studied.

Hu and Cui [105] extended their method for unstiffened plates to deal with combined loadings including longitudinal compression, transverse compression, lateral pressure and edge shear. Finally, Hu et al. [107] continued their work by proposing a methodology to assess the time-variant ultimate strength of a ship hull girder under the degradations of corrosion and fatigue, by examining $1,000\,\text{mm} \times 1,000\,\text{mm} \times 10\,\text{mm}$ (length-breadth-thickness) center cracked plates

subjected to longitudinal uniform loads.

Sano et al. [273] proposed a simple model to simulate buckling/plastic collapse behavior of an ultra-wide rectangular plate subjected to in-plane compression on its wider edges. The buckling and post-buckling strength behavior are simulated by performing elastic large deflection analysis applying analytical methods. On the other hand, post-ultimate strength behavior is simulated according to the rigid plastic mechanism analysis. Using the proposed method, the average stress-average strain relationship was constructed, which can be applied to transversely stiffened parts of the hull girder when ultimate longitudinal strength analysis is performed with Smith's method.

Byklum et al. [39] derived a computational model for global buckling and postbuckling analysis of stiffened panels subjected to biaxial in-plane compression or tension, shear and lateral pressure. The global buckling model is based on Marguerre nonlinear plate theory and the local buckling is treated in a separate local model. The two models provide a tool for buckling assessment of stiffened panels. The local and global stresses are combined in an incremental procedure. Ultimate limit state estimates for design were obtained by calculating the stresses at certain critical points, and using the onset of yielding due to membrane stress as the limiting criterion.

Harada and Fujikubo [96] performed a series of buckling eigenvalue calculations and elasto-plastic large deflection analyses by FEM to examine buckling/plastic collapse behavior of a stiffened web plating with cutout as a part of the ship bottom girder together with those of an isolated plate with cutout. Based on the observations of the FEM calculation results, a set of closed simple formulae were proposed to estimate the elastic buckling and ultimate strength of a stiffened web plating with cutout. The predicted ultimate strength showed good correlations with FEM results.

Zheng and Hu [358] derived a differential equation to analyze tripping of thin-walled stiffeners and solved it with Galerkin's method to obtain a general eigenvalue problem. A computer code was developed applying the proposed method to evaluate the tripping strength. After confirming the accuracy of the calculated results with FEM results by MARC, a series of calculations was performed applying axial force, lateral pressure and end moments, respectively. Regression of the calculated results gave out a correlativity formula of the three kinds of applied

loads.

Xiao and Dexter [339] used finite element analysis to calculate the applied J-integral as a function of applied displacement for cracked full-scale test specimens which were representative of ship structural components. The specimens were welded from thin (9 mm) HSLA80 (ASTM A710) and EH36 (ASTM A131) steel plates. It was found that the applied J vs. displacement relationship for shell cracks bridged by stiffeners or girders can be calculated from an idealized CCT model incorporating all of the sections as if they are coplanar.

Some analytical and semi-analytical formulations were developed to evaluate ultimate strength of steel and / or aluminum plates without and with stiffeners subjected to various loads by Paik et al. [206]; Paik and Thayamballi [210]; Yanagihara et al. [345]; Paik and Duran [211]; Steen et al. [293]; Harada et al. [95]; Paik et al. [214] and [219]; Wang et al. [324]; Paik and Lee [218]. Some of them are introduced in the following chapters accompanied by obtained results.

For the strength assessment, it is very important to predict damages which may affect the strength. Cho and Lee [43] proposed a simple analytical method to predict the denting damage of stiffened plates under small lateral collision. They assumed that the plate can absorb some portion of the collision energy by the plastic rotation along plastic hinge lines and the membrane plastic tension, and the remaining collision energy can be dissipated by those in the stiffener flanges and the plastic shear deformation of stiffener webs. The proposed method was substantiated with thirty-three test data.

The evaluation of the ultimate strength of plates and stiffened plates is the most fundamental criterion for marine structures, and a great deal of progress has been achieved in the past decades. There are a variety of methods and computer codes available for the ultimate strength analysis of plates and stiffened plates, ranging from simple analytical formulae to complicated numerical methods. The analysis costs typically increase with the level of detail modeling and the fidelity of the analysis procedure used. Therefore, the studies on ultimate strength of plates and stiffened plates have been and shall continue to be a large area of active research in marine structures.

2.7.1 Strength and failure of unstiffened plates

The studies on the ultimate strength of plated structures have continued over several decades and significant progress has been achieved. However, there are some aspects of this subject still unresolved and interesting. In recent years, the research efforts in the ultimate strength of plated structures are devoted to:

- development of analytical formulae,
- development of simplified methods,
- assessment of effects of initial imperfections, and
- assessment of effects of fatigue cracks.

Hu and Cui [104] [105] have carried out a comparative study between simplified analytical methods and design formulae for the ultimate strength of unstiffened and stiffened plates. The simplified analytical method was developed based on the combination of elastic large deflection analysis and rigid plastic mechanism analysis. Paik and Thayamballi [210] and Paik and Lee [218] have presented a semi-analytical method for the elastoplastic large deflection analysis of unstiffened plates and stiffened plates under typical loads until the ultimate strength is reached. The effect of initial imperfections is accounted for in the calculations. Shariat et al. [275] performed studies on the buckling behavior of functionally graded rectangular plates with geometrical imperfections.

The initial imperfections in the forms of initial distortion and welding residual stress are inevitable in marine structures due to the nature of fabrication technology. They have very significant effects on the ultimate strength of plates and stiffened plates and should be accounted for the ultimate strength evaluation of marine structures. An energy measure is suggested by Sadovský et al. [269] to provide an integral measure of the degree of initial deflections according to the comparison between the energy measure and the commonly employed amplitude to thickness ratio. The effects of initial deflections on the collapse strength of thin rectangular plates in longitudinal compression were analyzed by using measured data of distortions.

El-Sawy et al. [61] present the curves representing both elastic and elastoplastic buckling stresses versus the slenderness ratio of perforated plates for different grades of steel according to a series of finite element analysis results. The results show that the critical buckling stress for perforated plates always decreases as the plate slenderness ratio and/or hole size increases.

It is recommended to avoid punching the hole near the plate edge.

In addition to initial imperfections, the fatigue cracks have an important effect on the ultimate strength of marine structures and should be accounted for in residual strength evaluation of aged ship hulls. A systematic investigation is carried out by Hu and Cui [106] on the effects of the crack damage on the residual strength by using the finite element method. Regression formulae are provided for the residual strength evaluation of the damaged plates and stiffened plates.

Brighenti [27] and [28] has carried out the theoretical and numerical studies on the elastic buckling of cracked thin-plates under tension or compression. A series of finite element analyses was performed to evaluate elastic buckling strength of rectangular thin-plates with various cracks under tension and compression and a simple approximate theoretical model was proposed to explain and predict the buckling phenomena in cracked plates subjected to tensile load.

Vafai and Estekanchi ([313], [314]) studied the overall behavior in the elastic range of plates and shells as affected by the presence of a through crack. Paik et al. [217] have performed an experimental and numerical study on the ultimate strength of cracked steel plate elements subjected to uniaxial compressive or tensile loads. The ultimate strength reduction characteristics of plate elements due to cracking damage are investigated with varying size and location of the cracking damage. A theoretical model for predicting the ultimate strength of cracked plate elements under uniaxial compression or tension is developed based on experimental and numerical results. Paik and Kumar [220] at a further step performed a series of nonlinear finite element analyses for these experiments with varying size and location of cracking damage.

Kumar and Paik [145] deal with the estimation of buckling loads of plates with cracking damages. The hierarchical trigonometric functions are used to define the displacement function of the cracked plate. The buckling loads of plates with various types of cracks, such as an edge crack and a central crack are calculated under the in-plane compressive load and/or shear load.

Ramajeyathilagam et al. [248] [251] performed analysis of rectangular plates under shock loading, examining the response in order to simulate dynamic weapon effects against naval structures.

2.7.2 Strength and failure of stiffened plates and panels

Cylindrical stiffened panels are as important as stiffened plates. Stiffened cylindrical panels or cylinders are used in aircraft fuselage, rocket and missile structural components, and launch vehicle tank structures.

Simplified methods are very important in the ultimate strength assessment of plates and stiffened plates not only to provide initial guidance in the early stage of design but also to evaluate results obtained from time-consuming numerical simulations. Consequently, significant attention is paid to develop rational, robust and simplified methods for ultimate strength evaluation of plates and stiffened plates. The current topics of interest related to plated structures are:

- simplified method,
- idealized structural unit method (ISUM),
- effects of initial imperfections,
- sensitivity analysis.

Byklum et al. [39] have derived a computational model for global buckling and postbuckling analysis of stiffened panels. Deflections are assumed in the form of trigonometric function series and local and global stresses are combined in an incremental procedure. Ultimate limit state estimates for design are obtained by calculating the stresses at certain critical points, and using the onset of yielding due to membrane stress as the limiting criterion.

Zhang et al. [354] present a new solution of the elastic buckling and post-buckling behavior of imperfect stiffened plates based on the large deflection theory. The tangential stresses of the stiffeners are neglected and nonlinear membrane forces of the stiffeners are taken into account in the discretely stiffened plate model. The deflection as well as the initial imperfection and stress distribution of the plates are represented by Fourier series.

The analytical expression of buckling of the stiffener is obtained by using appropriate differential equations and boundary conditions. A simplified method is proposed by Yanagihara et al. [345] and Harada et al. [95] to estimate ultimate strength of a continuous stiffened plate under combined uni/biaxial thrust and lateral pressure on the basis of the results of a series of nonlinear finite element analyses. Three collapse modes are considered in a simplified method, namely stiffener induced failure, plate-induced failure and hinge-induced failure. The

accuracy of the proposed method is examined through comparison of the calculated results with FEM results. The numerical results show that the ultimate strength of a continuous stiffened plate under transverse thrust is significantly higher than that of a continuous unstiffened plate simply-supported along stiffener lines because of the stiffener's torsional stiffness.

Advanced nonlinear buckling models of thin-walled stiffened panels have been developed (Byklum and Amdahl [38]; Steen et al. [293]) based on the elastic large deflection plate theory of Marguerre and von Karman. The models cover geometrical proportions of plates and stiffeners typically used in ship hulls and offshore constructions. Improved expressions are developed by Hughes et al. [110] for elastic local plate buckling and overall panel buckling of uniaxially compressed panels with T-bar stiffeners. The expressions were validated with fifty-five ABAQUS eigenvalue buckling analyses over a wide range of typical panel geometries.

The ISUM provides an efficient method to evaluate the load carrying capacity of large structural systems. It can be used to simulate both stiffener collapse and plate panel collapse and evaluate the ultimate strength at the structural system level by employing particular definitions of elements. Fujikubo and Kaeding [73] have developed a new simplified model for collapse analysis of stiffened plates within the framework of ISUM by employing accurate shape functions. The proposed stiffened plate model consists of ISUM plate elements and beam-column elements. Combination of plate and beam-column elements allows for both local buckling of the plate panel and overall buckling of the stiffened plate.

Kaeding et al. [124] presented the state-of-the-art in ISUM modeling and extend the formulation to include lateral pressure. Two shape functions have been investigated for unstiffened double-span/double-bay models. The combined models of present ISUM plate elements and beam-column elements are employed to analyze the ultimate strength of stiffened plates under biaxial compression and lateral pressure and good agreements are observed between the results by the ISUM and the FEM analyses. Paik and Thayamballi [210] present a summary of their ISUM theory and its application to nonlinear analysis of steel plated structures. Some important concepts for development of various ISUM elements are discussed.

Finally, the strength of naval panels subjected to underwater explosion loading has been examined. Numerical analysis of underwater explosion damage of ship hull panels was performed by Ramajeyathilagam and Vedhan [250] using commercial codes (DYNA3D).

Hoo Fatt [101] at her study of crack propagation in stiffened panels describes the detachment of a stiffener from a plate by the fully-plastic crack propagation in the web of a non-symmetric I-beam. She performed a parametric study which shows that bifurcation load increases approximately linearly with an increasing ratio of web to flange widths for some chosen material constants. The effective width of the stiffened plate is thus an important parameter in the detachment of the plate from the stiffener.

2.7.3 Prediction of the crack pattern

As it is well known, most of the engineering structures and components contain cracks or flaws and, therefore, crack growth must be examined both in design and in the analysis of failures. The complete solution of a crack growth problem includes the determination of the crack pattern. This path in a critical component or structure can determine whether catastrophic failure is imminent or not. Knowledge of potential crack patterns is also required for the selection of the appropriate testing procedure.

It is usually assumed that the crack pattern is known or expected either from theoretical considerations or from the results of laboratory tests, but at the present state of the art, the factors controlling the path followed by a crack are not completely understood. Agreement between theoretically predicted and experimentally determined crack paths is sometimes poor. Paik et al. [216] [217] categorize the cracks in stiffened panels in three general categories, namely vertical, horizontal and angular, Fig. 2-18.

The prediction of the crack path in naval structures has been examined mainly from a fatigue point of view. Dobroskok et al. [59] simulated fatigue cracks initiated at a cavity in fillet-welded joints. The growth of such cracks is usually assessed by using finite element analysis. However a fine mesh, especially along an expected crack path, is needed. Furthermore, the crack trajectory must be traced through iterations at each of the crack extensions via analysis of the stress field. An improvement may be achieved by using special forms of the Boundary Element Method (BEM) with elements located only along the crack. An automated procedure for modeling the crack trajectory and evaluating stress intensities was developed based on the complex variable hypersingular boundary integral equation. It provided substantial economy of time and expert labour, and easily allows for changes in boundary conditions and stress flow through the joint

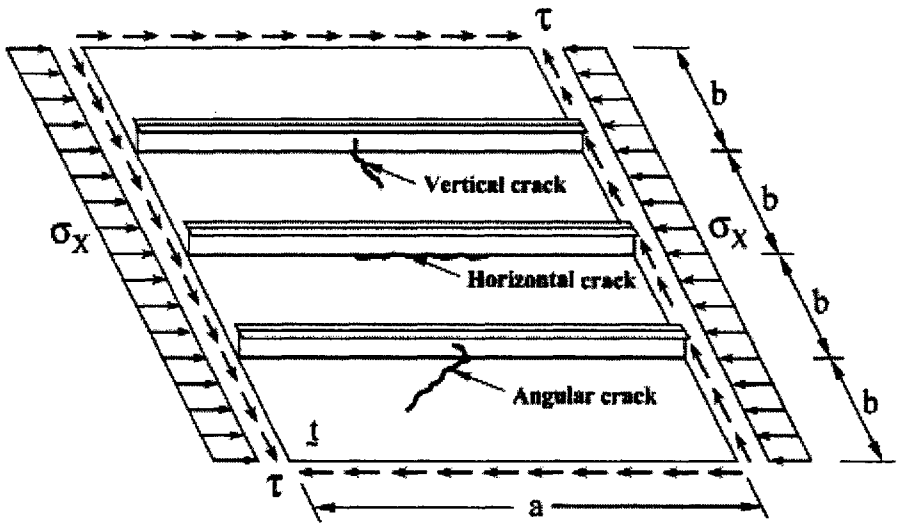

Figure 2-18: A schematic of a steel stiffened panel with three types of crack orientations under axial loads or edge shear from Paik et al. [216]

with necessary accuracy.

The characteristics of fatigue crack propagation and the remaining life assessment of ship structures have been investigated, focusing attention on curved crack paths, the effects of the weld, complicated stress distributions at three-dimensional structural joints and structural redundancy. Sumi et al. [295] presented an advanced numerical simulation system, so that realistic phenomena of fatigue crack propagation can be predicted. The presented method may offer an efficient simulation-based tool for the fatigue crack management of critical details.

A new parameter, which can quantitatively describe fatigue crack propagation, was proposed by Toyosada et al. [304]. This parameter reflects the cyclic plastic behavior near the crack tip, and the resulting build up of layers with residual plastic deformations on the crack surfaces. A fatigue crack closure model suitable for an arbitrary applied stress distribution and an arbitrary residual stress distribution was developed based on the appropriately modified Dugdale's concept of crack tip plasticity. A re-tensile plastic zone generated (RPG) load, at which the tensile plastic zone starts to develop ahead of a crack tip, was defined. An effective stress intensity factor range was redefined by replacing the crack opening load with the RPG load. This redefined effective stress intensity factor was termed ΔK_{RPG}. When ΔK_{RPG} is substituted for ΔK or the crack opening load based on ΔK_{eff}, the "knee" in the threshold

region was not seen any longer. As a result, it was confirmed that a stopping phenomenon of fatigue crack propagation can be quantitatively and appropriately described without the threshold value such as $(\Delta K_{eff})_{th}$. It was also confirmed that the proposed crack closure model can provide quantitative estimates of the fatigue life under various loading conditions and in a pre-existing residual stress field.

Zabavsky et al. [351] studied fatigue of a welded connection with incomplete penetration in ship hull details. The fatigue failure which developed from an incomplete penetration was analyzed. The crack growth in the weld metal was governed by normal and shear modes of shifting crack surfaces. The authors' many years of experience in experimental and theoretical investigations permitted replacement of a curvilinear crack trajectory by planes and a composition of flat and conical fragments under spatial crack propagation in the connection of a limited length. A condition of equivalency of the normal opening displacement stress intensity factors under the curvilinear path and composition of stress intensity factors of normal and shear modes for the equivalent flat path was used. When analyzing the initial failure phase, the cavity was considered as a through crack. However, the stress intensity factor calculated for a crack propagating from the cavity tip was corrected accounting for the actual spatial character of the detailed strain. To calculate crack growth in the welded connection, experimentally obtained parameters of the Paris-Erdogan relationship for the weld metal were utilized. A rather satisfactory match between the calculated and experimental endurance characteristics in the range of loads, under which crack growth was controlled mostly by the elastic stress field in the weld material, was obtained.

2.8 Fracture of Relative Structures

2.8.1 Fracture of aircraft fuselages

Aluminum alloys have been used for decades in the aerospace industry because of their high strength to density ratio and their relative low price. One of the critical fields in aircraft design is damage tolerance, which represents the ability of a material to sustain loads when damaged. The Federal Aviation Administration (FAA) requires aircraft manufacturers to show that the residual strength of the stiffened panels that constitute most of current aerospace structures is

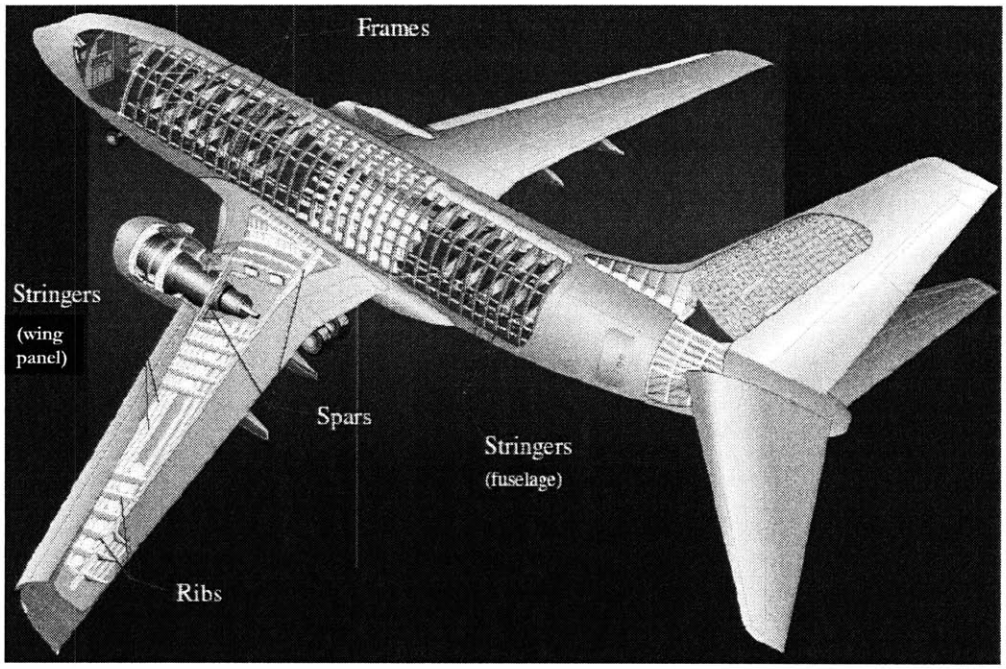

Figure 2-19: Typical aircraft: most of an it is made of thin aluminum sheets on which are assembled extruded stiffeners. The fuselage contains longitudinal stringers and circumferential frames to sustain a multiple bending / pressure loading. Wings are boxes containing two panels stiffened longitudinally that are linked together with ribs in the transverse direction and spars in the longitudinal direction

high enough, Fig. 2-19 and 2-20.

The aerospace industry is setting more and more aggressive targets for weight and cost of aircraft along with a new focus on reduced development time. Achieving those targets requires not only optimized design and processes but also improved material properties, therefore in-depth ongoing research on fatigue fracture of stiffened panels is underway (see Fig. 2-21).

The aging of the commercial air transport fleets around the world is of constant concern because of the loss of structural integrity through fatigue cracking, Fig. 2-22. Methods for computing the energy release rate for cracks of varying length in typical stiffened metallic shells under general loading conditions have been developed by Rankin et al. [253] in order to predict analytically the structural integrity and residual strength of aircraft fuselage structures containing cracks. This work was built on the finite element procedure developed by Riks et al. [261] for the analysis of the buckling and post-buckling behavior of cracks in plates loaded

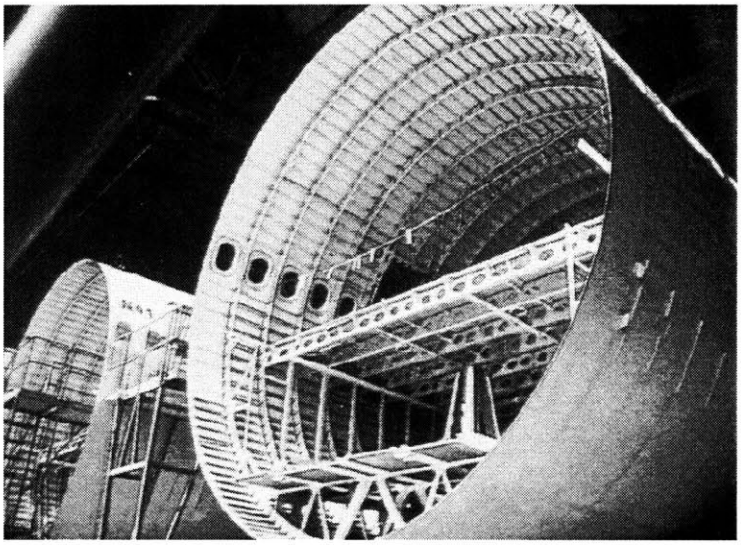

Figure 2-20: Al–Cu and Al–Zn–Mg alloys used for aircract

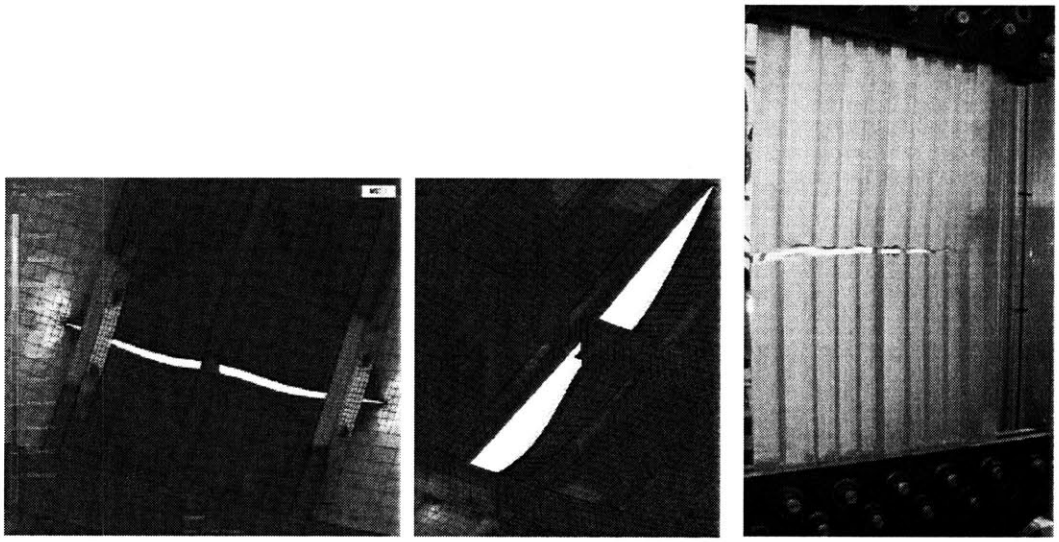

Figure 2-21: Finite element modeling of two stringer bay cracks (left), two frame bay cracks (middle), and actual tests on 2027 T351 lower wing skin alloy (right) [188]

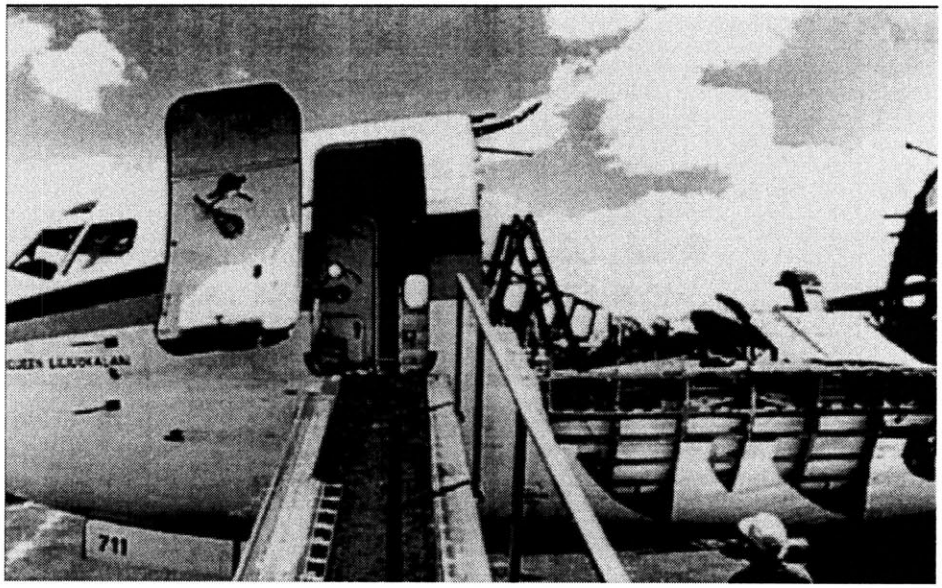

Figure 2-22: Failed fuselage of the Aloha Airlines Boeing 737 in 1988, attributed to multiple-site damage [courtesy of the National Aeronautics and Space Administration]

in tension, for centrally cracked specimens.

In one design approach for aircraft fuselages using semi-monocoque construction, circumferential rings or frames are intended to steer dangerous longitudinal cracks, if they appear, in the less threatening circumferential direction around the fuselage. However, in the case of aging aircraft in which damage, such as short fatigue cracks emanating from rivet holes, is present, cracks that start running longitudinally may continue to do so because the cracked rivet holes may provide a path of lesser resistance. The ongoing research in aircraft fuselages includes all types of failures, Fig. 2-23.

The residual strength of stiffened panels with large damage, such as a two-bay crack, is an important design parameter for large transport aircraft typically required to satisfy fail-safety criteria. The crack-stopping role of the stiffeners has long been recognized and utilized for structures with mechanically fastened structure, but has historically been considered less effective for integrally stiffened structures (Swift [298]), due to the potential of the crack to spread directly from the skin into an integral stiffener. Newman et al. [192] performed experiments with stiffened and unstiffened panels for the aircraft industry calculating the residual strength using finite element shell code and the critical crack-tip-opening angle (CTOA) fracture crite-

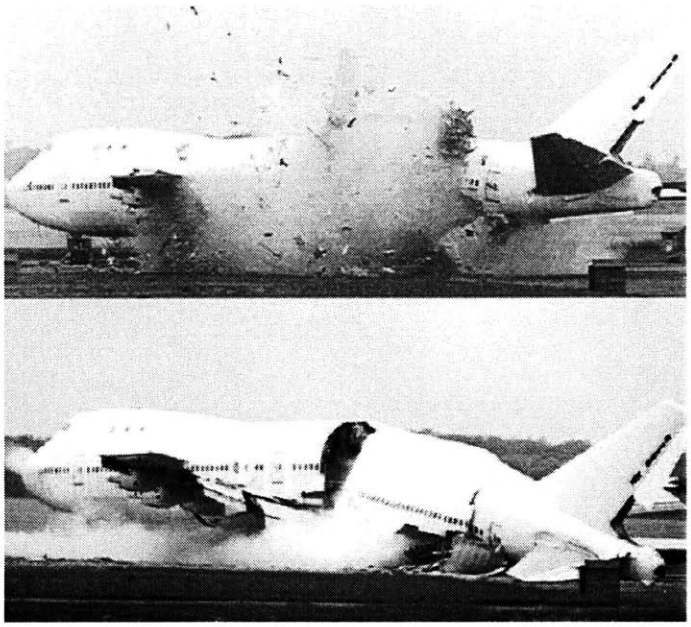

Figure 2-23: Fracture of aluminum fuselage (pressurized Boing 747) due to controlled explosion (200 grams of Semtex)

rion for the benefit of a NASA/FAA program. A study at NASA performed by Pettit [235] has shown that crack turning phenomena can enhance the residual strength of an integrally stiffened structure by turning a crack as it approaches a stiffener as shown in Fig. 2-24.

The results of that study also suggested that even in cases where the crack did not turn, the observed residual strength of integral test panels was higher than would have been anticipated, possibly due to the peculiar three-dimensional profile of the crack as it tunnels under the stiffener. Fracture orthotropy is also believed to play a significant role (Boone [23]). Better understanding of these phenomena could enable future aerospace programs to utilize low-cost

Figure 2-24: Up-close photographs of failed 2096-T8X panel with integral stiffeners

integral structures with greater freedom and confidence than at present.

Labeas and Diamantakos [147] developed a methodology for the case of crack link-up prediction of unstiffened plates and extended it for the case of typical cracked stiffened aircraft panels. They focused on the prediction of the coalescence of adjacent cracks and the residual strength estimation of structures under multiple site damage conditions.

2.8.2 Fracture of pipes and pipelines

Gas pipelines have experienced several types of dynamic fracture propagation and their behavior has been analyzed (Emery et al. [62] [63] [64] [65] [66] [67]; Kanninen et al. [125] [126]; O'Donoghue et al. [194]; You et al. [348]) and crack arrest systems have been implemented (O'Donoghue et al. [195]; Kanninen [129] [130]; Freund et al. [72]; Maxey et al. [170] [171] [172]).

The research covers dynamic crack propagation identifying the variables that govern the dynamic fracture process and their relationships (Zhuang and O'Donoghue [362]; Murtagian et. al. [186], [187]). The overall conclusion is that either an adequate pipeline design (crack arresters, pipeline layout, etc.) or a proper selection of material can minimize this effect, especially for axially propagating cracks (Zhuang and O'Donoghue [363]).

2.8.3 Fracture of pressure vessels

In the design of components such as pressure vessels and piping systems, the different modes of failure to be considered are:

1. excessive elastic deformation, including elastic instability,
2. excessive plastic deformation,
3. brittle fracture and unstable fracture after ductile tearing,
4. stress rupture and creep deformation,
5. plastic instability - incremental collapse,
6. high-strain low-cycle fatigue,

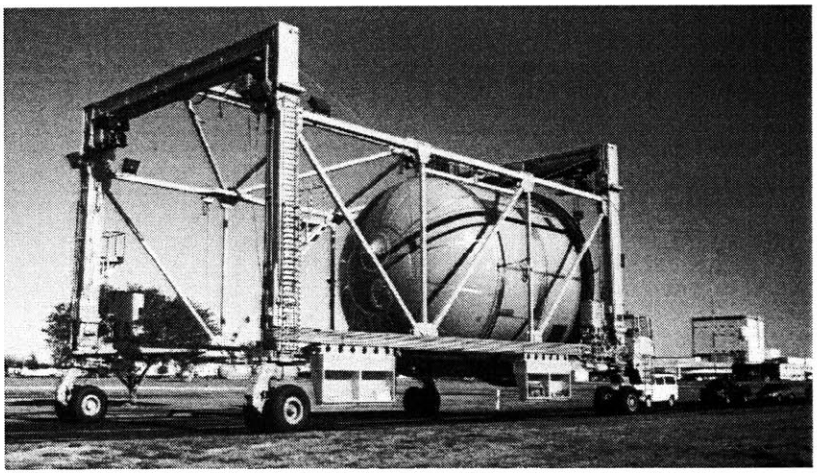

Figure 2-25: Fuel tanks and booster rockets, such as those of the Space Shuttle, are 2xxx alloys, originally 2219 and 2419, now Al–Li "Weldalite" alloy 2195

7. stress corrosion, and

8. corrosion fatigue.

These types of structures are very sensitive to fracture, because once occurred can cause severe damages to human beings and the environment, Fig. 2-25. Several researchers examined the crack propagation and arrest phenomena of stiffened structures. Structural plate systems stiffened by stringers and ribs are widely used in engineering structures, such as aircraft. Their behavior was studied in depth especially under the presence of cracks, since large fatigue cracks can develop in such structures. Configurations involving cracks in infinite or semi-infinite plates were examined (Romualdi et al. [265]; Sanders [271]; Greif and Sanders [91]). By using Reissner's plate theory and the Fourier integral transform technique, the analytical solution for a stiffened plate containing a through-crack under uniform bending load was obtained by Yahsi and Shahid [343]. The asymptotic stress rate near the crack tip terminating at the stiffener was examined.

The application of the boundary integral equation method to the plate bending problem was presented by Jaswon and Maiti [118] for the classical theory. For the Reissner plate model, the boundary integral equation was reported by Vander Weeën [315] and fundamental solutions were deduced by use of the Hormander method. The application of the boundary element

method for Reissner cracked plate can be found in Rashed et al. [254]. Comprehensive review of application of boundary element methods to plate bending methods can be found in the book of Aliabadi [7]. Finally, this method was implemented to analyze the deformation of stiffened cracked plates, using both concentric and eccentric stiffeners which contained single and double cracks subjected to uniform distributed moment on the crack surface and uniform shear load on the plate (Wen [325]).

Dynamic photoelasticity and static finite element analysis were also used to study the fracture mechanics of propagating cracks in stiffened panels by Wade and Kobayashi [320]. The arrest capabilities of the stiffened panel examined was assessed through the kinetic-energy release-rate concept and the bounded stiffeners were found to be more effective in arresting propagating cracks than corresponding pin-joined stringers under the same conditions.

A method that relates the crack resistance of a stiffened panel to that of an unstiffened sheet was proposed by Vlieger [319]. The ultimate panel failure after crack arrest was initiated either by subsequent unstable crack growth or by stiffener failure. It was found that, in case crack arrest does not occur, the residual strength of the unstiffened panel constitutes a safe lower bound. The tests were performed on bonded and riveted panels with symmetric strip stiffeners or eccentric Z-stringers.

Fracture of cylinders and conical shells

Das et al. [53] provided ultimate strength design formulations for ring stiffened and ring/stringer stiffened cylinders under various loading like axial compression, radial pressure and combined loading. Comparisons were made with screened test data, which have realistic imperfections and various radius to thickness ratio values in the range generally used in offshore structures.

Unlike ring-stiffened cylinders, the test results of stiffened conical shells are difficult to find in the open literatures. Cho and So [42] reported hydrostatic test results on four ring-stiffened conical shells together with those on six ring-stiffened cylinders. Among four conical shells, three were collapsed by inter-frame failure, but the other was by overall failure. Figure 2-26 shows the collapsed shapes of stiffened conical shells which are quite similar to those of ring-stiffened cylinders. Comparison of their ultimate strength with those predicted by relevant design codes showed reasonable agreements.

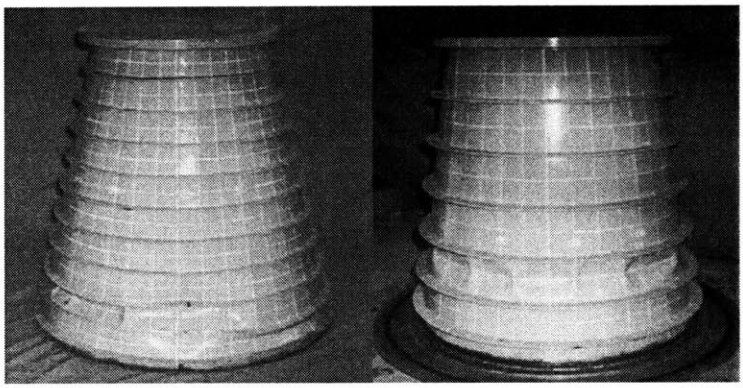

Figure 2-26: Collapse modes of ring-stiffened conical shells subjected to hydrostatic pressure: (a) inter-frame collapse (left) and (b) overall collapse (right)

Underwater explosion tests were performed by Hung et al. [111] on one unstiffened and two ring-stiffened cylinders of a small scale. In the tests, the deformed shapes were captured by a high-speed video recorder. The dynamic structural analysis of the test models was also performed using FEM together with USA code to take into account the fluid-structure interaction effects. They discussed the problems experienced in the underwater explosion tests.

Unstiffened and stiffened curved plates

Recently, structural behaviors of unstiffened and stiffened curved plates subjected to axial compression or combined with hydrostatic pressure were numerically investigated. Maeno et al. [161], [162] performed a series of elastoplastic large deflection analyses to investigate buckling/plastic collapse behavior of ship's bilge strakes which are unstiffened curved plates under axial compression. Based upon the analysis results, a simple formula is derived to calculate buckling/ultimate strength and to simulate average stress - strain relationship of the bilge structure under uniaxial compression. It is found that the bilge structure with a conventional shape and size reaches the ultimate strength by yielding before buckling. Therefore the hard corner elements could be used for bilge part in the ultimate hull girder strength evaluation by the Smith's method and the effects of buckling of bilge part should be accounted beyond the ultimate strength.

Yumura et al. [350] investigated buckling/plastic collapse behavior of cylindrically curved

plates under axial thrust. They, firstly, performed a series of elastic eigenvalue analysis changing curvature of a curved plate to clarify the fundamentals in its elastic buckling behavior. Then, giving a small initial deflection of a buckling mode, a series of elastic large deflection analyses are performed to investigate the characteristics of postbuckling behavior of a curved plate. Finally, a series of elastoplastic large deflection analyses were performed to clarify the buckling/plastic collapse behavior of cylindrically curved plates.

Unlike other ship types, container ships have bilge strakes having large radius of curvature, which should be stiffened with longitudinal stiffeners. In shipyards, however, those stiffened curved plates are designed using formulations for flat stiffened plates. Park et al. [222] performed non-linear FEM analyses using a commercial code for stiffened curved plates changing the curvature and spacing of stiffeners. In the analyses, initial shape imperfection and residual stresses were considered and combined axial compression and hydrostatic pressure loads were applied.

2.9 Scaling Effect

The testing of small-scale models is indispensable for obtaining the behavior of complex structural systems which are difficult to analyze theoretically and numerically, or to study experimentally. It is evident that to accurately predict the behavior of full-scale prototypes the only cost-effective solution is by numerical simulations. Scaling effect might be an important issue either for different size of specimens or for applications of different types of materials, which can also lead to significant deviations in the obtained results, as shown in Fig. 2-27. Therefore, a calibration of the code is required and sometimes the full-scale tests cannot be avoided, especially with critical structures. Small-scale tests are clearly much cheaper than full-scale tests. However, for a complete validation of the predictive tools on plates and panels made of typical Navy metals, full-scale tests must be run.

On the other hand, bridging micro-scale metallurgical examination with small and intermediate-scale specimens is needed to understand the fracture characteristics of a material and a structural component. Bouchaud [24] used nanotechnological approaches at her review concerning the scaling properties of cracks, from the morphology of fracture surface aspect, and concluded

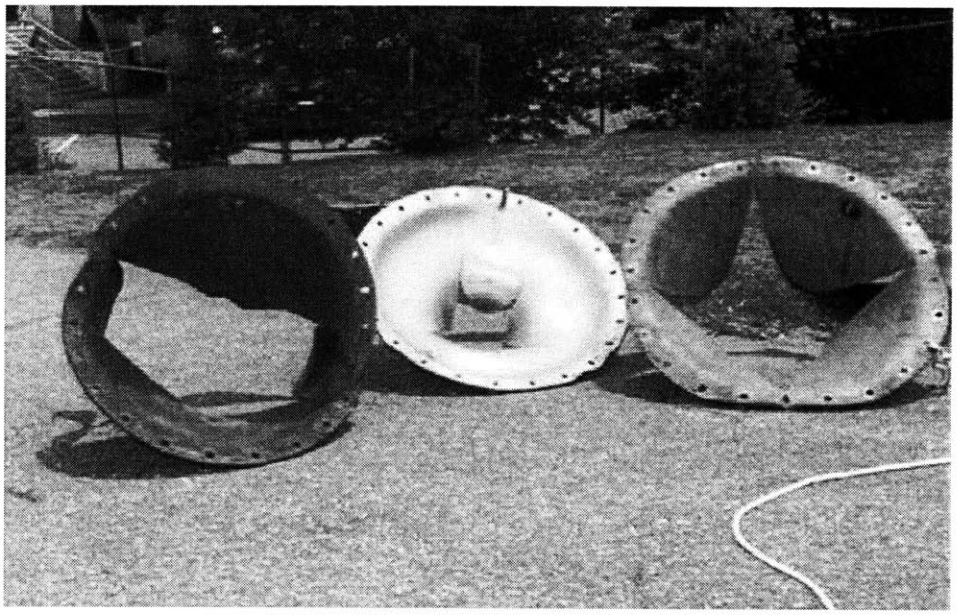

Figure 2-27: Behavior of unstiffened plates from naval steels (DH36, AL6XN and HY-130) subjected to contact blast loading. Different modes of fracture for same loading coniditions can be observed

that microstructural heterogeneities (grain boundaries, second phase precipitates, dislocation assemblies, etc.) control the ability of the material to resist crack initiation or propagation by examining several crack paths.

Chapter 3

Experimental Program

3.1 Methodology

Mapping the crack pattern in aluminum naval structures presents a challenging problem as this phenomenon occurs at various length scales, ranging from microscopic voids to necking and panel cracking. In order to efficiently study this in the laboratory, additional factors such as total cost of material, time, and usage of facilities have to be optimized. A methodology for designing the experiments in order to achieve the objective of this thesis is initially presented, aimed at including all major aspects of fracture. This methodology consists of careful specimens selection, exploitation of facilities capabilities, and examination of material behavior.

An extensive experimental program is conducted comprising of a series of test panels with varying degrees of complexity replicating typical naval vessel applications, which are designed and tested to quantify dimensional variations arising from the panel fabrication processes in a naval production environment. Crack growth depends strongly on material properties, structural configuration, loading and environmental conditions. It may be extremely fast, over $1,000$ m/s, and it may be extremely slow, less than 1 $mm/year$.

A naval structure usually contains thousands of macro-cracks (separation distance is of the order of grain size) and several million micro-cracks (separation distance of the order of atomic distance), Fig. 3-1. Only those cracks that are situated in highly strained regions should be regarded as potential fracture initiators. It is a major objective of naval architects to determine which cracks constitute an obvious risk for fracture and which do not, so they can either redesign

the structure or decide on the repair technique.

Figure 3-1: Macro-crack of 24 m in length on the weather deck of the tanker Castor [113] [courtecy of IMO]

3.2 Design of Experiments

A major challenge confronting researchers is how to efficiently allocate resources to an experimental effort in order to extract the maximum amount of information while minimizing the amount of required specimens. Design of experiments is a process of determining the functional relationships between independent experimental variables so that controlling factors can be predicted and stated with a statistical accuracy. Once a better understanding of the effects of the various parameters is achieved, the remaining resources can be directed more efficiently on those variables that can be controlled and that significantly influence the response.

Early on in any investigation, many factors are potential candidates for controlling variables that influence the response of naval structures. Rushing into experimentation with a full set of specimens, to evaluate all effects one at a time, would be inefficient. Even setting up a full factorial design to cover all possible combinations of factors, is prohibitive in terms of

experimental cost. A careful selection of the most representative naval structures and loading cases based on experience was thus performed by executing one test for each case.

The uniaxial tension test is one of the most widely used tests to characterize strength, ductility and other mechanical properties of a material. This type of test was selected because its analysis provides data about elastic and plastic deformation: modulus of elasticity or Young's modulus, Poisson's ratio, yield and tensile strengths, elongation and reduction in area, and strain-hardening characteristics. This data can also be used for quality control in production. It can also be used for ranking the performance of structural materials, evaluating newly developed alloys, and dealing with the static strength requirements of a design. Analytical calculations that give the value of the J-integral for mode-I loading are presented in Appendix A.

Furthermore, the uniaxial tests subject the specimens to a similar stress environment as the stiffened plates in ship structures are usually subjected to: a combination of lateral and in-plane loads. The lateral loads cause bending of the panel, while the in-plane loads cause axial tension or compression. However, the results of tensile tests of specimens machined from selected portions of a part or material may not totally represent the strength of the entire end product or its in-service behavior in different environments.

3.2.1 Specimen selection

Evaluation of materials may be performed using standard (e.g. ASTM B557M-06) or nonstandard test specimens, depending on the amount, size and shape of available material. Naturally, this thesis is concerned with the examination of fracture characteristics of a material with limited resources, and as a result, the experimental work has focused on the fundamentals of crack propagation in stiffened panels. The tests were, therefore, divided into three groups: (i) determination of material characteristics, (ii) small-scale tests of plates and panels, and (iii) intermediate-scale tests of structural configurations.

The first group consists of results obtained from six specimens that were tested in order to determine the material properties. Rectangular tensile thin sheet ("dogbone") type specimens were used. As it will be shown later, there was a fairly good agreement between measured values, documentation provided and results obtained from numerical simulations.

The choice of test in the second group was based on the international standard ISO12135:2002

(Metallic materials - Unified method of test for the determination of quasi-static fracture toughness) [115], utilizing the compact tension (CT) specimen without fabrication of the precrack often used for fatigue tests, but only the notch. A series of fracture tests on small scale aluminum alloy sheets and panels were performed to examine and characterize the process by which cracks propagate and coalesce in stiffened configurations. Specific test fixtures were designed to withstand the tension loads applied to the panel specimens in a $\pm$ 250 kN capacity MTS testing machine. Thirteen single sheets of bare naval aluminum alloy, approximately 120 mm high, 125 mm wide, and 4 mm thick were fabricated with artificial through-cracks oriented horizontally at mid-height. Additionally, nine tests of naval aluminum alloy panels in several geometries, stiffener types, stiffener configurations, and displacement rates were conducted.

In the third group, the results acquired from the small-scale tests were compared to the subsequent four tests with edge and central cracks in two common unstiffened and stiffened intermediate-scale structural configurations. The comparison showed that the crack pattern followed similar discrete steps proving that the scaling effect did not affect the crack pattern. Special test fixtures were designed for this particular experimental group as shown in Appendix B.

Notch geometry

Fracture is often considered as a process in which increased loading suddenly causes accelerated growth of a pre-existing crack. The author's experience working with damaged naval structures has shown that cracks can be formed in all possible variations. One parameter that needed to be examined in-depth was the effect of crack geometry, with emphasis on the length and the tip type of the crack (blunt or sharp), on the crack propagation and arrest in stiffened panels. This relates to the well accepted notion that material ductility depends on the stress state at the crack tip (crack tip constraint) [196].

Crack growth in ductile elastic-plastic materials have been thoroughly examined. In the case that the plastic zone is large compared to the geometric characteristics of the specimen (thickness, length and width), the crack tip loading modes are not precisely defined, as in Linear Elastic Fracture Mechanics. The most common methodologies for crack growth investigation include either fracture criteria on the macroscopic scale or local approaches based on damage

mechanics.

Introduction of a notch into the gage length of a steel tensile test specimen increases the tensile strength above that measured on an identical steel test specimen without a notch. The increased tensile strength of the notched specimen is caused by a subtle "distortion" of the applied uniaxial stress, resulting in a localized triaxial stress state at the root of the notch. This phenomenon was selected to be examined also for naval aluminum alloys.

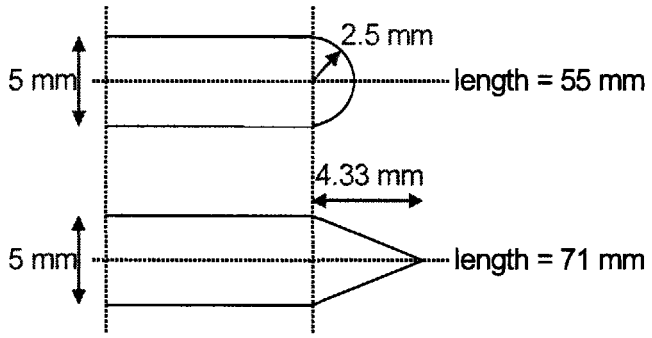

Figure 3-2: Geometry of the artificial cracks fabricated with various crack tip and initial crack length

Since the main objective of this research was to map the crack pattern in stiffened panels, the initial crack length was selected as a parameter in order to evaluate the potential crack path diversity in relation to the amount of plate material that the crack would have to travel prior to the stiffener's foot (either the web or the weld). Figure 3-2 shows schematics for two types of crack tips. Additionally, since the profile of the crack was selected in order to meet the general requirements of international standards, the crack tip geometry was set as a parameter and was further evaluated. Actual pictures prior to the tests were taken for both cases, where the initial geometries were measured, Fig. 3-3.

3.2.2 Material used

A wide variety of materials have been used for the construction of marine vessels, with steel being the primary choice. In an effort to reduce manufacturing, maintenance and operating costs, the shipbuilding industry is using aluminum alloys as a means of reducing plate thickness, and thus weight, in ship construction. Each type of aluminum alloy differs in the crack sensitivity

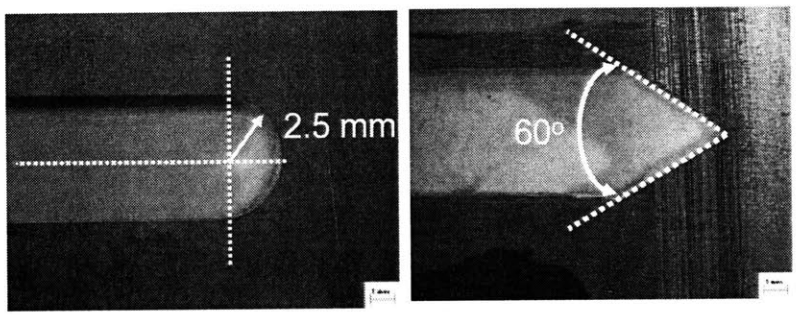

Figure 3-3: Stereoscopic data showing two types of initial crack tip examined, the semi-circular (left) and the triangular (right)

with respect to the solute concentration during the welding process, as shown in Fig. 3-4 [174].

In this research, a marine aluminum alloy, 1561 (equivalent to AlMg6MnZr based on ISO 209-1 [116]), which has already been used for the construction of naval applications was selected as the base material for the experiments. Yarema et al. [346] extensively studied the cyclic cracking resistance of this particular aluminum alloy (in air and NaCl solution) prior to its usage for hull structures in the Soviet shipbuilding industry.

Marine aluminum is usually offered in sheets, profiles, panels (sheets with extruded stiffeners) and pipes. The material tested in this research was cut from a $4 \times 8000 \times 1670$ (thickness $\times$ length $\times$ width in mm) panel, corresponding to a total mass of $201,600$ kg. The density of the material was 2.65×10^3 kg/ m^3 based on the specifications of the manufacturer. For the unstiffened specimens, the samples were cut from a sheet with $4 \times 1500 \times 400$ mm dimensions, corresponding to a total mass of $63,600$ kg. The material properties as documented by the manufacturer were: tensile strength $\sigma_t = 332.2$ MPa (34 kg/ mm^2), yield limit $\sigma_y = 186.2$ MPa (19.0 kg/ mm^2), and relative elongation (strength in cracking) along the fiber, $\delta_R = 11.0$ %.

This naval aluminum-magnesium alloy is described as an average strength heat non-hardenable alloy. Being heated by welding, an alloy of this group does not loose strength in the heat-affected zone. Bakulin et al. [14] found that press-forged panels of this type of aluminum alloy of 4.2 mm thick pieces, stiffened with ribs with a height of 100 mm at 200 mm intervals in the longitudinal direction, had a nonuniform structure across the section because of specifics of the

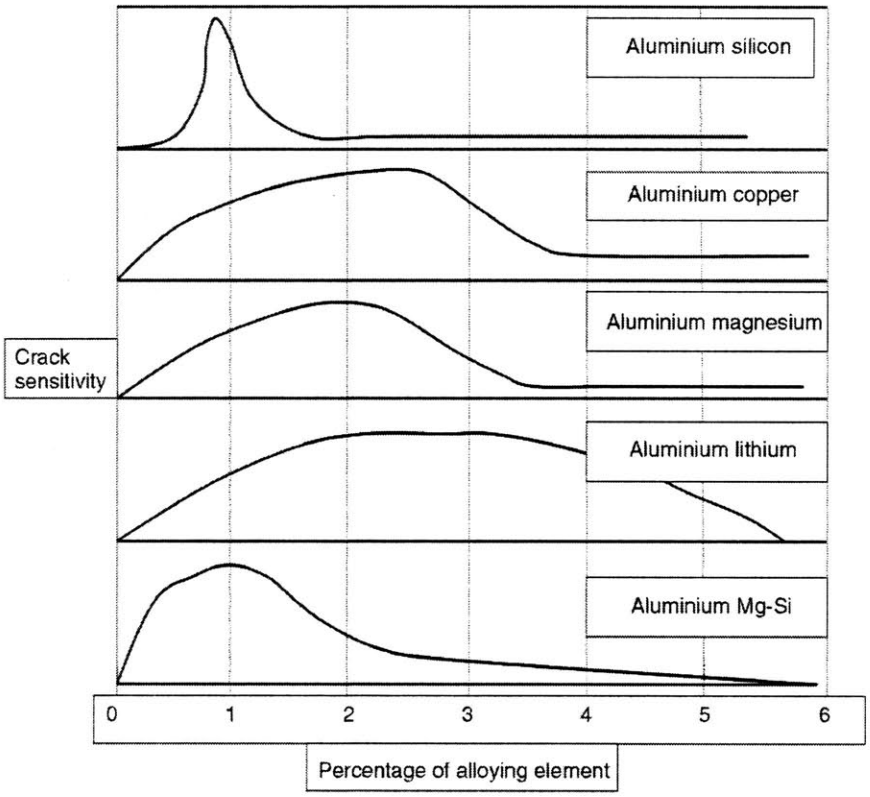

Figure 3-4: Effect of solute concentration on crack sensitivity in aluminum alloys [174]

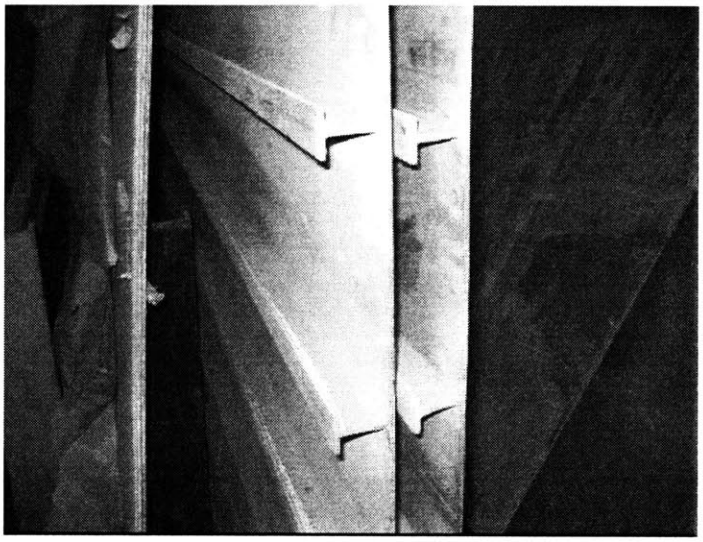

Figure 3-5: Marine aluminum sheets and extruded T-type stiffened panels used for naval vessels from which the specimens were extracted

temperature and strain conditions in press forging. This resulted in similar corrosion-mechanical characteristics between ribbed and unribbed specimens.

3.2.3 Stiffening systems

Though material ductility of naval construction steels has already been examined by Burch et al. [37] and Pussegoda et al. [245] [246], the effect of structural configuration has never been considered as a major parameter for fracture, but only treated as a crack arrest mechanism. The same approach has been followed by Chao et al. [40] when considering crack propagation for fillet-welded specimens and measuring the crack extension rate. The influence of structural dimensions on crack arrest for naval steels has been examined by Priest [241], indicating that both the width and the length of the structure govern the energy release rate at crack arrest.

Stiffener type

The most common types of stiffener used for marine vessels are the T-type, flatbar and the angle-type. In this case, the T-type stiffener was selected for the extruded specimens due to its availability, and its dimensions are shown in Fig. 3-6. The extruded panels with installed T-type stiffeners were cut from stiffened plated that are used for repair of an existing naval vessel. Therefore, this particular stiffener has already been designed and tested for operational loads, meaning that it can sustain the range of loading that naval architecture demands for marine structures, but had never been examined for its behavior towards fracture. For this reason, the effect of the plate thickness on the fracture characteristics was kept as a constant and it was not varied during the experimental program.

Stiffener configuration

Most wrought aluminum alloys are weldable by experienced operators using either the arc or resistance method. Arc welding is typically performed by Gas Tungsten Arc Welding (GTAW), commonly called TIG (for Tungsten Inert Gas) welding, or Gas Metal Arc Welding (GMAW), referred to as MIG (for Metal Inert Gas) welding. TIG welding is commonly used to join parts from about 0.8 to 3.2 mm thick; MIG welding being used for thicker parts.

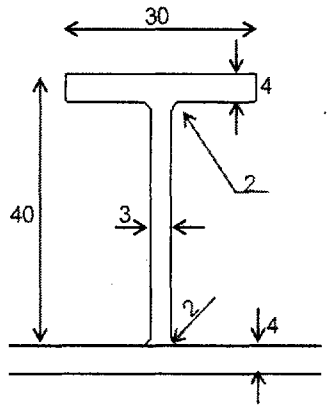

Figure 3-6: T-type stiffener geometry used for the tests on extruded panels (dimensions in mm)

All aluminum alloys suffer from strength reduction in the heat-affected weld zone, although this reduction is less in the aluminum-magnesium ($5xxx$ series) alloys. Rigo et al. [260] investigated the effects of welding on ultimate strength, concentrating on the location of welding, HAZ width, and the corresponding degradation on the material properties due to heating. It was concluded that the parameters that mostly influence the ultimate strength are the yield stress and the width of the HAZ. The level of residual stresses and initial imperfections are considered to have secondary effects. However, a more recent detailed work relating ultimate strength reduction of panels due to the degradation of the yield stress in the HAZ indicates that the reduction is less important than that initially expected (Richir [257]).

The welding of this naval aluminum alloy was based on the process described in the technical documentation provided from the shipyard. The welded specimen had initial distortions due to welding, which were kept to a maximum of 2 mm. Weld deformations are difficult to predict accurately since they depend on a number of parameters as described by Bruce et al. [33]. Many of these parameters are subjected to variations under different conditions. Zheng [359], a colleague of the Impact and Crashworthiness Laboratory at MIT, developed a comprehensive methodology for damage prediction of aluminum thin-walled structures, which includes material modeling, calibration, numerical simulation and experimental verification, Fig. 3-7. Prediction of crack growth using the discrete element removal technique in combination with the proposed fracture locus, was shown to be accurate and robust. Therefore, this technique was used at this

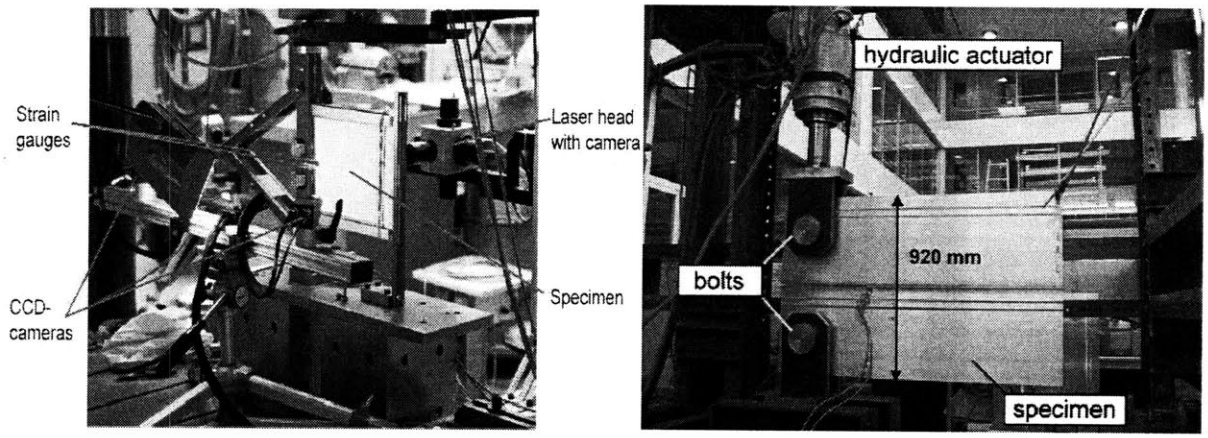

Figure 3-7: Intermediate and large-scale experiments performed under Mode I on aluminum welded plates (left) and thin-walled extruded panels (right), Zheng [359]

dissertation.

3.2.4 Experimental set-up

The tensile tests were performed on an MTS tensile machine with a maximum capacity of $\pm$ 250 kN. An extensometer was fastened on the rectangular tension "dogbone" specimens to measure the strain for the material properties experiment, Fig. 3-8. The digitized measurements were stored and analyzed with a Personal Computer connected directly to the logging device.

Sensitivity to strain rate is of major concern for marine structures due to the variety of loading. Fracture toughness of steel, which is the most commonly used material for marine structures, is known to be sensitive to strain rate. However, for most steels, material ductility (as measured by $\overline{\varepsilon}_f$) information is primarily available only at quasi-static testing rates ($\dot{\varepsilon} = 10^{-4}$ s^{-1}). However, in operation, ship structures can be subjected to significantly higher loading rates: intermediate ($\dot{\varepsilon} = 10^{-1}$ s^{-1}) due to slamming and increasing up to impact ($\dot{\varepsilon} = 2$ s^{-1}) in the case of, for example, collision. Full thickness fracture toughness of conventional ship plate grades, including modern high-strength steels, was determined at loading rates representing quasi-static, intermediate, and impact conditions by Pussegoda et al. [244]. Therefore, the experiments were carried out with a cross-head speed ranging from 0.5 up to 2 mm/min, resulting in low strain rates. The tests can thus be considered quasi-static.

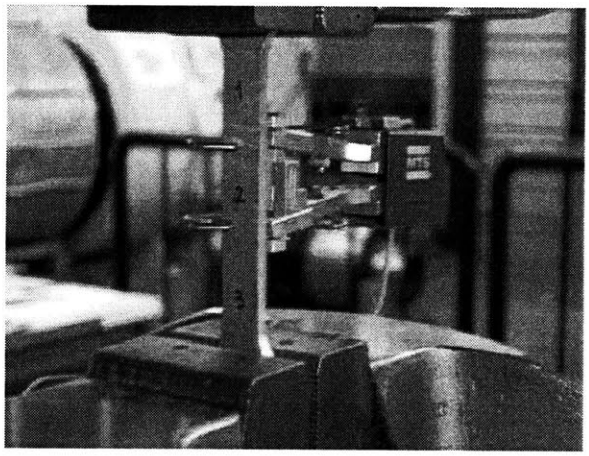

Figure 3-8: Experimental set-up used for the uniaxial tests to acquire the naval grade material characteristics

Figure 3-9: Experimental set-up used for the testing of CT specimens, where the specimen, fixture, pins, clevis, digital camera and PC are observed

All the CT specimens were machined prior to testing with parallel lines that have a 5 mm distance between them, perpendicular to the crack tip, in order to measure the crack using the stereoscope. The results of each fracture event were recorded on digital camera, computer, and occasionally optical microscope. The computer recorded the output of the testing machine load cell. A digital camera was used to record data from the specimens, Fig. 3-9. All experiments were performed at room temperature.

3.3 Group I: Coupon Uniaxial Testing

The orientation and location of the test specimen in a product can influence the measured tensile properties. Many ASTM standards, such as A370, E8 and B557, provide guidance in the selection of test specimen orientation relative to the rolling direction of the plate or the major forming axes of other types of products and in the selection of test specimen location relative to the surface of the product.

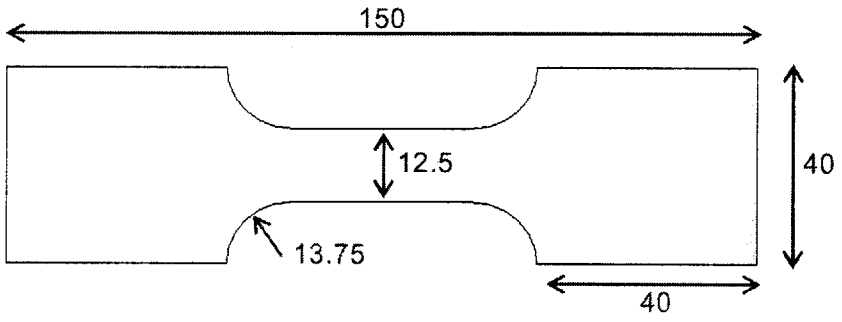

Figure 3-10: Dimensions of "dogbone" specimen used in the uniaxial tensile tests for the material characteristics (dimensions in mm)

Orientation is important to standardize test results relative to the directionality of properties that often develop in the microstructure of materials during processing. The location from which a test specimen is taken from the initial product form is important because the manner in which a material is processed influences the uniformity of microstructure along the length of the product as well as through its thickness. In addition, the fracture toughness of a material is usually dependent on the orientation and direction of propagation of the crack in relation to

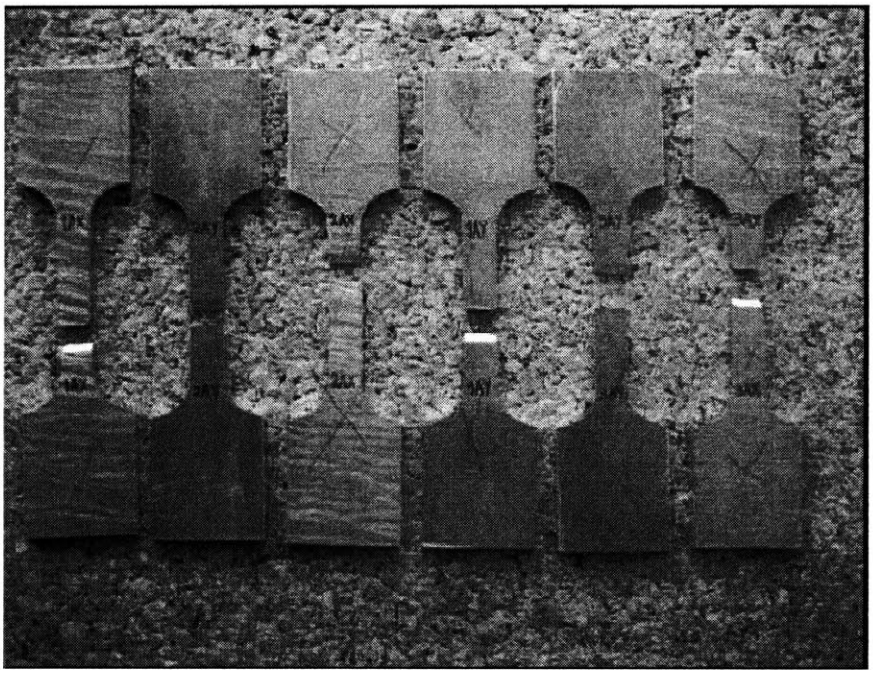

Figure 3-11: Set of uniaxial testing rectangular tension test ("dogbone") specimens

Property	**Documentation** (along the fiber)	**Test** $(L-T)$
Tensile Strength (MPa)	332.2	331.5
Yield Limit (MPa)	186.2	187.3

Table 3.1: Comparison between the documented properties of the naval aluminum and the experimental data

the principal directions of mechanical working or grain flow. Therefore, the specimens were cut in both longitudinal and transverse directions with respect to the rolling direction of the plate. Figure 3-10 shows a sketch of the "dogbone" specimen used for Group I of the experimental program.

The final stage of the specimens tested for this part of the experiment is shown in Fig. 3-11, where it can be observed that the slant fracture mode is dominant. A comparison between the documented and measured properties of the material is presented in Table 3.1.

The MTS device continuously monitored the relationship between the displacement (δ) and the force (P), where $P = P(\delta)$. In addition, the Young's modulus as measured from the stress-

Specimen	Engineering Strain [%]	Engineering Stress [MPa]	True Strain [%]	True Stress [MPa]
1AX	16.50	312.12	15.28	363.96
2AX	21.34	332.09	19.34	402.95
3AX	20.51	324.22	18.66	390.73
1AY	17.57	340.42	16.19	400.24
2AY	16.91	340.44	15.62	398.00
3AY	17.54	339.98	16.16	399.61
Average in L-direction	*19.45*	*322.81*	*17.76*	*385.88*
Average in T-direction	*17.34*	*340.28*	*15.99*	*399.28*
Total Average	**18.34**	**331.54**	**16.87**	**392.58**

Table 3.2: Results of rectangular tensile "dogbone" specimens at the point of failure

stain curve was found, $E = 65.87$ GPa. The results of the tests are shown in Fig. 3-12 and 3-13. Table 3.2 shows a summary of the results obtained from the tests.

The engineering stress-strain curve does not give a true indication of the deformation characteristics of a metallic material because it is based entirely on the original dimensions of the specimen, and these dimensions change continuously during the test. Therefore, the true stress-strain curves, which better represent the plastic-flow characteristics of the material, are shown in Fig. 3-14 and 3-15. A detailed discussion of engineering and true stress-strain curves for this experiment is presented in Chapter 4, which contains the numerical simulations.

3.3.1 Phenomena observed

The failure of all specimens resulted in a fractured surface that became slanted at about 45 degrees with respect to the loading direction, Fig. 3-16. A single shear lip was observed throughout the whole extent of the specimen. The mechanisms responsible for the transition to slant growth in thin sheets are not clear, even in the existing literature, and need to be resolved. Slant fracture is a common failure mode for thin aluminum sheets used in the aircraft and space industry subjected to the condition of transverse plane strain. Liang Xue [341], a colleague of Impact and Crashworthiness Laboratory at MIT, performed a complete set of theoretical, numerical and experimental analyses for ductile fracture of aluminum specimens where slant fracture was dominant.

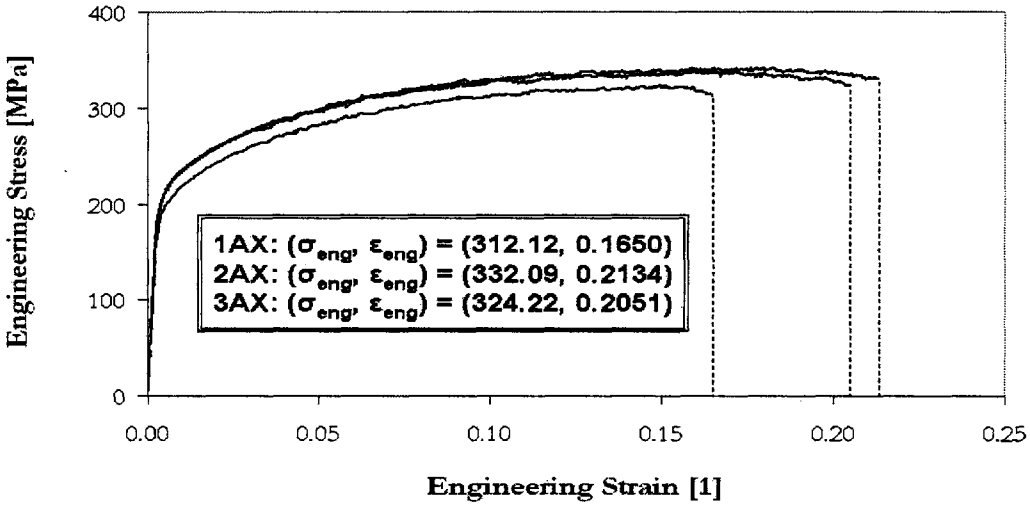

Figure 3-12: Stress-strain curves obtained from the experiments of three "dogbone" specimens cut in the L-direction

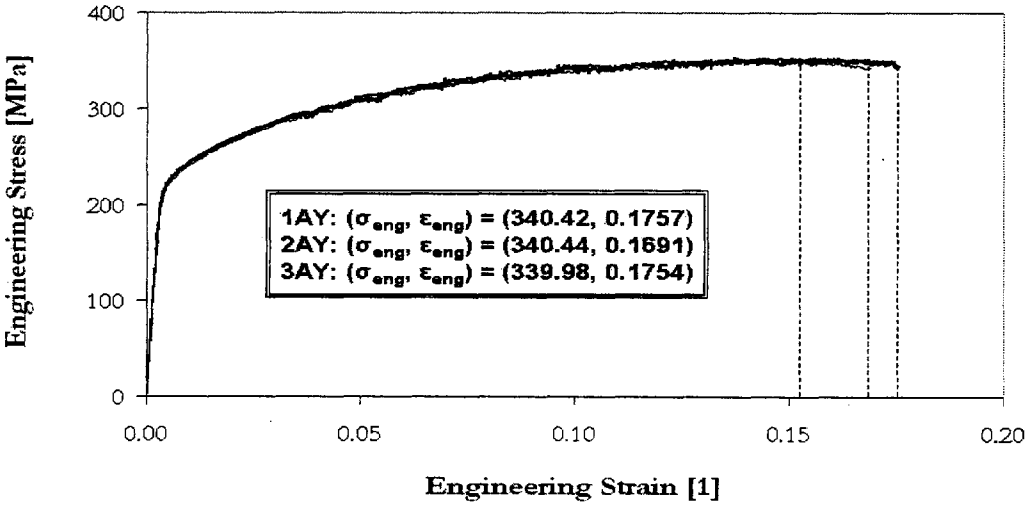

Figure 3-13: Stress-strain curves obtained from the experiments of three "dogbone" specimens cut in the T-direction

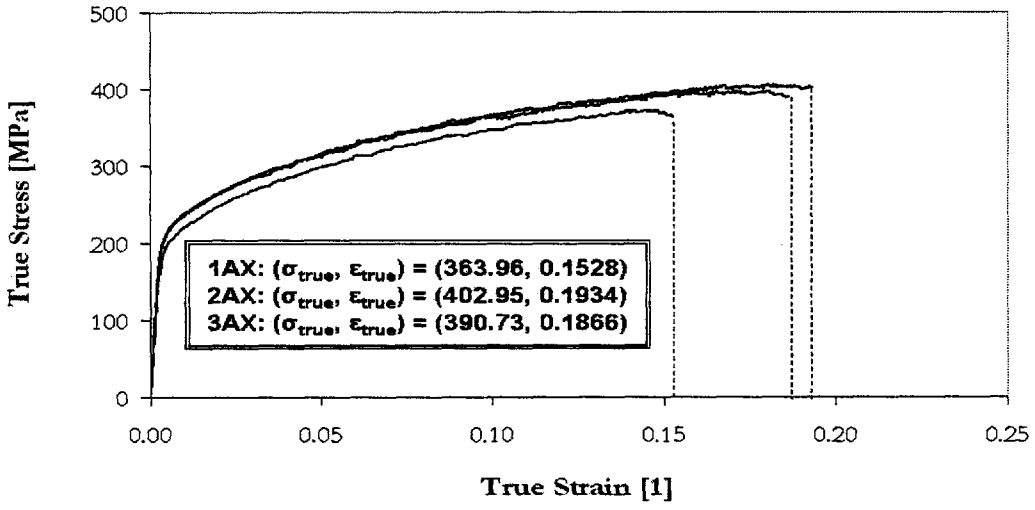

Figure 3-14: True stress-strain curves of three "dogbone" specimens cut in L-direction

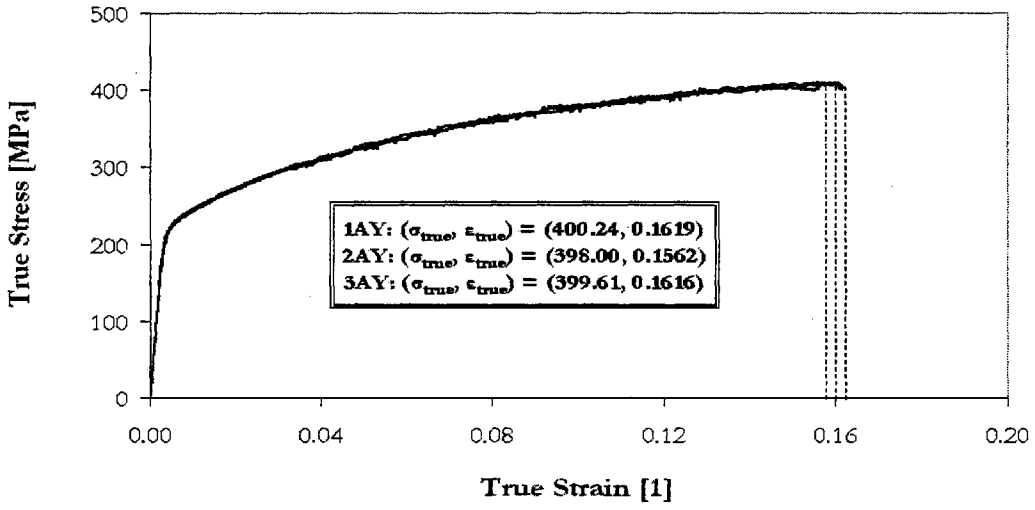

Figure 3-15: True stress-strain curves of three "dogbone" specimens cut in T-direction

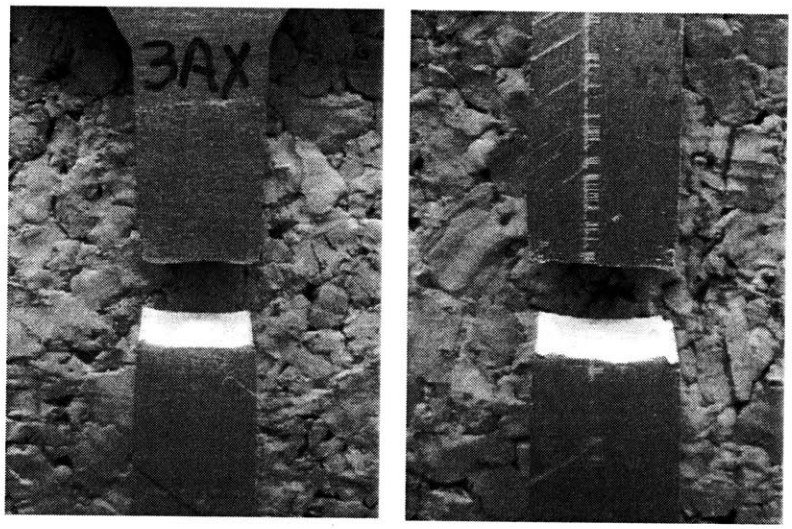

Figure 3-16: Fracture mode observed at the experimental tests of "dogbone" specimens

Several tests on Al2024-T3 aluminum thin sheets were performed by Lan et al. [148] in order to provide insight for establishing a slant fracture criterion, but the authors state that in-depth research is required in order to succeed in developing theoretical solutions and numerical methods that will accurately predict slant fracture phenomena. Material science and microscopic examinations can probably offer answers to the questions previously posted.

An examination of the results and especially the curves that present the relationship between stress and strain, either engineering or true, demonstrates that the measured values of the material characteristics are very close to the documented ones [98]. On the other hand, the dispersion of the experimental results related to the specimens cut in the L-direction proves the fact that the material presents non-uniform properties in this direction. The observation that the specimens did not present any major necking effect by themselves cannot categorize the material either in the ductile or the brittle behavior. The completion of this group of the experimental program provided the information required to examine the fracture characteristics of the selected naval aluminum alloy grade material used for existing naval vessels, as well as the required data for the calibration procedure needed to perform accurate numerical simulations.

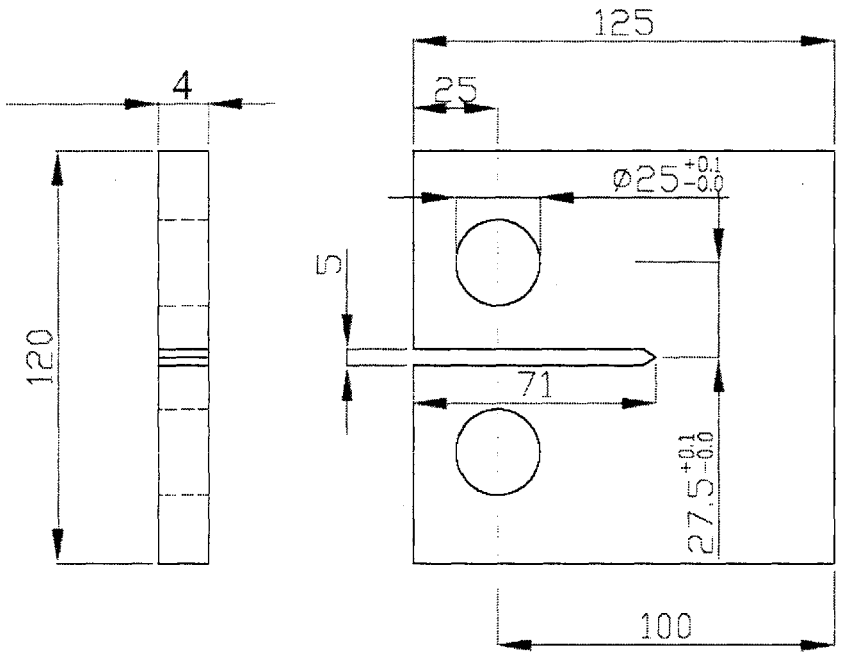

Figure 3-17: Geometry for the compact tension (CT) specimens (dimensions in mm)

3.4 Group II: Small-scale Tests

3.4.1 Compact tension (CT) specimen geometry

For the assessment of the safety level of a structure, it is of great importance to be able to evaluate the response of the structure under accidental loading and also to set appropriate criteria for acceptable damage levels caused by an accident. Therefore, the first step of the experimental work has been approached from a "macroscopic" point-of-view, meaning that the general behavior of a crack while facing a stiffening configuration had to be evaluated prior to testing larger specimens. A small-scale CT specimen was selected as the most appropriate for this type of testing. The dimensions of the specimen are shown in Fig. 3-17. It should be noted that no precrack (common technique for fatigue testing) but only the notch required by the ISO standard was fabricated [115].

Specimen	Length [mm]	Width [mm]	Displacement rate [mm/min]	Crack length [mm]	Crack tip profile
CT1UHC	124.9	120.4	0.5	71	*semi – circular*
CT2UHC	125.3	120.1	1.0	71	*semi – circular*
CT3UHC	125.2	120.6	1.5	71	*semi – circular*
CT4UHC	125.1	120.5	2.0	71	*semi – circular*
CT1UTR	125.1	120.5	0.5	71	*triangular*
CT2UTR	125.1	120.0	1.0	71	*triangular*
CT3UTR	125.1	120.5	1.5	71	*triangular*
CT4UTR	125.1	120.4	2.0	71	*triangular*

Table 3.3: Geometric characteristics of the unstiffened CT specimens

3.4.2 Unstiffened CT specimens

The first series of tests was performed on four unstiffened CT specimens with initial crack length of 71 mm and a semi-circular (blunt) crack tip of 2.5 mm radius. The effect of displacement rate was also examined: it varied from 0.5 to 2 mm/min, increased in 0.5 increments beginning from specimen labeled CT1UHC, which was tested with the minimum displacement rate. The second series of tests were performed on four unstiffened CT specimens with initial crack length of 71 mm and a triangular (sharp) crack tip of 2.5 mm width and 60 degree angle. Similarly to the first series of tests, the displacement rate varied from 0.5 to 2 mm/min, in 0.5 increments beginning from specimen labeled CT1UTR, which was tested with the minimum displacement rate. Table 3.3 summarizes the main geometric characteristics of the unstiffened CT specimens tested. The results of the unstiffened specimens revealed the expected case of crack propagation perpendicular to the loading direction, Figs. 3-18 and 3-19. It should be noted that only in-plane deformation was observed during the experiments with unstiffened CT specimens.

Figure 3-20 schematically presents the loading of the CT unstiffened and stiffened specimens. The displacement rate control technique enabled the user to observe the crack propagation with the naked eye at a low growth rate where the discrete steps of the crack pattern could be defined, a case that it is rare to experience during real case events of fractured structural components, where the crack usually propagates either with a high or a very slow growth rate. Additionally, it proved extremely useful for the comparison of crack patterns between similar unstiffened and stiffened specimens.

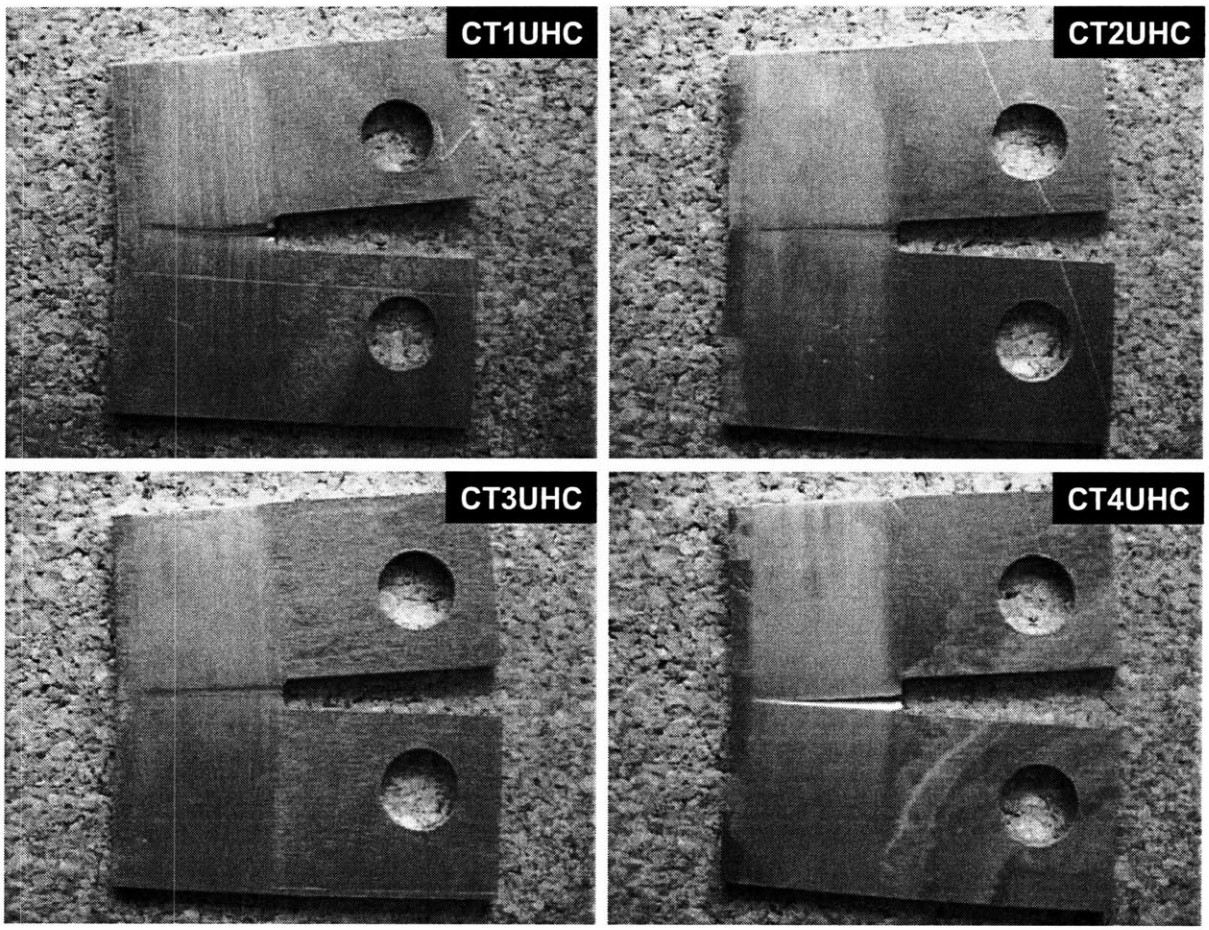

Figure 3-18: CT specimens with an initial crack length of 71 mm and semi-circular (blunt) crack tip subjected to various displacement rates (0.5 to 2 mm/ min). The crack pattern formulated perpendicular to the loading direction

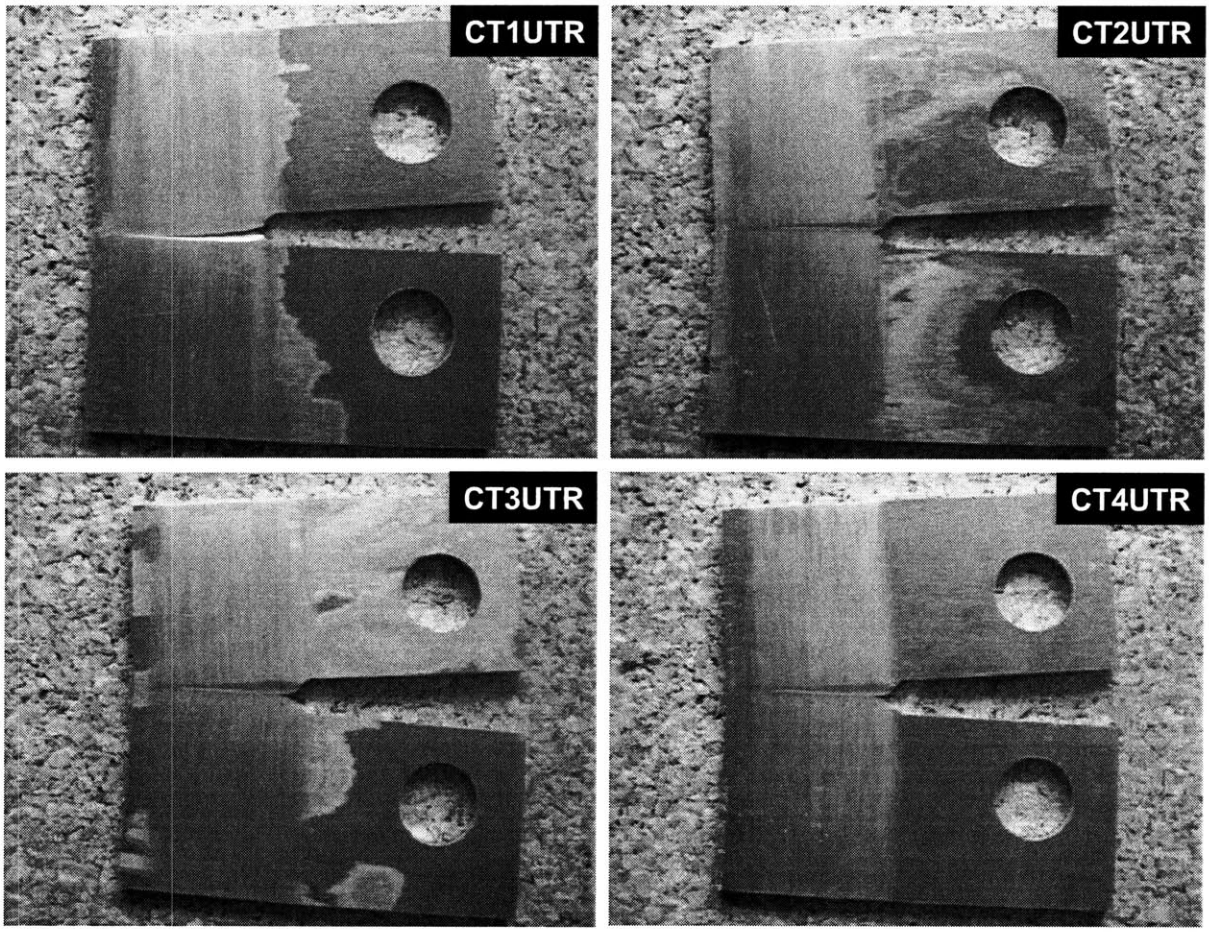

Figure 3-19: CT specimens with an initial crack length of 71 mm and triangular (sharp) crack tip subjected to various displacement rates (0.5 to 2 mm/ min). The crack pattern formulated perpendicular to the loading direction

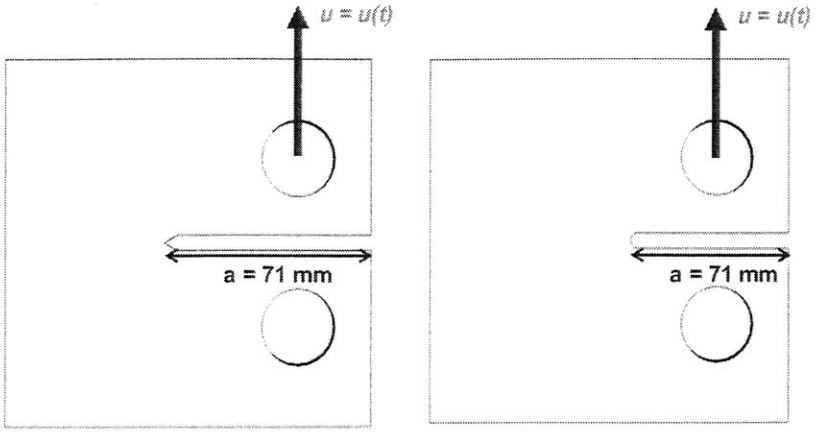

Figure 3-20: Mimic representation of the experimental procedure showing the unstiffened CT specimens with various crack geometries (sharp and blunt notch, initial crack length) subjected to various displacement rates

The load-displacement curves obtained from this series of tests are shown in Fig. 3-21. One can observe that the family of specimens with exact geometric characteristics lies within a region that varies with the displacement rate. The crack tip geometry was thus the main parameter affecting the result, which showed that the sharper the crack tip the less the ultimate strength of the plate is. Table 3.4 shows that the displacement to fracture differs significantly.

An analysis of the results of the unstiffened CT specimens reveals that no strong relation between maximum applied force and strain rate exists. Based on the results of Group I, a single test was performed for each type of specimen with respect to the displacement rate, the range of which was from 0.5 mm/ min up to 2 mm/ min.

3.4.3 Stiffened CT specimens

T-type extruded CT stiffened specimens

The T-type extruded CT stiffened specimens were tested with varying displacement rate, initial crack length and plate material at the rear part of the stiffener. Although the width of the specimen was kept the same with the unstiffened CT specimens (120 mm) the length of the specimen increased to 167 mm for the CTiE specimens ($i = 1, 2, 3$) and reduced to 114 mm for the CTEB specimen, where the material at the rear part of the stiffener was completely cut.

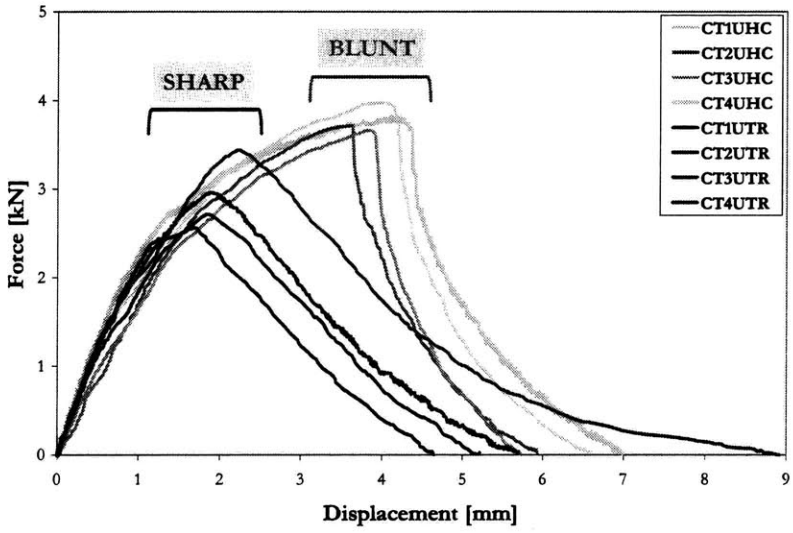

Figure 3-21: Load vs. displacement curves for the unstiffened CT specimens for various displacement rates (0.5 to 2.0 mm/min). Note that two families of curves exist that represent two different types of crack tip geometries

Specimen	Maximum Force [kN]	Displacement to fracture [mm]
CT1UHC	3.82	4.186
CT2UHC	3.71	3.635
CT3UHC	3.66	3.824
CT4UHC	3.97	3.979
CT1UTR	2.96	1.869
CT2UTR	2.56	1.697
CT3UTR	3.44	2.248
CT4UTR	2.71	1.860

Table 3.4: Results of force and displacement to fracture for the unstiffened CT specimens tested

Specimen	Length [mm]	Width [mm]	Displacement rate [mm/min]	Crack length [mm]	Rear plate material [mm]
CT1E	167.0	120.0	0.5	55	65.0
CT2E	123.5	121.5	0.5	71	20.0
CT3E	124.9	120.0	1.0	71	16.0
CTEB	101.0	120.3	1.0	55	0.0
CT1W	123.5	118.0	2.0	71	20.0
CT2W	124.6	118.0	0.5	71	10.0
CT3W	125.5	118.2	1.0	71	20.0
CT1WB	111.9	117.8	1.0	55	0.0
CT2WB	114.2	119.3	1.5	55	0.0

Table 3.5: Geometric characteristics of the CT specimens tested

Table 3.5 summarizes the geometric characteristics of the stiffened specimens.

Figure 3-22 shows pictures of the failed specimens. The four specimens examined had three different geometries (CT2E and CT3E are identical) concerning the rear plate material with respect to the stiffener. Additionally, the CT1E specimen presented out-of-plane deformation during the test. It was generally observed that the crack pattern presented similar characteristics and phenomena: (i) crack initiation with an initial 60 degree angle, (ii) crack paused almost at mid-distance between initial crack tip and the stiffener, (iii) crack flips and redirects, and (iv) crack propagates parallel to the foot of the stiffener failing to propagate through the stiffener in all cases examined.

The load-displacement curves of the experiments performed are shown in Fig. 3-23. In this

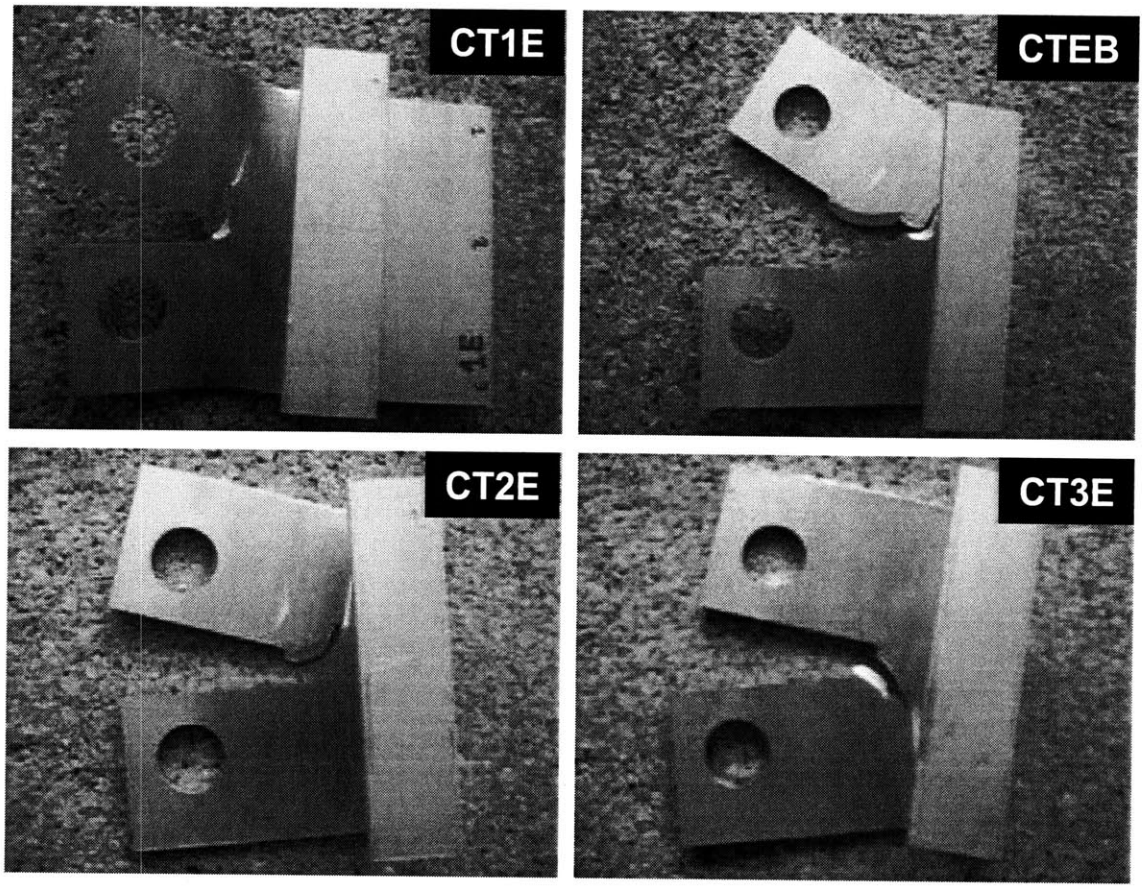

Figure 3-22: Compact Tension specimens (CTE) with T-type extruded stiffeners

graph, the crack onset, pause/flip and redirection can be easily observed. Table 3.6 summarizes the results obtained from the tests on the T-type extruded stiffened CT specimens, where the relationship between force and cross-head displacement at two different locations (fracture and flip) is examined.

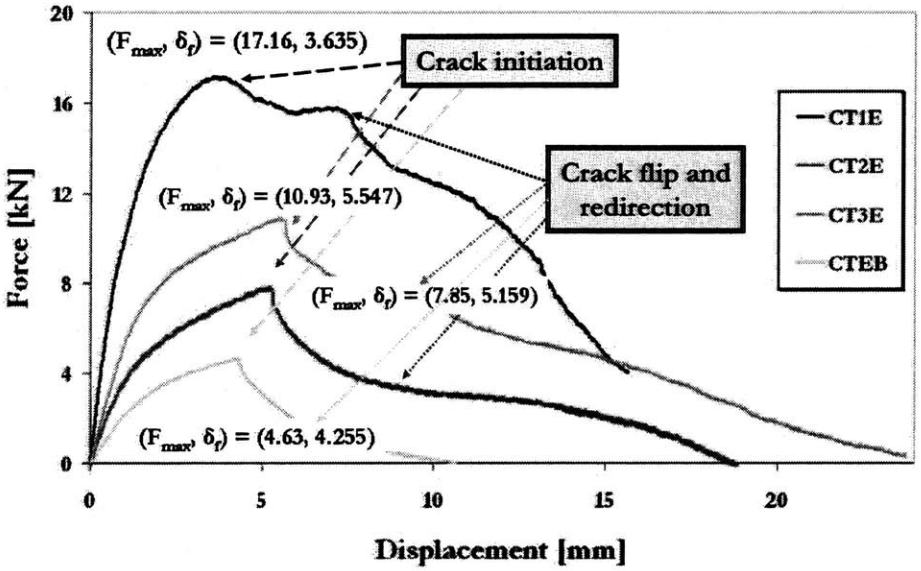

Figure 3-23: Load vs. displacement curves for the T-type extruded CT stiffened specimens

The first test was performed on specimen CT1E with a T-type extruded stiffener installed. It was observed that the crack propagated for 7.2 mm and kinked sharply at a 90 degree direction, parallel to the loading direction, Fig. 3-24. It can also be observed that the CT1E specimen showed a significant out-of-plane deformation, which was an effect of the wide plate at the rear part of the stiffener. The crack initiated at a maximum force of 17.16 kN corresponding to a 3.635 mm cross-head displacement to fracture.

In contrast to specimen CT1E, specimen CT2E was a different case. The main dimension of this specimen were similar to the ones used for the unstiffened ones with the exception of the existence of the stiffener. The specimen was loaded with a 0.5 mm/ min displacement rate. The crack initiated at a maximum force of 7.85 kN corresponding to a 5.159 mm displacement

Specimen	Maximum Force [kN]	Displacement to fracture [mm]	Force at flip point [kN]	Displacement at flip point [mm]
CT1E	17.16	3.635	15.67	6.132
CT2E	7.85	5.159	3.02	10.215
CT3E	10.93	5.547	7.26	8.768
CTEB	4.63	4.255	1.27	6.959

Table 3.6: Maximum values of force vs. cross-head displacement to fracture for the T-type extruded stiffened CT specimens tested

to fracture. The crack propagated at a 60 degree angle with respect to the loading direction and almost at mid-distance between the initial crack tip and the web of the stiffener (stereoscopic measurement showed 15.3 mm from the initial crack tip at a total distance of 31 mm), the crack redirected itself to a 30 degrees angle, and after 1.5 mm suddenly "paused". At that point, the crack flipped (the tunneling angle of the crack during the slant fracture mode changed 180 degrees with respect to the initial angle), re-initiated with a direction parallel (0 degrees) to the loading direction and propagated, following this path up to the point that the test stopped, Fig. 3-25.

The third test (specimen CT3E) was very similar to the previous one (CT2E), but loaded with a 1.0 mm/min displacement rate. The crack initiated at a maximum force of 10.93 kN corresponding to a 5.547 mm cross-head displacement to fracture. The crack propagated at a 60 degree angle with respect to the loading direction but in this case the angle had a 180 degrees difference with the previous test. Similarly, almost at mid-distance between the initial crack tip and the web of the stiffener (stereoscopic measurement showed 15.1 mm from the initial crack tip at a total distance of 31 mm), the crack redirected itself to a 30 degrees angle, and after 1.7 mm suddenly "paused". At that point, the crack flipped 180 degrees, re-initiated itself with a direction parallel (180 degrees) to the loading direction (opposite at this case) and propagated following this direction up to the point that the test stopped, Fig. 3-26.

The final test on specimen CTEB with a T-type extruded stiffener installed on a CT specimen, was performed on a specimen similar to the previous one (CT3E) but without any plate material at the rear part of the stiffener, since this was decided to be removed by machining. The specimen was loaded with a 1.0 mm/min displacement rate. The crack initiated at a max-

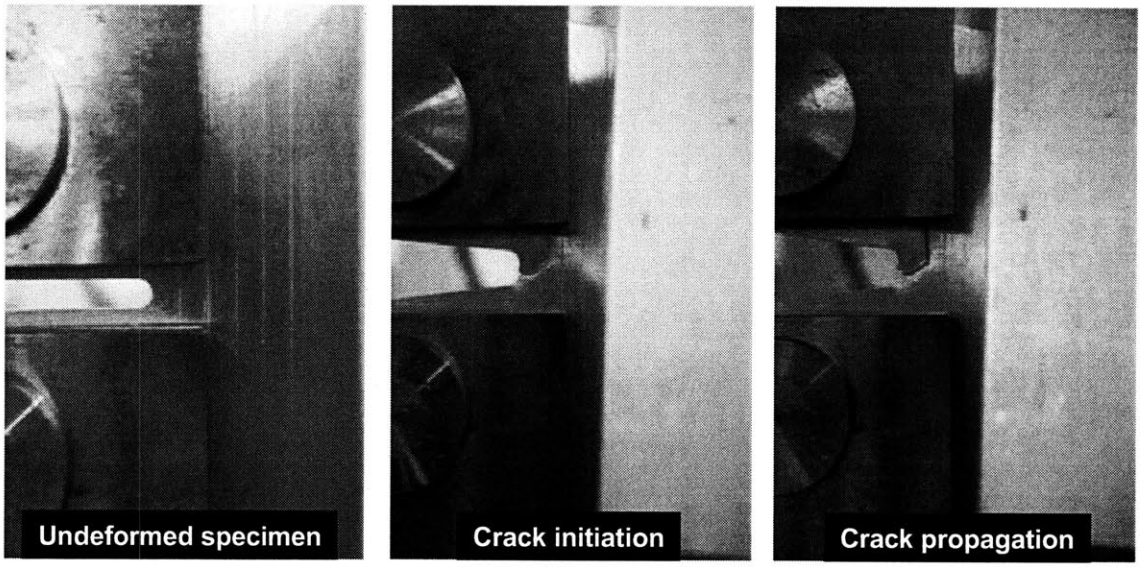

Figure 3-24: CT1E specimen with blunt initial crack tip and 20 × 120 × 4 mm plate material at the rear part of the T-type extruded stiffener. The crack pattern is characterized by crack initiation, flip, redirection, and propagation parallel to the loading direction

imum force of 4.63 kN corresponding to a 4.255 mm cross-head displacement to fracture. The crack initially propagated at an almost 90 degree angle with respect to the loading direction. While the crack propagated, it kinked with an almost 60 degrees angle. At almost 3/4 of the distance between the initial crack tip and the web of the stiffener (stereoscopic measurement showed 21.4 mm from the initial crack tip at a total distance of 31 mm), the crack redirected to a 90 degrees angle, and suddenly "paused". At that point, the crack flipped 180 degrees, re-initiated with a direction perpendicular (90 degrees) to the loading direction and propagated towards the web of the stiffener. At the foot of the stiffener the crack "paused" again in an effort to propagate through the stiffener, failed, redirected itself, and propagated parallel to the stiffener foot up to the point that the test stopped, Fig. 3-27.

Flatbar welded CT stiffened specimens

The flatbar welded specimens were tested for various displacement rates, initial crack lengths and plate material at the rear part of the stiffener. The specimens were cut from a larger welded structural configuration. The specimens presented minor differences in width and length

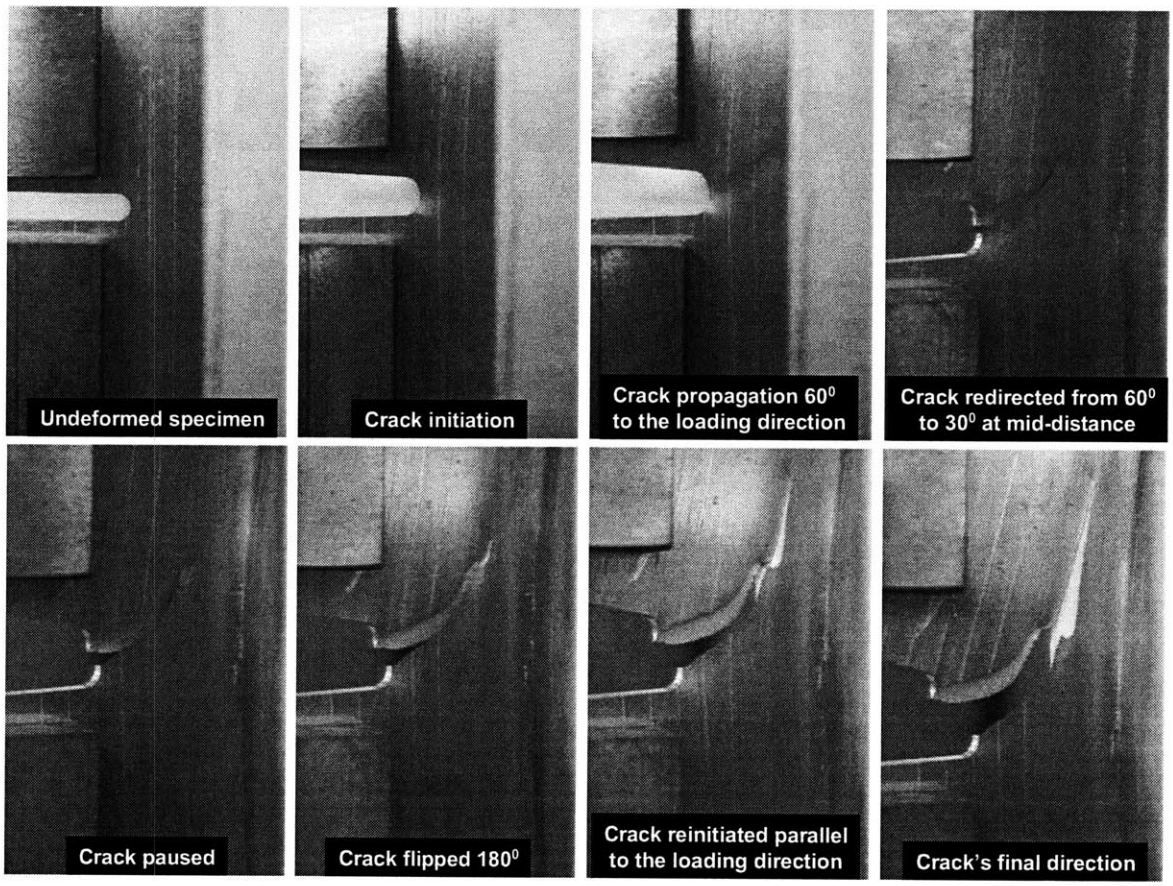

Figure 3-25: Stepwise crack propagation in CT2E specimen showing the phenomena observed: crack initiation, propagation with 60 degrees angle with respect to loading direction, pause and flip, reinitiation, redirection, and propagation parallel to loading direction

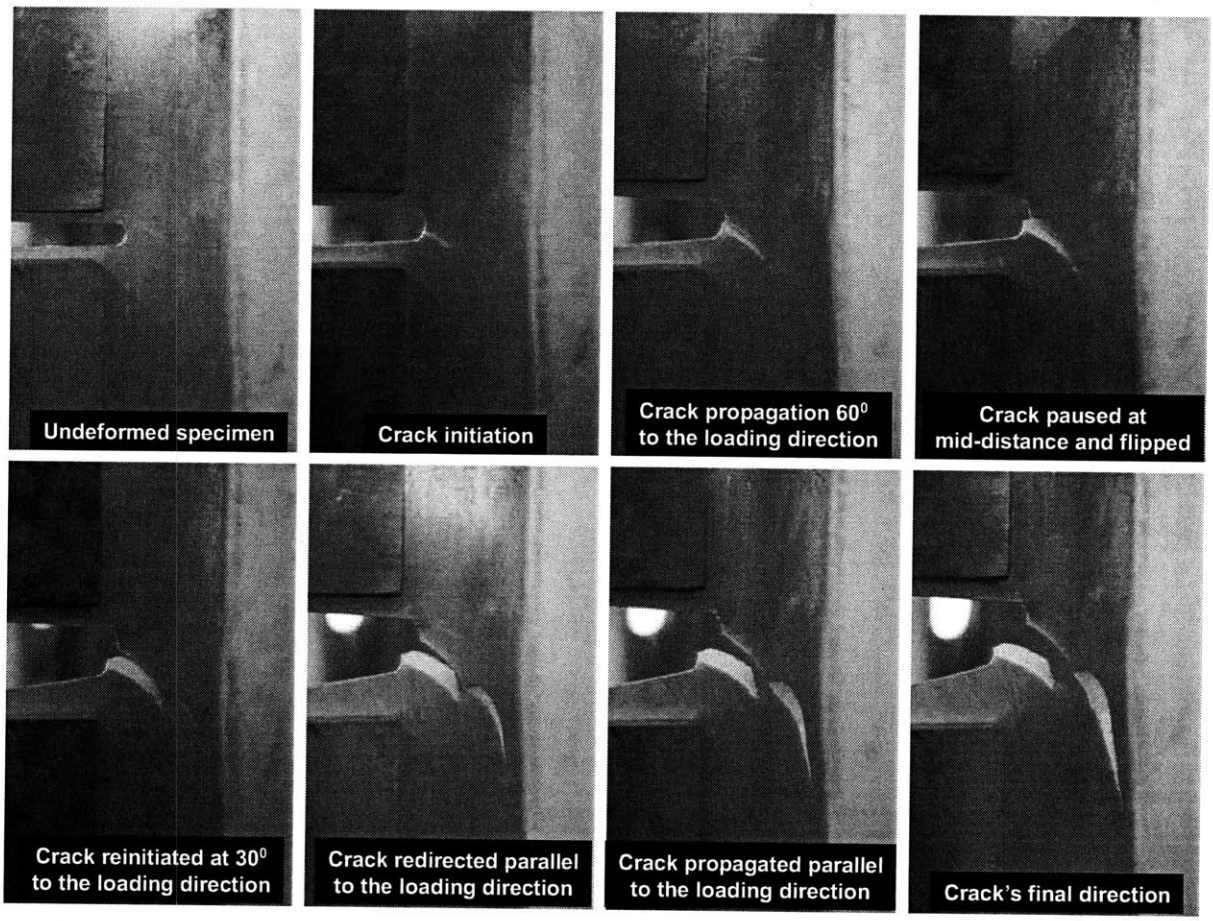

Figure 3-26: Stepwise crack propagation in CT3E specimen with extruded T-type stiffener showing the phenomena observed: crack propagation with 60 degrees angle with respect to the loading direction, pause, flip, reinitiation and redirection to 30 degrees to the loading direction, and propagation opposite to the loading direction

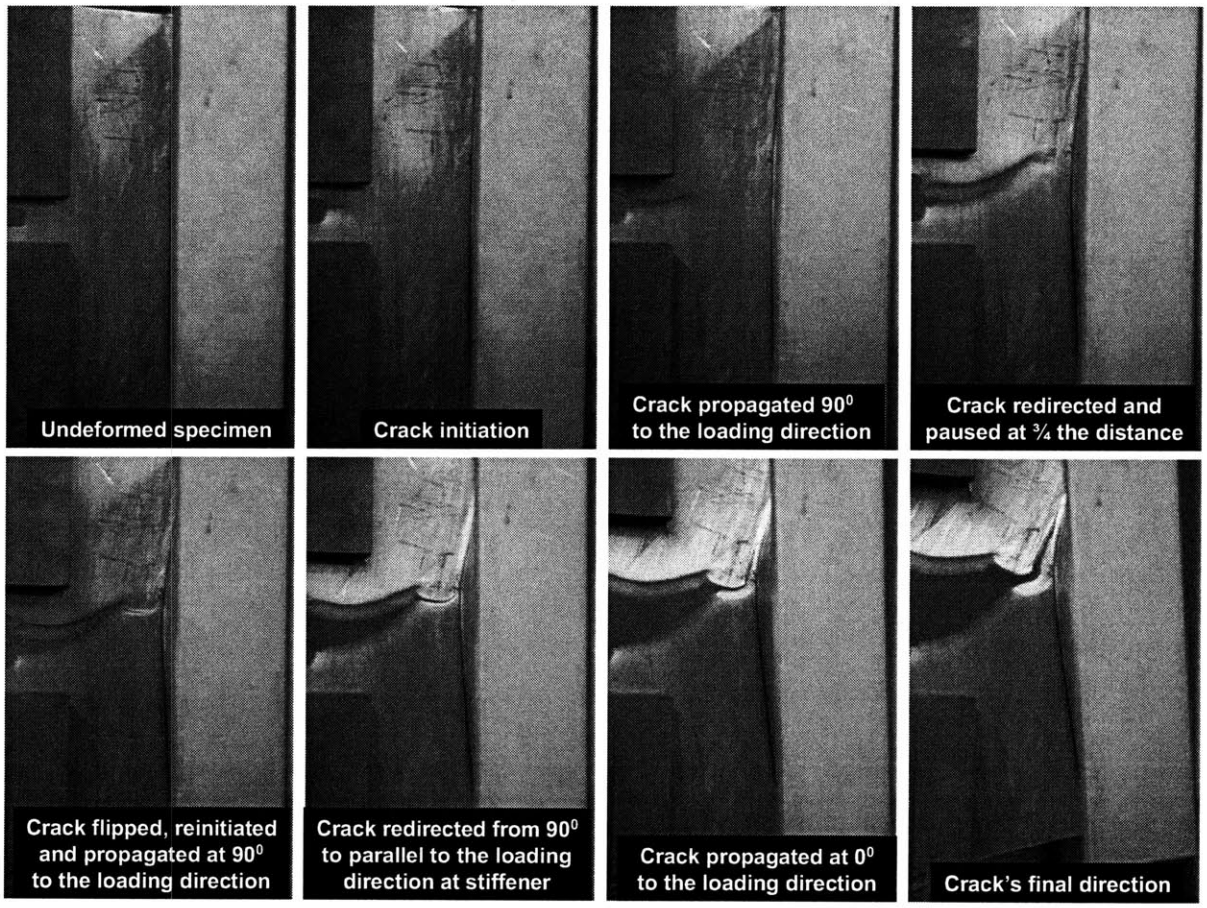

Figure 3-27: Stepwise crack propagation in T-type extruded stiffened specimen (CTEB) that has no plate material at the rear part of the stiffener showing the phenomena observed: crack propagation with 30 degrees angle with respect to the loading direction, pause, flip, reinitiation and redirection to 90 degrees to the loading direction, and propagation parallel to the loading direction

Specimen	Distance between crack & stiffener [mm]	Weldment Height [mm]	Weldment Width [mm]
CT1W	31.0	4.9	18.5
CT2W	33.4	4.9	18.3
CT3W	27.2	5.0	19.2
CT1WB	45.0	5.6	18.1
CT2WB	48.4	5.1	18.5

Table 3.7: Values of maximum force and displacement to fracture for the flatbar welded stiffened CT specimens tested

Specimen	Maximum Force [kN]	Displacement to fracture [mm]
CT1W	11.83	6.735
CT2W	3.85	5.822
CT3W	4.79	6.201
CT1WB	5.76	5.349
CT2WB	5.37	4.823

Table 3.8: Results of maximum value of force and displacement to fracture for the flatbar welded stiffened CT specimens tested

compared to the unstiffened specimens. The height and thickness of the web of the stiffener were similar to the extruded T-type stiffener, meaning thickness of $t_w = 3$ mm and height of $h_w = 40$ mm. Table 3.7 shows a detailed geometric description of the CTiW ($i = 1, 2, 3$) and CTiWB ($i = 1, 2$) specimens. Figure 3-28 shows pictures of the failed specimens.

The first test (specimen CT1W) had identical main dimensions to the unstiffened specimens with the exemption of the stiffener. The specimen was loaded at a displacement rate of 2.0 mm/ min. Table 3.8 shows the maximum force and displacement to fracture for each specimen. The crack initiated at a maximum force of 11.83 kN corresponding to a 6.735 mm cross-head displacement to fracture. Then, propagated at an initial 60 degree angle with respect to the loading direction and almost at 3/4 of the distance between the initial crack tip and the web of the stiffener (stereoscopic measurement shows 21.4 mm from the initial crack tip at a total distance of 31 mm), the crack redirected itself to a parallel direction with respect to the loading and propagated following this direction up to the point that the test stopped (see Fig. 3-29).

The second test (specimen CT2W) had similar main dimensions with the previous one

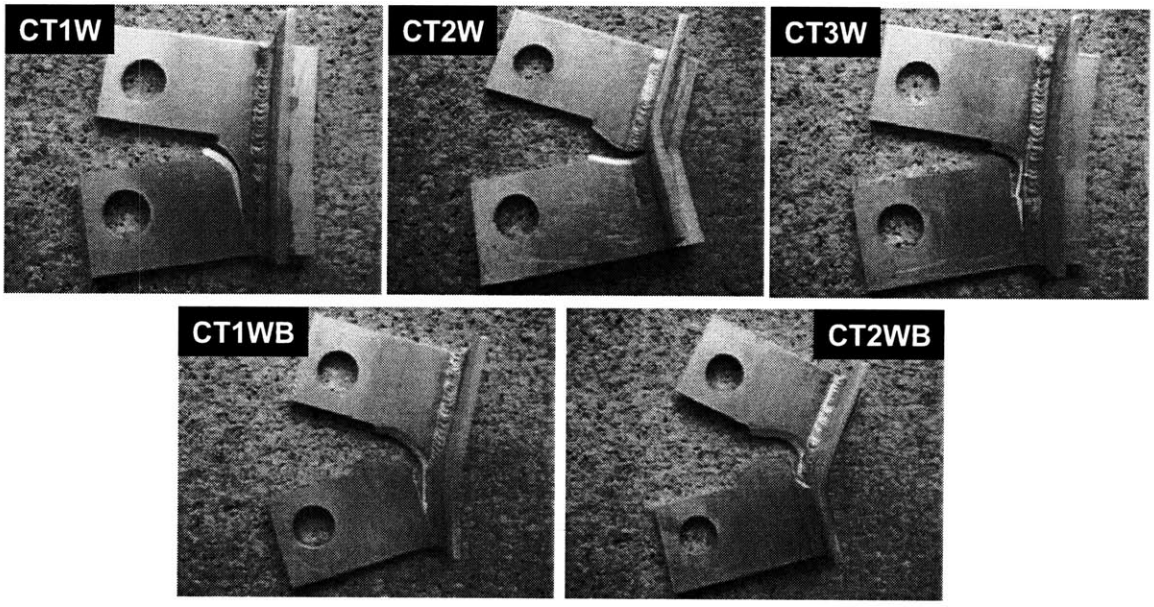

Figure 3-28: Final stage of stiffened CT specimen with welded flatbar stiffener. Note that the crack propagates through the stiffener in specimens labeled CT2W (enters through the weld while the crack reaches the stiffener) and CT2WB (enters through the weld with an angle during an intial failed attempt and while propagating opposite to the loading direction)

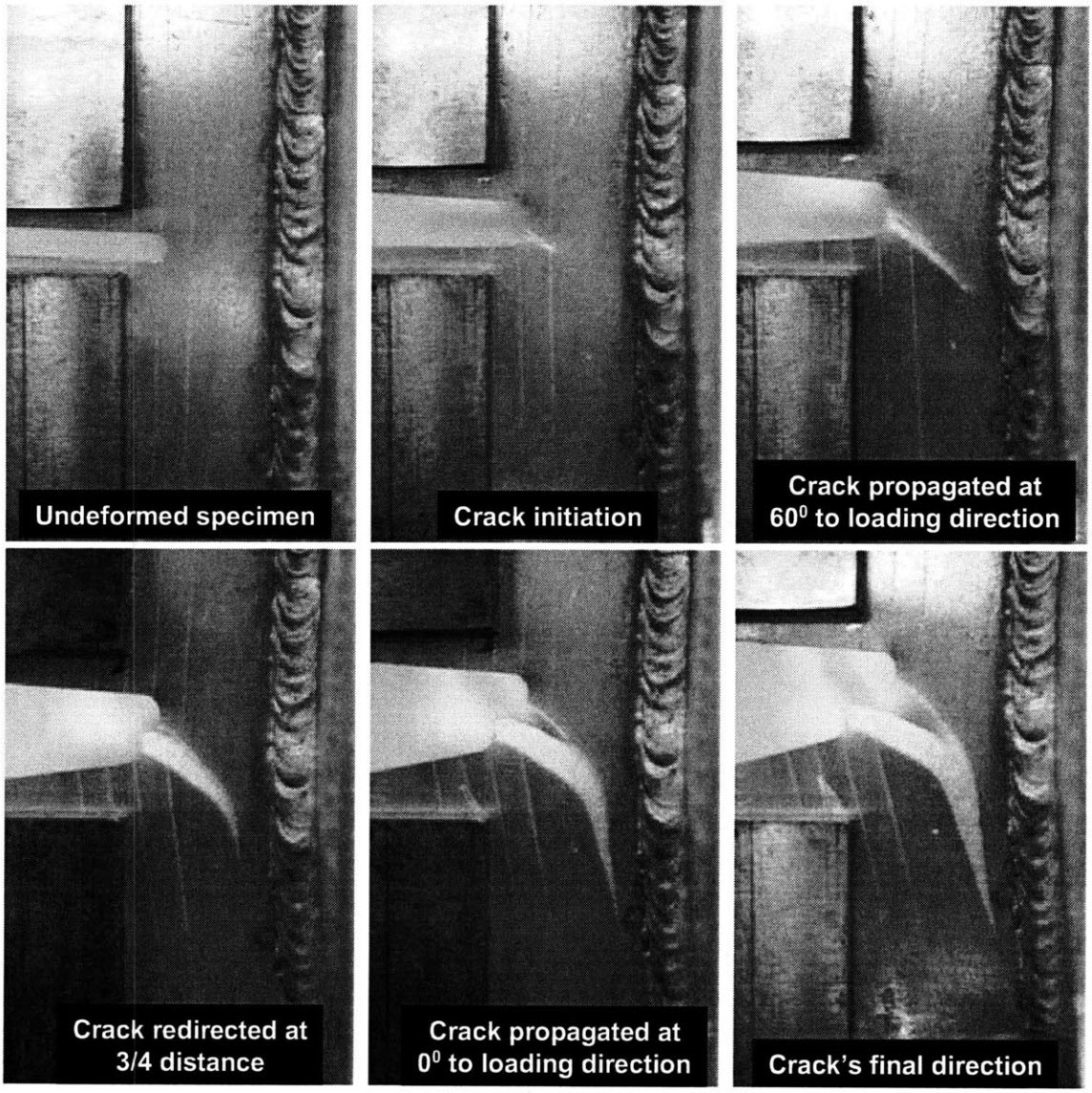

Figure 3-29: Stepwise crack propagation showing the phenomena observed at CT1W specimen: crack propagation with 60 degrees angle with respect to the loading direction and crack redirection to 180 degrees to the loading direction

(CT1W) but was loaded with a 0.5 mm/min displacement rate. The crack initiated at a maximum force of 3.85 kN corresponding to a 5.822 mm cross-head displacement to fracture. The crack propagated at an initial 60 degree angle with respect to the loading direction and almost at 3/4 of the distance between the initial crack tip and the web of the stiffener (stereoscopic measurement showed 22.6 mm from the initial crack tip at a total distance of 31 mm), the crack redirected itself to a direction perpendicular with respect to the loading and propagated through the weld. One can observe that the crack then propagated concurrently at the stiffener and the rear plate material travelling with the same growth rate, meaning that the growth rate of the crack on the stiffener web was similar to the growth rate of the crack that propagated at the rear plate material (see Fig. 3-30).

Specimen CT3W had similar main dimensions with the first specimen (CT1W) tested but is loaded with a 1.0 mm/min displacement rate. The crack initiated at a maximum force of 4.79 kN corresponding to a 6.201 mm displacement to fracture. The crack pattern was similar to specimen CT1W.

Specimen CT1WB had similar main dimensions with the previous ones but did not have any additional material at the rear part of the stiffener and it was loaded with a 1.0 mm/min displacement rate. The crack initiated at a maximum force of 5.76 kN corresponding to a 5.349 mm displacement to fracture. The crack propagated at an initial 60 degree angle with respect to the loading direction up to the foot of the stiffener where initially the crack "failed" to propagate through the stiffener and redirected itself to a direction parallel with respect to the loading following this direction up to the point that the test stopped (see Fig. 3-31).

The last test (specimen CT2WB) had similar dimensions with the previous one (CT1WB) and also did not have any additional material at the rear part of the stiffener. It was loaded at a displacement rate of 1.5 mm/min. The crack initiated at a maximum force of 5.37 kN corresponding to a 4.823 mm cross-head displacement to fracture. The crack propagated at an initial 30 degree angle with respect to the loading direction and at the mid-distance between the initial crack tip and the stiffener redirected itself perpendicular to the loading direction up to the foot of the stiffener where initially the crack "failed" to propagate through the stiffener and redirected itself to a direction parallel with respect to the loading following initially this direction. Once it had propagated for almost 5 mm, the crack penetrated through the weld

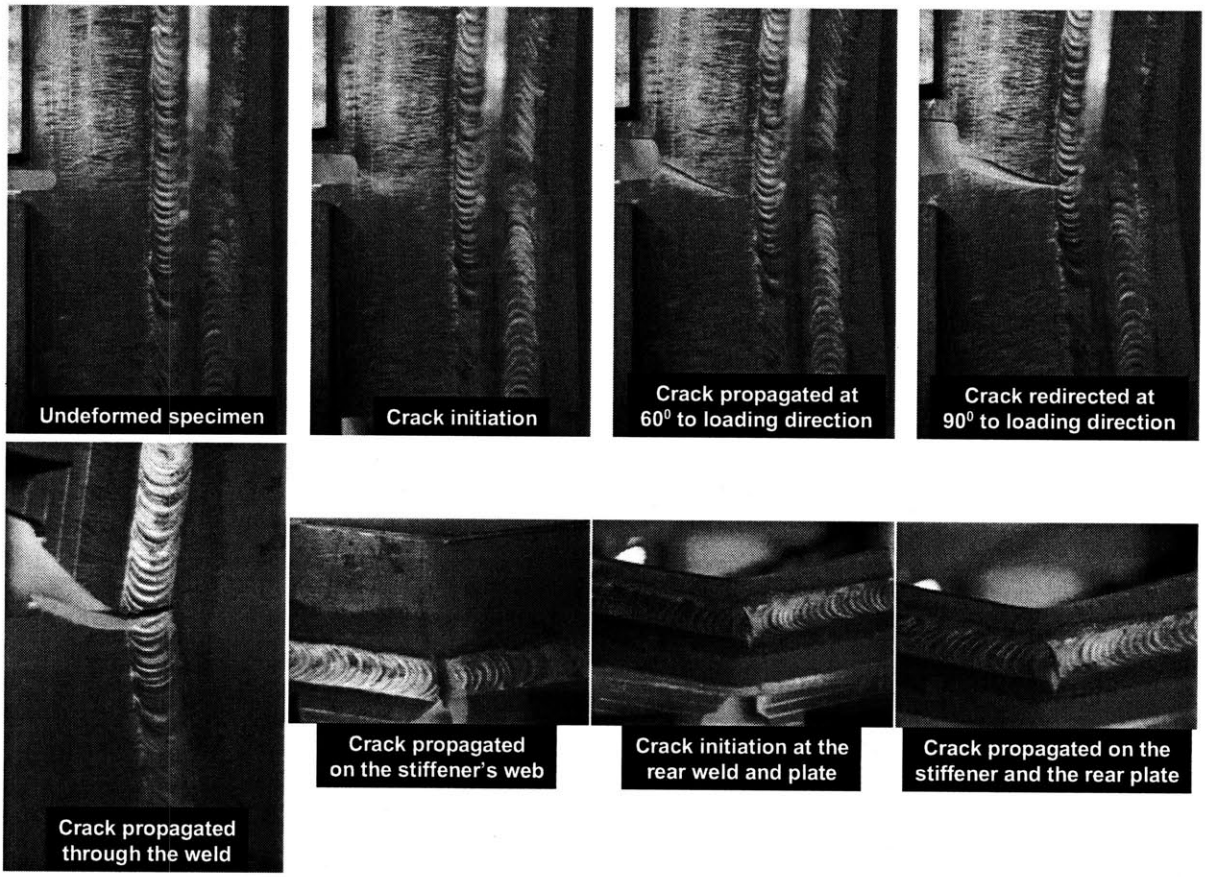

Figure 3-30: Stepwise crack propagation showing the phenomena observed at CT2W specimen: crack propagation with 30 degrees angle with respect to the loading direction, crack kinking to a direction perpendicular to the loading, propagation through the weld and the stiffener, and, simultaneous propagation on the stiffener and the rear plate material with similar growth rate

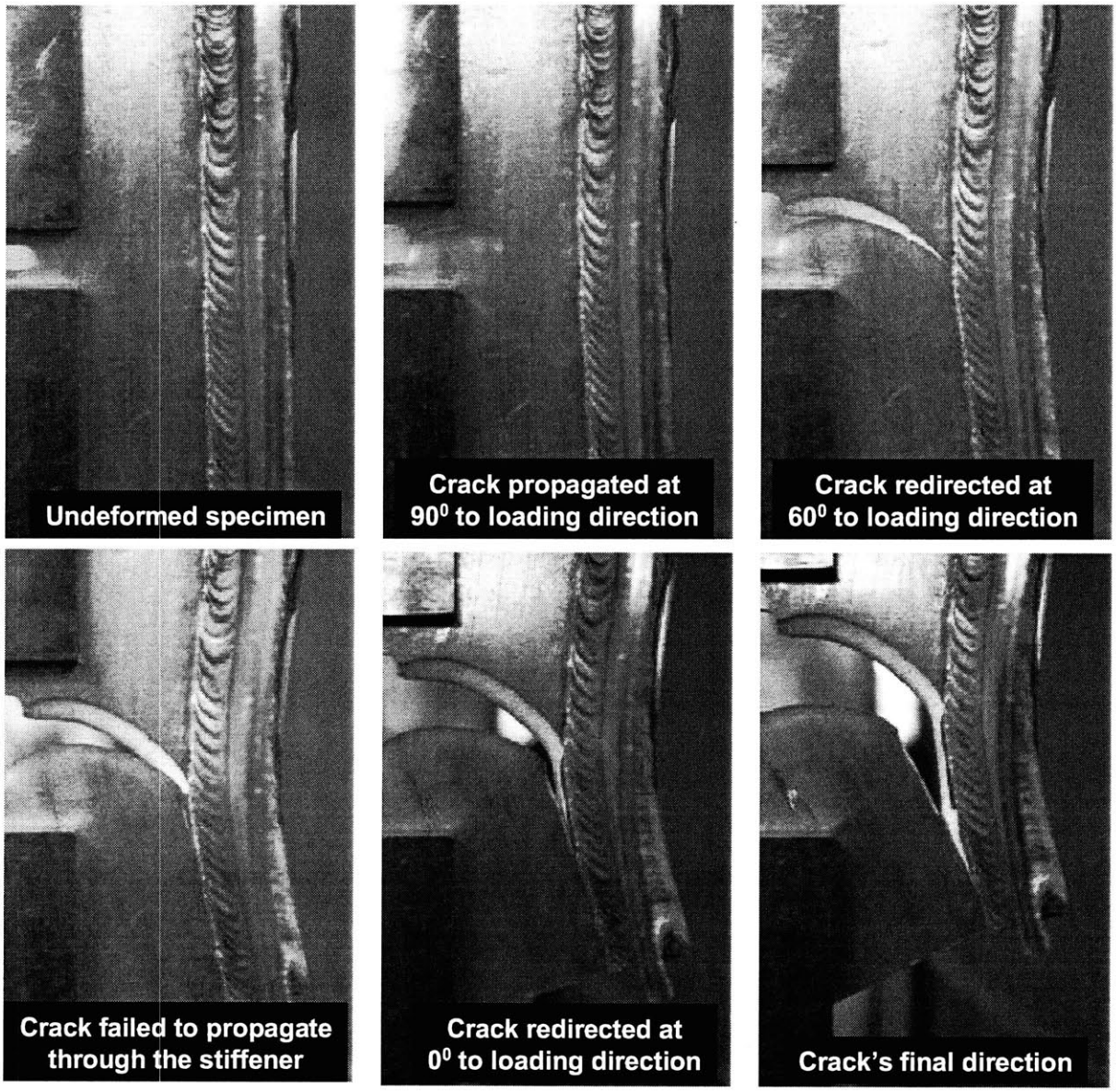

Figure 3-31: Stepwise crack propagation showing the phenomena observed at CT2WB specimen: crack propagation with 60 degrees angle with respect to the loading direction, failure to propagate through the stiffener and 180 degrees redirection with respect to the loading direction

and the stiffener, following a similar pattern to the CT2W specimen up to the point that the test stopped (see Fig. 3-32).

Figure 3-33 shows the load-displacement curves of all the experiments. It can be observed that the crack pattern regarding success or failure in propagation through the stiffener is not related to the amount of work needed but it is mainly a function of the physical characteristics of the crack, the stiffening configuration, the type of the stiffener and the quality of the manufacturing process.

3.4.4 Phenomena observed

Crack initiation

The initiation of a crack is indeed one of the major parameters because the consequences of the incident may change dramatically upon this effect. McClintock [176] studied the combined effects of root radius, stress, crack growth and rate on fracture instability of metallic materials. Conditions of plane stress dominate in very thin plates where it can be assumed that the transverse stress σ_z is zero through the plate thickness. On the other hand, for thick plates, the state of stress is primarily that of plane strain. The type of plastic deformation associated with these two cases is shown in Fig. 3-34. Under plane stress, slip takes place on 45 degrees planes, producing a rather large strain through the thickness, while in plane strain, slip occurs on planes perpendicular to the plate surface, giving a hinge-type deformation pattern. Zuidema and Blaauw [364] had observed that aluminum alloys often show regions of fatigue fracture surfaces which are inclined at about 45 degrees to the plate surface.

The size of plastic zone relative to the thickness of the body influences whether the crack tip state of stress is essentially plane stress, plane strain, or a combination of the two. Conversely, the type of stress field dictates the size of the plastic zone. The classification of the stress field is not a simple task, particularly in light of the fact that tranction-free lateral surfaces of the body are in a state of plane stress. The thickness of the specimen relative to the size of the plastic zone, therefore influences the state of stress and the deformation within the zone. Consequently, the fracture characteristics of the specimen can also be expected to depend upon its thickness. Crack initiation followed similar formation in almost all cases, Fig. 3-35.

For very small thicknesses, the loss of triaxiality contributes to an apparent increase in the

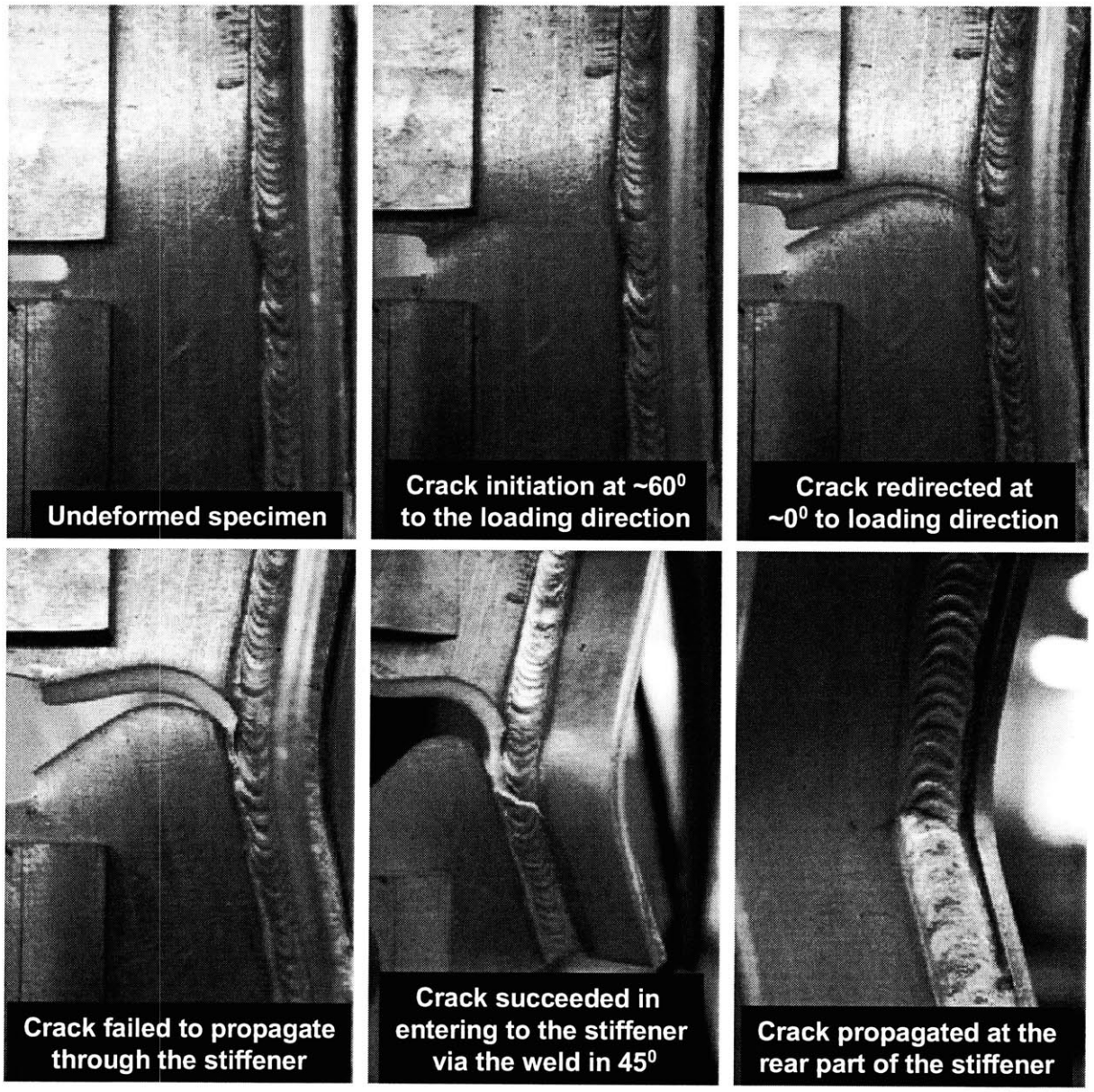

Figure 3-32: Stepwise crack propagation showing the phenomena observed at CT2WB specimen: crack propagation with 60 degrees angle with respect to the loading direction, kinking to a direction perpendicular to the loading, initial failure to propagate through the weld and the stiffener, propagations opposite to the loading direction, success to propagate through the weld and the stiffener with an angle, and, propagations simultaneously at the stiffener and the rear plate material with similar growth rate

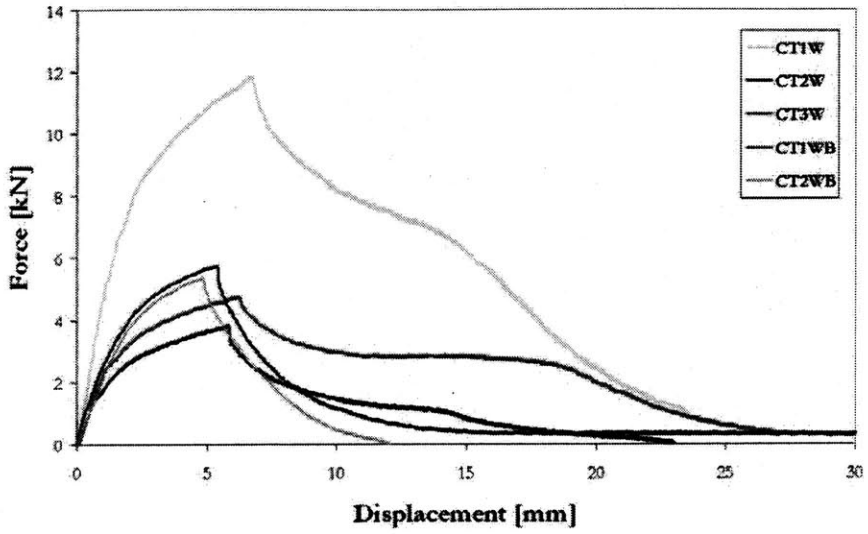

Figure 3-33: Load vs. displacement graph for the welded flatbar stiffened CT specimens

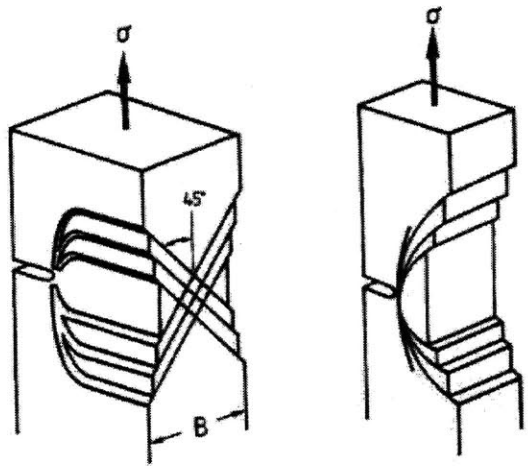

Figure 3-34: Slip-planes around a mode-I crack for plane stress (left) and plane strain (right), Gdoutos [83]

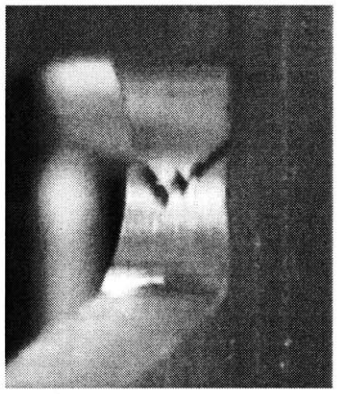

Figure 3-35: Formation of the onset of a crack observed at the experiments

ductility and, hence in the fracture resistance. In this case, the fracture surfaces are slanted at 45 degrees to the specimen's surfaces and are composed entirely of shear lips.

Crack propagation

A crack in an engineering structure will generally grow in a plane normal to the maximum principal stress. If the original crack orientation does not coincide with such a plane, a smooth adjustment occurs after initial kinking, i.e. change of direction, which is abrupt at the small scale of yielding. Kinking is a result of incipient crack growth under mixed mode loading. Under small scale yielding conditions, cracks in plates appear to grow with local mode I symmetry at the crack edge, except when mode I growth is suppressed by a sufficiently high superposed pressure [30].

The crack propagation is important to be properly modeled as the resistance of the structure following crack initiation is highly dependent on the crack pattern. Figure 3-36 shows results concerning crack tip geometry. The extent of damage and impact forces on a marine structure are very sensitive to the initiation and propagation of cracks. The micro-mechanics of the crack formation and propagation is normally of less direct interest in marine structural analyses. Therefore, naval architecture uses fracture criteria which do not provide in-depth information concerning the micro-mechanics of cracks. If the macroscopic behavior of the whole structure is predicted satisfactorily, a correct global structural response will be obtained. It is important to discuss about the crack propagation at the welded flatbar CT specimens and the effect of

failure and success of the crack to propagate through the stiffener. A closer view of this type of specimens revealed that the crack propagated through the stiffener when the stiffener deformed and the point of entrance was the location where the stiffener presented maximum deformation (CT2W and CT2WB). The rest of the specimens presented minor or no deformation of the stiffener and the crack failed to propagate through the web. Especially at the case of CT1W, where the stiffener remained intact, the crack did not even approach the welding and was redirected, showing the maximum applied force to fracture.

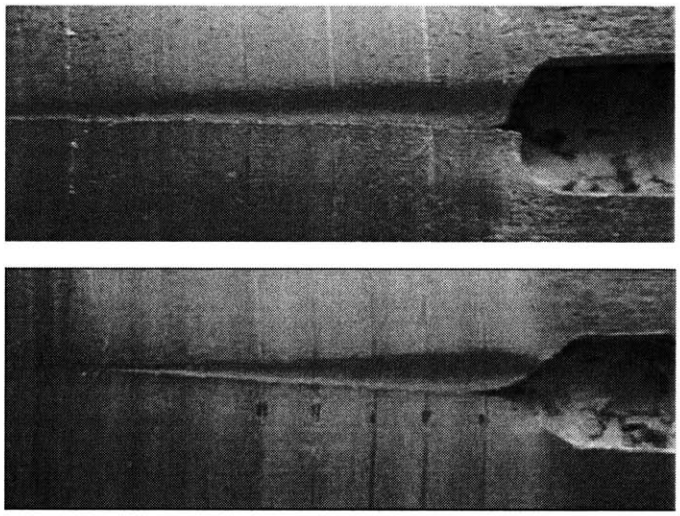

Figure 3-36: Comparison of crack initiation and propagation between two different crack tip geometries examined, blunt (top) and sharp (bottom)

Similar fracture mode, slant fracture, was observed by Forsyth, [69]. The fast fatigue crack advances may be explained by the preceding plastic deformation of material at the crack tip, i.e., damage accumulation in the process. This is shown schematically in Fig. 3-37, where the crack propagation becomes macroscopically discrete with the transition of the crack plane from the direction normal to loading (to the maximum principal stress) to a direction inclined at about 45 degrees to that in the final cycles.

This phenomenon, often observed in stable tearing crack growth experiments on thin plate specimens made of ductile materials (e.g., aluminum alloys), is that a crack tends to grow in slant mode at the initiation or during the propagation phase. This behavior has been reported widely in fatigue experiments (Rickerby and Fenici [258]; Zuidema and Blaauw [364]; Zehnder et

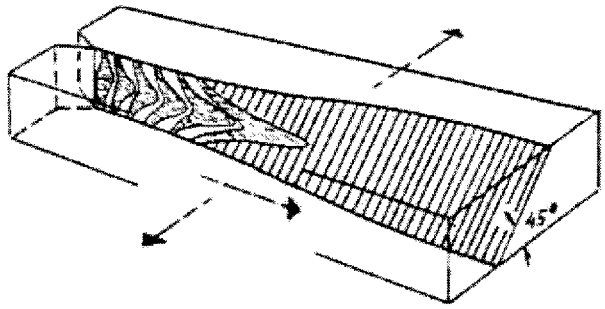

Figure 3-37: Transition of the crack plane (Forsyth [69])

al. [352]; Richard et al. [256]), and stable tearing experiments (Meyn et al. [182]; Narasimhan et al. [190]; Mahmoud and Lease [164]; Simonsen and Tőrnqvist [289]).

Experiments on compact tension or CT specimens with initial slant cracks have also been carried our for different ductile materials, for instance steel (Kumar and Hirth [144]) and aluminum alloys (Manoharan [167]). An investigation has been performed by Mahgoub et al. [163] to understand the mechanics of slant fracture, using three-dimensional finite element analyses of selected Al 2024-T3 specimen geometries with initial flat and slant cracks under nominal Mode I condition. Finally, James and Newman Jr. [117] examined experimentally the effect of crack tunneling on crack growth on 2024-T351 aluminum alloy plate.

Sumi et al. [297] examined experimentally and developed a numerical method of analyzing the characteristics of fatigue crack propagation and the remaining life assessment of ship structures focusing on a curved crack path due to the effects of welds, complicated stress distributions at three-dimensional structural joints and structural redundancy. For both theory and experiments, the cracks tend to form and become unstable at lower stresses, the longer the crack, as stated also by McClintock [175]. Figure 3-38 shows a schematic of the expected crack pattern for the stiffened CT specimens. It shows that the crack pattern is related to the amount of plate material at the rear part of the stiffener and follows specific paths that can be mapped. The stiffener type and the stiffening configuration are of primary importance for the crack propagation.

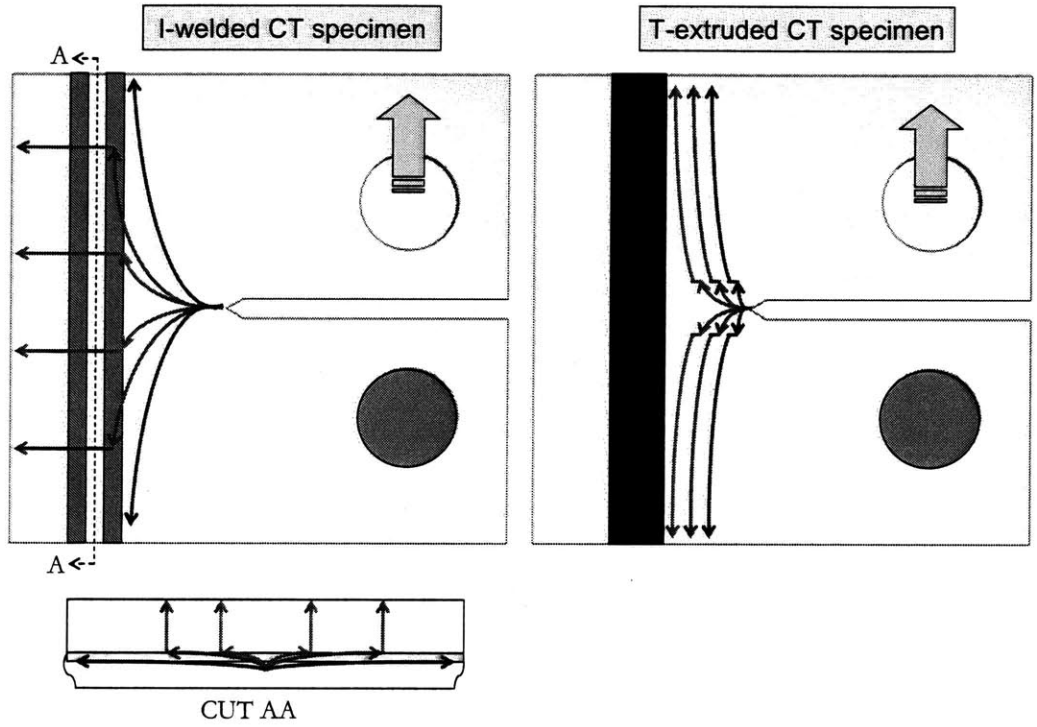

Figure 3-38: Conceptual schematic of the possible crack pattern in stiffened CT specimens as a function of the plate material at the rear part of the stiffening configuration

3.5 Group III: Intermediate-scale Tests

Standards related to fracture mechanics testing (issued by ISO, ASTM, etc.) are inappropriate for the examination of crack initiation and propagation in intermediate and large-scale structures. The existing specimen guidelines described within these standards are commonly used to investigate material fracture toughness caused by fatigue and are typically 25 mm thick.

Scaling effects should always be addressed during the evaluation of the experimental analyses, for a set of tests to be as complete as possible. In contrast to fluid mechanics, the problems of scaling and size in solid mechanics have not come to the forefront of attention until late in the last century. The classical view that any observed size effect was statistical was reversed during the 1980's. Ductile materials might exhibit size effects on the mean structural strength that are deterministic in nature, being caused by stress redistribution and energy release associated with stable propagation of large fractures or with formation of large zones of distributed cracking.

While the motivation for the development of these blast resistant structures originated for naval defense projects, there is a transfer potential for internal and external explosions to other sectors of the industry. If it is envisioned that there will be impacts on steel weight and production costs, these should be noted as well. Park and Cho [223] proposed practical yet accurate formulae to predict the structural damage of rectangular unstiffened and stiffened plates under explosion loads, with emphasis on simplicity.

The scaled specimens were designed to meet the limitations of the experimental apparatus. The outcome of the calculations yielded specimens that could be called full-scale. It was decided instead to categorize them in the intermediate-scale, compared to the large size of marine structures, such as the size of a vessel. Due to the scarcity of material, we examined only the extruded case.

3.5.1 Double Edge Notched Tension (DENT) specimen

The first type of specimen tested was a version of the "dogbone" specimen used in Group I of the experiments but with increased dimensions and two artificial edge notches, each one having initial length of 22.5 mm, which were machined prior to testing. A schematic of the DENT specimen is shown in Fig. 3-39. The specimen was mounted on the MTS device using a fixture

designed specifically for the intermediate-scale specimens (see Fig. 3-40). Two cracks were initiated at both notches but it was observed that one of the cracks propagated at a greater distance compared to the opposite crack and they finally coalesced. The cracks initiated at different initial angles having an 180 degrees difference between them with respect to the tunneling angle. The crack propagated with a very high growth rate. The crack path coalescenced the two artificial cracks and it was perpendicular to the loading direction.

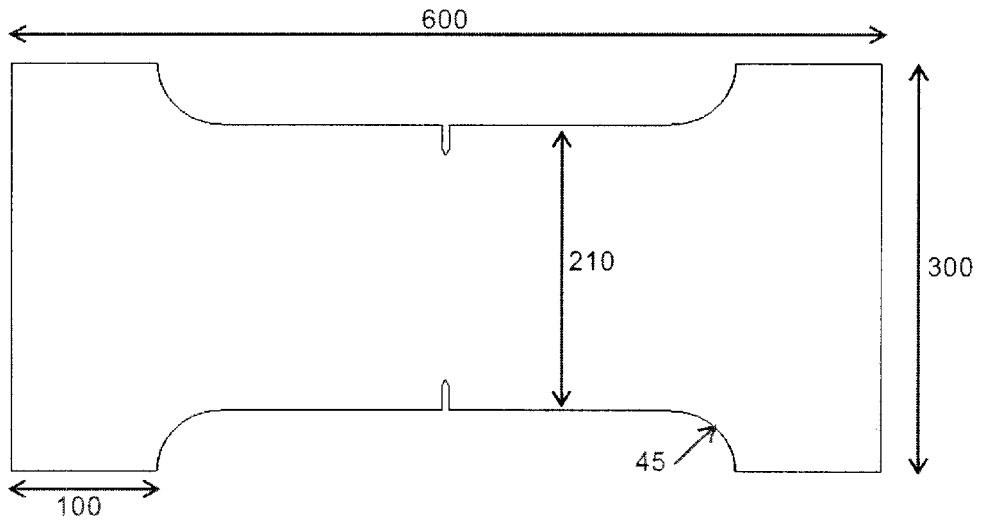

Figure 3-39: Double Edge Notched Tension (DENT) specimen geometry subjected to quasi-static uniaxial tensile loading (dimensions in mm)

The duration of the test was 726 seconds (from test initiation up to the failure of the specimen) and the displacement rate for this test was 0.5 mm/min. Figure 3-41 shows the load vs. displacement curve obtained from the test. The phenomena observed during this test can also be well visualized through a stepwise examination of this graph. The maximum force of 154.98 kN and cross-head displacement of 5.237 mm corresponds to the onset of fracture. The second "knee" of the graph, corresponds to a force of 65.16 kN and 5.486 mm cross-head displacement, where the crack propagated and at a force of 45.41 kN and 5.995 mm cross-head displacement the onset of the opposite crack commenced and the cracks coalescenced which resulted in specimen failure. Data were obtained in 1 s increments.

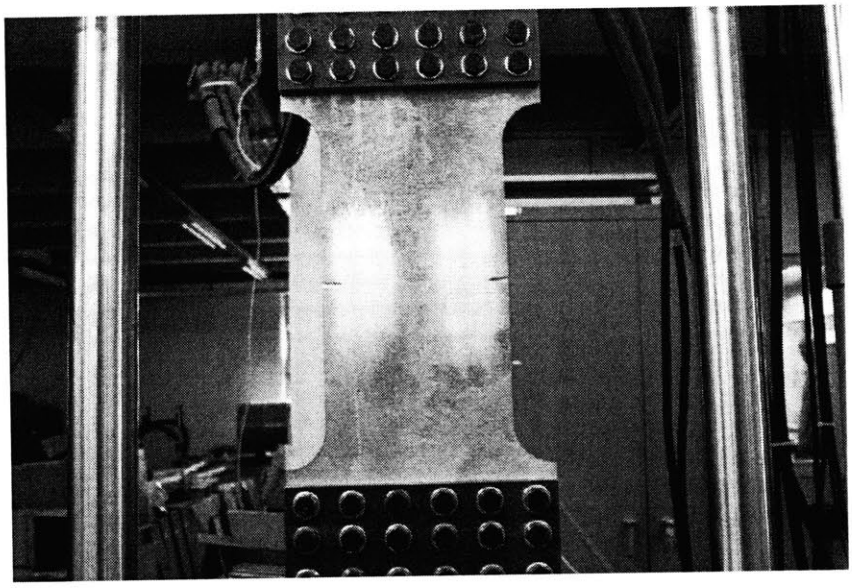

Figure 3-40: Experimental setup for the testing of the Double Edge Notched Tension (DENT) specimen

3.5.2 Single Stiffened Double Edge Notched Tension (SSDENT) specimen

This experiment was similar to the previous one (DENT) with the existence of a T-type extruded stiffener installed in the center of the specimen, as shown in Fig. 3-42. The stiffener was machined at both ends to avoid any interference with the fixture. A schematic of the SSDENT specimen is shown in Fig. 3-43, where the geometric characteristics of the specimen are presented.

Prior to the onset of fracture, the specimen presented out-of-plane deformation due to the existence of the stiffener. At the point of maximum deformation the onset of fracture occurs. The phenomena that followed (see Fig. 3-44) can be summarized as follows:

(i) at a force of 141.23 kN and 7.993 mm cross-head displacement the onset of fracture was observed at one of the artificial cracks,

(ii) at a force of 142.78 kN and 11.447 mm cross-head displacement, and after the crack had covered a distance of 25 mm at an angle of 60 degrees with respect to the loading direction, flipped and redirected itself,

(iii) at a force of 139.71 kN and 13.066 mm cross-head displacement, and while the first

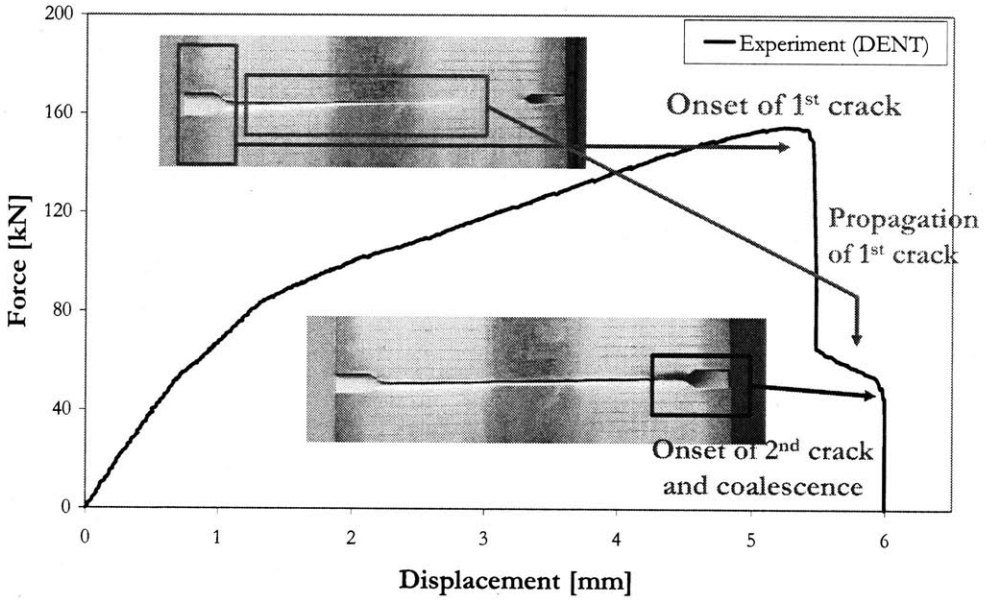

Figure 3-41: Force vs. displacement graph of the Double Edge Notched Tension (DENT) specimen

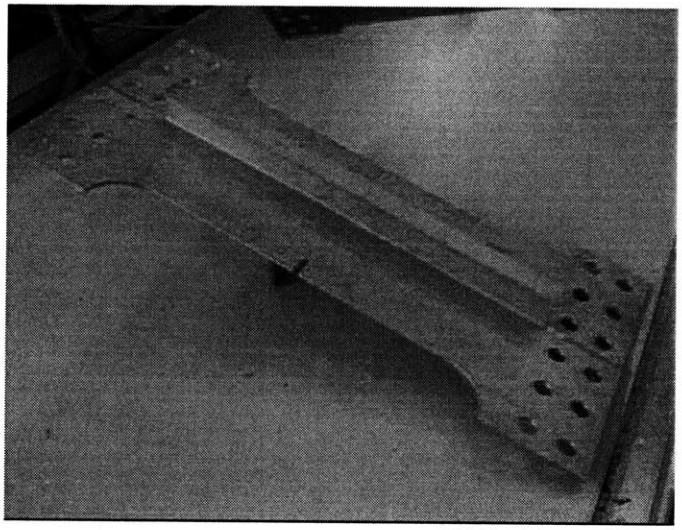

Figure 3-42: Intact Single Stiffened Double Edge Notched Tension (SSDENT) specimen prior to testing

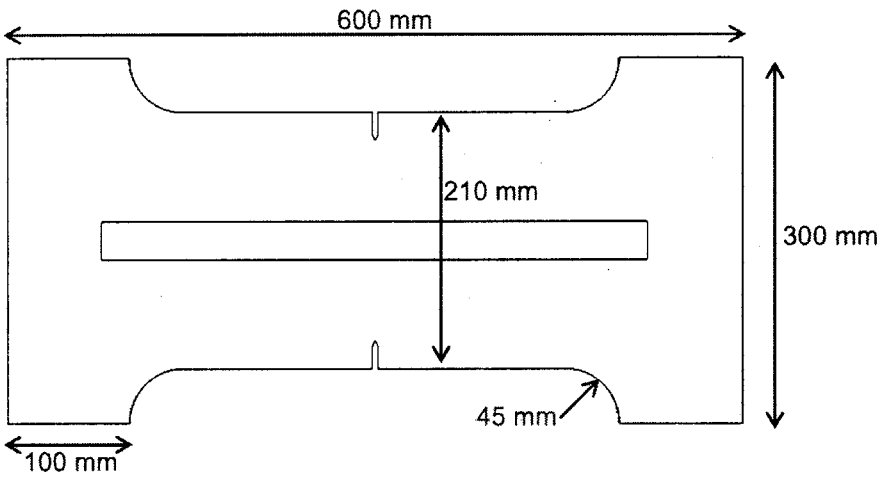

Figure 3-43: Single Stiffened Double Edge Notched Tension (SSDENT) specimen geometry subjected to quasi-static uniaxial tensile loading (dimensions in mm)

crack had traveled for 31 mm the onset of fracture occurred at the second notch and propagated with a similar initial angle of 60 degrees with respect to the loading direction,

(iv) at a force of 129.70 kN and 13.987 mm cross-head displacement the first crack had propagated almost all the way up to the foot of the stiffener and the second crack flipped and redirected itself,

(v) the second crack propagated for a distance of 26 mm where it redirected towards to the coalescence point and at a force of 105.29 kN and 14.478 mm cross-head displacement the cracks coalescenced and the single crack propagated on the stiffener, and

(vi) at a force of 62.20 kN and 14.694 mm cross-head displacement the crack completed its propagation on the web of the stiffener, reached the flange of the stiffener and fracture of the flange occurred. The test was then interrupted.

The duration of the test was 1765 seconds (from test initiation up to the point that the crack reached the flange of the stiffener) and the displacement rate for this test was 0.5 mm/min. The corresponding load vs. displacement curve is shown in Fig. 3-45. This stepwise process can be clearly observed at the graph, and for visualization purposes photographs taken during the experiment (every 15 s) present the series of events. Data were obtained in 1 s increments.

Observations often show that cracks and micro-cracks growing in the same plane appear

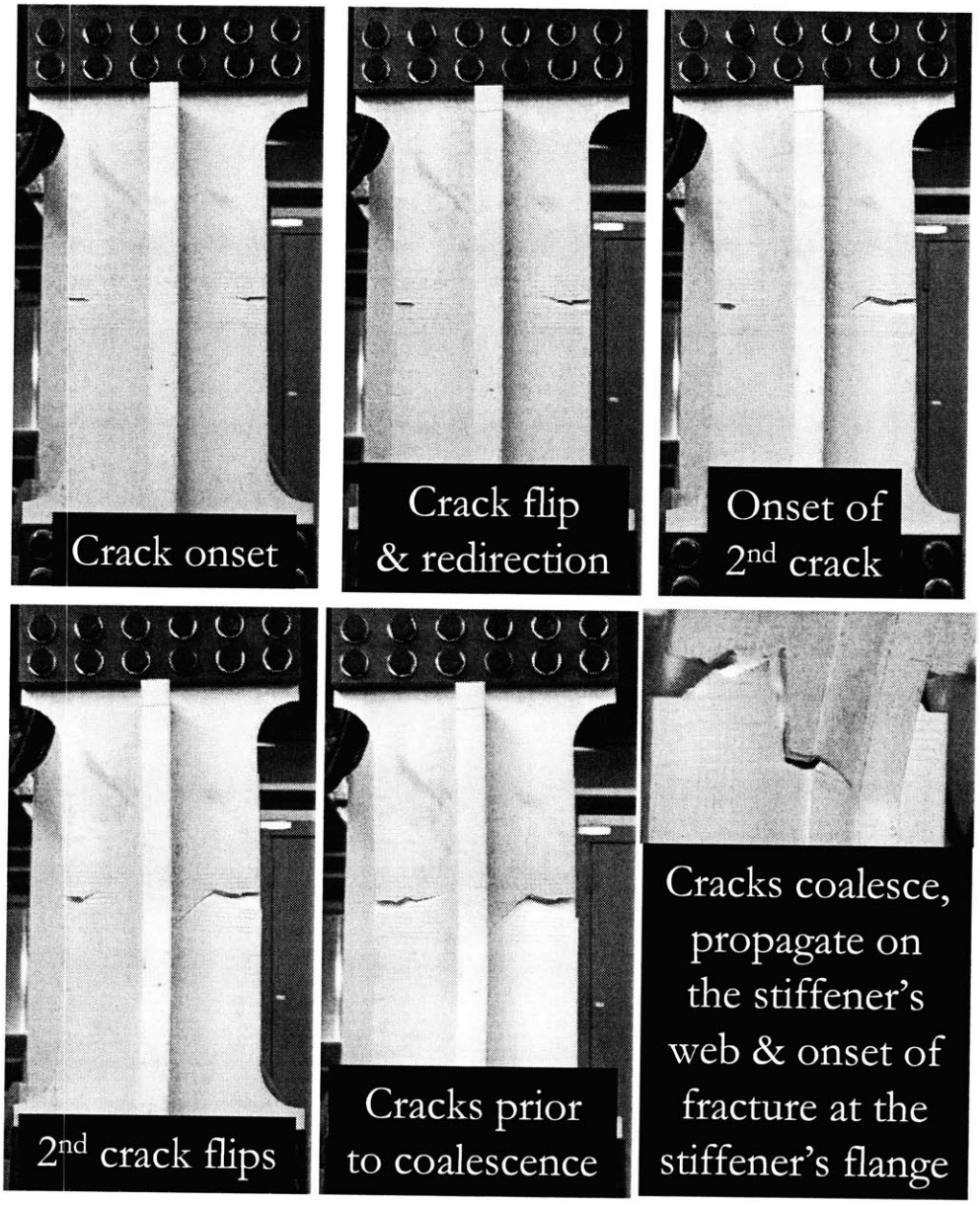

Figure 3-44: Series of photographs taken during the test of the SSDENT specimen. The phenomena observed can be summarized at the following phases: onset of fracture at the artificial crack on the right after the completion of the out-of-plane deformation, crack on the right flipped and redirected itself, onset of fracture on the artificial crack on the left, flipping and redirection of the crack on the left , both cracks propagated in order to coalensce at the web of the stiffener, and, cracks coalescence, propagation on the web of the stiffener and onset of fracture at the flange of the stiffener (side close-view photograph)

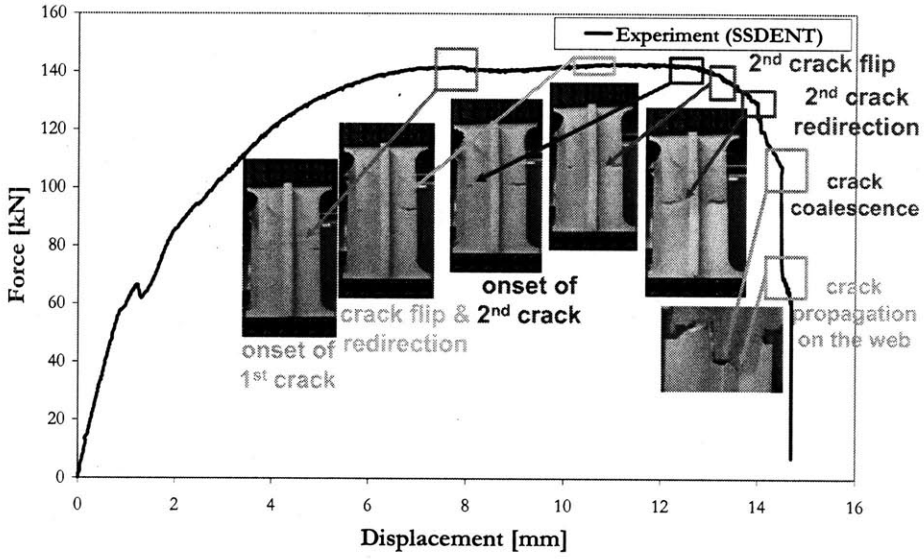

Figure 3-45: Force vs. displacement graph for the SSDENT specimen

to avoid each other rather than coalesce edge to edge (Broberg, [30]). The symmetry is quite typical in experiments and because the cracks usually obtain a high velocity, both cross-fractures become completed, so that the small piece in the middle becomes cut out.

3.5.3 Center Cracked Tension (CCT) specimen

Prior to the examination of the behavior of the twin stiffened specimen an unstiffened center cracked tension (CCT) specimen with similar dimensions was tested under displacement-control conditions (see Fig. 3-46). This test was similar to the previous ones but the geometry of the CCT specimen differed slightly to the DENT one concerning the width of the plate machined (see Fig. 3-47). During this test the only phenomenon observed was the crack initiation at both ends of the artificial central crack of 44.5 mm initial length and its propagation at both sides. The maximum load was 150.95 kN at a cross-head displacement of 3.910 mm. The duration of the test was 553 seconds (from test initiation up to the failure of the specimen) and the displacement rate for this test was 0.5 mm/ min. Data were obtained in 1 s increments.

Figure 3-48 shows the experimental data obtained from the test on the CCT specimen. The relationship between the applied force vs. the cross-head displacement shows the three main observations during this case, which are the initial deformation a the center of the artificial crack, initiation at both crack tips and the failure of the specimen while the crack on the left propagated all the way through the plate.

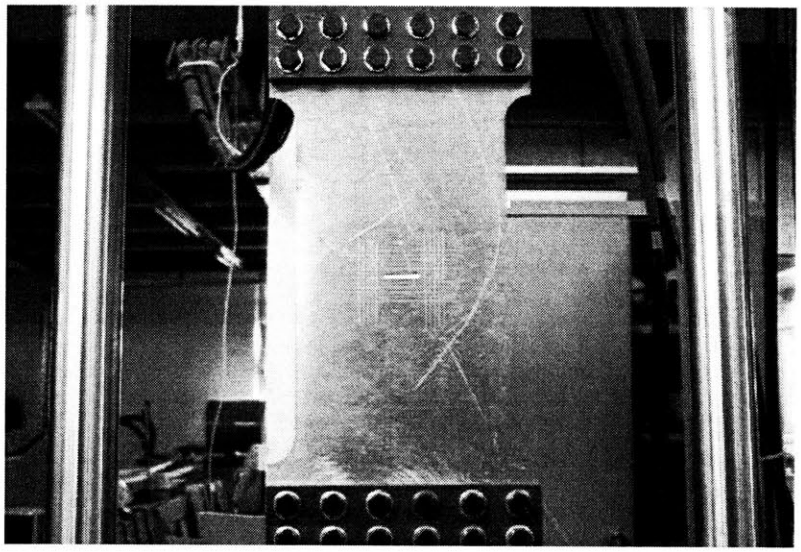

Figure 3-46: Center Cracked Tension (CCT) specimen prior to testing mounted on the MTS device

Similar tests to the ones described were performed by Galatolo and Lanciotti [79] on welded small CT and large-scale CCT aluminum specimens. The specimens were made from aluminum alloy 2219−T851 a commonly used material in the aerospace industry. Two cases were examined, with the welding either parallel or perpendicular to the loading direction. Their objective was to evaluate the fatigue fracture mechanics properties, principally the crack propagation rate of plasma welded aluminum joints. The residual stresses were measured in cracked and uncracked plates by means of strain gauges. Their results showed that the crack propagated along the weld bead, in the heat-affected zone, as the residual stress effect was quite low, while the crack propagation rate in the CT specimens was lower than that in the CCT ones in the case of a crack which propagates perpendicular to the weld bread. Finally, tests performed by Paik and Thayamballi [210] on steel CCT specimens showed same crack pattern with the one

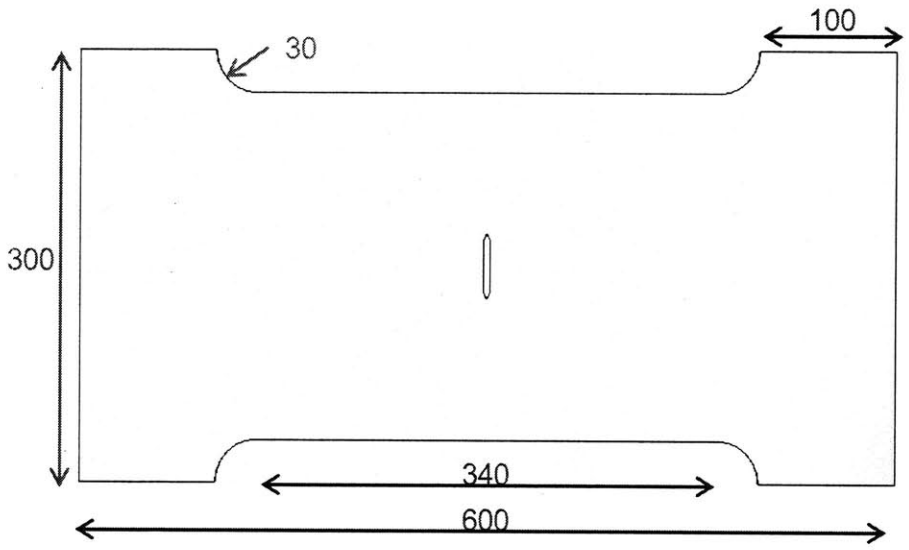

Figure 3-47: CCT specimen geometry subjected to quasi-static uniaxial tensile loading (dimensions in mm)

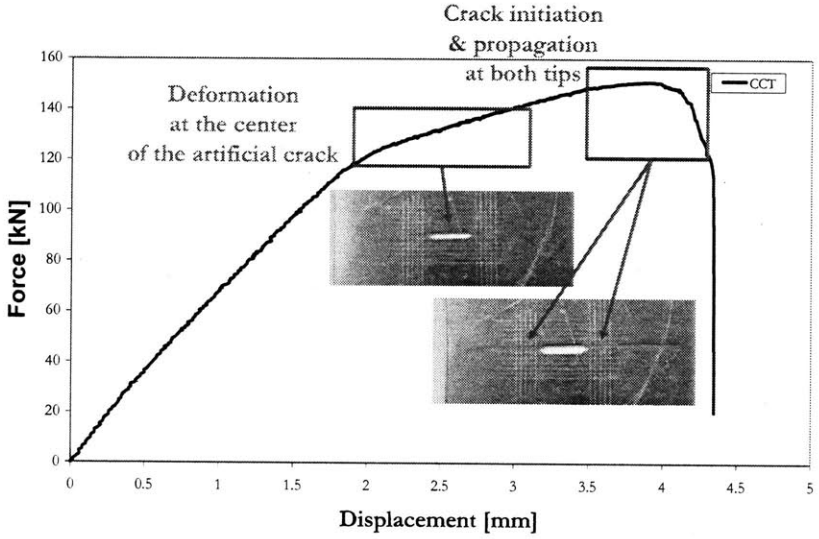

Figure 3-48: Force vs. displacement graph of the CCT specimen

obtained during this group of experiments, Fig. 3-49.

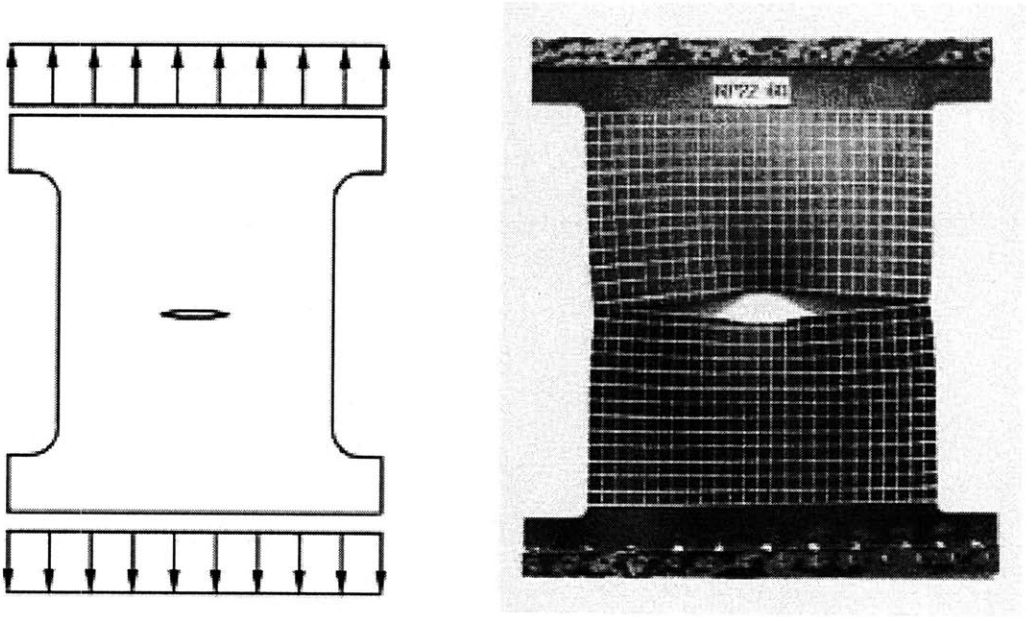

Figure 3-49: Schematic (left) and failed specimen (right) from tests perfomed by Paik and Thayamballi [210] on steel central precracked specimens

3.5.4 Twin Stiffened Center Cracked Tension (TSCCT) specimen

In this experiment a similar specimen to the CCT was used with the existence of two T-type extruded stiffeners located symmetrically at each side of the specimen, as shown in Fig. 3-50. The stiffeners were machined at both ends to avoid any interference with the fixture. A schematic of the SSDENT specimen is shown in Fig. 3-51. It has to be noted that the distance between the stiffeners is preselected since the specimen was cut from a panel that is designed and manufactured to be used for an existing naval vessel so as to be capable of withstanding sufficiently all types of loading defined in naval architecture for marine vessels (see Fig. 3-52). This case allowed us to examine the behavior towards fracture of this panel as an additional parameter.

Prior to the onset of fracture, the specimen presented out-of-plane deformation due to the existence of the stiffeners. Initially the whole specimen deformed out-of-plane, and at a second step a dishing out-of-plane deformation was observed around the region of the artificial crack in

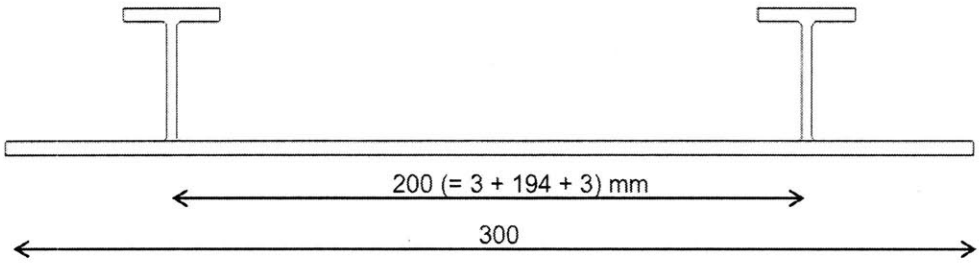

Figure 3-50: Side view of a schematic representation of the extruded stiffener configuration geometry

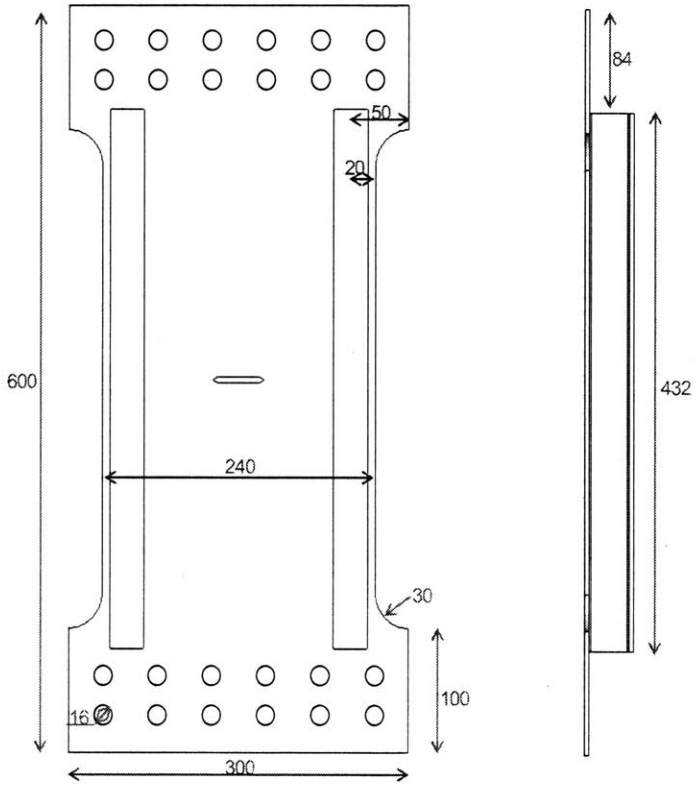

Figure 3-51: Twin Stiffened Center Cracked Tension (TSCCT) specimen geometry subjected to quasi-static uniaxial tensile loading (dimensions in mm)

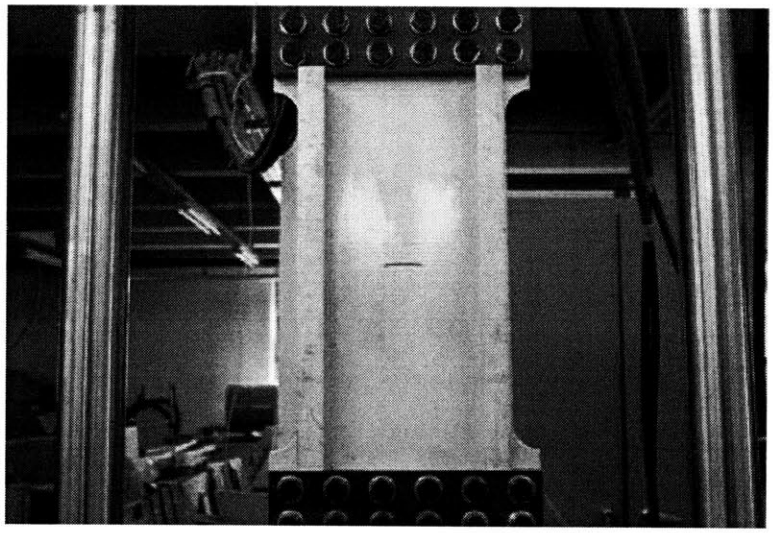

Figure 3-52: TSCCT specimen prior to testing mounted on the MTS device

the center of the specimen, with direction opposite to the one occurred in the whole specimen.

The phenomena regarding fracture of the specimen, shown in Fig. 3-53 can be summarized at the following steps:

(i) at a maximum force of 201.50 kN and 8.983 mm cross-head displacement the onset of fracture was observed at both the crack tips of the artificial crack. The crack on the right propagated with an initial angle of 60 degrees with respect to the loading direction and the crack on the right with a smoother angle of 75 degrees with respect to the loading direction,

(ii) at a force of 200.28 kN and 9.087 mm cross-head displacement after having already travelled for 12 mm, the crack on the left flipped, redirected itself and propagated with a 90 degrees angle with respect to its previous path. The same phenomenon was observed after a while for the crack on the right, where at a force of 194.53 kN and 9.629 mm cross-head displacement after having already travelled for 13 mm, the crack redirected itself with a direction perpendicular to the loading,

(iii) at a force of 179.30 kN and 10.465 mm cross-head displacement, the crack on the left already travelled for 16 mm more, redirected itself towards the stiffener and the crack on the right already travelled for 14 mm more, redirected smoothly with a 30 degrees angle towards the stiffener,

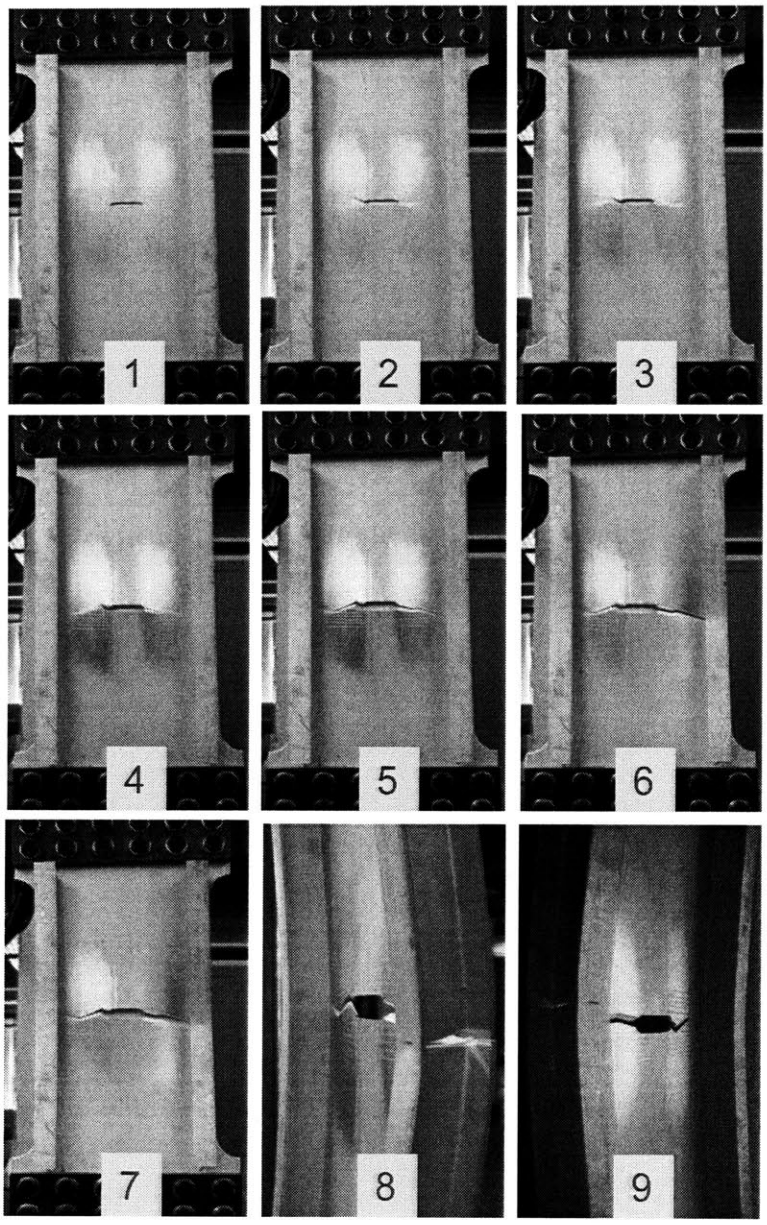

Figure 3-53: Series of photographs taken during the test of the TSCCT specimen. The phenomena observed can be summarized at the following phases: (1) onset of fracture at both tips of the artificial cracks occured after out-of-plane deformation, (2) both cracks pause, flip and redirect, (3) cracks redirect propagating towards to the stiffeners, (4) crack on the right becomes unstable and propagates with an increased growth rate, (5) cracks propagate on stable crack pattern, (6) crack on the right reaches the foot of the stiffener, splits the stiffener from the plate and begins to propagate on the web, (7) crack traveled all the distance on the web of the stiffener and the onset of fracture on the flange of the stiffener occurs, (8) side photograph showing a close-view of the cracked specimen at the right-hand-side, and (9) side photograph at a reverse angle

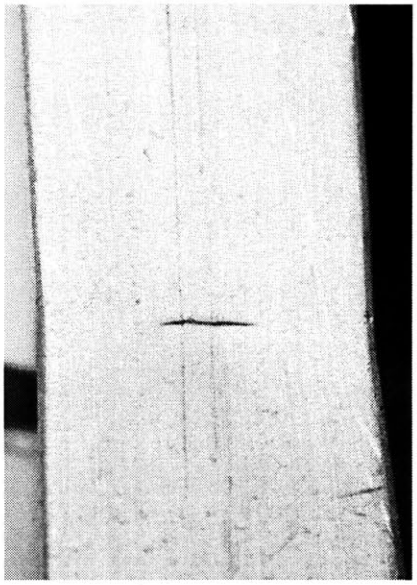

Figure 3-54: TSCCT specimen: crack intiation and propagation on the flange of the T-type extruded stiffener

(iv) at a force of 147.72 kN and 12.592 mm cross-head displacement, the crack on the right already travelled for 16 mm more, became unstable and begun its propagation towards the stiffener keeping the same direction while the crack on the left already travelled for 15 mm propagates towards the opposite stiffener too,

(v) the crack on the right propagated towards the foot of the stiffener and at a force of 149.71 kN and 12.634 mm cross-head displacement the crack teared the stiffener from the plate and propagated on the stiffener,

(vi) the crack on the right at a force of 47.97 kN and 12.635 mm cross-head displacement begun its propagation on the stiffener, and

(vii) at a force of 91.71 kN and 14.159 mm cross-head displacement the crack on the right completed its propagation on the web of the stiffener, reached the flange of the stiffener and fracture of the flange occurred, Fig 3-54. The test was then interrupted.

The duration of the test was 1711 seconds (from test initiation up to the point that the crack reached the flange of the stiffener) and the displacement rate for this test was 0.5 mm/ min. Figure 3-45 shows the load vs. displacement curve obtained from the test. This stepwise process can be clearly observed at the graph, and for visualization purposes photographs taken (every

15 s at the beginning, 10 s in the middle, and 5 s at the end) during the experiment present the series of events. Data were obtained in 1 s increments.

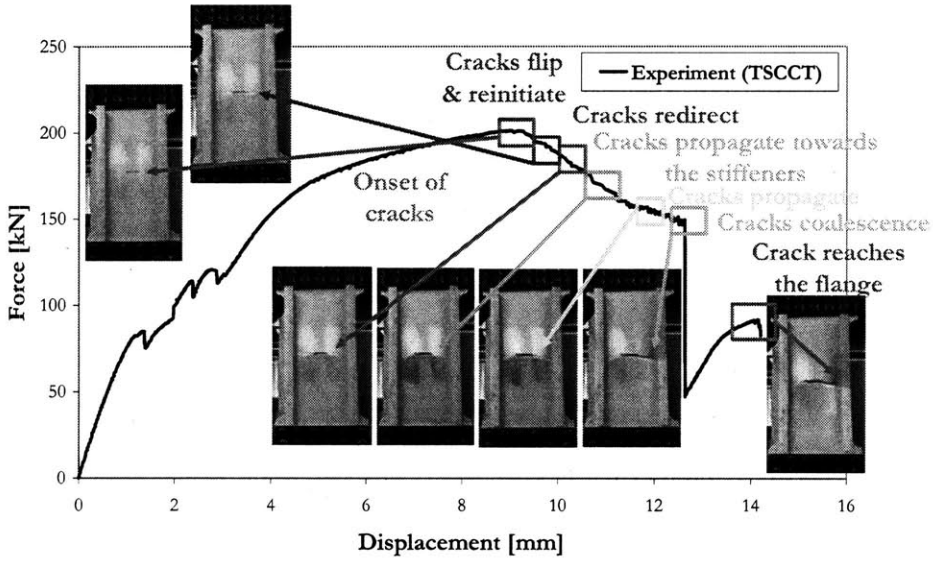

Figure 3-55: Force vs. displacement graph of the TSCCT specimen

3.5.5 Phenomena observed

As the specimen size increased, various design challenges appeared. These challenges include the loss of stiffness of aluminum structures compared to the steel ones that result in excessive deformation, buckling and plastic collapse. The lack of information on fabrication relating to initial imperfections can be solved with detailed analysis of the behavior of the structure against fracture.

A visual examination of the CCT specimen indicated that the crack initiated and propagated from both directions, Fig. 3-56. From one side the crack propagated with an angle of 45 degrees and from the opposite side the crack propagated with a reverse angle. Cracks were coalescenced close to one side of the specimen, while one crack has propagated for 2 cm. Both cracks propagated totally perpendicular to the loading direction. In order to find the effect

of shear lips on the stress intensity factor, Zuidema et al. [366], performed three-dimensional finite element calculations on the stress intensity distribution in centre-cracked plates. They concluded that there was a decrease of about 40 % in K_I, when a complete single shear condition is compared with a tensile test. At the same time K_{II} and K_{III} raised to a level of about 40 % of the original K_I. Pardoen et al. [221] studied the thickness dependence of cracking resistance in thin aluminum plates by examining experimentally and numerically cracked DENT specimens subjected to tensile loading.

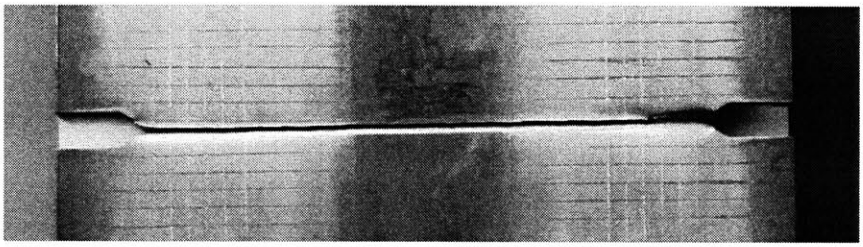

Figure 3-56: Final stage of the DENT specimen. Note that the cracks although initiated at both crack tips linked up on the right-hand side

On the other hand, observations on the SSDENT specimen reveal that the crack changes direction three times from one side and one from the other side. Bending of the specimen preceeded fracture and the maximum deflection was 7.5 cm (see Fig. 3-57). Crack paths are similar, except for the difference that on one side we observe two "knees" related to change of direction (see Fig. 3-58). When the cracks are linked at the foot of the stiffener, they form a crack that propagates almost vertically, Fig. 3-59. Measurements of the crack pattern gives a first "knee" at 0.75 cm, a second one at 2 cm and a third at 6 cm. From the opposite side, only one "knee" at 2.5 cm from the edge existed.

Observations at the CCT specimen showed that the parallel sides of the notch actually shifted in parallel prior to the crack initiation at the crack tips. It was noticed that once fracture initiated, within less than a second, the crack propagated with very high speed from one side. Both cracks propagated perpendicular to the loading direction (see Fig. 3-60). A 45 degree angle crack was observed from the specimen side (see Fig. 3-61). At the angle that the crack propagated further, a necking effect was noticed. Neither bending of the specimen nor out-of-plane deformation was observed. One crack propagated 60% of the distance compared

Figure 3-57: Side view of the final stage of the SSDENT specimen where the final deformation is observed

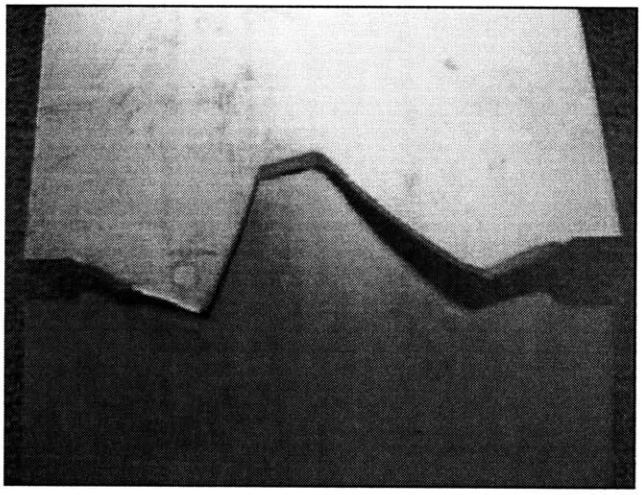

Figure 3-58: Rear view of the SSDENT specimen where the crack pattern is observed

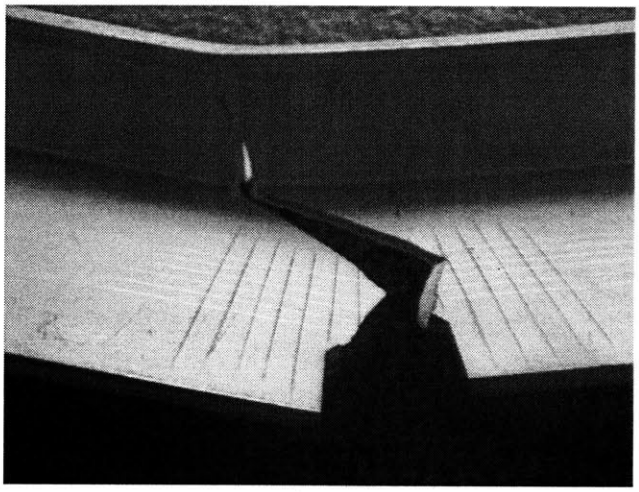

Figure 3-59: Side view of the SSDENT specimen, where the crack pattern is observed to the other crack.

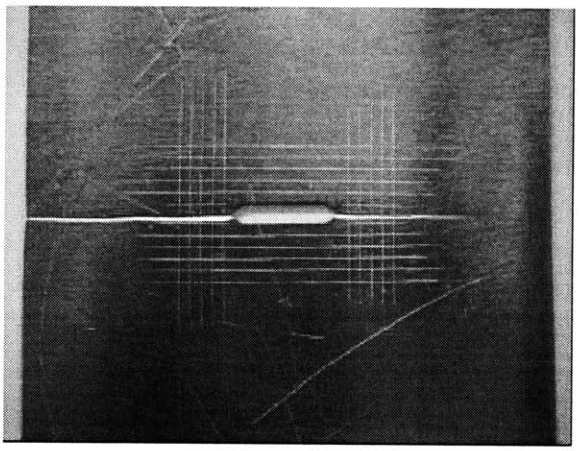

Figure 3-60: Final stage of the CCT specimen where the crack pattern is observed

Closer examination of the TSCCT specimen reveals deflection in the middle of the specimen, the maximum deflection was 4.5 cm (see Fig. 3-62). The crack propagated up to the stiffener only from one side and reached the flange. Two "knees" related to change of direction can be observed from one side (see Fig. 3-63). The first one at 1 cm and the second at 4 cm and one "knee" from the opposite side at 2.5 cm. Cracks initiated at both crack tips. Dishing was observed in the center of the specimen prior to crack initiation.

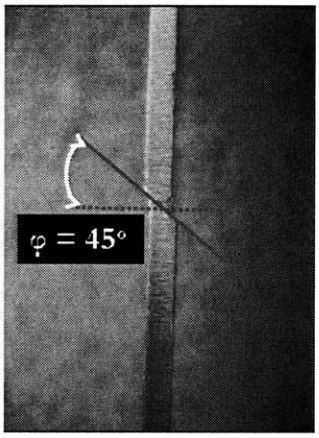

Figure 3-61: Photograph of the CCT showing the through-the-thickness crack angle

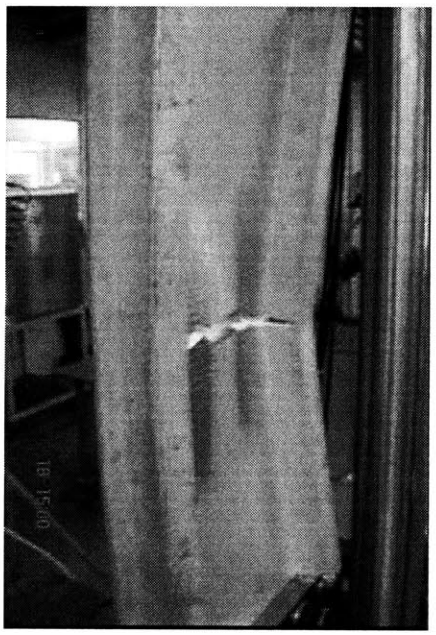

Figure 3-62: Final deformed shape of the TSCCT specimen

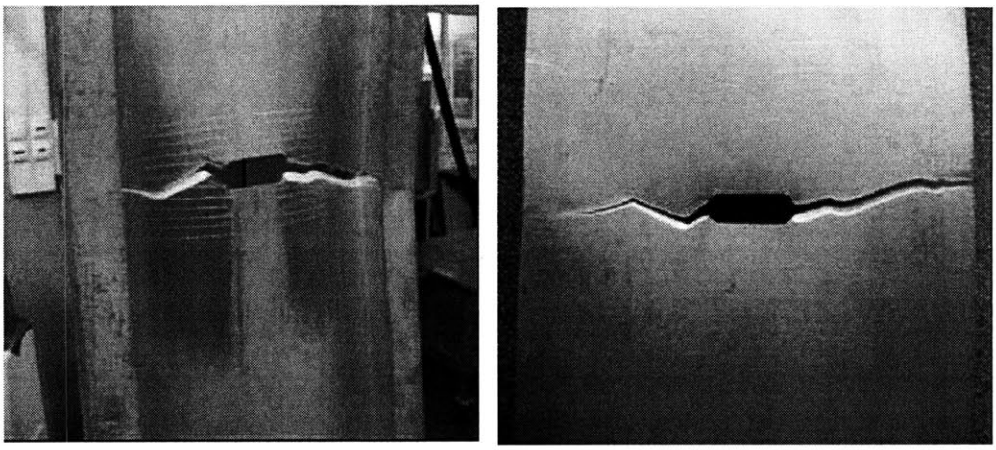

Figure 3-63: Front view of the TSCCT specimen (left) and rear view (right) showing the crack path

When assessing structural damage, one of the most important factors is the initial crack size (depth), especially when the damage is related to fatigue. This value provides a reliable link between the crack initiation and propagation stages. Although the problem of the initial crack size in crack propagation analysis has been frequently examined in fatigue (Petinov [234]), it needs to be evaluated. Continuum mechanics falls short in describing the stress field surrounding a microstructurally short crack, and hence the linear elastic fracture mechanics methodologies cannot be accurately used to model the growth.

A comparison among the four different specimens is presented in Fig. 3-64. The graph shows that the stiffened panels do not always present higher ultimate strength, but require significantly higher work to fracture. It is also interesting to observe that the position of the artificial crack in the unstiffened plates does not actually affect the ultimate strength of the structure. Finally, a stiffer structure (two stiffeners) fractures earlier than the one that is less stiff (one stiffener). This result further demonstrates the imminent need for consideration of fracture mechanics concepts into the design of marine vessels.

Another major insight obtained during the intermediate-scale tests is that as the crack length increases, the tensile strength and the elongation to failure decrease significantly. This is a consequence of the cross-sectional area reduction caused by the crack growth.

Paik and Thayamballi [210] have conducted experiments on steel for the case of a center-

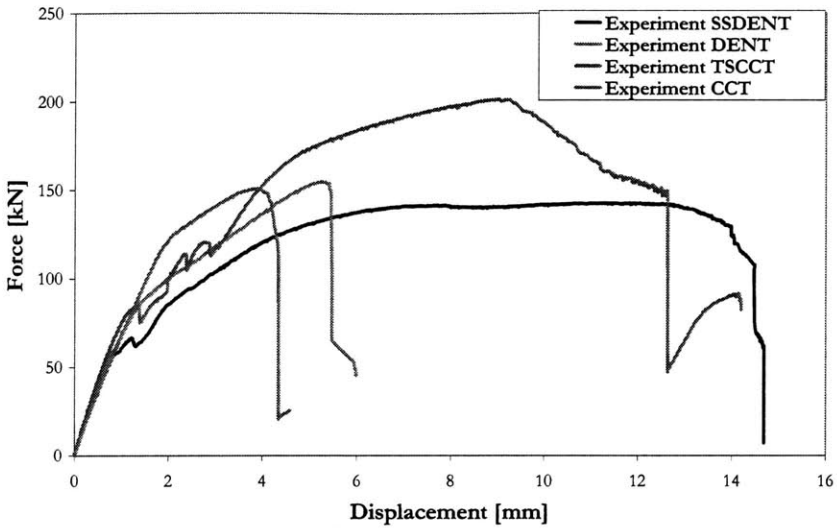

Figure 3-64: Force vs. displacement graph for the four intermediate-scale specimens tested

or edge-cracked plate under controlled displacement conditions. Furthermore, they developed an analysis that predicts the ultimate strength on the basis of the reduced cross-sectional area, taking into account the loss of load-carrying material due to the crack damage (see Fig. 3-65). For that case, the ultimate strength of a steel-plated structural component with existing cracks and under monotonic extreme loading may be approximately obtained by

$$\sigma_u = \frac{A_c}{A_o}\sigma_{uo} \tag{3.1}$$

where σ_u/σ_{uo} is the ratio of the ultimate strengths of cracked/uncracked (intact) structure, A_c/A_o is the ratio of the cross-sectional areas of the cracked/uncracked (intact) structural component.

Figure 3-66 shows a steel plate component with existing crack damage subjected to monotonic axial tensile load. The simplified model of Eq. (3.1) predicts the ultimate strength of the cracked plate as follows:

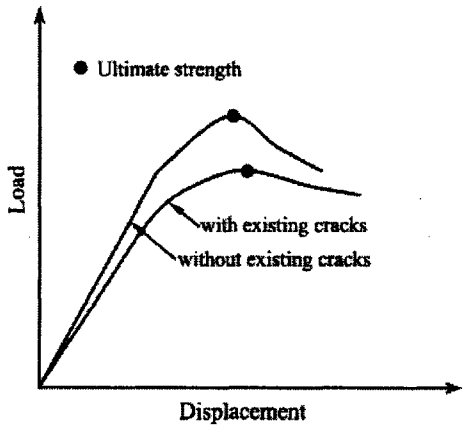

Figure 3-65: Graphical estimation of the relationship between the ultimate strength of steel structures with respect to the existence of cracks by Paik and Thayamballi, [210]

$$\sigma_u = \frac{b - c_p}{b}\sigma_{uo} \tag{3.2}$$

where σ_{uo} is the ultimate strength of the uncracked plate.

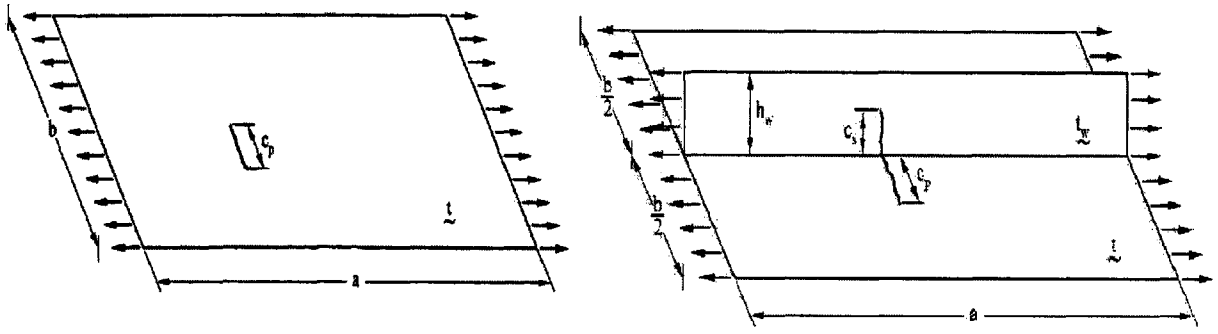

Figure 3-66: Schematics of cracked unstiffened and stiffened plates proposed by Paik and Thayamballi [210]

While a refined procedure for the collapse analysis of cracked stiffened panels is presented by Broek [31], the ultimate (tensile) strength for this case can be predicted using the simplified model noted in Equation 3.1:

$$\sigma_u = \frac{(b - c_p)t\sigma_{yp} + (h_w - c_s)t_w\sigma_{ys}}{bt + h_w t_w} \tag{3.3}$$

where c_p is the crack length of the plating, c_s is the crack length for the stiffener, σ_{yp} is the yield strength of plating, and σ_{ys} is the yield strength of the stiffener.

3.6 Summary of Results

The main experimental observations generated from this study can be summarized:

1. crack propagation depends strongly on the existence of stiffeners,
2. bending precedes crack initiation at stiffened panels,
3. some cracks propagate while others initiate,
4. the extruded panels arrest cracks more efficiently than the welded ones,
5. the crack path can be mapped knowing the design parameters,
6. crack propagation follows discrete steps at stiffened panels, and
7. four evolution phases exist for each critical site: crack initiation, propagation, linkage and arrest or failure.

The completion of this set of experiments provides fracture data on aluminum stiffened plate structures, which was one of the objectives of this research. This data, with proper analyses can fill the gap in our knowledge of the crack initiation, propagation and arrest processes that exists for aluminum and other metallic structures. The experimental results will also form a benchmark for the validity of computational simulations that are presented in the next chapter.

Chapter 4

Numerical Simulations

Today's shipyards are pressured by international competition for increasing production efficiency and each shipyard is forced to establish continuous improvement and cost-saving methods in production. If vessels can be produced cost effectively and delivered on time with the customer's quality requirements satisfied, more orders will be won and the future of the shipyard becomes more secure. In the highly competitive shipbuilding industry, the main aim is to produce a vessel by meeting the specification of the owner/client on time, with the required quality and within budget, while providing an acceptable level of profit to the shipbuilder. This goal is very challenging as shipbuilding is a process involving many activities, and problems at any stage of the vessel production cycle can cause delays.

A naval vessel is a complex structure designed and built to withstand a variety of loads, namely, operational loads from installed weapons, loads resulting from an enemy attack, wave and wind loads which are ever changing, cargo loads as a result of ballast and full load operations and accidental loads such as collisions and groundings. Recently, Finite Element Modeling (FEM) and Analysis (FEA) techniques have been developed to a level where these can be applied to analyze complex naval structures during the design process. Moreover, when design innovations are pursued, useful information can be obtained from direct load, response, and strength analyses. In such cases, it is essential to identify the relationship between the limit states and the corresponding loading conditions in a precise manner.

Simplified analysis procedures for the quasi-static response calculations are of great importance since they provide initial guidance during the early design stage but are also used to

evaluate results obtained through more complex numerical calculations.

These innovative technologies open the window for research in fracture mechanics that govern naval structures and enable the designers to produce more sound vessels. Beyond numerical simulations, analytical solutions for crack initiation, propagation and "arrest" exist in the literature [52] but structures are in general complex and the numerical solutions serve as a unique tool for the engineers.

4.1 Finite Element Modeling of Fracture

The availability of finite element (FE) modeling techniques has gradually increased, not only by a dramatic decrease in computational time, in accordance with the advancement of computer technology, but also by improving the pre- and post-processing in FE analyses.

The commercial code, ABAQUS/Explicit^{TM}, is used in this dissertation to carry out all the numerical simulations. This code offers an element library for a wide variety of geometric models. The preliminary analysis is conducted with a relatively coarse mesh. However, increasing the number of elements also increases the required computational time to reach a solution and hence it increases cost. The meshing techniques implemented in this thesis require from 10 minutes to 20 hours of computational time using powerful personal computers already installed at the shipyards. The numerical simulations of this thesis were performed on a HP ProLiant DL 145 G3 workstation (2-CPUs, 64-digit and 6G-memory) with Linux environment.

4.1.1 Uncertainties on FE modeling

Rigo et al. [259] [260] presented the results of an extensive sensitivity analysis carried out by Committee III.1 "Ultimate Strength" of the International Ship and Offshore Structure Congress (ISSC) in 2003 within the framework of a benchmark on the ultimate strength of aluminum stiffened panels. The target of this benchmark was to present reliable finite element models to study the behavior of axially compressed stiffened aluminium panels, including extruded profiles. The main objectives were to compare codes/models and to perform quantitative sensitivity analysis of the ultimate strength of a welded aluminium panel on various parameters (typically the heat-affected zone). This approach is similar to the work presented in this thesis,

since a methodology is developed including calibrations with coupon testing and applications to various types of small and intermediate-scale specimens to examine the effect of various parameters on unstiffened and stiffened naval aluminum plates.

Additionally, and within the area of interest of this dissertation, Nakasumi et al. [189] presented a new approach to crack propagation analysis for large-scale or complicated geometric structures. The approach utilizes the connection of mesh superposition method and extended finite element method. In the former technique, two types of meshes were used and displacement was represented as the sum of them. And in the latter technique, discontinuity across the crack segment and singularity around the crack tips were represented in the approximation by enriching the nodal degrees. This technique does not require meshes to conform to the crack geometry, a fact enabling crack propagation simulation with no re-meshing.

It then becomes obvious that the use of FE in the numerical analysis of complex structures is of great importance for the examination of aluminum naval structures with numerous models converging to the physical behavior of the structure. A critical parameter for the designer is the selection of the appropriate technique and theory that will apply to simulate the behavior of the real structure. A method that provides accurate results optimizing the computational time is presented in this chapter.

4.1.2 Crack propagation

The list of available fracture criteria in the literature is long. Prediction of the onset of fracture of crack-free bodies has traditionally been treated in the field of metal forming, while ductile fracture from a pre-existing crack has been treated by researchers in the area of fracture and damage mechanics. Research in the two closely related areas has proceeded almost independently over the past four decades. Atkins [12] gave an excellent historical overview of the development of fracture criteria in the two fields.

So far, various failure criteria have been explored from researchers, such as maximum strain criterion, rupture strain, equivalent plastic work, damage models and energy density models. Four methods are currently used for modeling crack initiation and propagation in finite element codes:

1. unzipping, often called cohesive crack models, where the crack is modeled by releasing

the constraints between adjacent elements,

2. the extended finite element method (XFEM), where the crack can be inserted arbitrarily within the element,

3. remeshing, where a new mesh is constructed in each time step to follow the crack, and,

4. the element deletion.

Unzipping limits the crack path to the edges of the element, so that crack paths which are not aligned with the element edges are not calculated accurately. It can also exhibit mesh size dependence in ductile fracture problems, since the complicated strain patterns around the crack tip are not well represented. XFEM can represent arbitrary crack paths. Furthermore, using similar partition of unity concepts will enable us to enrich the strain fields around the crack tip, so that accurate, mesh-independent predictions can be made of crack progression. Its disadvantages are a somewhat more complicated algorithmic structure and its relatively recent state of development, so it will require extensive research and development effort to achieve a high degree of robustness. Remeshing is terribly awkward, especially for dynamic problems, so it will not be considered here. As a result, the element deletion method is selected for this thesis.

4.1.3 Element removal method

Many numerical techniques have already been proposed to enable accurate and reliable simulations of crack propagation under arbitrary geometry, material and loading conditions. A commonly used approach that has enjoyed a high degree of acceptance is the use of standard finite element methods in conjunction with an "Element Removal" procedure [309] [22]. This approach was adopted in this dissertation.

The element deletion technique of the formation and growth of cracks has been implemented in leading commercial finite element codes, which is termed "Element Deletion" in ABAQUS/Explicit^{TM} [1]. When the damage indicator, D, exceeds the prescribed critical value at an integration point of an element, all the deviatoric stress components are instantaneously set to zero. The whole element is considered to fail if the damage indicator at all integration

points exceeds the critical value. ABAQUS/Explicit^{TM} provides two options to treat failed elements.

Either a failed element completely loses its load carrying ability, or a failed element is still capable of resisting pressure but neither tension nor shear. If the former option is used, the failed element will no longer participate in the calculation, and it can deform arbitrarily. The time step required for the computational stability will not be determined from these severely distorted elements.

Element deletion is the simplest of the methods, which makes it very attractive. It involves only insertion of a constitutive equation into a FE program that reflects the process of the stress drop as the material fails. The formulation is entirely element-specific, so that the algorithmic structure is straightforward. The "Element Removal" method offers the advantages of convenience and efficiency in terms of implementation and application with standard finite element methods. With a sufficiently fine discretization and the appropriate constitutive law, this finite element based approach is able to predict fracture accurately. However, in practice, the finite element models normally need to use a relatively coarse mesh, which introduces a potential drawback to this method in terms of solution accuracy. In other words, it can exhibit element-size dependence and it requires that the width of the crack is the size of one element, which may create problems in capturing the fluid-structure effects.

4.2 Fracture Criterion Selection

Fracture criterion selection is the determination of how much material ductility is necessary for a particular structural application. Some of the factors involved in the application of a fracture criterion are the knowledge of service conditions (temperature, loading, strain rate, etc.) to which the structure will be subjected, the desired level of performance in the structure (plane-strain, elastic-plastic, or plastic) and the consequences of structural failure. Two fracture criteria are selected for this thesis, the "constant equivalent strain" and the "Rice - Tracey" models. The reason is that both of them are simple and can be applied to a wide range of marine metal structures.

4.2.1 Constant equivalent strain criterion

In common industrial practice, fracture is assumed to occur in a material element when the equivalent plastic strain $\overline{\varepsilon}$ reaches a critical value $\overline{\varepsilon}_f$. To obtain the critical value from large-scale tests, real-life observations or tensile tests are required

$$\overline{\varepsilon} = \overline{\varepsilon}_f \tag{4.1}$$

For an incompressible plastic material $\overline{\varepsilon}$ is defined by

$$\overline{\varepsilon} = \sqrt{\frac{2}{3}}\sqrt{\varepsilon_1^2 + \varepsilon_2^2 + \varepsilon_3^2} \tag{4.2}$$

where ε_1, ε_2, ε_3 are the principal strains. There is an understanding that Eq. (4.1) is valid for all possible stress states. Even though the origin of this criterion goes back to the beginning of the 20^{th} century [108], it has found its way into almost all nonlinear commercial codes in the 21^{st} century. While this criterion lacks generality, practitioners like it because location of the possible fracture sites can be determined simply by constructing color-coded plots of the equivalent strain and data can be easily found in existing handbooks.

4.2.2 Rice and Tracey fracture criterion

Many constitutive models with evolving damage have been proposed over the past few decades, and most of them are based on the fundamental assertion that degradation of the stress carrying capacity of the material is caused by void initiation, growth and coalescence. The void growth is caused by simultaneous plastic deformation and hydrostatic tensile loading in the material. Therefore, the hydrostatic stress

$$\sigma_H = \frac{1}{3}\sigma_{ii} \tag{4.3}$$

becomes of primary importance. The simplest methods among these are called damage indicators. Rice and Tracey criterion [255], used for the numerical simulations throughout this dissertation, does not include any coupling between the constitutive behavior and the material damage, except at the point of fracture where the stress carrying capacity is removed

instantaneously. This model states that material damage evolves when

$$D = \int \frac{1}{1.65} \exp(\frac{3\sigma_H}{2\sigma_{eq}}) d\varepsilon_{eq} \tag{4.4}$$

where ε_{eq} and σ_{eq} are the equivalent strain and stress, respectively. For this case, at the uniaxial tension test with no necking effect, with $\sigma_2 = \sigma_3 = 0$, then $\sigma_H = \frac{1}{3}\sigma_1$ using Eq. (4.3), $\sigma_{eq} = \sigma_1$ and the damage from Eq. (4.4) becomes

$$D = \int d\varepsilon_{eq}$$

meaning that simply $D_{cr} = (\varepsilon_{eq})_f$.

4.3 Calibration

Material calibration for fracture analysis is a procedure that identifies a true stress-stain curve up to the fracture of the material by tracing an experimental load-displacement curve with finite element (FE) simulations of a uniaxial test on a standard specimen. This curve fitting procedure is a hybrid methodology which combines testing and numerical simulations. The calibration method must be modified if the necking effect is observed.

4.3.1 Stress-Strain curve

The output of the experimental data give a relationship between the displacement (δ) and the force (P), $P = P(\delta)$. The engineering stress and strain before necking (σ_{eng} and ε_{eng}) can then be calculated from the standard equations:

$$\sigma_{eng} = \frac{P}{A_o} \tag{4.5}$$

$$\varepsilon_{eng} = \frac{\delta}{L_o} \tag{4.6}$$

where A_o and L_o are the initial area and length of the specimen, respectively, Fig. 4-1. The corresponding true stress and strain (σ_{tr} and ε_{tr}) can then be obtained from the following

conversion laws:

$$\sigma_{tr} = \sigma_{eng}(1 + \varepsilon_{eng}) \tag{4.7}$$

$$\varepsilon_{tr} = \ln(1 + \varepsilon_{eng}) \tag{4.8}$$

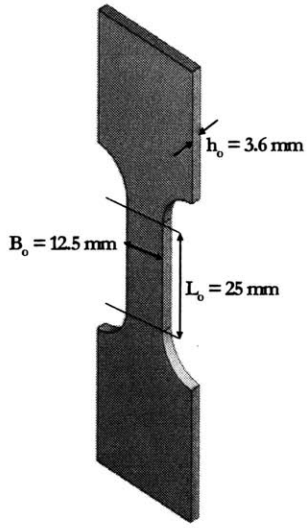

Figure 4-1: Gauge section of the "dogbone" model in the FE code

The data obtained from the tests of six specimens performed (see Section 3.3) show the relationship between load and displacement (see Figs. 4-2, 4-3). As previously mentioned, due to the fabrication of the structures, the material thickness presents up to 8 % variation with respect to the different orientations (longitudinal and transverse). Additionally, the coupon testing was performed only on specimens cut from plate, due to material availability, and not also from the extruded panels, resulting in expected experimental error. To minimize this error, the input data to the FE code were derived only from the coupon tests performed in the T-direction that showed variation within less than 1.5 % with respect to displacement.

It can be observed from the failed "dogbone" specimen and the data analysis, that fracture occurred prior to any significant diffuse necking. Therefore, the true stress-strain curves (see Figs. 3-14 and 3-15) that were obtained in Chapter 3 using Eqs. (4.7) and (4.8), do not require

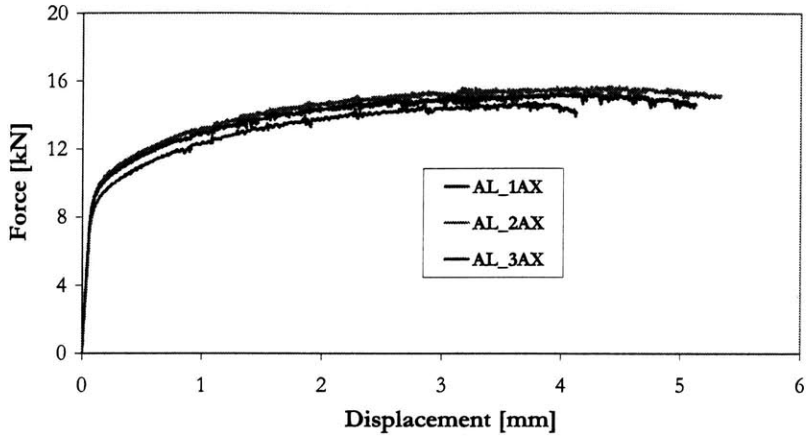

Figure 4-2: Load vs. displacement curves obtained from three "dogbone" specimens cut in L-direction subjected to uniaxial tensile loading

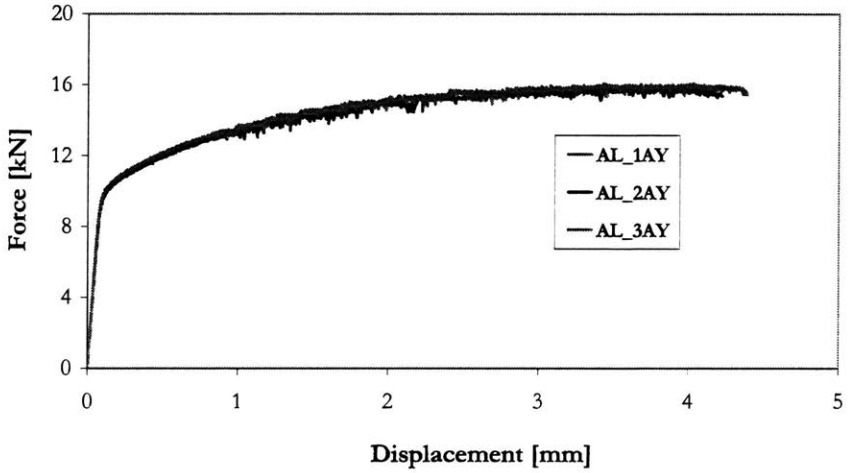

Figure 4-3: Load vs. displacement curves obtained from three "dogbone" specimens cut in T-direction subjected to uniaxial tensile loading

any further calibration. In addition, Young's modulus was measured from the stress-stain curve, $E = 65.87\ GPa$. As material input data for the numerical analysis in ABAQUS^{TM}, the manufacturer's provided values are used for Poisson's ratio and mass density of naval aluminum, i.e. $\nu = 0.3$ and $\rho = 2650\ \text{kg/m}^3$.

4.3.2 Mesh densities

In order to obtain the most reliable results from the numerical analysis, it is necessary to study the mesh sensitivity. Thus, the effect of the mesh size is investigated by developing three different meshes, with different numbers of layers of elements through the thickness for the uniaxial tensile specimen ("dogbone"), Figs. 4-4 and 4-5. Table 4.1 presents a summary of the details for each mesh. Quasi-static analyses using ABAQUS/Explicit^{TM} were performed throughout this calibration procedure, using reduced integration 3-D solid elements (C3D8R and C3D6, 8-node linear brick reduced integration and 6-node linear triangular prism, respectively).

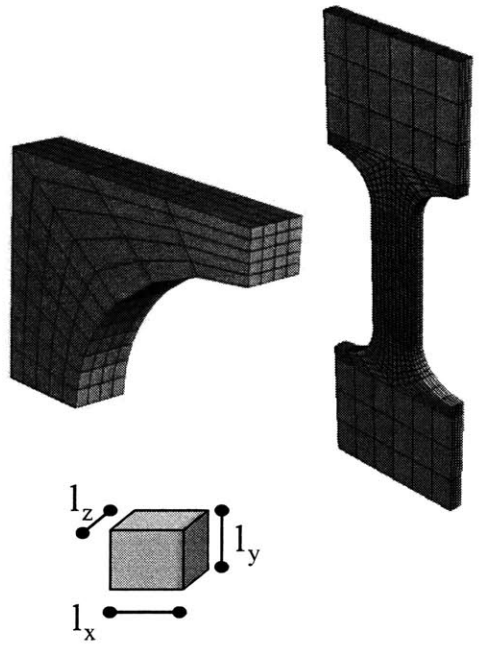

Figure 4-4: "Dogbone" model using FE code for coarse mesh with four through-the-thickness elements

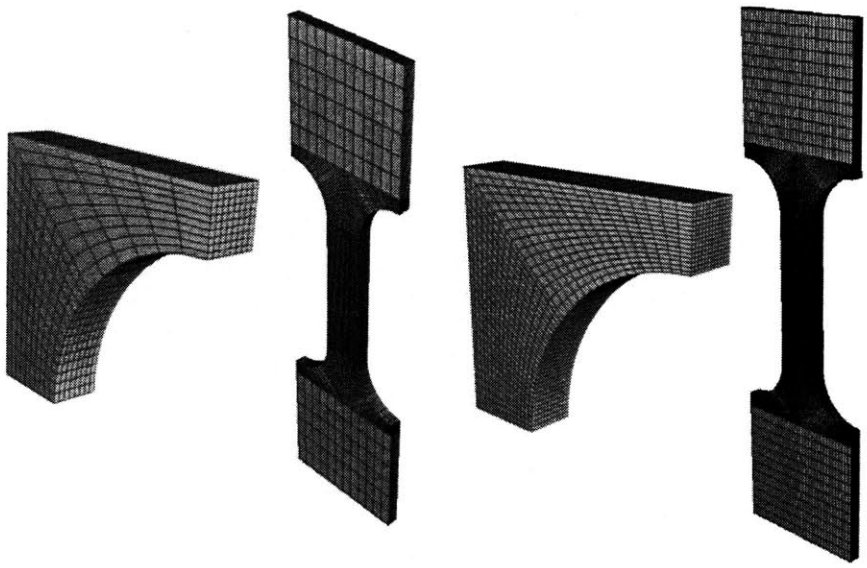

Figure 4-5: FE modeling of the "dogbone" specimen for the intermediate and fine mesh with eight and twelve through-the-thickness elements, respectively

4.3.3 Boundary conditions

The boundary condition is imposed to simulate the experimental setting by fixing the bottom of the specimen and assigning an upward moving roller to the top of the specimen. Displacement control tests were simulated by imposing displacement on the top with a smooth amplitude curve whose first and second derivatives are smooth and whose slopes are zero at the beginning and ending of loading. Therefore, the displacement and rotation of nodes on the lower end parts of the specimen were fixed. The upper end parts of the specimen were assumed to move with a prescribed displacement. Figure 4-6 shows the boundary condition in the numerical simulation.

4.3.4 Numerical analysis parameters

The appropriate loading rate and total time step for a quasi-static analysis can be estimated. By using a coarse mesh for the purpose of reducing computational time, we can determine an approximate lower bound on the total time step by calculating the stability time limit and the lowest natural frequency in the loading direction. In explicit analysis, the stability time is automatically calculated in the main solver of a FE program. It has to be greater than the

Mesh Type		Coarse	Intermediate	Fine
Total number of elements		2,144	19,072	62,568
Finest element size in FE model [mm]	l_x	1.250	0.625	0.417
	l_y	1.136	0.568	0.379
	l_z	0.9	0.45	0.3
Number of element layer through the thickness		4	8	12
Aspect ratio of in-plane mesh l_x/l_y		1.1		
Normalized mesh size in loading direction $\xi_l = l_y/h_o$		0.217	0.162	0.081

Table 4.1: Mesh densities for the calibration procedure

total time step, and it can be expressed as:

$$\Delta t = \frac{L_e}{c_d} = L_e\sqrt{\frac{\rho}{E}} \qquad (4.9)$$
$$= 9 \times 10^{-4} \times \sqrt{\frac{2650}{65.87 \times 10^9}} = 1.8 \times 10^{-7} \text{ [s]}$$

where L_e is the characteristic element length, usually the smallest element dimension, and c_d is the dilatational wave speed for a linear elastic material. As another lower bound for the time step, the lowest natural frequency in the loading direction $f = 7523.6$ Hz is obtained by running a frequency analysis in ABAQUS/Standard^{TM}.

Thus the total time step should be larger than the period, $T = 1.33 \times 10^{-4}$ s, corresponding to the lowest natural frequency in order to increase the likelihood of a quasi-static result. It was decided to perform the FE simulation with a total time step, $t_{total} = 0.0125$ s, which is about 100 times longer than the period corresponding to the lowest natural frequency in the loading direction.

Moreover, it was observed from the tests that the aluminum specimens failed when the head-to-head displacement was about 4.5 mm, so the maximum displacement is set to 6 mm. This value, therefore, leads to the following loading rate:

Figure 4-6: Boundary conditions imposed to the "dogbone" specimen at the numerical simulation. Note that the degree of freedom in the loading direction is released on the top of the specimen

$$V_{load} = \frac{\delta_{\max}}{t_{total}} = \frac{6 \times 10^{-3}}{0.0125} = 0.48 \ [\mathrm{m/s}] \tag{4.10}$$

Therefore, the ramping time is 0.0125 s and the constant velocity 480 mm/s. Figures 4-7 and 4-8 show a comparison among the load-displacement curves obtained from experiment and simulations, for the three different meshes and the two fracture criteria used. The fine mesh discretization agrees very closely with the experimental deformation and fracture mode obtained from the tests.

4.3.5 Comparison between experiment and numerical simulation

Prior to investigating the damage parameters that can be calculated from the calibration procedure, it is crucial to compare the deformed shape produced by the numerical simulations to the fracture mode of the experimental results.

Figures 4-9 and 4-10 show a closer view of the center part of the "dogbone" model for

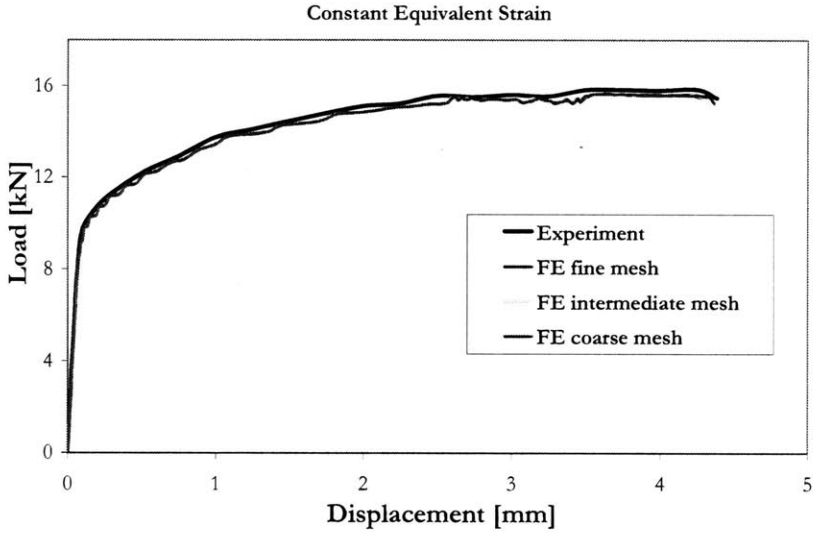

Figure 4-7: Load vs. displacement graph obtained from experiment and numerical simulations using finite element code and the constant strain fracture criterion

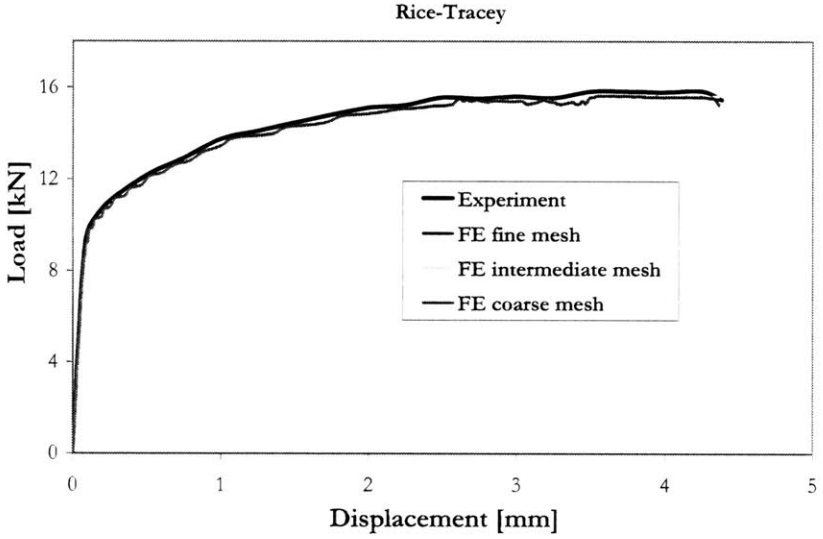

Figure 4-8: Load vs. displacement graph obtained from experiment and numerical simulations using finite element code and the Rice and Tracey fracture criterion

the three type of meshes and the two fracture criteria embedded, where it is observed that shear fracture is dominant. This deformed shape is obtained from numerical simulations with the different types of meshes while acquiring the equivalent plastic strain to fracture from the corresponding displacement to fracture obtained from the experiment ($\delta_f = 4.385\,\text{mm}$). The fine mesh captures very closely the failure mode from the test in both cases. Table 4.2 summarizes the load, displacement, true stress and true strain at the point of fracture, results obtained from the numerical simulations.

Additionally, the true stress-strain curves obtained from the experiment and the numerical simulations are presented showing a relatively good approximation, Figs. 4-11 and 4-12.

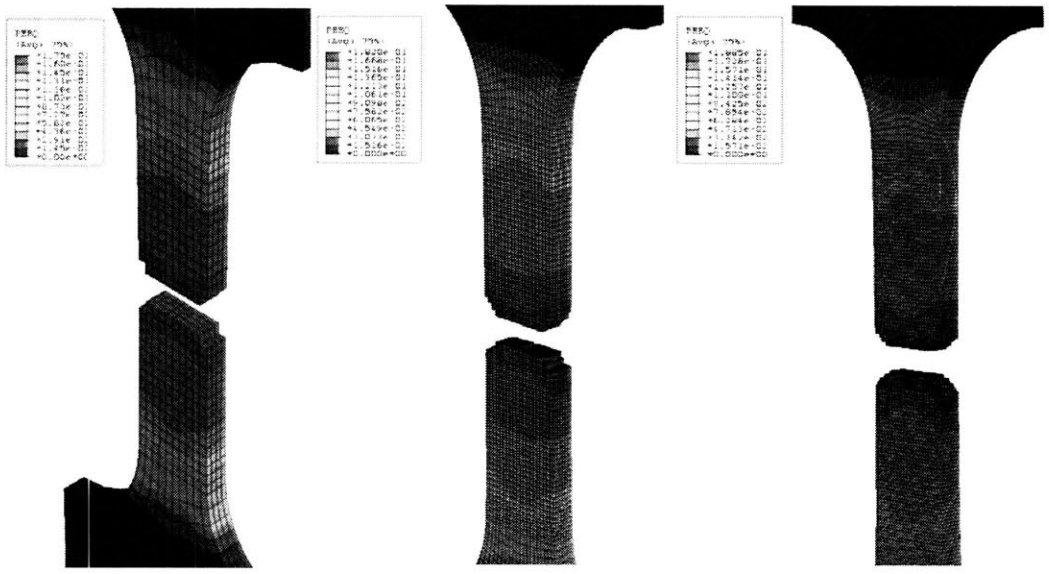

Figure 4-9: Results obtained from numerical simulations using the constant strain fracture criterion for three different meshes examined, coarse, intermediate and fine (from left to right, respectively)

4.3.6 Critical damage parameters

The damage parameters include the equivalent plastic strain to fracture ($\bar{\varepsilon}_f$), the corresponding stress triaxiality ($\frac{\sigma_m}{\bar{\sigma}}$), and the critical damage value (D_c). Bao and Wierzbicki [16] [17] predicted that fracture occurs when the accumulated equivalent plastic strain with a suitable weighting function reaches a critical value:

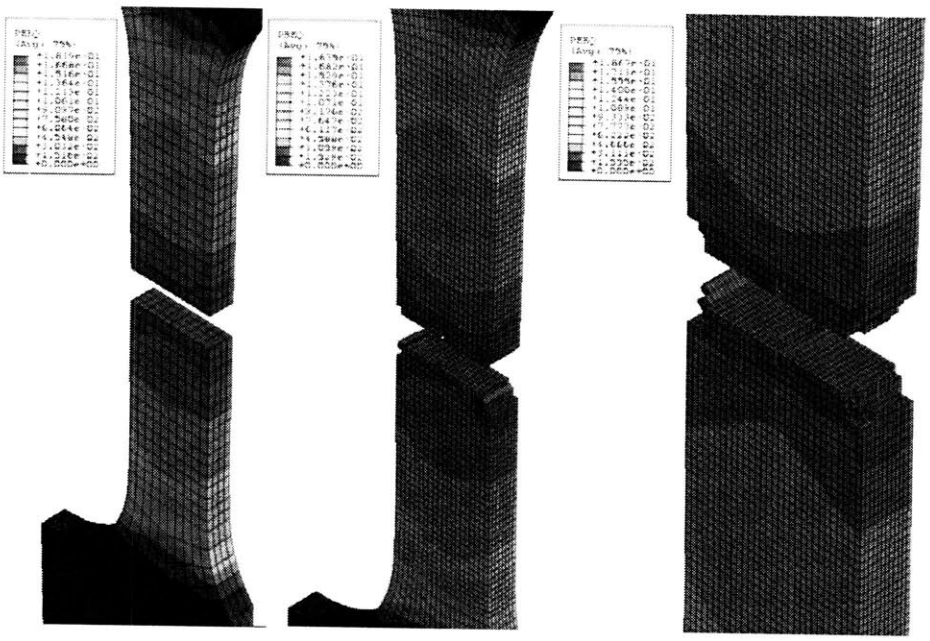

Figure 4-10: Results obtained from numerical simulations using the Rice - Tracey fracture criterion for three different meshes examined, coarse, intermediate and fine (from left to right, respectively)

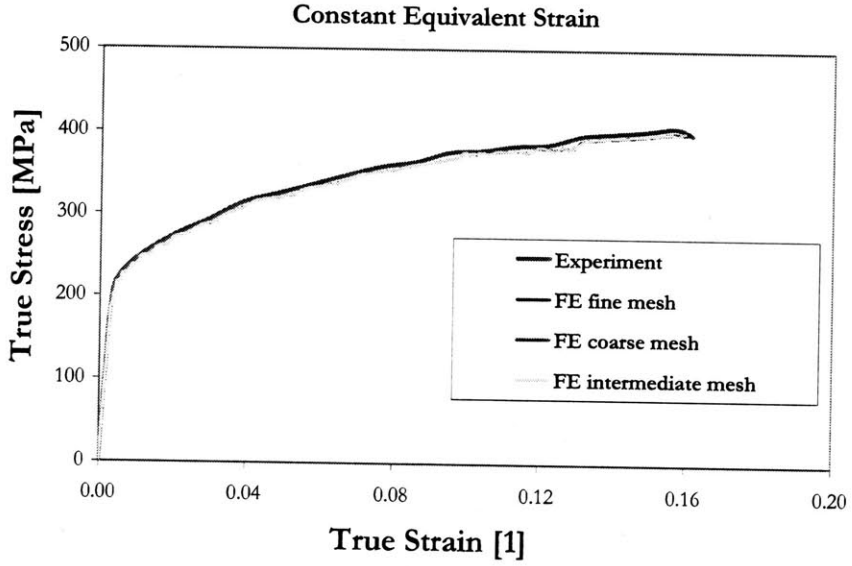

Figure 4-11: Stress-strain curves obtained from experiment and numerical simulations using finite element code and the constant strain fracture criterion

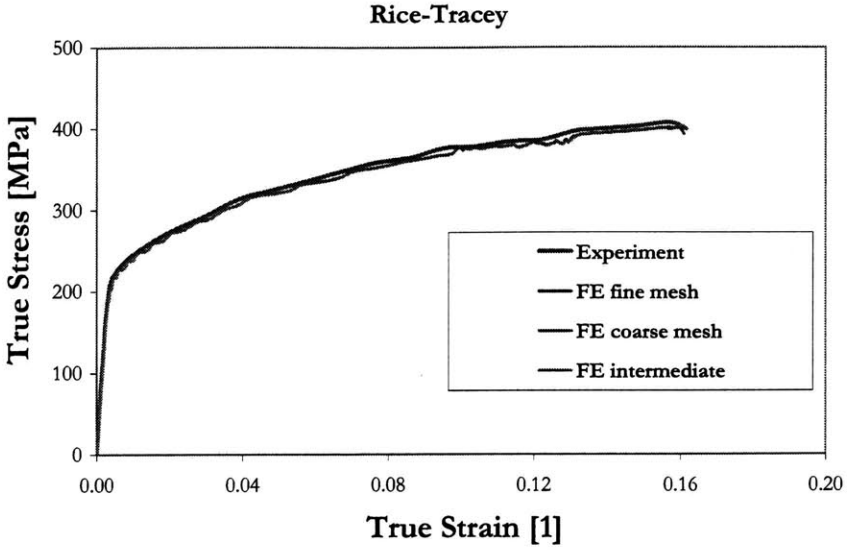

Figure 4-12: Stress-strain curves obtained from experiment and numerical simulations using finite element code and the Rice-Tracey fracture criterion

$$D_c = \int_0^{\overline{\varepsilon}_f} f(\frac{\sigma_m}{\overline{\sigma}}) d\overline{\varepsilon} \tag{4.11}$$

where D_c is the critical damage value, and f is a weighting function depending on the stress triaxiality, $\frac{\sigma_m}{\overline{\sigma}}$. They reported that in the range of high stress triaxiality, $\frac{\sigma_m}{\overline{\sigma}} > \frac{1}{3}$, the weighting function f in the integral of Eq. (4.11) can be taken approximately equal to its argument. Furthermore, by introducing the average stress triaxiality $(\frac{\sigma_m}{\overline{\sigma}})_{av}$, Eq. (4.11) can be rewritten as follows:

$$D_c = \int_0^{\overline{\varepsilon}_f} \frac{\sigma_m}{\overline{\sigma}} d\overline{\varepsilon} = (\frac{\sigma_m}{\overline{\sigma}})_{av} \overline{\varepsilon}_f \tag{4.12}$$

In order to evaluate the critical damage value for this naval aluminum alloy, two unknowns, $\overline{\varepsilon}_f$ and $(\frac{\sigma_m}{\overline{\sigma}})_{av}$ have to be determined. The history of the stress triaxiality parameter, $\frac{\sigma_m}{\overline{\sigma}}$, is found from numerical simulations. From the output data, the average stress triaxiality, $(\frac{\sigma_m}{\overline{\sigma}})_{av}$, can then be easily calculated.

Mesh Type	Fracture Criterion	Force [kN]	Displacement [mm]	True Stress [MPa]	True Strain [%]
Coarse	CES	15.23	4.367	393.33	16.10
	R-T	15.22	4.367	393.33	16.10
Intermediate	CES	15.60	4.328	402.44	15.97
	R-T	15.61	4.361	402.97	16.08
Fine	CES	15.59	4.324	402.13	15.95
	R-T	15.61	4.356	403.07	16.06

Table 4.2: Results obtained from the numerical simulations of the dogbone model (CES stands for the Constant Equivalent Strain and R-T for the Rice and Tracey ctiteria)

Equivalent plastic strain

The equivalent plastic strain to fracture was determined from the output of the FE calculations. In order to construct a complete fracture envelope in the plane of equivalent plastic strain to fracture $\overline{\varepsilon}_f$ and the average stress triaxiality $(\frac{\sigma_m}{\overline{\sigma}})_{av}$ a set of various coupon tests is required. Figure 4-13 shows such an envelope constructed by Lee and Wierzbicki [154].

Additionally, Figure 4-14 shows the history of the equivalent plastic strain at the center point of the "dogbone" model for three different meshes as a function of the measured relative displacement in the gauge section. Figure 4-14 clearly shows that there is no significant mesh dependency. The values obtained for the equivalent strain at fracture for the three different meshes are $(\overline{\varepsilon}_f)_{coarse} = 0.174$ for the coarse mesh, $(\overline{\varepsilon}_f)_{intermediate} = 0.181$ for the intermediate mesh, and $(\overline{\varepsilon}_f)_{fine} = 0.1875$ for the fine mesh, corresponding, as mentioned previously, to a displacement to fracture obtained from the experiment, $\delta_f = 4.385\,\text{mm}$. Moreover, Figure 4-15 shows the distribution of the equivalent plastic strain at failure obtained without applying the Rice and Tracey criterion, where the failure mode can also be clearly observed but the element removal technique is not applied. Since the difference between the values obtained from the application of both criteria is less than 5 %, only one case is shown. Finally, Figure 4-16 shows a 3D view of the crack formation prior to the application of any fracture criterion.

Stress triaxiality

Similarly, the stress triaxiality and the average stress triaxiality can be also shown as a function of the displacement (see Fig. 4-17). The stress triaxiality remains constant, $\frac{\sigma_m}{\overline{\sigma}} =$

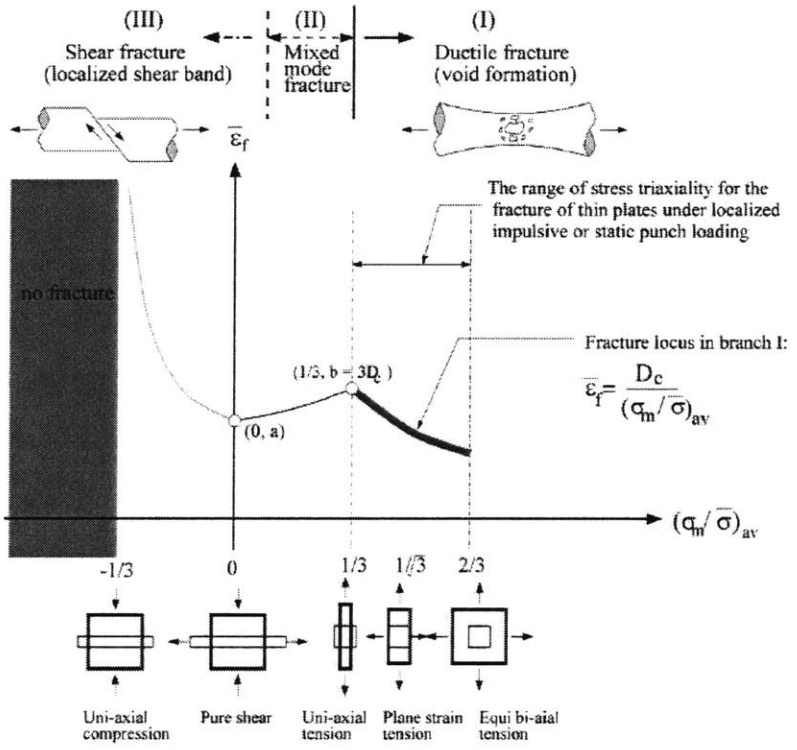

Figure 4-13: A schematic showing the fracture envelope constructed in the plane of equivalent plastic strain to fracture $\overline{\varepsilon}_f$ and average stress triaxiality $(\sigma_m/\overline{\sigma})_{av}$, Lee and Wierzbicki [154]

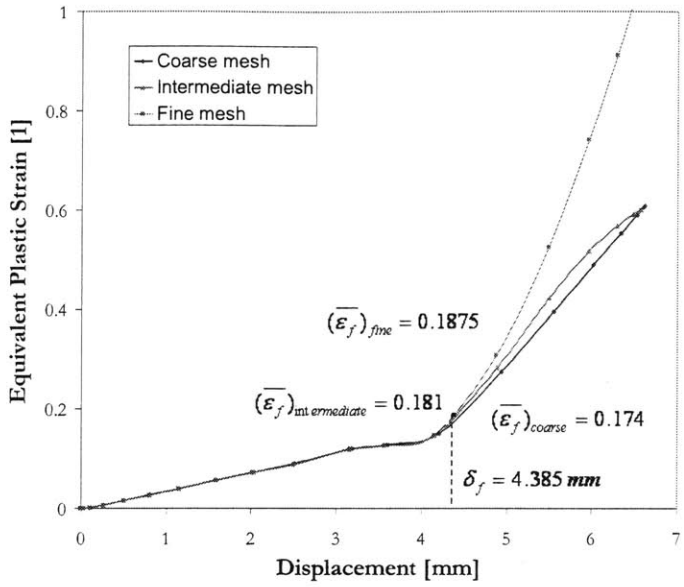

Figure 4-14: Calculated equivalent plastic strain *at the center of the specimen* versus the relative displacement

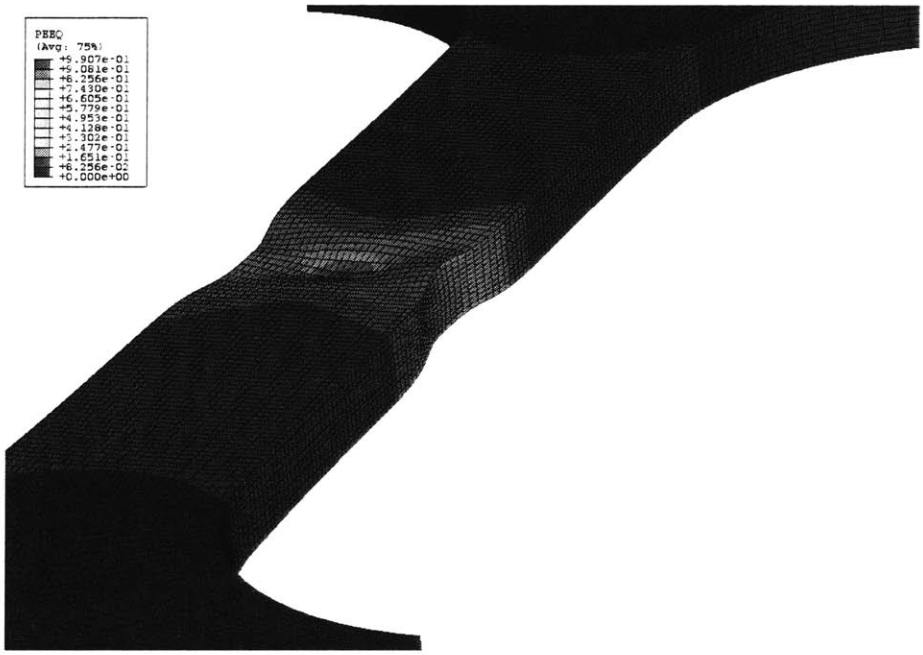

Figure 4-15: Distribution of equivalent plastic strain at failure using the fine mesh (no fracture criterion is embedded)

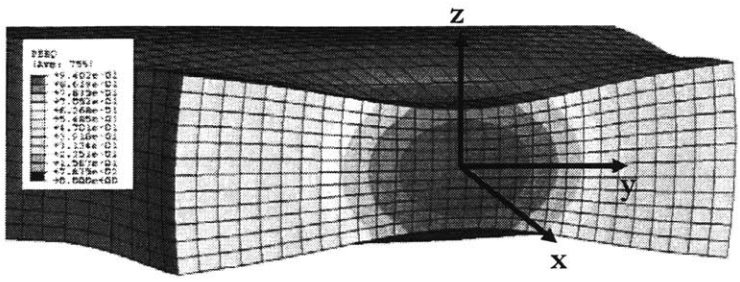

Figure 4-16: 3D view of crack formation (cut through view of the center of the dogbone specimen with the fine mesh)

0.333. The stress triaxiality for each mesh is $(\frac{\sigma_m}{\overline{\sigma}})_{av,\ coarse} = 0.349$ for the coarse mesh, $(\frac{\sigma_m}{\overline{\sigma}})_{av,\ intermediate} = 0.36$ for the intermediate mesh, and $(\frac{\sigma_m}{\overline{\sigma}})_{av,\ fine} = 0.362$ for the fine mesh, obtained, as the equivalent plastic strain to fracture, for a displacement to fracture obtained from the experiment, $\delta_f = 4.385\,\text{mm}$. The distribution of the von Mises stress at failure without applying any fracture criterion is shown in Fig. 4-18. It can be observed that failure can be predicted without the application of any fracture criterion but the crack pattern can not be visualized in this case.

Critical damage value

In order to calculate the critical damage failure, the history of the stress triaxiality is plotted as a function of the equivalent plastic strain (see Fig. 4-19). Geometrically, the critical damage value is simply the area under the curve. It is straightforward to calculate this value for each mesh size. As expected the value changes from $(D_c)_{coarse} = 0.061$, and $(D_c)_{intermediate} = 0.065$ to $(D_c)_{fine} = 0.068$ indicating the independence on the mesh density.

4.4 Small-scale FE Models

In order to perform the analysis of the small-scale tests, the intermediate mesh was selected, since it captures fracture similarly to the fine mesh and simultaneously gives very good results concerning the through-the-thickness behavior compared to the coarse mesh. Additionally, the application of Rice and Tracey fracture criterion is applied throughout the rest of the thesis,

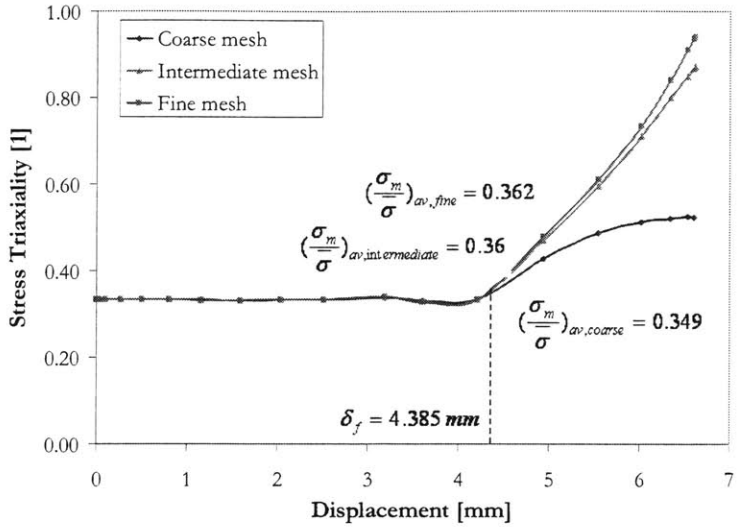

Figure 4-17: Calculated stress triaxiality *at the center of the specimen* versus the relative displacement

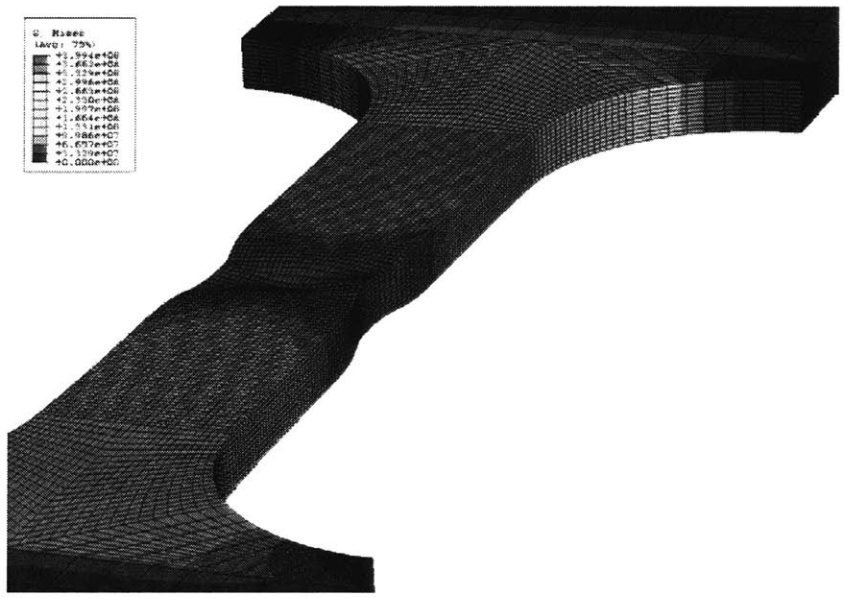

Figure 4-18: Distribution of Von Mises stress at failure for the fine mesh (no fracture criterion is embedded)

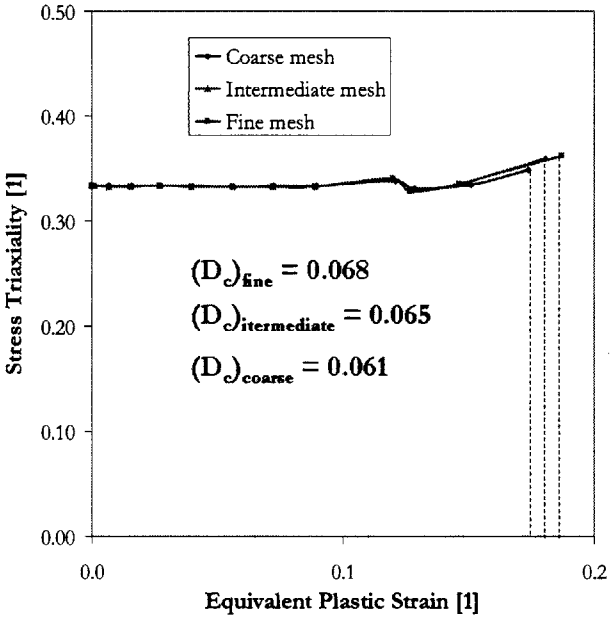

Figure 4-19: Evolution of stress triaxiality *at the center of the specimen* versus the equivalent plastic strain

since the constant equivalent strain fracture criterion does not work well at the compression side.

4.4.1 FE analysis of the unstiffened CT specimens

The first three models are the unstiffened CT specimens with different notch geometries. The differences are the initial crack length (55 and 71 mm) and the crack tip geometry (blunt and sharp crack tip) (see Fig. 4-20).

As detailed in Chapter 3, a fixture was designed to minimize the out-of-plane deformation of the specimens (see Appendix B - Fixture for small-scale tests). Therefore, the boundary condition imposed on the unstiffened CT specimens is shown in Fig. 4-21. For the simplicity of the analysis only the pins are modeled from the test setup configuration.

Initially, the appropriate loading rate and total time step for a quasi-static analysis of the unstiffened CT specimens has to be estimated. By using the intermediate mesh, one can determine an approximate lower bound on the total time step by calculating the stability time

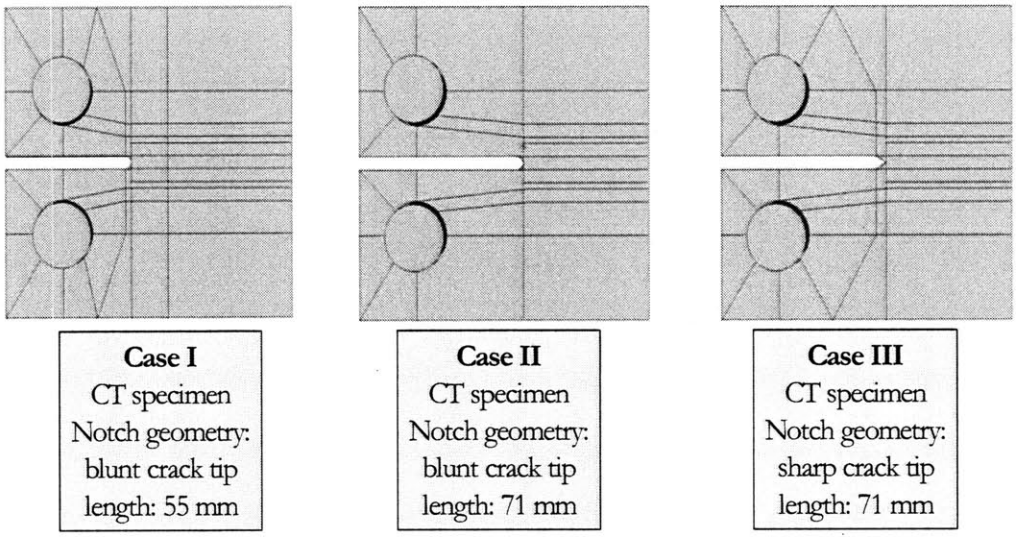

Figure 4-20: CT model in finite element code examined for three different cases: (i) case I with an initial notch length of 55 mm and blunt crack tip (left), (ii) case II with an initial notch length of 71 mm and blunt crack tip (center), and, (iii) case III with an initial notch length of 71 mm and sharp crack tip (right)

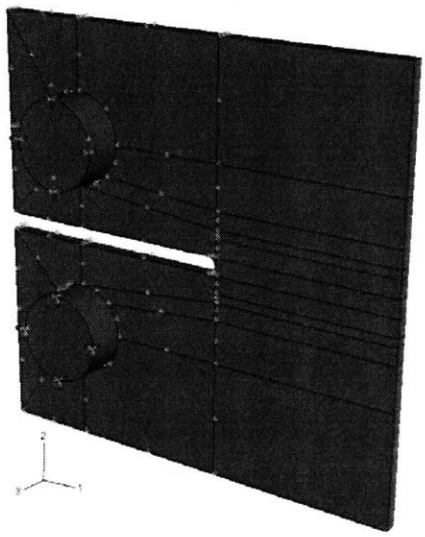

Figure 4-21: Boundary conditions for the CT model with an initial notch length of 71 mm and blunt crack tip geometry

limit and the lowest natural frequency in the loading direction. In explicit analysis, the stability time that is automatically calculated in the main solver of the FE program has to be higher than the total time step, and it can be expressed as:

$$\Delta t = \frac{L_e}{c_d} = L_e\sqrt{\frac{\rho}{E}}$$
$$= 4.5 \times 10^{-4} \times \sqrt{\frac{2650}{65.87 \times 10^9}} = 9 \times 10^{-8}[\mathrm{s}] \tag{4.13}$$

where L_e is the characteristic element length, usually the smallest element dimension, and c_d is the dilatational wave speed for a linear elastic material. As another lower bound for the time step, the lowest natural frequency in the loading direction $f = 2924.7$ Hz was obtained by running a frequency analysis in ABAQUS/Standard^{TM}.

Thus the total time step should be larger than the period, $T = 3.42 \times 10^{-4}$ s, corresponding to the lowest natural frequency in order to increase the likelihood of a quasi-static result. It was decided to perform the FE simulation with a total time step, $t_{total} = 0.035$ s, which is about 100 times longer than the period corresponding to the lowest natural frequency in the loading direction.

Moreover, it was observed from the tests that the aluminum specimens failed when the head-to-head displacement was about 15 mm, so the maximum displacement is set to 20 mm. This value, therefore, leads to the following loading rate:

$$V_{load} = \frac{\delta_{\max}}{t_{total}}$$
$$= \frac{20 \times 10^{-3}}{0.035} = 0.57\ [\mathrm{m/s}] \tag{4.14}$$

Therefore, the ramping time is 0.035 s and the constant velocity 570 mm/s.

The crack initiation and propagation obtained from the FE analyses capture extremely well the ones observed at the experimental program for both CT specimens with different notch geometries, Figs. 4-22, 4-23 and 4-24.

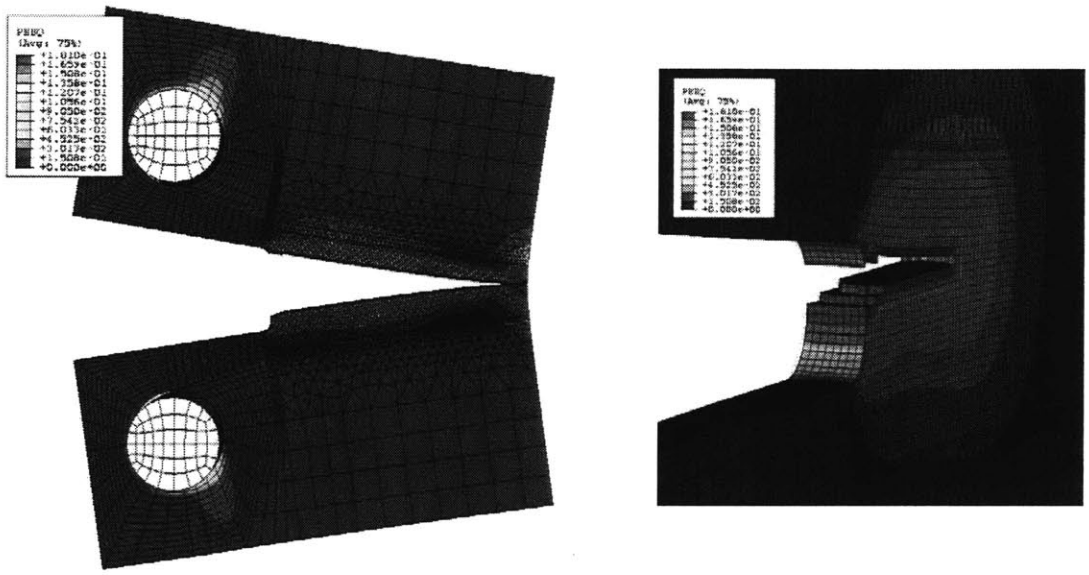

Figure 4-22: CT specimen with initial notch length of 55 mm and blunt crack tip: crack path (left) and crack tip initiation obtained from the FE simulation

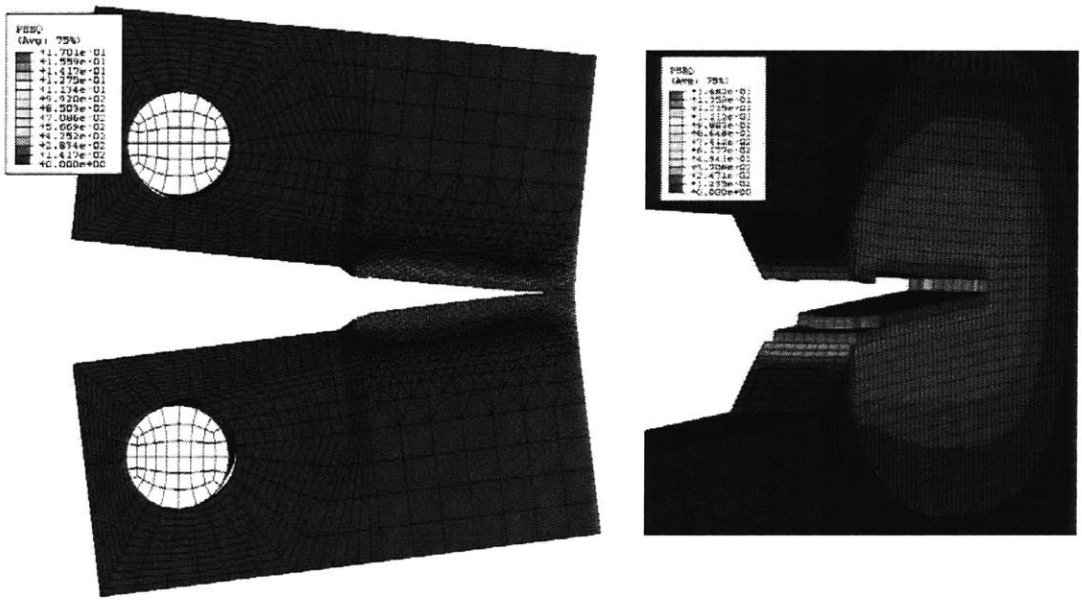

Figure 4-23: CT specimen with initial notch length of 71 mm and sharp crack tip: crack path (left) and crack tip initiation obtained from the FE simulation

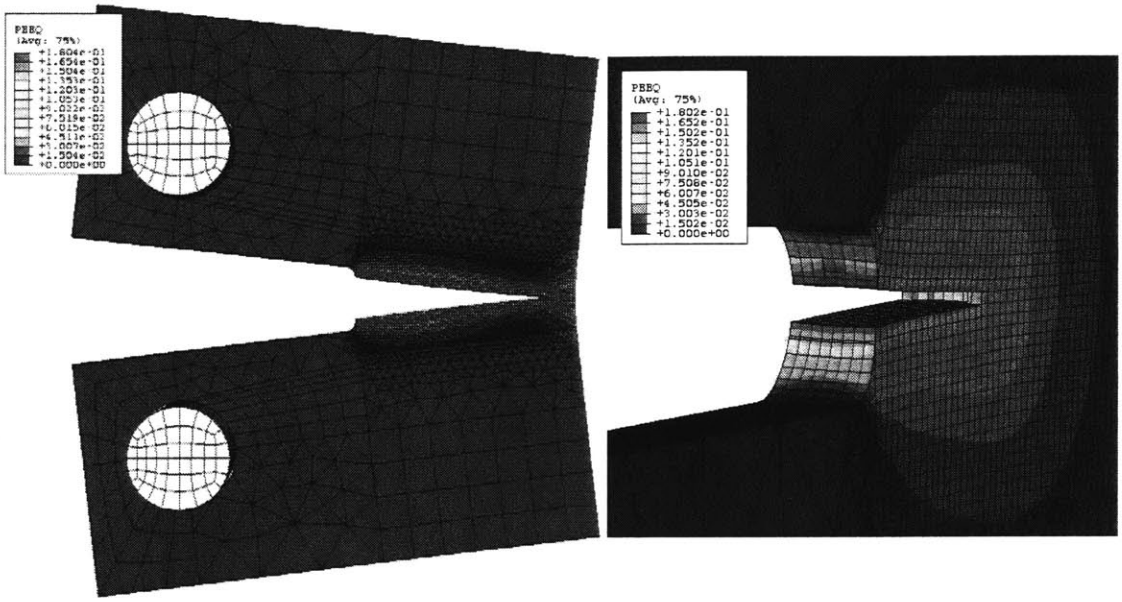

Figure 4-24: CT specimen with initial notch length of 71 mm and blunt crack tip: crack path (left) and crack tip initiation obtained from the FE simulation

4.4.2 FE analysis of the stiffened CT specimens

For the numerical simulation and analysis of the stiffened CT specimen, with an extruded T-type stiffener, the mass scaling technique was used since a dense mesh was selected around the expected crack path reducing drastically the computational cost. Mass scaling enables an analysis to be performed economically without artificially increasing the loading rate [1].

Although non-linear FE codes and inexpensive computational power have reached a state where the mechanics of very complex problems can be estimated with good accuracy by use of a PC, mass scaling is often used to increase computational efficiency for the case of quasi-static analysis where few very tiny elements control the stable time increment. The analysis requires over one month on a workstation with double processor of 2.2 GHz CPU without the application of mass scaling technique.

The FE model for the stiffened CT specimen shows that the crack fails to propagate through the stiffener. The crack path is similar to the pattern observed at the experimental program, Fig. 4-25. Additionally, the global behavior of the stiffener is captured extremely well, Fig.

4-26. Examining the crack pattern obtained from the numerical simulation it is observed that the condition in which the crack flips cannot be captured from this model, Fig. 4-27. Further investigation is needed in this area with emphasis on the understanding of the mechanisms that govern this change in tunneling. Prior to the application of other FE models, a microstructural analysis and observation might be needed to examine this particular condition. Although this phenomenon of crack flipping was observed throughout all the tests performed on extruded T-type stiffeners, the examination of different types of naval aluminum alloys might help explain this effect.

Nevertheless, as far as this thesis is concerned, the objective of mapping the crack pattern is achieved. For a naval architect who desires to examine macroscopically the effect of fracture on an entire vessel, the goal is achieved, since the understanding of this phenomenon will increase the capabilities of an optimized structure to withstand damage.

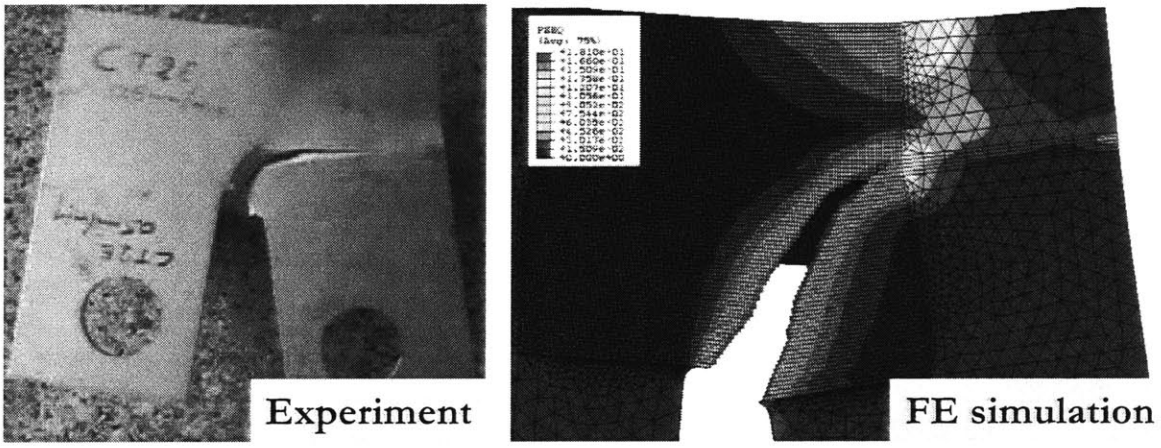

Figure 4-25: Comparison between the crack pattern obtained from the experiment (left) and the numerical simulation (right) for the T-type extruded CT specimen

4.5 Intermediate-scale FE Models

The numerical modeling of the intermediate-scale specimens is performed by utilizing symmetry taking advantage of the specimens' geometry. A similar scheme to the small-scale FE modeling method is followed for the intermediate-scale models. As a first step the total time step, Δt, is

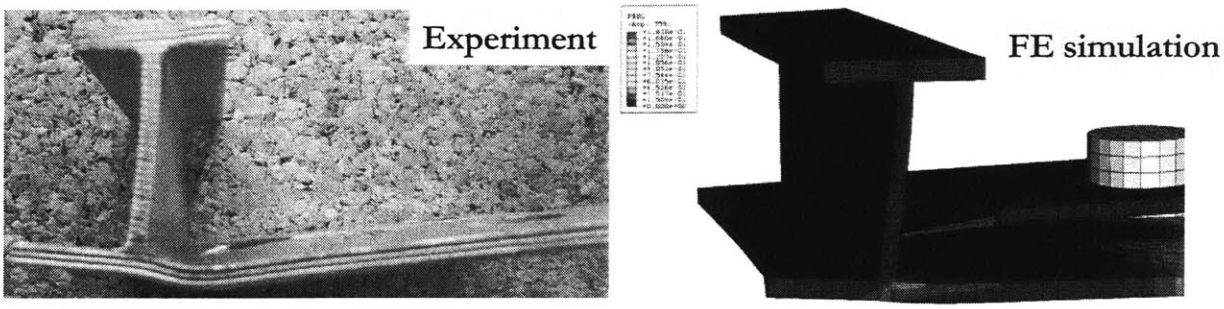

Figure 4-26: Comparison between experimental result (left) and numerical simulation (right) with respect to the behavior of the T-type stiffener during the loading

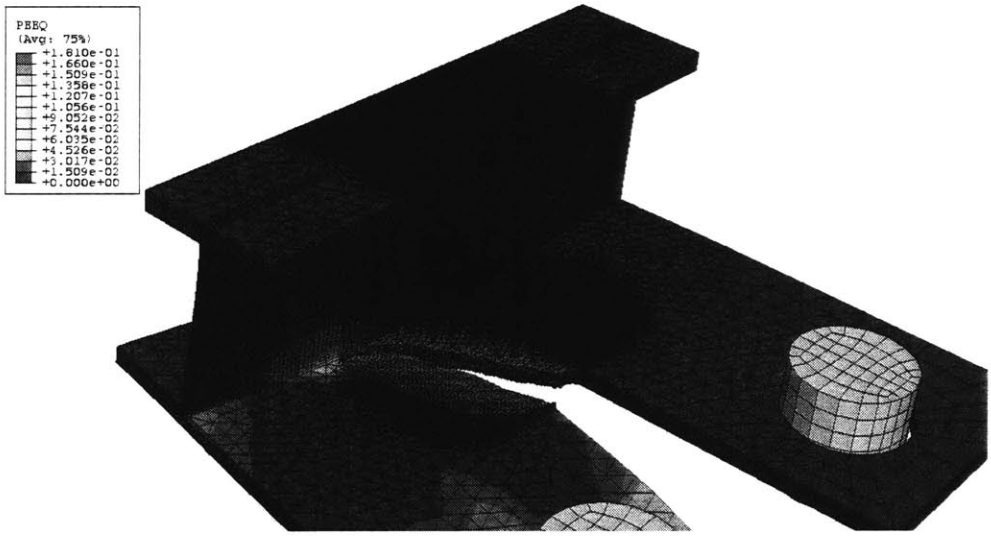

Figure 4-27: Crack propagation in the T-type extruded CT specimen. The crack pattern is similar to the one obtained from the experimental program

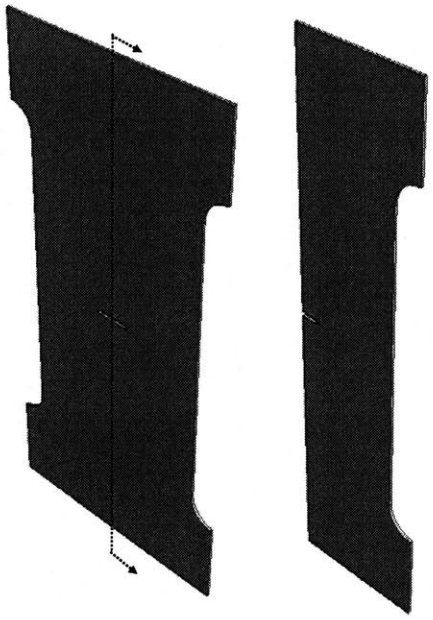

Figure 4-28: CCT finite element models, whole (left) and half (right). The half model was selected to reduce computational cost

calculated. Since the material and mesh size remain the same,we have that $\Delta t = 9 \times 10^{-8}$[s].

4.5.1 Center Cracked Tension (CCT) model

As another lower bound for the time step, the lowest natural frequency in the loading direction for the CCT model, Fig. 4-28, is $f = 2267.7$ Hz and it is obtained by running a frequency analysis in ABAQUS/Standard^{TM}. Thus the total time step should be larger than the period, $T = 4.41 \times 10^{-4}$ s, corresponding to the lowest natural frequency in order to increase the likelihood of a quasi-static result. This result is based on the intermediate mesh that was selected for this model, as shown in Fig. 4-29.

It was decided to perform the FE simulation with a total time step, $t_{total} = 0.045$ s, which is about 100 times longer than the period corresponding to the lowest natural frequency in the loading direction.

Moreover, it is observed from the tests that the aluminum specimens failed when the head-to-head displacement was about 4.6 mm, so the maximum displacement is set to 5.0 mm. This value, therefore, leads to the following loading rate:

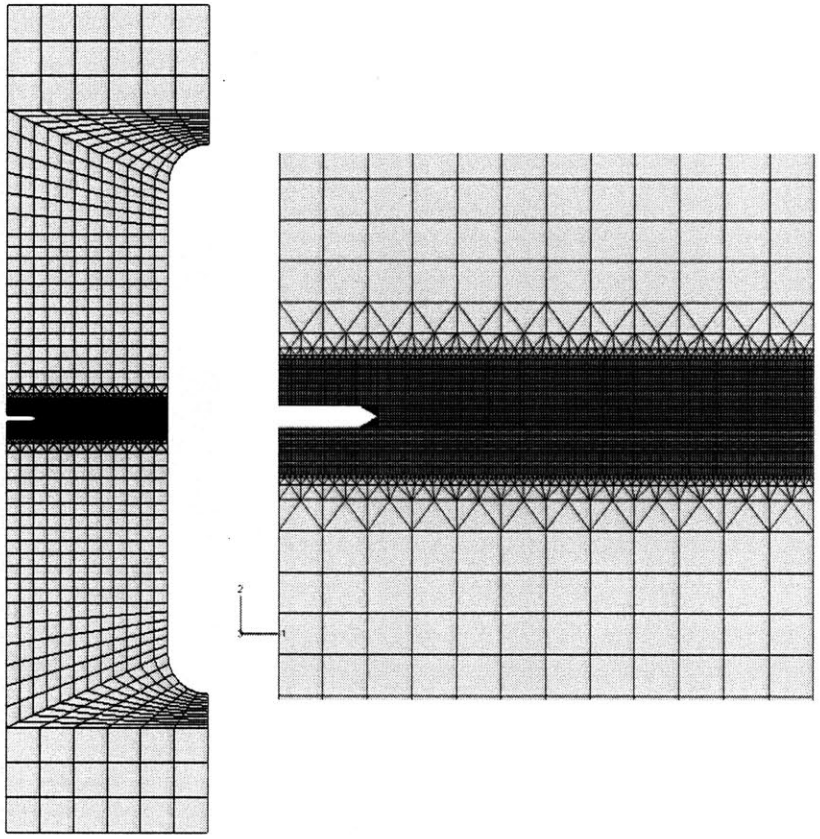

Figure 4-29: Finite element mesh of the half CCT model, whole (left) using large elements to reduce the computational cost and close view (right) that shows the dense mesh around the expected region of crack propagation

$$V_{load} = \frac{\delta_{\max}}{t_{total}}$$
$$= \frac{5.0 \times 10^{-3}}{0.045} = 0.11 \ [\mathrm{m/s}] \tag{4.15}$$

Therefore, the ramping time is 0.045 s and the constant velocity 111 mm/s. Figure 4-30 shows the boundary conditions imposed on the CCT model in order to simulate the experiment. This model consisted of 93,072 3D-solid elements and is completed within 10 hours (CPU time).

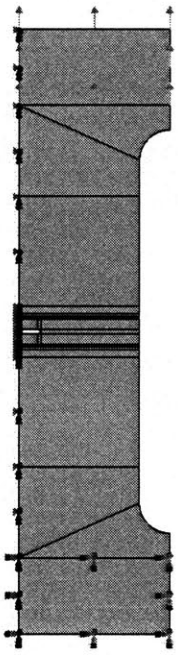

Figure 4-30: Boundary conditions for the Center Cracked Tension specimen modeled in commercial FE code

The distribution of the equivalent plastic strain for the crack at the stages of initiation, propagation and failure are shown in Figs. 4-31 and 4-32. Additionally, the distributions of von Mises stress and equivalent plastic strain at the crack initiation are shown in Fig. 4-33.

The results obtained from the numerical simulations with respect to the mapping of the crack path present very good correlation with the experimental ones.

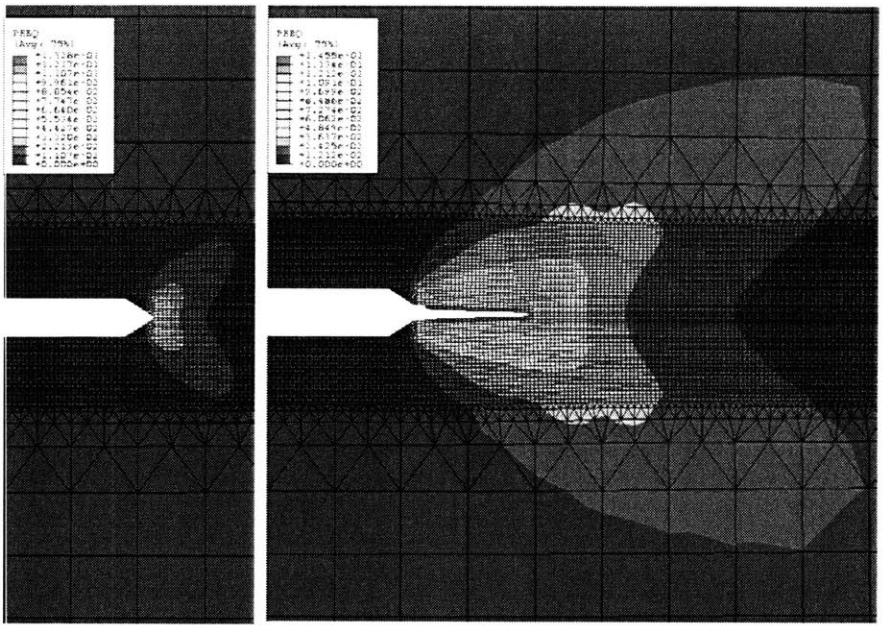

Figure 4-31: Distribution of equivalent plastic strain for CCT model at crack initiation (left) and during propagation (right)

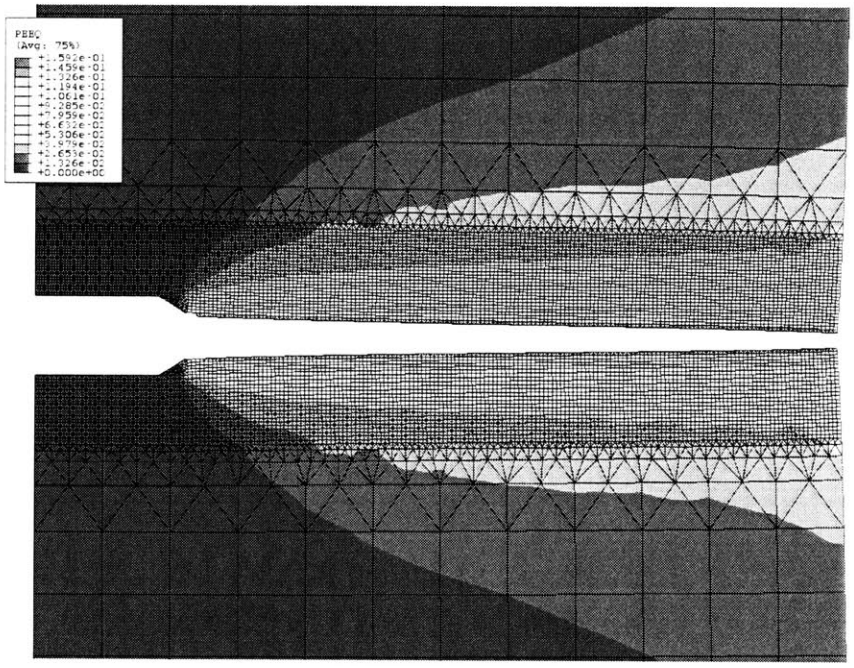

Figure 4-32: Distribution of equivalent plastic strain for CCT model at failure

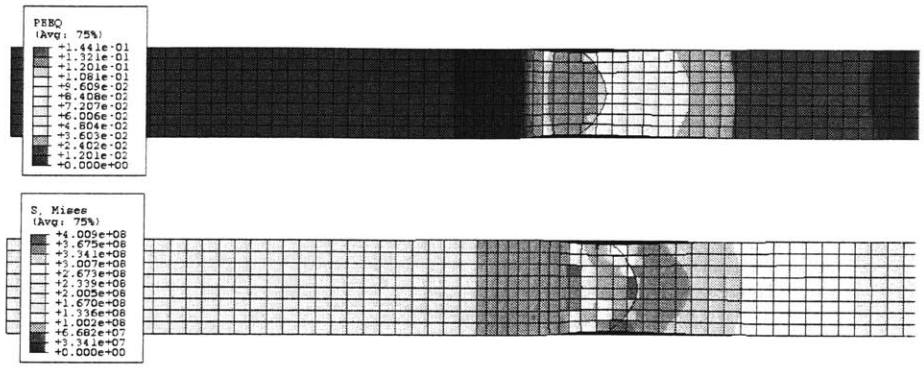

Figure 4-33: CCT crack initiation: distributions of equivalent plastic strain (top) and von Mises stress (bottom)

4.5.2 Twin Stiffened Center Cracked Tension (TSCCT) model

The lowest natural frequency in the loading direction for this case is $f = 2514.9$ Hz and it is obtained by running a frequency analysis in ABAQUS/Standard^{TM}. Thus the total time step should be larger than the period, $T = 3.97 \times 10^{-4}$ s, corresponding to the lowest natural frequency in order to increase the likelihood of a quasi-static result. It was decided to perform the FE simulation with a total time step, $t_{total} = 0.04$ s, which is about 100 times longer than the period corresponding to the lowest natural frequency in the loading direction.

Moreover, it is observed from the tests that the aluminum specimens failed when the head-to-head displacement was about 14.2 mm, so initially the maximum displacement is set to 20 mm. The output of this simulation shows that the FE model fails at a maximum displacement of 9.9 mm, which is finally used for the numerical simulation. This value, leads to a constant velocity of 0.2475 m/s. Figure 4-34 shows a FE model of the entire TSCCT specimen. It can be observed that this model is symmetrical in the centerline, therefore, half of the model is simulated to reduce the computational cost, Fig. 4-35. A very dense mesh around the expected crack path is created and this model requires the use of 138,898 3D-solid elements and computational cost of 13 hours (CPU time).

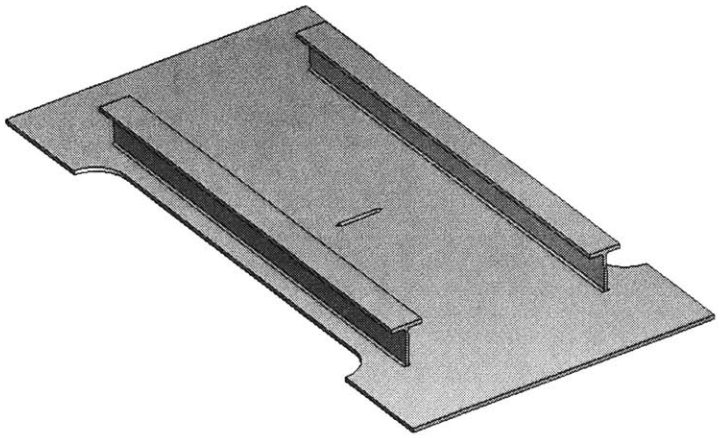

Figure 4-34: Twin Stiffened Center Cracked Tension (TSCCT) model. Half of this model was simulated at the commercial FE code ABAQUS

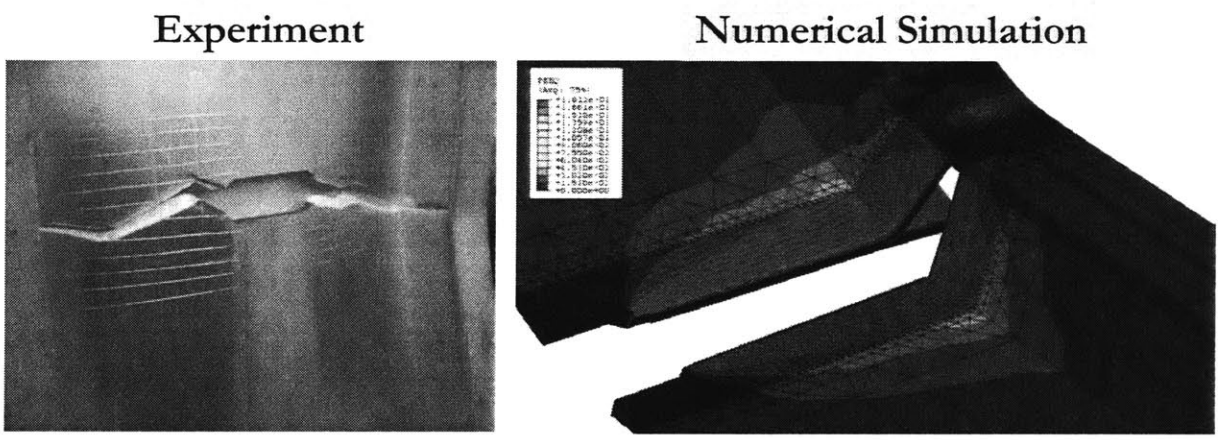

Figure 4-35: Comparison between the results obtained at the experimental program and the FE simulation for the TSCCT model

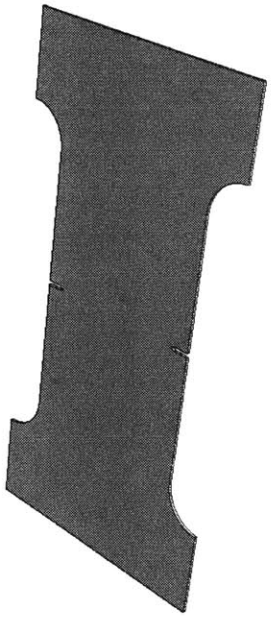

Figure 4-36: Whole model of the Double Edge Notched Tension (DENT) specimen at the FE code

4.5.3 Double Edge Notched Tension (DENT) model

The lowest natural frequency in the loading direction for this case is $f = 2193.0$ Hz and it is obtained by running a frequency analysis in ABAQUS/Standard^{TM}. Thus the total time step should be larger than the period, $T = 4.56 \times 10^{-4}$ s, corresponding to the lowest natural frequency in order to increase the likelihood of a quasi-static result. It was decided to perform the FE simulation with a total time step, $t_{total} = 0.045$ s, which is about 100 times longer than the period corresponding to the lowest natural frequency in the loading direction.

Moreover, it is observed from the tests that the aluminum specimens failed when the head-to-head displacement was about 6.0 mm, so initially the maximum displacement is set to 10 mm. From the output of the analysis it is observed that the FE model fails at a maximum displacement of 3.1 mm. Using this value, therefore, we create a constant velocity of 0.6889 m/s, Fig. 4-36.

The distributions of the von Mises stress at the crack initiation step and the equivalent plastic strain for the failed DENT FE model are shown in Fig. 4-37. The crack pattern that

includes, crack initiation, propagation and failure are well-captured in the model used for the numerical simulation. This model consisted of 72,784 3D-solid elements due to a very dense mesh around the area of the expected crack pattern and the computational cost was 6.5 hours (CPU time).

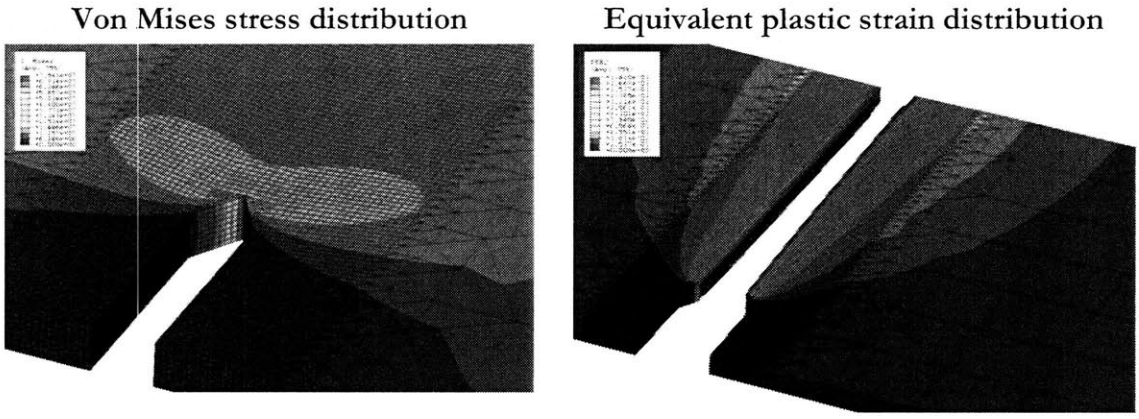

Figure 4-37: DENT results from FE simulation showing the distributions of the von Mises stress at the crack initiation step (left) and the equivalent plastic strain (right) for the failed case

4.5.4 Single Stiffened Double Edge Notched Tension (SSDENT) model

For the SSDENT model, symmetry is observed in the center part of the specimen that enables the user to reduce significantly the required computational time or increase the density at the expected crack path to acquire more accurate results, Figs. 4-38 and 4-39. The lowest natural frequency in the loading direction for this case is $f = 2514.8$ Hz and it is obtained by running a frequency analysis in ABAQUS/Standard^{TM}. Thus the total time step should be larger than the period, $T = 3.98 \times 10^{-4}$ s, corresponding to the lowest natural frequency in order to increase the likelihood of a quasi-static result. It was decided to perform the FE simulation with a total time step, $t_{total} = 0.04$ s, which is about 100 times longer than the period corresponding to the lowest natural frequency in the loading direction.

Moreover, it is observed from the tests that the aluminum specimens failed when the head-to-head displacement was about 14.97 mm, so initially, the maximum displacement is set to 20 mm. From the analysis, it is then measured that the FE model fails at a maximum displacement

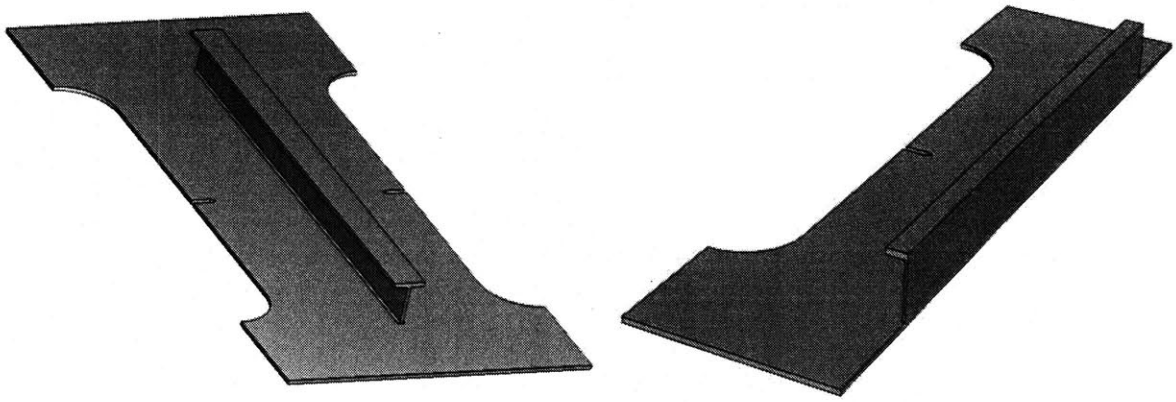

Figure 4-38: Single Stiffened Center Cracked Tension specimen (on the left) modeled in the FE code using symmetry (on the right)

of 10.19 mm, therefore this value is used. This value, leads to the a constant velocity of 0.25475 m/s.

The applied boundary conditions are similar to the previous cases examined and correspond to the ones imposed during the experimental program, Fig. 4-40. The FE result captured very well the phenomena observed at the experimental program, Fig. 4-41. This model consisted of 116,018 3D-solid elements due to a very dense mesh around the area of the expected crack pattern and the computational cost was 9.5 hours (CPU time).

4.5.5 Summary of the FE analysis for the intermediate-scale models

Figure 4-42 shows the results obtained from the FE analysis of the intermediate-scale models.

Table 4.3 presents a summary of the values obtained from the experiment and the numerical simulations. A comparison between the data obtained from the experimental program and the results of the FE analysis show that for the maximum forces we have an over-estimation that is from 11.60 % up to 60.50 %. It is noticed that the difference increases significantly in the cases where the model has a stiffener installed on the plate. This is an outcome of the operation of the experimental facilities near their limitation, where a lot of the energy is stored in the device. Additionally, the difference between the values of the displacements obtained comes from the fact that the experimental ones refer to the device's cross-head displacement which includes an

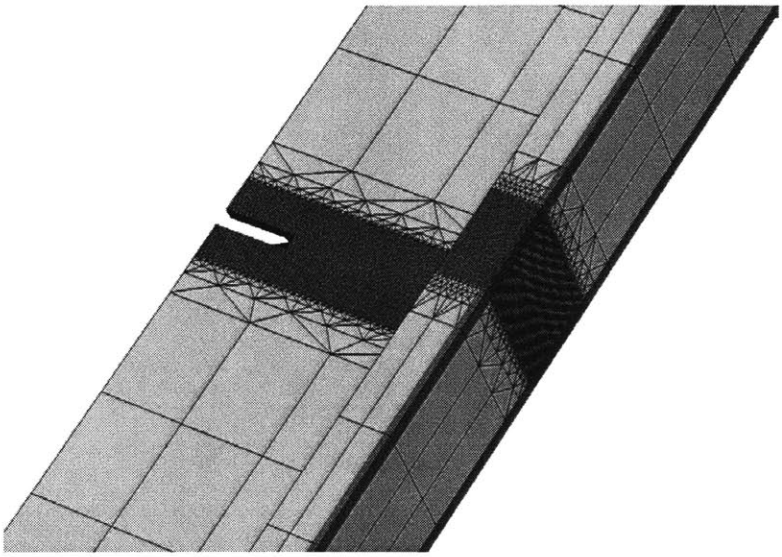

Figure 4-39: Close view of the mesh used for the half-SSDENT model utilizing the intermediate mesh used for the "dogbone" specimen

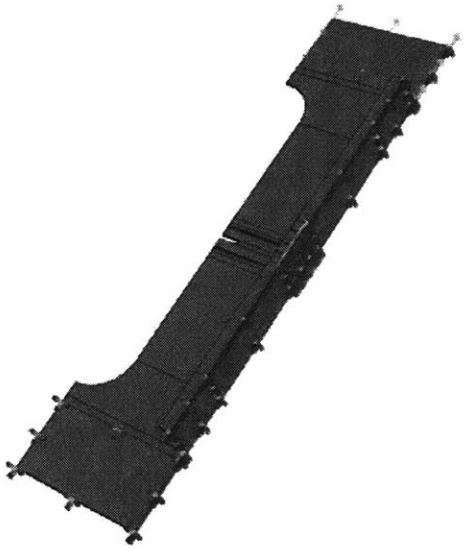

Figure 4-40: Boundary conditions imposed to the half-SSDENT model in the FE code

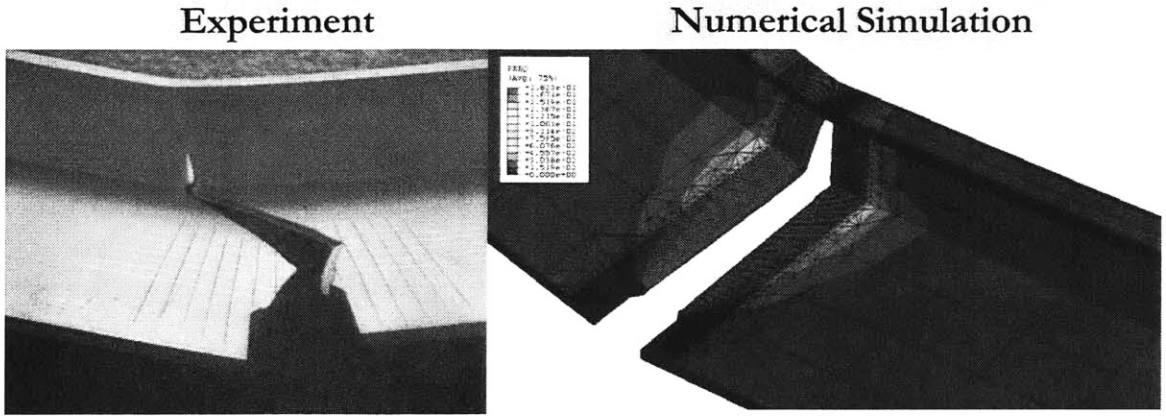

Figure 4-41: Crack pattern observed in the experimental program (left) and the FE code (right). Note that minor deformations or crack kinking can alternate the crack path which is expected to be perpendicular to the loading direction at the "perfect" case

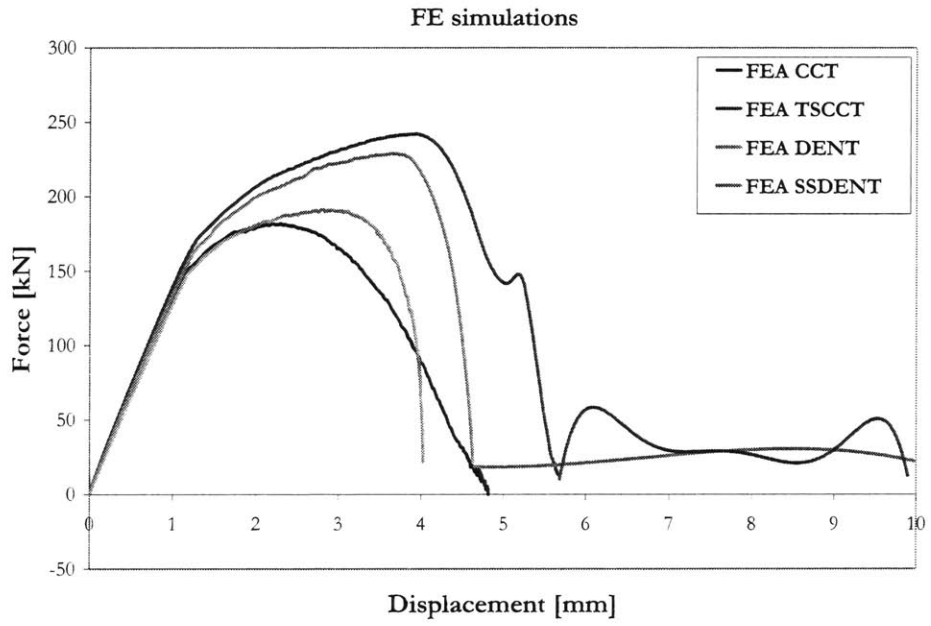

Figure 4-42: Force vs. displacement graph showing the results obtained from the FE analysis for the intermediate-scale models using symmetry

Model	Experiment		FE simulation	
	Maximum force [kN]	Cross-head displacement to failure [mm]	Maximum force [kN]	Displacement to failure [mm]
CCT	150.95	4.349	182.01	4.857
TSCCT	201.50	14.168	269.12	9.837
DENT	154.98	5.995	172.96	4.017
SSDENT	142.82	14.943	229.28	10.190

Table 4.3: Comparison between experiment and numerical simulations for the intermediate-scale group

experimental error coming from the displacement of the gripping components.

4.6 Fundamentals of Stiffener Effect on the Crack Pattern

Usually, material separation is a result of a complex physical process which occurs at the micromechanical scale. On a macro-scale the only variables that control fracture are current values of components of the stress and strain tensors and their histories. These quantities are readily available as output in all commercial nonlinear FE codes.

In order to examine the fundamentals embedded in the mechanics that govern the fracture mechanics of stiffened plates and panels, a series of numerical simulations were performed varying the web height to thickness ratio for the extruded flatbar stiffener. The initial flatbar stiffener used for the welded stiffened CT specimens has a value of $A_{web} = t_w \times h_w = 120$ mm^2, where t_w and h_w, are the thickness and height of the stiffener's web, resulting from initial values of $t_{w,initial} = 3$ mm and $h_{w,initial} = 40$ mm. This product was set as a constant and the thickness of the web of the stiffener varied from 1 to 6 mm for six different cases ($t = 1, 2, 3, 4, 5$ and 6 mm), Fig. 4-43. The geometry of the stiffened CT specimen is similar to the small-scale models, 125 × 120 × 3.6 mm (length × width × thickness).

4.6.1 Sensitivity analysis of extruded flatbar CT stiffened model

The evaluation of a model during numerical simulation is a complex procedure, especially when several parameters are entered into the code as inputs to achieve lower simulation costs. Table

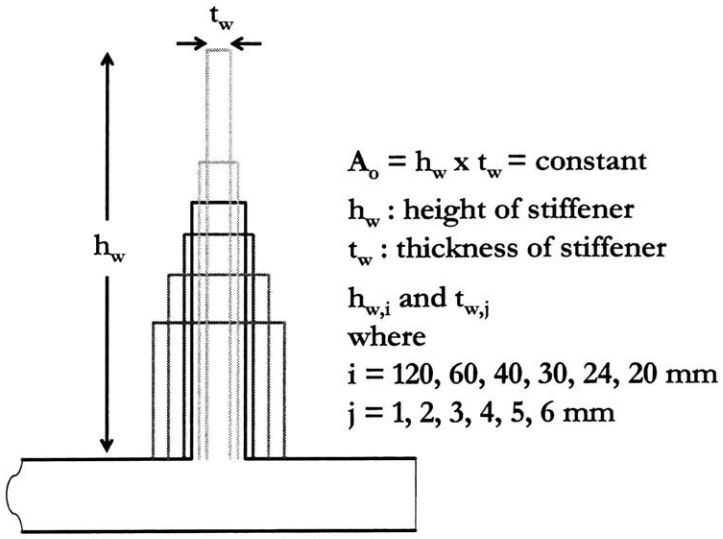

Figure 4-43: Schematic of the extruded flatbar stiffened CT models examined

4.4 shows the geometry characteristics. In order to examine the effect of one type of stiffener by varying its geometry, a sensitivity analysis is performed, using six different cases and the results are shown in Figs. 4-44, 4-45, and 4-46. It can be observed that the bigger the height of the stiffener is the more the crack propagates on it. Therefore, the crack propagates at a longer distance in the case I compared to the other cases, while at the case VI, the crack does not propagate on the stiffener but the stiffener is tripped.

The outcome of this sensitivity analysis reveals that the application of different stiffener geometry that might carry the same load, since the area remains constant, shows different behavior towards fracture, Fig. 4-47. A selection of the desired objective function from the naval architect will offer then the optimum type of stiffener geometry that will not only meet the naval architecture requirement but also will increase damage tolerance. It can be optimized versus either the maximum applied load or the maximum displacement to failure, as shows Table 4.5. This result is extremely critical in the modern shipbuilding industry and diverges from the traditional design approach that ships need to be extremely stiff as it is shown that the stiffening configuration affects even more the failure of structural components. The modern philosophy, already applied in other industries, such as automobile, aircraft, space and transportation, requires the structures to be capable of absorbing the maximum possible energy while increasing

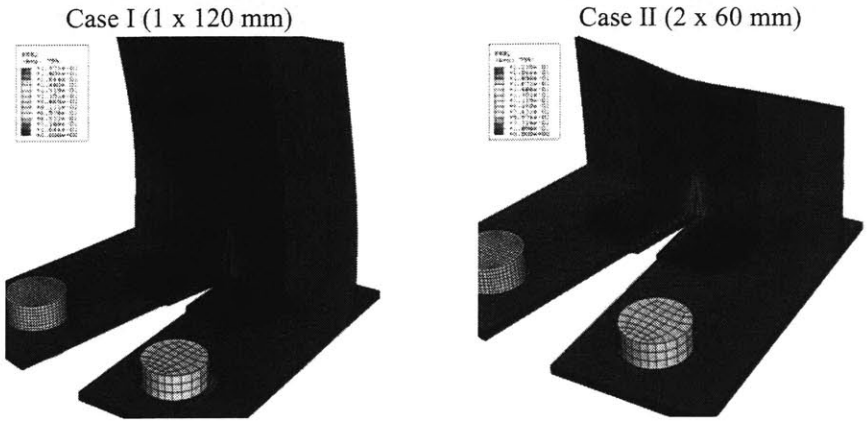

Figure 4-44: Cases I & II examined for an extruded flatbar stiffened CTEI model with 1×120 mm and 2×60 mm stiffener web thickness and height, respectively

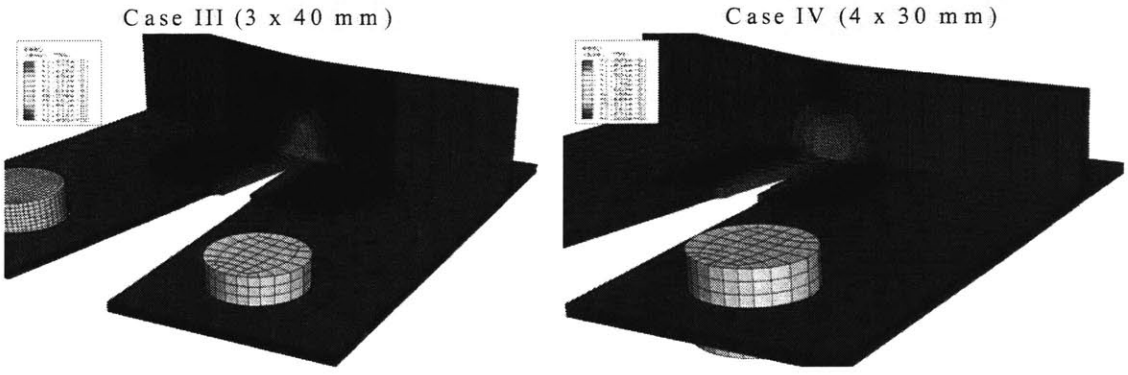

Figure 4-45: Cases III & IV examined for an extruded flatbar stiffened CTEI model with 3×40 mm and 4×30 mm stiffener web thickness and height, respectively

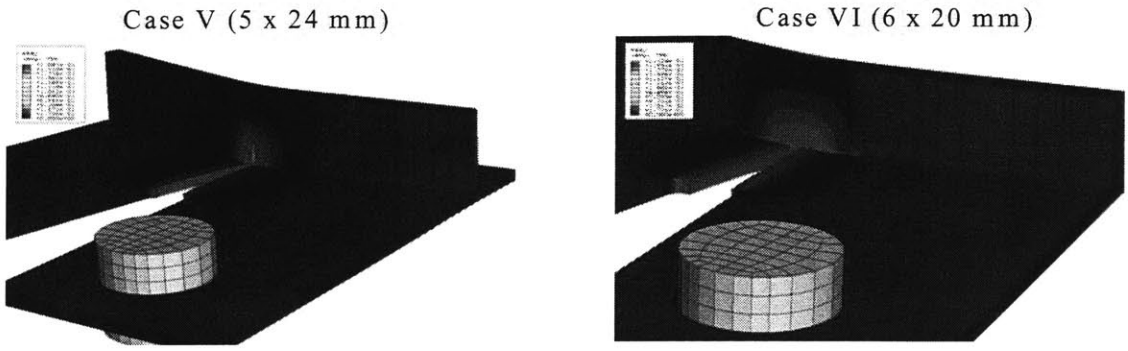

Figure 4-46: Cases V & VI examined for an extruded flatbar stiffened CTEI model with 5×24 mm and 6×20 mm stiffener thickness and height, respectively

	Stiffener's web		**CTEI geometry**	
Case	thickness [mm]	height [mm]	Distance from end of rear plate [mm]	Distance from crack tip [mm]
I	1	120	21.0	32.0
II	2	60	20.5	31.5
III	3	40	20.0	31.0
IV	4	30	19.5	30.5
V	5	24	19.0	30.0
VI	6	20	18.5	29.5

Table 4.4: Geometric characteristics of the flatbar stiffened CT models

the envelope of positive safety that includes speed and mobility.

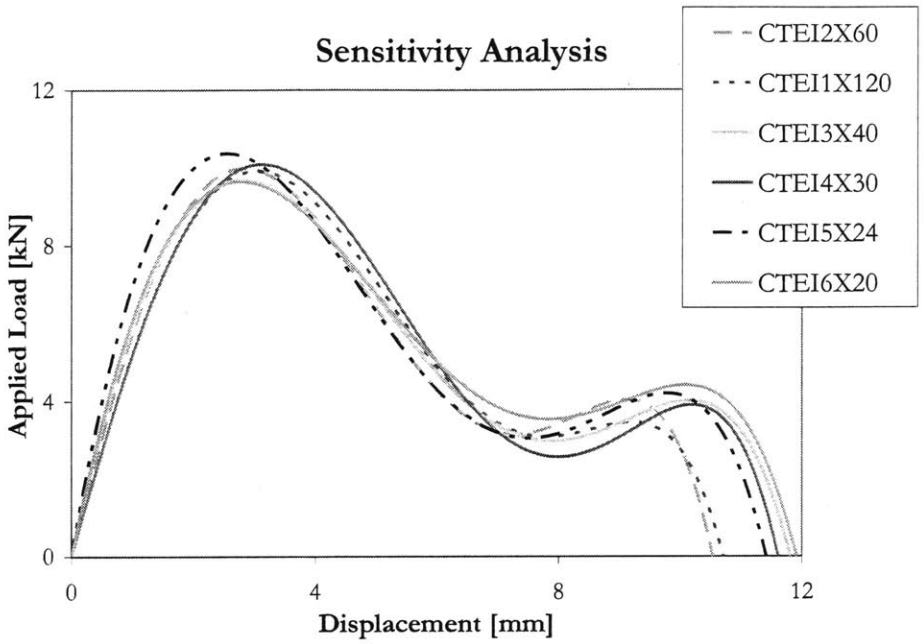

Figure 4-47: Load vs. displacement curves for the six different models using numerical simulations

Case	Max Load [kN]	Displacement to fracture [mm]	Displacement to failure [mm]
I	11.75	2.851	10.7
II	11.40	2.377	10.5
III	11.21	2.851	11.8
IV	11.73	2.515	11.6
V	11.85	2.802	11.4
VI	11.45	2.287	11.9

Table 4.5: Results from analysis of six different flatbar stiffened CT models with constast cross section of the stiffener's web

Chapter 5

Conclusions and Recommendations

5.1 Synopsis

Modern vessels vary from conventional ones, which were built of mild steel and designed on the basis of experience, to front-end technology high speed craft made by sophisticated lightweight materials such as composites, high-strength steels and aluminum alloys. It is obvious that design procedures have to cover a wide range of applications and materials, and with the continuing development of faster vessels in highly optimized designs, the demand for research in this area will continue as the accidental loads and consequences, due to lack of experience, are more or less unknown.

Since the tragic loss of the Titanic, which gained public attention across the world, the demand for improved safety in marine transportation has been a major long-standing issue. Accidents at sea usually receive enormous media coverage when they are related with human life losses or environmental disasters, such as the Exxon Valdez in Alaskan waters, the sinking of the Estonia due to a defective bow door, the grounding and sinking of the Norwegian high-speed ferry Sleipner, and lately the sinking of the tanker Prestige off the coast of France, due to structural failure of the hull beam. The public and political focus associated with the media coverage of shipping disasters has historically put a huge pressure on the marine industry to improve regulations for safety at sea which shows that this area of naval architecture is highly relevant. A thorough understanding of damage mechanics and mechanisms is required prior to setting new rules and regulations.

The shipbuilding industry is seeking to achieve advanced and more efficient concepts and designs for ships and underwater vehicles with improved safety and performance using optimized structural design. To increase the ship's survivability, in-depth understanding and vast experience is required to study the methodology and dynamic effects of complex damage mechanisms on marine structures and ship systems. Damage prediction models should be created to enhance the ability of the ship to withstand all types of loads. Verification and validation of modeling and simulation is required for the models to be functional. The modeling could be either numerical or physical. All these will lead to the improvement of existing design procedures and criteria, which may lead to more affordable designs.

Ships represent some of the most complex thin-walled structures seen in engineering. The development of finite element methods, together with high-speed computers, has allowed rational approaches to ship structural analysis to be adopted.

Structural failure due to extreme loads such as underwater and/or air explosion, high velocity impact or hydrodynamic loads is primarily caused by **fracture**. It is a common practice to design ships with adequate resistance to yielding, buckling and fatigue, but not fracture. Consequently, adequate methods and procedures to design ships against fracture have not been developed. Even more importantly, a fundamental understanding of mechanisms and mechanics of fracture under high intensity and short duration loads is lacking. Therefore, a need to increase the survivability envelope of naval combatants and other types of vessels through a comprehensive research on fracture based on the results of this dissertation and further research is needed.

5.2 Achievement of thesis objectives

The ultimate goal of this thesis is to understand the mechanics and mechanisms of fracture that govern the structural response of naval structures. This work is primarily focused on high-speed craft built with lightweight materials such as naval aluminum, because a significant increase in the use of its alloys is observed in the shipbuilding industry and these vessels. To pursue this objective an extended experimental program including coupon small and intermediate-scale tests is conducted examining the macroscopic effect of various parameters of stiffening

mechanisms towards fracture.

Marine vessels are always subjected to external or internal dynamic loading, operating in extreme environmental and functional conditions that can lead to the loss of the entire structure and human lives. Stiffened plates are the most commonly used built-up structural elements in marine vessels, which form the backbone of ships, appearing in decks, bottoms, bulkheads, and side shell. The damage of stiffened plates will result in the collapse of overall system structures. An increasingly popular approach to undertake ship hull ultimate strength analysis is to consider the failure of the individual stiffened plates and combine these to determine the failure load of the entire hull cross-section.

The results of the experiments on aluminum plates and panels reveal that the crack propagation and arrest phenomena highly depend on the presence of stiffeners, the type of stiffener and the stiffening configuration. Observations of the crack pattern in both experimental and numerical analyses show that the type of stiffener and its configuration can significantly affect the effect of fracture. A careful selection of stiffener type and its geometry can improve the global behavior of a naval structure based on the requirements set by the customer. Nevertheless, this selection should always take place in conjuction and with respect to the other types of loading that a vessel is designed to withstand.

Many civil and defense applications require a blast-resistant performance. The threat from a sudden overpressure can arise from a number of situations, ranging from accidents to attack by an enemy weapon. The impact of an explosive is one of the most threatening scenarios for a naval platform. A naval engineer has various options to reduce the vulnerability of the platform design, like structural arrangement and protection. One of the most important options is to increase the blast resistance of the hull. The methodology proposed in this thesis provides a tool for engineers and designers to include blast resistance during design and evaluation of naval structures.

Fracture mechanics concerns the design and analysis of structures which contain cracks or flaws. On some size/scale all materials contain flaws, either microscopic, due to cracked inclusions, debonded fibers, etc., or macroscopic, due to corrosion, fatigue, welding flaws, etc. Thus, fracture mechanics is involved in any detailed design or safety assessment of a structure. As cracks can grow during service due to fatigue, fracture mechanics assessments are required

throughout the life of a structure or component, not just at the start of the life cycle of a naval vessel. In which direction will a crack propagate when a stiffening mechanism is present? Which type of stiffener arrests a crack better? Which parameters affect the crack path? What should be done by a designer to improve the damage tolerance of a naval structure without penalty to the rest of the existing requirements? This thesis fully or partially answers these questions.

Moreover, the author has a strong belief that this research will eventually lead to very important knowledge concerning the effect of stiffeners on the crack propagation and arrest phenomena especially with the recent rapid expansion of naval applications of marine aluminum alloys. These results will enhance the capabilities of the naval architect to create stronger and safer structures by optimizing the amount of material, structural design and operational life of the structure. Further gains in structural performance can be anticipated via stiffened panel construction optimization. This research provides new knowledge which will increase manufacturing affordability, passive damage protection and will improve damage containment.

5.3 Major Contributions

Marine structures such as ships and offshore platforms are designed to be damage tolerant. The level of damage tolerance is empirically set and requires accurate prediction of crack growth under operational conditions. Accurate prediction of crack growth in naval and marine aluminum structures plays a key role in the structural analysis of a vessel. In the advancing marine high speed market the evolution tends towards larger and faster vessels and this makes it difficult to base new designs on past experience. The result is an intensified need for rational procedures for design of both main structural parts and details in such high speed vessels.

The application of the proposed methodology in the shipbuilding industry will lead to the reduction of parameters that critically affect the operation of vessels. This includes the preparations, demand for skilled personnel, and special environmental conditions required for the replacement of a panel. On the other hand, it will decrease the inherent risk, cost and time while increasing the operational availability of the vessel. The major contributions of this dissertation can be summarized as follows:

- Development of a methodology to study the mechanisms that govern the fracture of

aluminum structures,

- Completion of a unique series of fracture tests on various structural components,
- Mapping of crack patterns in small and intermediate scale tests,
- Quantification of the stiffening effect on fracture of structures,
- Analysis of relative merits of various stiffener configurations with respect to damage tolerance, and
- Evaluation of design parameters that affect fracture of naval aluminum structures.

Despite the increased application of aluminum in the shipbuilding industry, lack of information on fracture exists in the current literature. This information includes critical data, that consist of fracture tests of aluminum stiffened plate structures, crack initiation, propagation and "arrest". This thesis contributes to the study of these issues, which will hopefully lead to better vessel designs, decrease of maintenance requirements and estimation of the criticality of an existing damaged part of a vessel and the method to select for repairing it.

One important issue is the determination of the crack path. The macroscopic direction in which a crack is growing in an isotropic material is influenced by various factors, some of which are related to features at some distance from the crack edge, such as severe material deformation that may attract the crack, necking from the crack edge, micro-separations in a long process region or anisotropy introduced by flow in the plastic region. In other cases, it appears that the local stress field at the crack edge governs the direction of continued crack growth.

The reason why shear lips develop has its origin in the material structure and the type and amount of texture. Further analysis is needed using microscopic observations. Quite recently [365] it was found that shear lips in AA 5083 could be surpressed by making a small scratch along the crack growth direction.

The simplest condition for cracks in isotropic materials is that of symmetry, which implies that a crack would propagate in the opening mode, unless this mode is surpressed by sufficiently high compressive stresses. The apparent preference for mode I appears to be most pronounced for small scale yielding. Under massive plastic flow, a crack may propagate in a shearing mode, as evidenced by shear lips in tensile tests.

As aluminum high-speed vessels grow larger and venture into increasingly hostile operating environments, ensuring their structural safety becomes more and more complex. The design of this new generation of aluminum vessels has created the need for improved structural engineering methods. Fracture mechanics has developed into a useful tool in the design of crack-tolerant structures and in fracture control; it also useful in failure analysis. The present thesis provides helpful quantitative and qualitative information on the circumstances that lead to failure, and it can be used to substantiate preventive measures to avoid the recurrence of failures in similar components.

Applicability to other type of structures

The approach used in this thesis is very general, therefore, the material is also applicable to a wide variety of other metallic structures, both fixed and floating. Consideration of additional types of loads and failure modes, plus some new examples would be required to illustrate these other applications.

Paik et al. [215] [217] made a comparison of the various methods for ultimate limit state predictions of aluminum stiffened panels used for aerospace, marine and civil engineering applications and concluded that due to the different structural characteristics, material types (depending on structure types of each industry application) and the primary failure pattern, the analyses using same principles present different results.

5.4 Recommendations for Future Research

To achieve further validation of this method, each type of test should be repeated to verify the behavior of either the material or the design, and compared to a single test for each case performed in this thesis. Fracture mechanics is the mathematical analysis of the mechanical processes that lead to fracture failure. Although fracture and crack-growth analysis can be performed manually, most problems are not easily solved in this manner. A computer analysis is usually necessary. The results of fracture mechanics analysis often have limited accuracy. Although fracture mechanics can certainly be improved, most of the inaccuracies are due to scatter in the data of the material and inaccuracies in the input data for stress and stress

history. The involvement with this research opens new areas of research for expanding the results obtained. These areas can be classified in three major categories.

Microscopic analysis of material

Despite the need of macroscopic examination of a naval structure, the application of new materials should be associated with in-depth examination of its behavior to understand the characteristics of the failure modes. The academic community strives to bridge materials science to mechanics. The objective of this effort is to relate macroscopic fracture characteristics (K_{IC}, J_{IC}) to microscopic fracture mechanisms and microstructural length scales using local fracture criteria. The size of structures is increasing, causing various design challenges. Aluminum naval structures are less stiff compared to the steel ones, causing excessive deformation, buckling and plastic collapse. Initiation of microscale defects can cause crack propagation from rapidly applied loading of neighboring structural components and rapid propagation of an existing crack or defect due to slowly varying loading conditions.

Future objectives should include the development of experimental and numerical tools at multiple scales for analyzing and designing naval vessels. The basic knowledge on the material and component level should be used to assess the overall performance of a ship fitted with optimized damage tolerant panels in a realistic ship structural design.

Structural assessment for various loads and modes of failure

The assessment of a naval structure should be performed for a wide range of loading conditions and modes of failure. This thesis examined the mode-I type of loading at the quasi-static field. Ships are generally exposed to a large variety of loads in a rather complex manner. To gain a clear overall understanding of these loads and their impact on the hull structure, different ways of classifying the loads are used. One way is to classify the loads according to the sources producing them. The primary sources are weight, buoyancy, waves, wind, loading and unloading in port, and temperature differences. These loads are well expected and more or less predictable. However, ships may also be exposed to unexpected or accidental loads arising from collision, grounding, fire, flooding, weapon effects, etc. The rate of loading often influences the direction of crack growth. Shear banding followed by crack propagation in a shearing mode

may occur only if the rate of loading is sufficiently high, whereas otherwise an opening mode crack may develop. Other parameters, such as strain rate and different loading (biaxial or mixed mode, dynamic), should be examined and evaluated. The effect of plate thickness, other types of complex structural configurations and welding procedures might result in important observations.

Comparison with other metal structures and scaling effects

This method should be applied to other metal structures, with emphasis on steel. Finally, the final approval of these techniques will be validated with full-scale tests of relevant structures minimizing the scaling effect. Future naval ships and submarines must be designed to survive exposure to extreme loading conditions from impact and explosions. Various structural failure modes contribute to the loss of integrity of naval vessels subject to blast loading; these being dependent on material selection and structural configuration. Modeling vessel response encompasses material constitutive equations, fracture and damage mechanics, nonlinear dynamics simulation codes and structural finite element analyses. The advancement and integration of these disciplines are necessary in order to provide a design framework for developing optimum structural configurations and materials.

Bibliography

[1] ABAQUS Analysis User's Manual, Version 6.6, Iogo, USA: Hibbitt, Karlsson and Sorensen, Inc., 2005.

[2] Abramowicz, W., Crush resistance of "T", "Y" and "X" sections, Joint MIT - Industry Program on Tanker Safety, Report No 24, January 1994.

[3] Abramowicz, W. and Simonsen, B. C., Effect of fracture on crushing of ship structures, *Journal of Ship Research* **47**(3): 194-207, 2003.

[4] America Bureau of Shipping, Rules for building and classing aluminum vessels, 1975.

[5] America Bureau of Shipping, Rule requirements for materials and welding, Part 2, Supplementary requirements for naval vessels, May 2000.

[6] America Bureau of Shipping, Guide for building and classing high-speed naval craft, 2007.

[7] Aliabadi, M. H., *Plate bending analysis with boundary elements*, Southampton, UK; Boston, Computational Mechanics Publications, 353 p., May 1998.

[8] Anderson, T. L., *Fracture mechanics: fundamentals and applications*, 3rd Ed., Boca Raton, FL: Taylor & Francis, 621 p., 2005.

[9] Standard Specification for High Magnesium Aluminum Alloy Sheet and Plate for Marine Service, ASTM B928-03, ASTM International, 2003.

[10] Astrup, O., Cutting of thick plate by a wedge: an experimental study, Joint MIT - Industry Program on Tanker Safety, Report No 27, 1994.

[11] Atkins, A. G. and Liu, J. H., A single curl failure of metal plates in ship grounding, Joint MIT - Industry Program on Tanker Safety, Report No 17, June 1993.

[12] Atkins, A. G., Fracture Mechanics and Metal forming: Damage Mechanics and the local approach of yesterday and today, Fracture Research in Retrospect, An Anniversary Volume in Honour of George R. Irwin's 90^{th} Birthday, Ed. H. P. Rossmanith, A. A. Balkema / Rotterdam / Brookfield, 327-350, 1997.

[13] Atmadja, J., Weld failures in oil tankers due to grounding - finite element approach, Joint MIT - Industry Program on Tanker Safety, Report No 51, August 1995.

[14] Bakulin, A. V., Kobzaruk, A. V. and Olik, A. P., Corrosion fatigue resistance of 1561 aluminum alloy in sea water, *Materials Science* **21**(1): 32-34, 1985.

[15] Bakulin, A. V., Andreev, G. N., Zolotarevskii, Y. S. and Olik, A. P., Effect of aging on the strength and corrosion-resistance of an alloy of the Al Zn Mg system, *Soviet Materials Science* **26**(1): 109-110, 1990.

[16] Bao, Y., Prediction of ductile crack formation in uncracked body, PhD Dissertation, Massachusetts Institute of Technology, Cambridge, Massachusetts, 2003.

[17] Bao, Y. and Wierzbicki, T., On fracture locus in the equivalent strain and stress triaxiality space, *International Journal of Mechanical Sciences* **46**(1): 81-98, 2004.

[18] Barsom, J. M., *Fracture and fatigue control in structures: applications of fracture mechanics applications of fracture mechanics*, 3rd Ed., Woburn, MA, West Conshohocken, Pa.: Butterworth - Heinemann; ASTM, 1999.

[19] Beach, J. E., Advanced surface ship hull technology - Cluster - B, *Naval Engineers Journal* **103**(6): 27-37, 1991.

[20] Bell, R. A., Beaver, P. W., Mann, J. Y. and Sparrow, J. G., Fatigue of thick-section cold-expanded holes with and without cracks, *Fatigue & Fracture of Engineering Materials and Structures* **12**(6): 553-567, 1989.

[21] Bernard, M., Buiquoc, T. and Burlat, M., Effect of re-cold working on fatigue life enhancement of a fastener hole, *Fatigue & Fracture of Engineering Materials and Structures* **18**(7-8): 765-775, 1995.

[22] Besson, J., Steglich, D. and Brocks, W., Modeling of crack growth in round bars and plane strain specimens, *International Journal of Solids and Structures* **38**: 8259-8284, 2001.

[23] Boone, T. J., Wawrzynek, P. A. and Ingraffea, A. R., Finite element modeling of fracture propagation in orthotropic materials, *Engineering Fracture Mechanics* **26**(2): 185-201, 1987.

[24] Bouchaud, E., Scaling properties of cracks, *Journal of Physics* **9**(21): 4319-4344, 1997.

[25] Bracco, M., Grounding resistance of longitudinally stiffened single and double hulls, Joint MIT - Industry Program on Tanker Safety, Report No 30, June 1994.

[26] Bracco, M. D. and Wierzbicki, T., Tearing resistance of advanced double hulls, *Journal of Ship Research* **41**(1): 69-80, 1997.

[27] Brighenti, R., Numerical buckling analysis of compressed or tensioned cracked thin plates, *Engineering Structures* **27**(2): 265-276, 2005.

[28] Brighenti, R., Buckling of cracked thin-plates under tension or compression, *Thin-Walled Structures* **43**(2): 209-224, 2005.

[29] British Standard BS EN 13195-1:2002 Aluminium and aluminium alloys - Wrought and cast products for marine applications (shipbuilding, marine and offshore), 2002.

[30] Broberg, K. B., *Cracks and fracture*, San Diego: Academic Press. xvi, 752 p, 1999.

[31] Broek, D., *Elementary engineering fracture mechanics*, Martinus Nijhoff, Dordrecht/Boston/Lancaster, 1986.

[32] Brooks, C., Weld strength and crack growth ductility from the Lazy - L test, Joint MIT - Industry Program on Tanker Safety, Report No 49, May 1995.

[33] Bruce, G. J., Yuliadi, M. Z. and Shahab, A., Towards a practical means of prediction weld distortion, *Journal of Ship Production* **17**(2): 62-68, 2001.

[34] Bryan, G. H., On the stability of a plane plate under thrusts in its own plane, with application to the "buckling" of the sides of a ship, *London Mathematics Society* **s1-22**(1): 54-67, 1890.

[35] British Standard BS 8118, Structural use of aluminum, Part I: Code of practice for design, 1991.

[36] Bulson, P. S., *Explosive Loading of Engineering Structures: a history of research and a review of recent developments*, 1st Ed., London; New York: E & FN Spon. xxxi, 236 p., 1997.

[37] Burch, I. A., Ritter, J. C., Saunders, D. S. and Underwood, J. H., Crack arrest fracture toughness testing of naval construction steels, *Journal of Testing and Evaluation* **26**(3): 269-276, 1998.

[38] Byklum, E. and Amdahl, J., A simplified model for elastic large deflection analysis of plates and stiffened panels due to local buckling, *Thin-Walled Structures* **40**(11): 925-953, 2002.

[39] Byklum, E., Steen, E. and Amdahl, J., A semi-analytical model for global buckling and postbuckling analysis of stiffened panels, *Thin-walled Structures* **42**(5): 701-717, 2004.

[40] Chao, R.-M., Chen, Y. R. and Kuo, J.-C, Crack propagation in high tensile steel, *Ship Technology Research* **47**: 95-101, 2000.

[41] Chen, Q., Zimmerman, T. J. E., DeGeer, D. D. and Kennely,B. W., Strength and stability testing of stiffened plate components, Ship Structure Committee, Report No SSC-399, 1997.

[42] Cho, S.-R. and So, H.-Y., Ultimate strength tests on ring-stiffened cylinders and conical shells subjected to hydrostatic pressure, *Proceedings of the 17th Asian-Pacific Technical Exchange and Advisory Meeting on Marine Structures*, Tainan, Taiwan, 579-588, 2003.

[43] Cho, S.-R. and Lee, H.-S., Experimental and analytical investigations on the response of stiffened plates subjected to lateral collisions, *Proceedings of 3rd International Conference on Collision and Grounding of Ships*, Izu, Japan, 295-301, 2004.

[44] Choi, S. K., Wierzbicki, T. and Driscoll, J. C., Crushing strength of a web girder, Joint MIT - Industry Program on Tanker Safety, Report No 23, January 1994.

[45] Choi, S. K., Wierzbicki, T., Goksoyr, O. and Driscoll, J. C., Crushing resistance of a web-girder with application to ship structures, Joint MIT - Industry Program on Tanker Safety, Report No 38, January 1995.

[46] Choi, S. K. and Wierzbicki, T., Correlation of NSWC grounding tests with Minorsky/Vaughan Method, Joint MIT - Industry Program on Tanker Safety, Report No 39, January 1995.

[47] Chu, H. P., Hauser, J. A. and Sikora, J. P., Fatigue-crack growth in weldbonded-aluminum-alloy stiffened panels under pressure loading, *Experimental Mechanics* **19**(5): N39-N39, 1979.

[48] Cichocki, K., Effects of underwater blast loading on structures with protective elements, *International Journal of Impact Engineering* **22**(6): 609-617, 1999.

[49] Cichocki, K. and Ruchwa, M., Steel stiffened plates subjected to a blast load, *Journal De Physique IV* **10**(P9): 535-540, 2000.

[50] Cole, R. H., *Underwater Explosions*, Princeton: Princeton Univ. Press. ix, 437 p., 1948.

[51] Cole, R. H., *Underwater Explosions*, New York, Dover Publications. ix, 437 p, 1965.

[52] Cotterell, B. and Rice, J. R., Slightly curved or kinked cracks, *International Journal of Fracture* **16**(2): 155-169, 1980.

[53] Das, P. K., Thavalingam, A. and Bai, Y., Buckling and ultimate strength criteria of stiffened shells under combined loading for reliability analysis, *Thin-Walled Structures* **41**(1): 69-88, 2003.

[54] Dexter, R. J. and Pilarski, P. J., Effect of welded stiffeners on crack growth rate, Ship Structure Committee, Report No SSC-413, 2000.

[55] Dexter, R. J. and Pilarski, P. J., Crack propagation in welded stiffened panels, *Journal of Constructional Steel Research* **58**(5-8): 1081-1102, 2002.

[56] Dexter, R. J., Pilarski, P. J. and Mahmoud, H. N., Analysis of crack propagation in welded stiffened panels, *International Journal of Fatigue* **25**(9-11): 1169-1174, 2003.

[57] Dexter, R. J. and Mahmoud, H.N., Predicting stable fatigue crack propagation in stiffened panels, Ship Structure Committee Report, No SSC-435, 2004.

[58] Dinovitzer, A. S. and Pussegoda, N., Fracture toughness of a ship structure, Ship Structure Committee, Report No SSC-430, 2003.

[59] Dobroskok, A. A., Frumen, A. I. and Petinov, S. V., Modeling of fatigue cracks initiated at a cavity in fillet-welded joints, *International Conference on Marine Intellectual Technologies "Marintech-2003"*, St. Petesburg, 2003.

[60] Driscoll, J. C., Crushing characteristics of web girders in unidirectionally stiffened double hull structures, Joint MIT - Industry Program on Tanker Safety, Report No 10, May 1992.

[61] El-Sawy, K. M., Nazmy, A. S. and Martini, M. I., Elastoplastic buckling of perforated plates under uniaxial compression, *Thin-Walled Structures* **42**(8): 1083-1101, 2004.

[62] Emery, A. F., Love, W. J. and Kobayashi, A. S., Dynamic finite difference analysis of an axially cracked pressurized pipe undergoing large deformations, ASTM STP 627, p. 143-158, 1977.

[63] Emery, A. F., Love, W. J. and Kobayashi, A. S., Fracture in straight pipes under large deflection conditions. Part I: structural deformation, *Journal of Pressure Vessel Technology* **99**: 122-127, 1977.

[64] Emery, A. F., Love, W. J. and Kobayashi, A. S., Fracture in straight pipes under large deflection conditions. Part II: pipe pressure, *Journal of Pressure Vessel Technology* **99**: 128-136, 1977.

[65] Emery, A. F., Perl, M., Kobayashi, A. S. and Love, W. J., The use of the split ring in modeling ductile axial crack extension in pipes, *Journal of Pressure Vessel Technology* **103**(2): 151-154, 1981.

[66] Emery, A. F., Perl, M., Love, W. J. and Kobayashi, A. S., On the motion of a axial through crack extension in pipes, *Journal of Pressure Vessel Technology* **103**(3): 281-286, 1981.

[67] Emery, A. F., Kobayashi, A. S., Love, W. J., Place, C. L. and Chao, Y. H., An experimental and analytical investigation of axial crack propagation in long pipes, *Engineering Fracture Mechanics* **23**(1): 215-226, 1986.

[68] Fang, C. and Das, P. K., Survivability and reliability of damaged ships after collision and grounding, *Ocean Engineering* **32**(3-4): 293-307, 2005.

[69] Forsyth, P. J. E., *The Physical Basis of Metal Fatigue*, New York; American Elsevier Pub. Co. vii, 200 p., 1969.

[70] Forsyth, P. J. E., Some observations and measurements on mixed fatigue tensile crack growth in aluminum-alloys, *Scripta Metallurgica* **10**(5): 383-386, 1976.

[71] Frankel, E. G., Economics and management of American shipbuilding and the potential for commercial competitiveness, *Journal of Ship Production* **12**(1): 1-10, 1996.

[72] Freund, L. B., Li, V. C. F. and Parks, D. M., Analysis of a wire-wrapped mechanical crack arrester for pressurized pipelines, *Journal of Pressure Vessel Technology - Transactions of ASME* **101**(1): 51-58, 1979.

[73] Fujikubo, M. and Kaeding, P., New simplified approach to collapse analysis of stiffened plates, *Marine Structures* **15**(3): 251-283, 2002.

[74] Fujikubo, M., Yanagihara, D., Matsuda, I. and Olaru, D. V., Collapse analysis of a pontoon-type VLFS in waves, *Proceedings of the Fourth International Workshop on Very Large Floating Structures*, 207-214, 2003.

[75] Fujikubo, M., Xiao, T. and Yamamura, K., Structural safety assessment of a pontoon-type VLFS considering damage to the breakwater, *Journal of Marine Science and Technology* **7**(3): 119-127, 2003.

[76] Fujikubo, M. and Pei, J., Progressive collapse analysis of ship's hull girder in longitudinal bending using Idealized Structural Unit Method, *Journal of the Japan Society of Naval Architects and Ocean Engineers* **1:** 187-196 (in Japanese), 2005.

[77] Fujikubo, M., Yao, T., Khedmati, M. R., Harada, M. and Yanagihara, D., Estimation of ultimate strength of continuous stiffened panel under combined transverse thrust and lateral pressure - Part 1: Continuous plate, *Marine Structures* **18**(5-6): 383-410, 2005.

[78] Fujikubo, M., Harada, M., Yao, T., Khedmati, M. R. and Yanagihara, D., Estimation of ultimate strength of continuous stiffened panel under combined transverse thrust and lateral pressure - Part 2: Continuous stiffened panel, *Marine Structures* **18**(5-6): 411-427, 2005.

[79] Galatolo, R. and Lanciotti, A., Fatigue crack propagation in residual stress fields of welded plates, *International Journal of Fatigue* **19**(1): 43-49, 1997.

[80] Garwood, S. J., Investigation of the MV Kurdistan casualty, *Engineering Failure Analysis* **4**(1): 3-24, 1997.

[81] Gdoutos, E. E., *Problems of mixed mode crack propagation*, The Hague; Boston, Hingham, MA, USA: M. Nijhoff; Distributors for the U.S. and Canada, Kluwer Boston. xiii, 204 p, 1984.

[82] Gdoutos, E. E., Rodopoulos, C. A. and Yates, J. R., *Problems of fracture mechanics and fatigue: a solution guide*, Dordrecht; Boston: Kluwer Academic Publishers. xxiv, 618 p., 2003.

[83] Gdoutos, E. E., *Fracture mechanics: an introduction,* 2nd Ed. Solid mechanics and its applications; v. 123, Dordrecht, Norwell, MA: Springer; Distributed in North, Central and South America by Springer. xv, 369 p, 2005.

[84] Geers, T. L., Residual potential and approximate methods for three dimensional fluid structure interaction problems, *Journal of Acoustical Society of America* **49**(5)Prt 2: 1505-1510, 1971.

[85] Ghfiri, R, Shi, H.-J., Guo, R. and Mesmacque, G., Effects of expanded and non-expanded hole on the delay of arresting crack propagation for aluminum alloys, *Materials Science and Engineering* **286**(2): 244-249, 2000.

[86] Ghose, D. J., Nappi, N. S. and Wiernicki, C. J., Residual strength of damaged marine structures, Ship Structure Committee, Report No SSC-381, 1994.

[87] Glen, I. F., Dinovitzer, A., Malik, L. and Yee, R., Guide to damage tolerance analysis of marine structures, Ship Structure Committee, Report No SSC-409, 1999.

[88] Goksoyr, O., Crushing resistance of web girders in unidirectionally stiffened double hulls, Joint MIT - Industry Program on Tanker Safety, Report No 20, January 1994.

[89] Gonzalez, F. F., Modeling of ship - Obstacle interaction and hull structure definition for damage calculations, Joint MIT - Industry Program on Tanker Safety, Report No 32, June 1994.

[90] Goto, M., Miyagawa, H. and Nisitani, H., Crack growth arresting property of a hole and Brinell-type dimple, *Fatigue and Fracture Engineering Materials & Structures* **19**(1): 39-49, 1996.

[91] Greif, R. and Sanders, J. L., The effect of a stringer on the stress in a cracked sheet, *Journal of Applied Mechanics* **32:** 59-66, 1965.

[92] Guerra, A. and McClintock, F. A., Upper bounds to the tensile limit loads of cracked welded T-joints, Joint MIT - Industry Program on Tanker Safety, Report No 28, January 1994.

[93] Guruprasad, S. and Mukherjee, A., Layered sacrificial claddings under blast loading Part I – Analytical studies, *International Journal of Impact Engineering* **24**(9): 957-973, 2000.

[94] Guruprasad, S. and Mukherjee, A., Layered sacrificial claddings under blast loading Part II – Experimental studies, *International Journal of Impact Engineering* **24**(9): 975-984, 2000.

[95] Harada, M., Fujikubo, M. and Yanagihara, D., Estimation of ultimate strength of continuous stiffened plate under combined biaxial thrust and lateral pressure, *Journal of the Society of Naval Architects of Japan* **196**: 189-198, (in Japanese), 2004.

[96] Harada, M. and Fujikubo, M., Estimation of buckling and ultimate strength of a stiffened web plating with cutout, *Proceedings of the 15th International Offshore and Polar Engineering Conference*, Seoul, Korea, 745-751, 2005.

[97] Haxton, R. S. and Haywood, J. H., Linear elastic response of a ring-stiffened cylinder to underwater explosion loading, *Proceedings of Conference: Advances in Marine Structures*, ARE Dunfermline, Scotland, May 1986.

[98] Hellenic Navy classified documentation with respest to the marine aluminum alloy for naval vessels.

[99] Herrington, P. D. and Latorre, R. G., Development of an aluminum hull panel for high-speed craft, *Marine Structures* **11**(1-2): 47-71, 1998.

[100] Hertzberg, R. W., *Deformation and fracture mechanics of engineering materials*, 4th Ed., New York: J. Wiley & Sons. xxiv, 786 p., 1996.

[101] Hoo Fatt, M. S., Fully-plastic crack propagation in stiffened plates, *International Journal of Solids and Structures* **33**(5): 629-645, 1996.

[102] Houlston, R., Slater, J. E., Pegg, N. and Desrochers, C. G., On analysis of structural response of ship panels subjected to air blast loading, *Computers & Structures* **21**(1-2): 273-289, 1985.

[103] Houlston, R., Slater, J. E., Global and local modeling of naval panels subjected to shock loads, *Computers & Structures* **40**(2): 353-364, 1991.

[104] Hu, Y. and Cui, W. C., A comparison between simplified analytical method and design formulas for ultimate strength of unstiffened plates, *Shipbuilding of China* **44**(2): 8-16 (in Chinese), 2003.

[105] Hu, Y. and Cui, W. C., A simplified analytical method to predict the ultimate strength of unstiffened plates under combined loading including edge shear, *Journal of Ship Mechanics* **7**(6): 60-74 (in Chinese), 2003.

[106] Hu, Y. and Cui, W.C., Residual ultimate strength of cracked plates and stiffened panels under combined loading, *Journal of Ship Mechanics* **7**(1): 63-78 (in Chinese), 2003.

[107] Hu, Y., Cui, W. C. and Pedersen, P. T., Maintained ship hull xcgirxcder ultimate strength reliability considering corrosion and fatigue, *Marine Structures* **17**(2): 91-123, 2004.

[108] Huber, M. T., Contribution to the foundation of the strength of the material, *Czasopismo Techniczne, Lwow* 22, 81, in Polish (translated to English by Professor M. Zyczkowski in connection with the M. T. Huber Century Symposium, Krakow, August, 2004.

[109] Hughes, O. F. and Society of Naval Architects and Marine Engineers (U.S.), *Ship Structural Design: a rationally-based, computer-aided optimization approach*, SNAME edition, Jersey City, N.J.:Society of Naval Architects and Marine Engineers, xv, 566 p., 1998.

[110] Hughes, O. F., Ghosh, B. and Chen, Y., Improved prediction of simultaneous local and overall buckling of stiffened panels, *Thin-Walled Structures* **42**(6): 827-856, 2004.

[111] Hung, C. F., Hwang-Fuu, J. J. and Chow, C. L., Comparison study on dynamic response of cylindrical shell structure subjected to underwater explosion, *Proceedings of the 19th Asian-Pacific Technical Exchange and Advisory Meeting on Marine Structures*, Singapore, 98-106, 2005.

[112] International Association of Classification Societies (IACS), Guidelines for assessment of the fatigue design of ship structures, Paris La Defence, November 30, 1998.

[113] International Maritime Organization (IMO) website http://www.imo.org/

[114] Irwin, G. R., *Fracture Mechanics*, Report of Naval Research Laboratory Progress, Washington, D.C., 36 p., 1973.

[115] International Standard ISO 12135: 2002(E), Metallic materials – unified method of test for the determination of quasistatic fracture toughness, 2002.

[116] International Standard ISO 209 – 1: 1989, Wrought aluminum and aluminium alloys – Chemical composition and froms of products - Part 1: Chemical composition, 1989.

[117] James, M. A. and Newman Jr., J. C., The effect of crack tunneling on crack growth: experiments and CTOA analyses, *Engineering Fracture Mechanics* **70**(3-4): 457-468, 2003.

[118] Jaswon, M. A. and Maiti, M., An integral equation formulation of plate bending problems, *Journal Engineering Mathematics* **2**(1): 59-66, 1968.

[119] Jones, N., A literature survey on the collision and grounding protection of ships, Ship Structure Committee, Report No SSC-283, 1979.

[120] Jones, N., Jouri, W. S. and Birch, R. S., On the scaling of ship collision damage, *Proceedings of 3rd International Congress on Marine Technology* **2**, International Maritime Association of East Mediterranean, Hellenic Institute of Marine Technology, Athens, 1984.

[121] Jones, N. and Jouri, W. S., A study of plate tearing for ship collision and grounding damage, *Journal of Ship Research* **31**(4): 253-268, 1987.

[122] Jones, N., *Structural Impact,* Cambridge; New York, Cambridge University Press xvi, 575 p., 1989.

[123] Jones, N. and Jones, C., Inelastic failure of fully clamped beams and circular plates under impact loading, *Proceedings of the Institution of Mechanical Engineers Part C-Journal of Mechanical Engineering Science Proceedings of International Mechanical Engineering* **216**(2):133-149, 2002.

[124] Kaeding, P., Olaru, D. V. and Fujikubo, M., Development of ISUM plate element with consideration of lateral pressure effects and its application to stiffened plates of ships, *Proceedings of Practical Design of Ships and other Floating Structures* **1**: 148-155, 2004.

[125] Kanninen, M. F., Sampath, S. G. and Popelar, C., Steady state crack propagation in pressurized pipelines without backfill, *Journal of Pressure Vessel Technology* **98**: 56-64, 1976.

[126] Kanninen, M. F. and Battelle Memorial Institute, Columbus Laboratories, A study of ship hull crack arrester systems, Final technical report on Project SR-226 "Hull crack arrester systems", Washington: ill.;. x, 98 p, 1977.

[127] Kanninen, M. F., Popelar, C. and Rosenfield, A. R., Steady state crack propagation in pressurized pipelines, *Journal of Pressure Vessel Technology* **99**: 112-121, 1977.

[128] Kanninen, M. F. and Popelar, C. H., *Advanced fracture mechanics,* Oxford engineering science series; 15, New York: Oxford University Press. xv, 563 p, 1985.

[129] Kanninen, M. F., Applications of dynamic fracture mechanics for the prediction of crack arrest in engineering structures, *International Journal of Fracture* **27**(3-4): 299-312, 1985.

[130] Kanninen, M. F., Hudak, S. J., Couque, H. R., Dexter, R. J. and O'Donoghue, P. E., Viscoplastic-dynamic crack propagation: experimental and analysis research for crack arrest applications in engineering structures, *International Journal of Fracture* **42**(3): 239-260, 1990.

[131] Kee, A., Matic, P., Darby, I. and Rodd, J. L., Finite-element analysis of the quarter scale advanced double-hull design, *Naval Engineers Journal* **107**(3): 185-196, 1995.

[132] Keesecker, A. L., Davila, C. G., Johnson, E. R. and Starnes, J. H., Crack path bifurcation at a tear strap in a pressurized shell, *Computers & Structures* **81**(16): 1633-1642, 2003.

[133] Keil, A. H., *Introduction to Underwater Explosion Research*, UERD, Norfolk Naval Ship Yard, Portsmouth, Virginia, 1956.

[134] Keil, A. H., The response of ships to underwater explosions, *Transactions of Society of Naval Architects and Marine Engineers* **69**: 366-410, 1961.

[135] Kennell, C., Lavis, D. R. and Templeman, M. T., High-speed sealift technology, *Marine Technology and SNAME News* **35**(3): 135-150, 1998.

[136] Khalil, M. R., Olson, M. D. and Anderson, D. L., Nonlinear dynamic analysis of stiffened plates, *Computers & Structures* **29**(6): 929-941, 1988.

[137] Khan, M. Z. S., Saunders, D. S., Burch, I. A. and Mouritz, A. P., Materials aspects of damage tolerance and reliability of ship structures and components, *Naval Engineers Journal* **106**(4): 192-207, 1994.

[138] Kirkov, K., Tearing resistance for fillet welds in ships exposed to grounding - A full-scale test and cost implications, Joint MIT - Industry Program on Tanker Safety, Report No 29, June 1994.

[139] Kitamura, K., Okumoto, Y. and Shibue, T., On the model tests of double bottom strength for stranding, *Journal of the Society of Naval Architects of Japan* **143**: 346-356, 1978.

[140] Kitamura, O., FEM approach to the simulation of collision and grounding damage, *Marine Structures* **15**(4-5): 403-428, 2002.

[141] Koko, T. S. and Olson, M. D., Nonlinear transient response of stiffened plates to air blast loading by a superelement approach, *Computer Methods in Applied Mechanics and Engineering* **90**(1-3): 737-760, 1991.

[142] Kotousov, A. and Tan, P. J., Effect of the plate thickness on the out-of-plane displacement field of a cracked elastic plate loaded in mode-I, *International Journal of Fracture* **127**(1): L97-L103, 2004.

[143] Kristensen, O. H. H. and Moan, T., Ultimate strength of aluminum plates under biaxial loading, *PRADS'1999*, 1999.

[144] Kumar, A. M. and Hirth, J. P., Mixed-mode I/III fracture testing, *Scripta Metallurgica et Materialia* **25**(5): 985-990, 1991.

[145] Kumar, Y. V. S. and Paik, J. K., Buckling analysis of cracked plates using hierarchical trigonometric functions, *Thin-Walled Structures* **42**(5): 687-700, 2004.

[146] Kutz, M., *Handbook of materials selection*, New York: J. Wiley. xvii, 1497 p, 2002.

[147] Labeas, G. and Diamantakos, J., Residual strength prediction of multiple cracked stiffened panels, *Fatigue & Fracture of Engineering Materials & Structures* **29**(5): 365-371, 2006.

[148] Lan, W., Deng, X., Sutton, M. A. and Cheng, C.-S., Study of slant fracture in ductile materials, *International Journal of Fracture* **141**(3-4): 469-496, 2006.

[149] Langdon, G. S., Yuen, S. C. K. and Nurick, G. N., Experimental and numerical studies on the response of quadrangular stiffened plates. Part II: localized blast loading, *International Journal of Impact Engineering* **31**(1): 85-111, 2005.

[150] Latorre, R. G., Herrington, P. D. and Mattei, N. J., Design of a 33-knot aluminum catamaran ferry, *Marine Technology and Sname News* **37**(2): 88-99, 2000.

[151] Latorre, R. G., Herrington, P. D. and Mattei, N. J., Stress analysis of a transversely loaded aluminum weldment, *Marine Structures* **15**(2): 175-191, 2002.

[152] Lee, J. W. and Song, J. Y., A study on the tearing and crushing behavior of isotropic aluminium alloy plate, *Korean Register of Shipping*, Report No 10053, pp. 3-16, 1983.

[153] Lee, Y. W., Paik, J. K., Thayamballi, A. K. and Currey, R., A novel concept for structural design and construction of vessels using aluminum honeycomb sandwich panels, *Transactions of the Society of Naval Architects and Marine Engineers* **105:** 285-302, 1996.

[154] Lee, Y.-W. and Wierzbicki, T., Fracture prediction of thin plates under localized impulsive loading. Part II: discing and petalling, *International Journal of Impact Engineering* **31**(10): 1277-1308, 2005.

[155] Liang, C-C., Lai, W-H. and Hsu, C-Y., Study of the nonlinear responses of a submersible pressure hull, *International Journal of Vessels and Piping* **75**(2): 131-149, 1998.

[156] Little, P., A study of the wedge cutting force through transversely stiffened plate: an application to ship grounding resistance, Master Thesis, Department of Ocean Engineering and Mechanical Engineering, Massachusetts Institute of Technology, May 1994.

[157] Little, P., Failure of transverse frames and bulkheads in grounding, Joint MIT - Industry Program on Tanker Safety, Report No 31, June 1994.

[158] Llopart, L., Kurz, B., Wellhausen, C., Anglada, M., Drechsler, K. and Wolf, K., Investigation of fatigue crack growth and crack turning on integral stiffened structures under mode I loading, *Engineering Fracture Mechanics* **73**(15): 2139-2152, 2006.

[159] Louca, L. A., Pan, Y. G. and Harding, J. E., Response of stiffened and unstiffened plates subjected to blast loading, *Engineering Structures* **20**(12): 1079-1086, 1998.

[160] Lu, G. and Calladine, C. R., On the cutting of a plate by a wedge, *International Journal of Mechanical Sciences* **32(4):** 293-313, 1990.

[161] Maeno, Y., Yamaguchi, H., Fujii, Y. and Yao, T., Study on buckling/ultimate strength of bilge part and its contribution to ultimate hull girder strength, *Journal of the Society of Naval Architects of Japan* **194:** 171-178 (in Japanese), 2003.

[162] Maeno, Y., Yamaguchi, H., Fujii, Y. and Yao, T., Buckling/plastic collapse behavior and strength of bilge circle and its contribution to ultimate longitudinal strength of ship's hull girder, *Proceedings of ISOPE'2004* **1**: 296-302, 2004.

[163] Mahgoub, E., Deng, X. and Sutton, M. A., Three-dimensional stress and deformation fields around flat and slant cracks under remote Mode I loading conditions, *Engineering Fracture Mechanics* **70**(18): 2527-2542, 2003.

[164] Mahmoud, S. and Lease, K., The effect of specimen thickness on the experimental characterization of critical crack-tip-opening angle in 2024-T351 aluminum alloy, *Engineering Fracture Mechanics* **70**(3-4): 443-456, 2003.

[165] Mahmoud, H. N. and Dexter, R. J., Propagation rate of large cracks in stiffened panels under tension loading, *Marine Structures* **18**(3): 265-288, 2005.

[166] Malik, L. and Tomin, L., Evaluation of toughness of conventional ship steels at intermediate loading rate and its implications, MTC, Fleet Technology Ltd., 1991.

[167] Manoharan, M., Development of a mixed-mode fracture mechanism map and its extension to mixed-mode fracture, In Proceedings: Recent advances in fracture, Metals and Materials Society, pp. 373-384, 1997.

[168] Masubuchi, K., McClintock, F. A. and Liang, L., Summary report on welding research from the tanker grounding project (preliminary version), Joint MIT - Industry Program on Tanker Safety, Report No 53, June 1995.

[169] Masubuchi, K., McClintock, F. A. and Liang, L., Summary report on welding research from the tanker grounding project (final version), Joint MIT - Industry Program on Tanker Safety, Report No 56, March 1996.

[170] Maxey, W. A., Eiber, R. J., Podlasek, R. J. and Duffy, A. R., Observations on shear fracture propagation behavior, *Symposium on Crack Propagation in Pipelines*, Institute of Gas Engineers, London, March 1974.

[171] Maxey, W. A., Fracture initiation, propagation and arrest, *5th Symposium on Line Pipe Research*, American Gas Association, 1974.

[172] Maxey, W. A., Kiefner, J. F. and Eiber, R. J., Ductile fracture arrest in gas pipelines, NG-18 Report 100, American Gas Association, 1975.

[173] Maxwell, L. M., Effect of rock geometry on the failure mode of plates and the forces in grounding experiments, Joint MIT - Industry Program on Tanker Safety, Report No 15, May 1993.

[174] Mazzolani, F. M., *Aluminum Alloy Structures*, E & FN Spon, 1995.

[175] McClintock, F. A., Ductile fracture instability in shear, *Journal of Applied Mechanics, Transactions of the ASME* **25**: 582-588, 1958.

[176] McClintock, F. A., Effects of root radius, stress, crack growth and rate on fracture instability, *Proceedings of the Royal Society of London*, Series A, Mathematical and Physical Sciences, **285:** 58-72, No. 1400, A Discussion on Damage and Failure Mechanisms of Heavy-Section Steel, 1965.

[177] McClintock, F. A., Zhou, Q. and Wierzbicki, T., Necking in plane strain under bending with constant tension, Joint MIT - Industry Program on Tanker Safety, Report No 11, February 1993.

[178] McClintock, F. A., Fully plastic mechanics for welded T-joints, Joint MIT - Industry Program on Tanker Safety, Report No 26, January 1994.

[179] McDermott, J. F., Kline, R. G., Jones, E. L., Maniar, N. M. and Chiang, W. P., Tanker structural analysis for minor collisions, *Transactions SNAME* **82:** 382-414, 1974.

[180] McDonald, H. A., Required strength and tear resistance for fillet welds in ships exposed to grounding or collision loads, Joint MIT - Industry Program on Tanker Safety, Report No 14, May 1993.

[181] McKenney, T. L., Grounding resistance of unidirectionally stiffened double hulls, Joint MIT - Industry Program on Tanker Safety, Report No 3, May 1991.

[182] Meyn, D. A., Webb, T. W. and Aifantis, E. C., Hydrogen-assisted cracking studies of 4340 steel by using the optical method of caustics, *Engineering Fracture Mechanics* **33**(6): 913-925, 1989.

[183] Middaugh, R. A., A knowledge-based expert system for analyzing welded structures, Joint MIT - Industry Program on Tanker Safety, Report No 43, February 1995.

[184] Minorsky, V. U., An analysis of ship collisions with reference to nuclear power plants, *Journal of Ship Research* **3**(2): 1-4, 1959.

[185] Moore, W. H., The grounding of Exxon-Valdez - an examination of the human organizational-factors, *Marine Technology & Sname News* **31**(1): 41-51, 1994.

[186] Murtagian, G. R., Johnson, D. H. and Ernst, H. A., Dynamic crack propagation in steel line pipes. Part I: experimental investigation, *Engineering Fracture Mechanics* **72**(16): 2519-2534, 2005.

[187] Murtagian, G. R. and Ernst, H. A., Dynamic axial crack propagation in steel line pipes. Part II: theoretical developments, *Engineering Fracture Mechanics* **72**(16): 2535-2548, 2005.

[188] Muzzolini, R., FEA optimizes airframe panels, *Advanced Materials & Processes* **163**(11): 37-39, 2005.

[189] Nakasumi, S., Suzuki, K. and Ohtsubo, H., Crack growth analysis using mesh superposition method and X-FEM, *Journal of the Society of Naval Architects of Japan* **195:** 79-86 (in Japanese), 2004.

[190] Narasimhan, R., Rosakis, A. J. and Moran, B., A three-dimensional numerical investigation of fracture initiation by ductile failure mechanisms in a 4340 steel, *International Journal of Fracture* **56**(1): 1-24, 1992.

[191] National Research Council (U.S.) Committee on Marine Structures and United States Ship Structure Committee, *Prevention of fracture in ship structure,* March 30-31, 1995, Washington, D.C., x, 441 p, 1997.

[192] Newman Jr., J. C., Dawicke, D. S. and Seshadri, B. R., Residual strength analyses of stiffened and un-stiffened panels - Part I: laboratory specimens, *Engineering Fracture Mechanics* **70**(3-4): 493-507, 2003.

[193] Nurick, G. N., Olson, M. D., Fagnan, J. R. and Levin, A., Deformation and tearing of blast-loaded stiffened square plates, *International Journal of Impact Engineering* **16**(2): 273-291, 1995.

[194] O'Donoghue, P. E., Kanninen, M. F., Leung, C. P., Demofonti, G. and Venzi, S., The development and validation of a dynamic fracture propagation model for gas transmission pipelines, *International Journal of Pressure Vessels and Piping* **70**(1): 11-25, 1997.

[195] O'Donoghue, P. E. and Zhuang, Z., A finite element model for crack arrestor design in gas pipelines, *Fatigue & Fracture of Engineering Materials & Structures* **22**(1): 59-66, 1999.

[196] O'Dowd, N. P. and Shih, C. F., Family of crack-tip fields characterized by a triaxiality parameter - I. Structure of fields, *Journal of the Mechanics and Physics of Solids* **39**(8): 989-1015, 1991.

[197] Olik, A. P., Petrov, L. N., Bakulin, A. V. and Kalinkov, A. Y., *Development of corrosion fatigue cracks in ship hull aluminum-alloys*, Soviet Materials Science **24**(2): 186-188, 1988.

[198] Olik, A. P. and Salamashenko, A. G., Effect of the asymmetry of the stress cycle on the corrosion fatigue resistance of 1561 aluminum-alloy, *Soviet Materials Science* **25**(1): 40-43, 1993.

[199] Olson, M.D., Nurick, G. N. and Fagnan, J. R., Deformation and rupture of blast loaded square plates–predictions and experiments, *International Journal of Impact Engineering* **13**(2): 279-291, 1993.

[200] Paik, J. K. and Suh, H. W., Ultimate fracture strength analysis of a cracked plate using 3-D isoparametric solid elements, *Proceedings of the 2nd International Offshore and Polar Engineering Conference (ISOPE'92)*, San Francisco, June, **IV:** 430-438, 1992.

[201] Paik, J. K., Cutting of a longitudinally stiffened plate by a wedge, *Journal of Ship Research* **38**(4): 340-348, 1994.

[202] Paik, J. K. and Pedersen, P. T., Ultimate and crushing strength of plated structures, *Journal of Ship Research*, **39**(3)**:** 250-261, 1995.

[203] Paik, J. K. and Pedersen, P. T., Collapse of a ship's hull due to grounding, *Proceedings of International Conference on Technologies for Marine Environment Preservation (MARIENV'95)* **1:** 75-80, Tokyo, September 1995.

[204] Paik, J. K. and Pedersen, P. T., Modeling of the internal mechanics in ship collisions, *Ocean Engineering* **23**(2): 107-142, 1996.

[205] Paik, J. K. and Wierzbicki, T., A benchmark study on crushing and cutting of plated structures, *Journal of Ship Research* **41**(2)**:** 147-160, 1997.

[206] Paik, J. K., Thayamballi, A. K. and Kim, D. H., An analytical method for the ultimate compressive strength and effective plating of stiffened panels, *Journal of Constructional Steel Research* **49**(1): 43-68, 1999.

[207] Paik, J. K., Thayamballi, A. K., Lee, S. and Kang, S., A semi-analytical model for the elastic-plastic large deflection analysis of welded steel or aluminum plating under combined in-plane and lateral pressure loads, *Thin-Walled Structures* **39**(2)**:** 125-152, 2001.

[208] Paik, J. K., Thayamballi, A. K. and Kim, B. J., Large deflection orthotropic plate approach to develop ultimate strength formulations for stiffened panels under combined bi-

axial compression/tension and lateral pressure, *Thin-Walled Structures* **39**(3): 215-246, 2001.

[209] Paik, J. K. and Kim, B. J., Ultimate strength formulations for stiffened panels under combined axial load, in-plane bending and lateral pressure: a benchmark study, *Thin-Walled Structures* **40**(1): 45-83, 2002.

[210] Paik, J. K. and Thayamballi, A. K., *Ultimate limit state design of steel plated structures*, Chichster, England; Hoboken, NJ: J. Wiley. xx, 521 p, 2003.

[211] Paik, J. K. and Duran, A., Ultimate strength of aluminum plates and stiffened panels for marine applications, *Marine Technology and SNAME News* **41**(3): 108-121, 2004.

[212] Paik, J. K., Principles and criteria for ultimate limit state design and strength assessment of ship hulls, *RINA Transactions (IJME)*, p. A3, 2004.

[213] Paik, J. K., Corrosion analysis of seawater ballast tank structures, *RINA Transactions Part A1 - International Journal of Maritime Engineering (IJME)*, 2004.

[214] Paik, J. K., Hess, P. E. and Hughes, O., Ultimate strength failure of lightweight, multi-hull ships, Report to US Office of Naval Research, Washington DC, 2004.

[215] Paik, J. K., van der Veen, S., Duran, A. and Collette, M., Considering aluminum welded panel structures for aerospace, marine and land-based applications: a comparison of ultimate compressive strength design methods, *9^{th} Symposium on Practical Design of Ships and Other Floating Structures*, Luebeck-Travemuende, Germany, **2**: 727-735, 2004.

[216] Paik, J. K., Kumar, Y. V. S. and Lee, J. M., Ultimate strength of cracked plate elements under axial compression or tension, *Thin-Walled Structures* **43**(2): 237-272, 2005.

[217] Paik, J. K., van der Veen, S., Duran, A. and Collette, M., Ultimate compressive strength design methods of aluminum welded stiffened panel structures for aerospace, marine and land-based applications: A benchmark study, *Thin-Walled Structures* **43**(10): 1550-1566, 2005.

[218] Paik, J. K. and Lee, M. S., A semi-analytical method for the elastic-plastic large deflection analysis of stiffened panels under combined biaxial compression/tension, biaxial in-plane bending, edge shear, and lateral pressure loads, *Thin-Walled Structures* **43**(3): 375-410, 2005.

[219] Paik, J. K., Hughes, O. F., Hess, P. E. and Renaud, C., Ultimate limit state design technology for aluminum multi-hull ship structures, *Transactions SNAME*, **113**: 1-37, 2005.

[220] Paik, J. K. and Kumar, Y. V. S., Ultimate strength of stiffened panels with cracking damage under axial compression or tension, *Journal of Ship Research* **50**(3): 231-238, 2006.

[221] Pardoen, T., Marchal, Y. and Delannay, F., Thickness dependence of cracking resistance in thin aluminium plates, *Journal of the Mechanics and Physics of Solids* **47**(10): 2093-2123, 1999.

[222] Park, H.-J., Cho, S.-R., Choung, J.-M. and Lee, D.-B., Ultimate strength analysis of curved stiffened shell of container bilge strake, *Proceedings of Annual Autumn Meeting, Society of Naval Architects of Korea*, Yongin, Korea, 189-195 (in Korean), 2005.

[223] Park, B.-W. and Cho, S.-R., Simple design formulae for predicting the residual damage of unstiffened and stiffened plates under explosion loadings, *International Journal of Impact Engineering* **32**(10): 1721-1736, 2006.

[224] Parks, D. M. and Freund, L. B., On the gas dynamics of running ductile fracture in a pressurized line pipe, *Journal of Pressure Vessel Technology - Transactions of the ASME* **100**(1): 13-17, 1978.

[225] Pedersen, P. T., Ship grounding on soft bottoms, Joint MIT - Industry Program on Tanker Safety, Report No 35, June 1994.

[226] Peer, D. B., Coupling global motion and local deformation in tanker grounding, Joint MIT - Industry Program on Tanker Safety, Report No 4, May 1991.

[227] Pellini, W. S., Fracture analysis diagram procedures for the fracture-safe engineering design of steel structures, *Welding Research Council Bulletin* **88**: 1-28, May 1963.

[228] Pellini, W. S., Principles of fracture safe design - Part I, Supplement to the Welding Journal, March 1971, pp. 91s-109s, 1971; Principles of fracture safe design - Part II, Supplement to the Welding Journal, April 1971, pp. 147s-162s, 1971.

[229] Pellini, W. S., Analytical design procedures for metals of elastic-plastic and plastic fracture properties, *Welding Research Council Bulletin* **186**: 17-25, 1973.

[230] Pellini, W. S., Design options for selection of fracture control procedures in modernization of codes, rules and standards, *Welding Research Council Bulletin* **186**: 1-16, 1973.

[231] Petersen, M. J., Dynamics of ship collisions, *Ocean Engineering* **9**(4): 295-329, 1982.

[232] Pedersen, P. T. and Zhang, S. M., Absorbed energy in ship collisions and grounding -revising Minarsky's empirical method, *Journal of Ship Research* **44**(2): 140-154, 2000.

[233] Pedersen, P. T. and Zhang, S. M., Effect of ship structure and size on grounding and collision damage distributions, *Ocean Engineering* **27**(11): 1161-1179, 2000.

[234] Petinov, S. V., *Fatigue Analysis of Ship Structures*, Fair Lawn, NJ: Backbone Pub. Co., 262 p., 2003.

[235] Pettit, R. G., Newman, J. C. and Domack, M. S., Crack turning damage tolerance approach for integrally stiffened structure, *19th ICAF Symposium*, Edinburgh, June 1997.

[236] Pippenger, D., Turheon, J. and Yahiaoui, M., Split wedge deformation experiments on stiffened plates, Joint MIT - Industry Program on Tanker Safety, Report No 40, January 1995.

[237] Pippenger, D., Coupled vertical and horizontal resistance of hull girder in grounding accidents, Joint MIT - Industry Program on Tanker Safety, Report No 46, May 1995.

[238] Porricelli, J. D. and Boyd, J. H., Analytical techniques for predicting grounded ship responses, Ship Structure Committee, Report No 324, 1984.

[239] Price, S. R., Plastic shear buckling of ship hull plating induced by grounding, Joint MIT - Industry Program on Tanker Safety, Report No 9, May 1992.

[240] Priest, A. H., An energy balance in crack propagation and arrest, *Engineering Fracture Mechanics* **61**(2): 231-251, 1998.

[241] Priest, A. H., The influence of structural dimensions on crack arrest, *Engineering Fracture Mechanics* **70**(17): 2421-2437, 2003.

[242] Puente, I. J., Correlation of NSWC grounding tests with MIT theory, Joint MIT - Industry Program on Tanker Safety, Report No 36, June 1994.

[243] Puente, I. J., Structural collapse of oil tanker hull due to stranding - a finite element approach, Joint MIT - Industry Program on Tanker Safety, Report No 44, May 1995.

[244] Pussegoda, L. N., Malik, L., Bouchard, R. and Tyson, W. R., Strain rate effects on fracture toughness of ship plate steels, *Journal of Offshore Mechanics and Arctic Engineering - Transactions of ASME* **118**(2):127-134, 1996.

[245] Pussegoda, L. N., Malik, L. and Tyson, W. R., Effects of plastic deformation on fracture toughness of ship plate steels, *Canadian Metallurgical Quarterly* **36**(1): 39-47, 1997.

[246] Pussegoda, L. N., Malik, L. and Morrison, J., Measurement of crack arrest fracture toughness of a ship steel plate, *Journal of Testing and Evaluation* **26**(3): 187-197, 1998.

[247] Rajendran, R., Paik, J. K. and Kim, B. J., Design of warship plates against underwater explosions, *Ships and Offshore Structures* **1**(4): 347-356, 2005.

[248] Ramajeyathilagam, K., Vendhan, C. P., and Rao, V. B., Non-linear transient dynamic response of rectangular plates under shock loading, *International Journal of Impact Engineering* **24**(10): 999-1015, 2000.

[249] Ramajeyathilagam, K., Vendhan, C. P. and Rao, V. B., Experimental and numerical investigations on deformation of cylindrical shell panels to underwater explosion, *Shock and Vibration* **8**(5): 253-268, 2001.

[250] Ramajeyathilagam, K. and Vendhan, C. P., Underwater explosion damage of ship hull panels. *Defence Science Journal* **53**(4): 393-402, 2003.

[251] Ramajeyathilagam, K. and Vendhan, C. P., Deformation and rupture of thin rectangular plates subjected to underwater shock, *International Journal of Impact Engineering* **30**(6): 699-719, 2004.

[252] Ramberg, W. and Osgood, W. R., Description of stress-strain curves by three parameters, *National Advisory Committee for Aeronautics*, Technical Note No 902, 1943.

[253] Rankin, C. C., Brogan, F. A. and Riks, E., Some computational tools for the analysis of through cracks in stiffened fuselage shells, *Computational Mechanics* **13**(3): 143-156, 1993.

[254] Rashed, Y. F., Aliabadi, M. H. and Brebbia, C. A., The boundary element method for Reissner plates resting on elastic foundations, Plate bending analysis with boundary elements (edited by M. H. Aliabadi), *Computational Mechanics Publications*, Southampton, 1998.

[255] Rice, J. R. and Tracey, D. M., On the ductile enlargement of voids in triaxial stress fields, *Journal of the Mechanics and Physics of Solids* **17**(3): 201-217, 1969.

[256] Richard, H. A., Fulland, M. and Sander, M., Theoretical crack path prediction, *Fatigue and Fracture of Engineering Materials and Structures* **28**(1-2): 3-12, 2005.

[257] Richir, T., Toderan, C., Paik, J. K. and Rigo, P., Effect of welding on ultimate compressive strength of aluminium stiffened panels, *High Performances Marine Vehicles (HIPER'2004)*, Rome, 129-139, 2004.

[258] Rickerby, D. G. and Fenici, P., Fatigue crack growth in thin section type 316 stainless steel, *Engineering Fracture Mechanics* **19**(4): 585-599, 1984.

[259] Rigo, P., Sarghiuta, R., Estefen, S., Lehmann, E., Otelea, S. C., Pasqualino, I., Simonsen, B. C., Wan, Z. and Yao, T., Sensitivity analysis on ultimate strength of aluminium stiffened panels, *Marine Structures* **16:** 437-468, 2003.

[260] Rigo, P., Sarghiuta, R., Otelea, S. C., Pasqualino, I., Wan, Z., Yao, T., Toderan, C. and Richir, T., Ultimate strength of aluminium stiffened panels: Sensitivity analysis, *Proceedings of Practical Design of Ships and other Floating Structures* **1:** 156-162, 2004.

[261] Riks, E., Rankin, C. C. and Bargon, F. A., Buckling behavior of a central crack in plate under tension, *Engineering Fracture Mechanics* **43**(4)**:** 529-548, 1992.

[262] Robles, L. B. R., Buelta, M. A., Goncalves, E. and Souza, G. F. M., A method for the evaluation of the fatigue operational life of submarine pressure hulls, *International Journal of Fatigue* **22**(1)**:** 41-52, 2000.

[263] Rodd, J. L., Phillips, M. P. and Anderson, E. D., Stranding experiments on double hull tanker structures, *Proceedings of The Advanced Double Hull (ADH) Technical Symposium*, October 1994.

[264] Rodd, J. L., Large scale tanker grounding experiments, *Proceedings of the 6th International Offshore and Polar Engineering Conference (ISOPE)* **IV:** 483-494, Los Angeles, May 1996.

[265] Romualdi, J. P., Frasier, J. T. and Irwin, G. R., Crack extension force near a riveted stiffener, N.R.L. report 4956, 1957.

[266] Rudrapatna, N. S., Vaziri, R. and Olson, M. D., Deformation and failure of blast-loaded square plates, *International Journal of Impact Engineering* **22**(4)**:** 449-467, 1999.

[267] Rudrapatna, N. S., Vaziri, R. and Olson, M.D., Deformation and failure of blast-loaded stiffened plates. *International Journal of Impact Engineering* **24**(5): 457-474, 2000.

[268] Sabelkin, V., Mall, S. and Avram, J. B., Fatigue crack growth analysis of stiffened cracked panel repaired with bonded composite patch, *Engineering Fracture Mechanics* **73**(11): 1553-1567, 2006.

[269] Sadovský, Z., Teixeira, A. P. and Soares, C. G., Degradation of the compressive strength of rectangular plates due to initial deflection, *Thin-Walled Structures* **43**(1)**:** 65-82, 2005.

[270] Salgado, N. K. and Aliabadi, M. H., Boundary element analysis of fatigue crack propagation in stiffened panels, *Journal of Aircraft* **35**(1): 122-130, 1998.

[271] Sanders, J. L., Effect of a stringer on the stress concentration due to a crack in a thin sheet, N.A.S.A.T.R R13, 1959.

[272] Sanford, R. J., *Principles of fracture mechanics*, Upper Saddle River, NJ: Prentice Hall. xi, 404 p, 2003.

[273] Sano, M., Miyaji, S., Iijima, K. and Yao, T., Development of simple calculation model to simulate buckling/plastic collapse behavior of ultra-wide rectangular plates under in-plane compression, *Proceedings of 19th Asian-Pacific Technical Exchange and Advisory Meeting on Marine Structures*, Singapore, 474-481, 2005.

[274] Sethuraman, R. and Maiti, S. K., Determination of mixed mode stress intensity factors for a crack-stiffened panel, *Engineering Fracture Mechanics* **33**(3): 355-369, 1989.

[275] Shariat, B. A. S., Javaheri, R. and Eslami, M. R., Buckling of imperfect functionally graded plates under in-plane compressive loading, *Thin-Walled Structures* **43**(7): 1020-1036, 2005.

[276] Shaw, D. and Huang, Y. H., Buckling behavior of a central cracked thin plate under tension, *Engineering Fracture Mechanics* **35**(6): 1019-1027, 1990.

[277] Sielski, R. A., Stopping cracks in aluminum plate, *U.S. Navy Deckplate,* NAVSEA **7**, 1986.

[278] Sielski, R. A., Fracture-mechanics of ship structures, *Naval Engineers Journal* **104**(3): 36-45, 1992.

[279] Sih, G. C., *Mechanics of Fracture Initiation and Propagation: surface and volume energy density applied as failure criterion*, Kluwer Academic Publishers, Dordrecht, Boston: Kluwer Academic. xxii., 410 p., 1991.

[280] Sikora, J., Grassman, J. M., Sensharma, P., Watts, J. and McNatt, T. R., Advanced double hull structural design technology, *Naval Engineers Journal* **109**(3): 117-128, 1997.

[281] Simonsen, B. C., User's manual for SOFTGROUND, PC computer program for analyzing ship groundings on sandy ocean beds, Joint MIT - Industry Program on Tanker Safety, Report No 45, March 1995.

[282] Simonsen, B. C., Wierzbicki, T. and Choi, S. K., Theoretical manual on grounding damage of a hull bottom structure, Volume I, Joint MIT - Industry Program on Tanker Safety, Report No 52, June 1995.

[283] Simonsen, B. C. and Wierzbicki, T., Theoretical manual on grounding damage of a hull bottom structure, Volume II, Joint MIT - Industry Program on Tanker Safety, Report No 55, March 1996.

[284] Simonsen, B. C. and Wierzbicki, T., Grounding bottom damage and ship motion over a rock, *Proceedings of the 6th International Offshore and Polar Engineering Conference (ISOPE)* **IV:** 476-482, Los Angeles, May 1996.

[285] Simonsen, B. C. and Wierzbicki, T., Plasticity, fracture, and friction in steady-state plate cutting, *International Journal of Impact Engineering* **19**(8): 667-691, 1997.

[286] Simonsen, B. C., Ship grounding on rock - I. Theory, *Marine Structures* **10**(7): 519-562, 1997.

[287] Simonsen, B. C. and Wierzbicki, T., Plasticity, fracture and friction in steady-state plate cutting, *International Journal of Impact Engineering* **21**(5): 387-411, 1998.

[288] Simonsen, B. C. and Ocakli, H., Experiments and theory on deck and girder crushing, *Thin-Walled Structures* **34**(3): 195-216, 1999.

[289] Simonsen, B. C. and Törnqvist, R., Experimental and numerical modeling of ductile crack propagation in large-scale shell structures, *Marine Structures* **17**(1): 1-27, 2004.

[290] Sinmao, M. V., Graphical user's interface (GUI) for grounding damage assessment of oil tanker structure, Joint MIT - Industry Program on Tanker Safety, Report No 47, May 1995.

[291] Sinmao, M. V., Abramowicz, W. and Wierzbicki, T., User's manual and modeling guide for the program DAMAGE, Joint MIT - Industry Program on Tanker Safety, Report No 54. June 1995.

[292] Smith, P. D. and Hetherington, J. G., *Blast and ballistic loading of structures*, Oxford; Boston, Butterworth - Heinemann Ltd, x., 320 p., 1994.

[293] Steen, E., Byklum, E., Vilming, K. G. and Ostvold, T. K., Computerized buckling models for ultimate strength assessment of stiffened ship hull panels, *Proceedings of PRADS'2004* **1:** 235-242, 2004.

[294] St. Germes, C. S., Davy, A. and Barrau, J. J., Prediction of the longitudinal crack behavior of stiffened curved panels, *International Journal of Fatigue* **23**(2): 147-158, 2001.

[295] Sumi, Y., Mohri, M. and Okawa, T., Simulation-based fatigue crack management for ship structural details, *Proceedings of Practical Design of Ships and other Floating Structures* **2:** 855-862, 2004.

[296] Sumi, Y., Yano, T. and Bashar, A. T. M. M., Numerical weight function method for the structural analysis of ships: a speedy direct calculation with condensed structural information, *Journal of Marine Science and Technology* **10**(2): 96-102, 2005.

[297] Sumi, Y., Mohri, M. and Kawamura, W., Computational prediction of fatigue crack paths in ship structural details, *Fatigue & Fracture of Engineering Materials & Structures* **28**(1-2): 107-115, 2005.

[298] Swift, T. and Wang, D. Y., Damage tolerant design-analysis methods and test verification of fuselage structure. *Air Force Conference on Fatigue of Aircraft Structures and Materials,* December, 1969.

[299] Thomas, P. F. and Wierzbicki, T., Performance criteria vs. design standards for commercial tank vessels, Joint MIT - Industry Program on Tanker Safety, Report No 5, October 1991.

[300] Thomas, P. F. and Wierzbicki, T., Grounding damage to double hull tank vessels, Joint MIT - Industry Program on Tanker Safety, Report No 7, April 1992.

[301] Thomas, P. F., Application of plate cutting mechanics to damage prediction in ship grounding, Joint MIT - Industry Program on Tanker Safety, Report No 8, May 1992.

[302] Thunes, R., Developed of analytical models of wedge unidirectionally stiffened and orthogonally stiffened double hulls, Joint MIT - Industry Program on Tanker Safety, Report No 21, January 1994.

[303] Timoshenko, S. P., *History of Strength of Materials*, McGraw-Hill Book Company, New York, 1953.

[304] Toyosada, M., Gotoh, K. and Niwa, T., Fatigue crack propagation for a through thickness crack: a crack propagation law considering cyclic plasticity near the crack tip, *International Journal of Fatigue* **26**(9): 983-992, 2004.

[305] Trauth, K. A. and Wierzbikci, T., Tearing failure of an infinite plate from a local cut, Joint MIT- Industry Program on Tanker Safety, Report No 16, June 1993.

[306] Trauth, K. A., Validation of concertina tearing solution, Joint MIT - Industry Program on Tanker Safety, Report No 34, June 1994.

[307] Tripathi, R. S., Rao, R. V. R., and Pattanaik, S. P., High cycle fatigue, crack propagation resistance and fracture toughness in ship steels, *Defence Science Journal* **51**(2): 201-210, 2001.

[308] Tryland, T., Larsen, P. and Langseth, M., Design of I beams and deck profiles under concentrated loading, *Journal of Structural Engineering* **129**(11): 1433–1440, 2003.

[309] Tvergaard, V. and Needleman, A., Analysis of the cup-cone fracture in a round tensile bar, *Acta Metallurgica* **32**: 157-169, 1984.

[310] Turgeon, J., Analysis of hull damage without fracture in single-bottom transversely framed ships subjected to grounding, Joint MIT - Industry Program on Tanker Safety, Report No 48, May 1995.

[311] Ueda, Y. and Rashed, S. M. H., The idealized structural unit method and its application to deep girder structures, *Computers and Structures* **18**(2): 277-293, 1984.

[312] Ueda, Y., Rashed, S. M. H. and Paik, J. K., An Incremental Galerkin method for plates and stiffened plates, *Computers & Structures* **27**(1): 147-156, 1987.

[313] Vafai, A. and Estekanchi, H. E., A parametric finite element study of cracked plates and shells, *Thin-Walled Structures* **33**(3): 211-229, 1999.

[314] Vafai, A., Javidruzi, M. and Estekanchi, H. E., Parametric instability of edge cracked plates, *Thin-Walled Structures* **40**(1): 29-44, 2002.

[315] Van der Weeën, F., Application of the boundary integral equation method to Reissner's plate model, *International Journal of Numerical Methods Engineering* **18:** 1-10, 1982.

[316] Vaughan, H., Damage to ship due to collision and grounding, Det norske Veritas, DnV Report 77-345, 1977.

[317] Vaughan, H., Bending and tearing of plate with application to ship-bottom damage, *The Naval Architect, RINA*, 97-99, May 1978.

[318] Vaughan, H., The tearing strength of mild steel plate, *Journal of Ship Research* **24**(2): 96-100, 1980.

[319] Vlieger, H., The residual strength characteristics of stiffened panels containing fatigue cracks, *Engineering Fracture Mechanics* **5**(2)**:** 447-477, 1973.

[320] Wade, B. G. and Kobayashi, A. S., Photoelastic investigation on the crack-arrest capability of a pretensioned stiffened plate, *Experimental Mechanics* **15**(1): 1-9, 1975.

[321] Wang, X., Peeling type fracture of ship hull plate due to grounding, Joint MIT - Industry Program on Tanker Safety, Report No 13, May 1993.

[322] Wang, Y. H., Liu, Z. H. and Wang, J., Dynamic fracture-analysis of a stiffened panel with an edge crack, *Engineering Fracture Mechanics* **46**(2): 329-338, 1993.

[323] Wang, G., Some recent studies on plastic behavior of plates subjected to large impact loads, *Journal of Offshore Mechanics and Arctic Engineering - Transactions of ASME* **124**(3)**:** 125-131, 2002.

[324] Wang, X., Sun, H., Akiyama, A. and Du, A., Buckling and ultimate strength of aluminum plates and stiffened panels in marine structures, *Fifth International Forum on Aluminum Ships*, Tokyo, Japan, 119-125, October 2005.

[325] Wen, P. H., Aliabadi, M. H. and Young, A., Stiffened cracked plates analysis by dual boundary element method, *International Journal of Fracture* **106**(3): 245-258, 2000.

[326] Wierzbicki, T. and Abramowicz, W., On the crushing mechanics of thin-walled structures, *Journal of Applied Mechanics, Transactions of the ASME* **50**(4A): 727-734, 1983.

[327] Wierzbicki, T., Crushing behavior of plate intersections, *Proceedings of the 1st International Symposium on Structural Crashworthiness*, University of Liverpool, 66-95, 1983.

[328] Wierzbicki, T., Rady, E., Peer, D. and Shin, J. G., Damage estimates in high energy grounding of ships, Joint MIT - Industry Program on Tanker Safety, Report No 1, 1990.

[329] Wierzbicki, T., Peer, D. and Rady, E., The anatomy of tanker grounding, Joint MIT - Industry Program on Tanker Safety, Report No 2, May 1991.

[330] Wierzbicki, T. and Thomas, P. F., Closed-form solution for wedge cutting force through thin metal sheets, Joint MIT - Industry Program on Tanker Safety, Report No 6, March 1992.

[331] Wierzbicki, T. and Thomas, D., Closed-form solution for wedge cutting force through thin metal sheets, *International Journal of Mechanical Sciences* **35**(3-4): 209-229, 1993.

[332] Wierzbicki, T., Concertina tearing of metal plates, Joint MIT - Industry Program on Tanker Safety, Report No 12, March 1993.

[333] Wierzbicki, T., Concertina tearing of metal plates: improved solution and comparison, Joint MIT - Industry Program on Tanker Safety, Report No 22, January 1994.

[334] Wierzbicki, T., Yahiaoui, M. and Sinmao, M., Research activities within the Joint MIT - Industry Project on Tanker Safety, Joint MIT - Industry Program on Tanker Safety, Report No 37, January 1995.

[335] Wierzbicki, T., Trauth, K. A. and Atkins, A. G., On diverging concertina tearing, *Journal of Applied Mechanics - Transaction of the ASME* **65**(4): 990-997, 1998.

[336] Wierzbicki, T., Petalling of plates under explosive and impact loading, *International Journal of Impact Engineering* **22**(9-10): 935-954, 1999.

[337] Wilcox, R., The effect of weld penetration on the tensile strength of fillet welded joints, Joint MIT - Industry Program on Tanker Safety, Report No 50, May 1995.

[338] Woisin, G., Design against collision, *Proceedings of the International Symposium on Advances in Marine Technology*, Trondheim, 1979.

[339] Xiao, D. Y. and Dexter, R. J., Finite element calculation of applied J-integral for cracked ship structural details, *Engineering Fracture Mechanics* **60**(1): 59-82, 1998.

[340] Xiao, Y. and Menzemer, C., Ultimate compressive strength of aluminium plate elements, *Journal of Structural Engineering* **129**(11): 1441-1447, 2003.

[341] Xue, L., Ductile fracture modeling - Theory, experimental investigation and numerical verification, PhD Thesis, Department of Mechanical Engineering, Massachusetts Institute of Technology, February 2007.

[342] Yahiaoui, M., Bracco, M., Little and Trauth, K. A., Experimental studies on scale models for grounding, Joint MIT - Industry Program on Tanker Safety, Report No 18, January 1994.

[343] Yahsi, O. S. and Shahid, M. M., The effect of a stiffener on a cracked plate under bending, International *Journal of Pressure Vessels and Piping* **23:** 133-148, 1986.

[344] Yanagihara, D., Fijikubo, M., Morita, R. and Setoyama, Y., Estimation of ultimate strength of continuous stiffened plate under combined thrust and lateral pressure, *Journal of the Society of Naval Architects of Japan* **192:** 697-705 (in Japanese), 2002.

[345] Yanagihara, D., Fujikubo, M. and Harada, M., Estimation of ultimate strength of continuous stiffened plate under combined thrust and lateral pressure, *Journal of the Society of Naval Architects of Japan* **194**: 161-170, (in Japanese), 2003.

[346] Yarema, S. Y., Zima, Y. V, Olik, A. P., Bakulin, A. V. and Borsukevich, V. I., Cyclic cracking resistance of 1561 aluminum-alloy in air and Nacl solution, *Soviet Materials Science* **24**(1): 87-91, 1988.

[347] Yeh, J. R. and Kulak, M., Fracture analysis of cracked orthotropic skin panels with riveted stiffeners, *International Journal of Solids and Structures* **37**(17): 2473-2487, 2000.

[348] You, X. C., Zhuang, Z., Huo, C. Y., Zhuang, C. J. and Feng, Y. R., Crack arrest in rupturing steel gas pipelines, *International Journal of Fracture* **123**(1-2): 1-14, 2003.

[349] Yuen, S. C. K. and Nurick, G. N., Experimental and numerical studies on the response of quadrangular stiffened plates. Part I: subjected to uniform blast load, *International Journal of Impact Engineering* **31**(1): 55-83, 2005.

[350] Yumura, K., Katsura, S., Iijima, K. and Yao, T., Simulation of buckling collapse behavior of cylindrically curved plates under axial compression, *Proceedings of 19th Asian - Pacific Technical Exchange and Advisory Meeting on Marine Structures*, Singapore, 482-489, 2005.

[351] Zabavsky, G., Kim, V. S., Lebova, T. I. and Manjula, K. P., Fatigue of welded connections with incomplete penetration in ship hull details, *Bubnov Lectures, St. Petersburg*, 66-68, 2004.

[352] Zehnder, A. T., Viz, M. J. and Potdar, Y., Fatigue fracture in plates in tension and out-of-plane shear, *Fatigue and Fracture of Engineering Materials and Structures* **23**(5): 401-413, 2000.

[353] Zha, Y. F. and Moan, T., Experimental and numerical prediction of collapse of flatbar stiffeners in aluminium panels, *Journal of Structural Engineering-ASCE* **129**(2): 160-168, 2003.

[354] Zhang, T., Liu, T. G., Zhao, Y. and Wang, X. Z., Buckling and postbuckling of imperfect stiffened plates, *Journal of Ship Mechanics*, **7**(1): 79-83, 2003.

[355] Zhang, S., Ocakli, H. and Pedersen, P. T., Crushing of ship bows in head-on collision, *RINA Transactions Part A2 - International Journal of Maritime Engineering (IJME)*, 2004.

[356] Zheng, Z. M. and Wierzbicki, T., Steady-state wedge indentation, Joint MIT - Industry Program on Tanker Safety, Report No 42, January 1995.

[357] Zheng, Z. M. and Wierzbicki, T., A theoretical study on the steady-state wedge cutting through metal plates, *International Journal of Fracture* **78**(1): 45-66, 1996.

[358] Zheng, G. and Hu, Y., Tripping of thin-walled stiffeners in the axially compressed stiffened panel with lateral pressure and end moment, *Thin-Walled Structures* **43**(5): 789-799, 2005.

[359] Zheng, L., Fracture of welded aluminum thin-walled structures, PhD Thesis, Department of Mechanical Engineering, Massachusetts Institute of Technology, June 2005.

[360] Zhou, Q. and Wierzbicki, T., A beam model for blanking and tearing of ductile metal plate, Joint MIT - Industry Program on Tanker Safety, Report No 25, January 1994.

[361] Zhuang, Z. and O'Donoghue, P. E., Steady state analysis for dynamic crack propagation in gas pipelines, *Fracture and Strength of Solids* Pts 1 and 2 **145-9**: 255-260, 1998.

[362] Zhuang, Z. and Guo, Y. J., Analysis of dynamic fracture mechanisms in gas pipelines, *Engineering Fracture Mechanics* **64**(3): 271-289, 1999.

[363] Zhuang, Z. and O'Donoghue, P. E., The recent development of analysis methodology for rapid crack propagation and arrest in gas pipelines, *International Journal of Fracture* **101**(3): 269-290, 2000.

[364] Zuidema, J. and Blaauw, H. S., Slant fatigue crack growth in Al 2024 sheet material, *Engineering Fracture Mechanics* **29**(4): 401-413, 1988.

[365] Zuidema, J., van Kranenburg, C., Riemslag, A. C., Veer, F. and Boljanovic, S., Anomalous fatigue crack growth behaviour in AA 2024 and AA 5083, In: *Proceedings of 3rd International Conference on Materials Structures and Micromechanics of Fracture*, Brno, 579-594, 2001.

[366] Zuidema, J., Veer, F. and van Kranenburg, C., Shear lips on fatigue fracture surfaces of aluminum alloys, *Fatigue and Fracture of Engineering Materials and Structures* **28**(1-2): 159-167, 2005.

Appendix A

Calculation of J-integral for Mode-I

The polar stresses and displacements for mode-I loading are given by:

$$\begin{bmatrix} \sigma_r \\ \sigma_\theta \\ \tau_{r\theta} \end{bmatrix} = \frac{K_I}{2\sqrt{2\pi r}} \cos\frac{\theta}{2} \begin{bmatrix} 3-\cos\theta \\ 1+\cos\theta \\ \sin\theta \end{bmatrix} \tag{A.1}$$

and

$$\begin{bmatrix} u_r \\ u_\theta \end{bmatrix} = \frac{K_I}{4\mu}\left(\frac{r}{2\pi}\right)^{1/2} \begin{bmatrix} (2\kappa-1)\cos\frac{\theta}{2} - \cos\frac{3\theta}{2} \\ -(2\kappa+1)\sin\frac{\theta}{2} + \sin\frac{3\theta}{2} \end{bmatrix} \tag{A.2}$$

We have

$$\varepsilon_r = \frac{\partial u_r}{\partial r}$$

$$\varepsilon_\theta = \frac{u_r}{r} + \frac{1}{r}\frac{\partial u_\theta}{\partial \theta} \tag{A.3}$$

$$\varepsilon_{r\theta} = \frac{1}{2}\left(\frac{1}{r}\frac{\partial u_r}{\partial \theta} + \frac{\partial u_\theta}{\partial r} - \frac{u_\theta}{r}\right)$$

From Eqs. (A.1) and (A.2) we obtain

$$\varepsilon_r = \frac{K_I}{8\mu}\frac{1}{\sqrt{2\pi r}}\left[(2\kappa - 1)\cos\frac{\theta}{2} - \cos\frac{3\theta}{2}\right]$$

$$\varepsilon_\theta = \frac{K_I}{8\mu}\frac{1}{\sqrt{2\pi r}}\left[(2\kappa - 3)\cos\frac{\theta}{2} + \cos\frac{3\theta}{2}\right] \tag{A.4}$$

$$\varepsilon_{r\theta} = \frac{K_I}{8\mu}\frac{1}{\sqrt{2\pi r}}\left[\sin\frac{\theta}{2} + \sin\frac{3\theta}{2}\right]$$

We have

$$J = \int_\Gamma \omega dy - T_k\frac{\partial u_k}{\partial x}ds = J_1 + J_2 \tag{A.5}$$

$$J_1 = \int_\Gamma \omega dy, \quad J_2 = -\int_\Gamma T_k\frac{\partial u_k}{\partial x}ds \tag{A.6}$$

Consider a circle Γ of radius r centered at the crack tip. We have

$$y = r\sin\theta, \quad dy = r\cos\theta d\theta \tag{A.7}$$

and

$$\omega = \frac{1}{2}(\sigma_r\varepsilon_r + \sigma_\theta\varepsilon_\theta + 2\tau_{r\theta}\varepsilon_{r\theta}) \tag{A.8}$$

Thus we obtain

$$J_1 = \frac{K_I^2}{32\mu\pi r}\frac{1}{2}\int_{-\pi}^{\pi}\cos\frac{\theta}{2}[(3-\cos\theta)\left[(2\kappa-1)\cos\frac{\theta}{2}-\cos\frac{3\theta}{2}\right]$$

$$+(1+\cos\theta)\left[(2\kappa-3)\cos\frac{\theta}{2}+\cos\frac{3\theta}{2}\right]$$

$$+2\sin\theta(\sin\frac{\theta}{2}+\sin\frac{3\theta}{2})r\cos\theta d\theta \tag{A.9}$$

$$=\frac{K_I^2}{32\pi\mu}\int_{-\pi}^{\pi}(4\kappa-3)\cos\frac{\theta}{2}-\cos\frac{\theta}{2}\cos\theta-\cos\frac{3\theta}{2}+\cos\theta\cos\frac{3\theta}{2}$$

$$+\sin\tfrac{\theta}{2}\sin\theta+\sin\theta\sin\frac{3\theta}{2}]\cos\frac{\theta}{2}\cos\theta d\theta$$

We have

$$(4\kappa-3)\cos^2\frac{\theta}{2}\cos\theta=\frac{4\kappa-3}{2}(1+\cos\theta)\cos\theta$$

$$-\cos^2\frac{\theta}{2}\cos^2\theta=-\frac{1}{2}\cos^2\theta(1+\cos\theta)$$

$$-\cos\frac{\theta}{2}\cos\frac{3\theta}{2}\cos\theta=-\frac{1}{2}\left(\cos^2\theta+2\cos^3\theta-\cos\theta\right) \tag{A.10}$$

$$\cos^2\theta\cos\frac{\theta}{2}\cos\frac{3\theta}{2}=\frac{1}{2}\left(\cos^3\theta+2\cos^4\theta-\cos^2\theta\right)$$

$$-\cos\frac{\theta}{2}\cos\theta\sin\frac{\theta}{2}\sin\theta=\frac{1}{2}\left(\cos\theta-\cos^3\theta\right)$$

$$\cos\frac{\theta}{2}\cos\theta\sin\theta\sin\frac{3\theta}{2}=\frac{1}{2}\left(-\cos\theta+2\cos^2\theta+\cos^3\theta-2\cos^4\theta\right)$$

Using the formula

$$\int_{-\pi}^{\pi}\cos^n\theta d\theta=0,\quad n=1,3,5... \tag{A.11}$$

we obtain

$$J_1 = \frac{K_I^2}{32\pi\mu}\int_{-\pi}^{\pi}\left(\frac{4\kappa-3}{2}-\frac{1}{2}-\frac{1}{2}-\frac{1}{2}+1\right)\cos^2\theta d\theta$$

$$= \frac{K_I^2}{32\pi\mu}\int_{-\pi}^{\pi} 2\left(\kappa-1\right)\cos^2\theta d\theta$$

$$= \frac{(\kappa-1)K_I^2}{16\pi\mu}\int_{-n}^{n}\cos^2\theta d\theta \tag{A.12}$$

$$= \frac{(\kappa-1)K_I^2}{16\pi\mu}\pi$$

$$= \frac{(\kappa-1)K_I^2}{16\mu}$$

We have for J_2

$$J_2 = -\int T_\kappa \frac{\partial u_k}{\partial x} ds \tag{A.13}$$

$$\frac{\partial u_1}{\partial x} = \frac{\partial u_1}{\partial r}\frac{\partial r}{\partial x} + \frac{\partial u_1}{\partial \theta}\frac{\partial \theta}{\partial x} \tag{A.14}$$

$$x = r\cos\theta \quad y = r\sin\theta \quad r = \sqrt{x^2+y^2} \quad \theta = \tan^{-1}\frac{y}{x} \tag{A.15}$$

$$\frac{\partial r}{\partial x} = \cos\theta \quad \frac{\partial \theta}{\partial x} = -\frac{\sin\theta}{r}$$

$$\frac{\partial u_i}{\partial x} = \cos\theta\frac{\partial u_i}{\partial r} - \frac{\sin\theta}{r}\frac{\partial u_i}{\partial \theta} \tag{A.16}$$

$$\underset{\sim}{T} = \sigma_r \underset{\sim}{\varepsilon_r} + \tau_{r\theta}\underset{\sim}{\varepsilon_\theta}$$

$$\tag{A.17}$$

$$\underset{\sim}{u} = u_r\underset{\sim}{\varepsilon_r} + u_\theta\underset{\sim}{\varepsilon_\theta}$$

where $\underset{\sim}{\varepsilon_r}$ and $\underset{\sim}{\varepsilon_\theta}$ are the unit vectors along the r and θ directions.

We have

$$\frac{\partial \underset{\sim}{\varepsilon_r}}{\partial \theta} = \underset{\sim}{\varepsilon_\theta} \quad \frac{\partial \underset{\sim}{\varepsilon_\theta}}{\partial \theta} = -\underset{\sim}{\varepsilon_r} \tag{A.18}$$

$$\frac{\partial \underset{\sim}{\varepsilon_r}}{\partial x} = -\frac{\sin\theta}{r}\underset{\sim}{\varepsilon_\theta}, \quad \frac{\partial \underset{\sim}{\varepsilon_\theta}}{\partial x} = \frac{\sin\theta}{r}\underset{\sim}{\varepsilon_r} \tag{A.19}$$

$$T_k \frac{\partial u_x}{\partial x} = \underset{\sim}{T_k} \frac{\partial \underset{\sim}{u}}{\partial x}$$

$$= \left(\sigma_r \underset{\sim}{\varepsilon_r} + \tau_{r\theta}\underset{\sim}{\varepsilon_\theta}\right)\left(\frac{\partial u_r}{\partial x}\underset{\sim}{\varepsilon_r} - \frac{\sin\theta}{r}u_r\underset{\sim}{\varepsilon_\theta} + \frac{\partial u_\theta}{\partial x}\underset{\sim}{\varepsilon_\theta} + \frac{\sin\theta}{r}u_\theta\underset{\sim}{\varepsilon_r}\right) \tag{A.20}$$

$$= \sigma_r\left[\cos\theta\frac{\partial u_r}{\partial r} - \frac{\sin\theta}{r}\left(\frac{\partial u_r}{\partial \theta} - u_\theta\right)\right] + \tau_{r\theta}\left[\cos\theta\frac{\partial u_\theta}{\partial r} - \frac{\sin\theta}{r}\left(\frac{\partial u_\theta}{\partial \theta} - u_r\right)\right]$$

We have

$$\begin{aligned}
\frac{\partial u_r}{\partial r} &= \frac{K_I}{8\mu}\left(\frac{1}{2\pi r}\right)^{1/2}\left[(2\kappa-1)\cos\frac{\theta}{2} - \cos\frac{3\theta}{2}\right] \\
\frac{\partial u_r}{\partial \theta} &= \frac{K_I}{8\mu}\left(\frac{1}{2\pi}\right)^{1/2}\left[-(2\kappa-1)\cos\frac{\theta}{2} + 3\sin\frac{3\theta}{2}\right] \\
\frac{\partial u_\theta}{\partial r} &= \frac{K_I}{8\mu}\left(\frac{1}{2\pi r}\right)^{1/2}\left[-(2\kappa+1)\sin\frac{\theta}{2} + \sin\frac{3\theta}{2}\right] \\
\frac{\partial u_\theta}{\partial \theta} &= \frac{K_I}{8\mu}\left(\frac{1}{2\pi}\right)^{1/2}\left[-(2\kappa-1)\cos\frac{\theta}{2} + 3\cos\frac{3\theta}{2}\right]
\end{aligned} \tag{A.21}$$

Thus

$$\begin{aligned}
&\frac{\partial u_r}{\partial \theta}\cos\theta - \left(\frac{\partial u_r}{\partial \theta} - u_\theta\right)\frac{\sin\theta}{r} = \\
&\frac{K_I}{8\mu}\sqrt{\frac{1}{2\pi r}}[(2\kappa-1)\cos\frac{\theta}{2}\cos\theta - \cos\frac{3\theta}{2}\cos\theta + (2\kappa-1)\sin\frac{\theta}{2}\sin\theta \\
&-3\sin\frac{3\theta}{2}\sin\theta - 2(2\kappa+1)\sin\frac{\theta}{2}\sin\theta + 2\sin\frac{3\theta}{2}\sin\theta]
\end{aligned} \tag{A.22}$$

and

$$\frac{\partial u_\theta}{\partial r}\cos\theta - \left(\frac{\partial u_\theta}{\partial \theta} + u_r\right)\frac{\sin\theta}{r} =$$
$$\frac{K_I}{8\mu}\sqrt{\frac{1}{2\pi r}}[-(2\kappa+1)\sin\frac{\theta}{2}\cos\theta + \sin\frac{3\theta}{2}\cos\theta + (2\kappa+1)\cos\frac{\theta}{2}\sin\theta \qquad \text{(A.23)}$$
$$-3\cos\frac{3\theta}{2}\sin\theta - 2(2\kappa-1)\cos\frac{\theta}{2}\sin\theta + 2\cos\frac{3\theta}{2}\sin\theta]$$

We have

$$T_k\frac{\partial u_k}{\partial x} = \frac{K_I^2}{32\pi r}[(2\kappa-1)\cos^2\frac{\theta}{2}\cos\theta(3-\cos\theta) - \cos\frac{3\theta}{2}\cos\theta\cos\frac{\theta}{2}(3-\cos\theta)$$

$$+(2\kappa-1)\sin\frac{\theta}{2}\sin\theta\cos\frac{\theta}{2}(3-\cos\theta) - 3\sin\frac{3\theta}{2}\sin\theta\cos\frac{\theta}{2}(3-\cos\theta)$$

$$-2(2\kappa+1)\sin\frac{\theta}{2}\cos\theta\sin\theta(3-\cos\theta) + 2\sin\frac{3\theta}{2}\cos\frac{\theta}{2}\sin\theta(3-\cos\theta) \qquad \text{(A.24)}$$

$$-2(2\kappa+1)\sin\frac{\theta}{2}\cos\theta\sin\theta\cos\frac{\theta}{2} + \sin\frac{3\theta}{2}\cos\theta\sin\theta\cos\frac{\theta}{2}$$

$$+(2\kappa+1)\cos^2\frac{\theta}{2}\sin^2\theta - 3\cos\frac{3\theta}{2}\sin^2\theta\cos\frac{\theta}{2}$$

$$-2(2\kappa-1)\cos^2\frac{\theta}{2}\sin^2\theta + 2\cos\frac{3\theta}{2}\sin^2\theta\cos\frac{\theta}{2}]$$

Furthermore, we have

$$3(2\kappa-1)\cos\theta\cos^2\tfrac{\theta}{2} = \tfrac{3}{2}(2\kappa-1)(\cos\theta+\cos^2\theta)$$

$$-(2\kappa-1)\cos^2\theta\cos^2\tfrac{\theta}{2} = -\tfrac{2\kappa-1}{2}(\cos^2\theta+\cos^3\theta)$$

$$-3\cos\tfrac{3\theta}{2}\cos\theta\cos\tfrac{\theta}{2} = -3\left(4\cos^4\tfrac{\theta}{2}-3\cos^2\tfrac{\theta}{2}\right)\cos\theta = \tfrac{3}{2}\cos\theta-\tfrac{3}{2}\cos^2\theta-3\cos^3\theta$$

$$\cos\tfrac{3\theta}{2}\cos^2\theta\cos\tfrac{\theta}{2} = -\tfrac{1}{2}\cos^2\theta+\tfrac{1}{2}\cos^3\theta+\cos^4\theta$$

$$-3(2\kappa+3)\sin\tfrac{\theta}{2}\sin\theta\cos\tfrac{\theta}{2} = -3\kappa-\tfrac{9}{2}+3\kappa\cos^2\theta+\tfrac{9}{2}\cos^2\theta \tag{A.25}$$

$$2\sin\tfrac{\theta}{2}\sin\theta\cos\tfrac{\theta}{2}\cos\theta = \sin^2\theta\cos\theta = \cos\theta-\cos^3\theta$$

$$-3\sin\tfrac{3\theta}{2}\sin\theta\cos\tfrac{\theta}{2} = -\tfrac{3}{2}-3\cos\theta+\tfrac{3}{2}\cos^2\theta+3\cos^3\theta$$

$$2\sin\tfrac{3\theta}{2}\cos\theta\sin\theta\cos\tfrac{\theta}{2} = \cos\theta-\cos^3\theta+2\cos^2\theta-2\cos^4\theta$$

$$(-2\kappa+3)\cos^2\tfrac{\theta}{2}\sin^2\theta = \left(-\kappa+\tfrac{3}{2}\right)\left(1-\cos^2\theta+\cos\theta-\cos^3\theta\right)$$

$$-\cos\tfrac{3\theta}{2}\sin^2\theta\cos\tfrac{\theta}{2} = \tfrac{1}{2}-\tfrac{1}{2}\cos\theta-\tfrac{3}{2}\cos^2\theta+\tfrac{1}{2}\cos^3\theta+\cos^4\theta$$

Considering that

$$\int_{-\pi}^{\pi}\cos^n\theta d\theta = 0, \quad n = 1,3,5... \tag{A.26}$$

we obtain

$$J_2 = \int_{-\pi}^{\pi} T_k \frac{\partial u_x}{\partial x} = -\frac{K_I^2}{32\mu\pi} \int_{-\pi}^{\pi} \left[2\left(3\kappa+1\right)\cos^2\theta - 4\left(1+\kappa\right)\right] d\theta$$

$$= -\frac{K_I^2}{32\mu\pi} \left[\left(3\kappa+1\right)\left(1+\cos 2\theta\right) - 4\left(1+\kappa\right)\theta\right]_{-\pi}^{\pi}$$

$$= -\frac{K_I^2}{32\mu\pi} \left[\left(3\kappa+1\right)2\pi - 8\left(1+\kappa\right)\pi\right] \tag{A.27}$$

$$= -\frac{K_I^2}{32\mu\pi} \left[-2\left(\kappa+3\right)\pi\right] = \frac{\left(\kappa+3\right)K_I^2}{16\mu}$$

$$J = J_1 + J_2 = \frac{\left(\kappa-1\right)K_I^2}{16\mu} + \frac{\left(\kappa+3\right)K_I^2}{16\mu}$$

$$= \frac{\kappa+1}{8\mu} K_I^2 = n\frac{K_I^2}{E} \tag{A.28}$$

$n = 1$ (plane stress), $n = 1 - \nu^2$ (plane strain)

Equation A.28 gives the value of the J-integral for mode-I loading.

Appendix B

Fixtures

B.1 Fixture for small-scale tests

B.2 Fixture for intermediate-scale tests

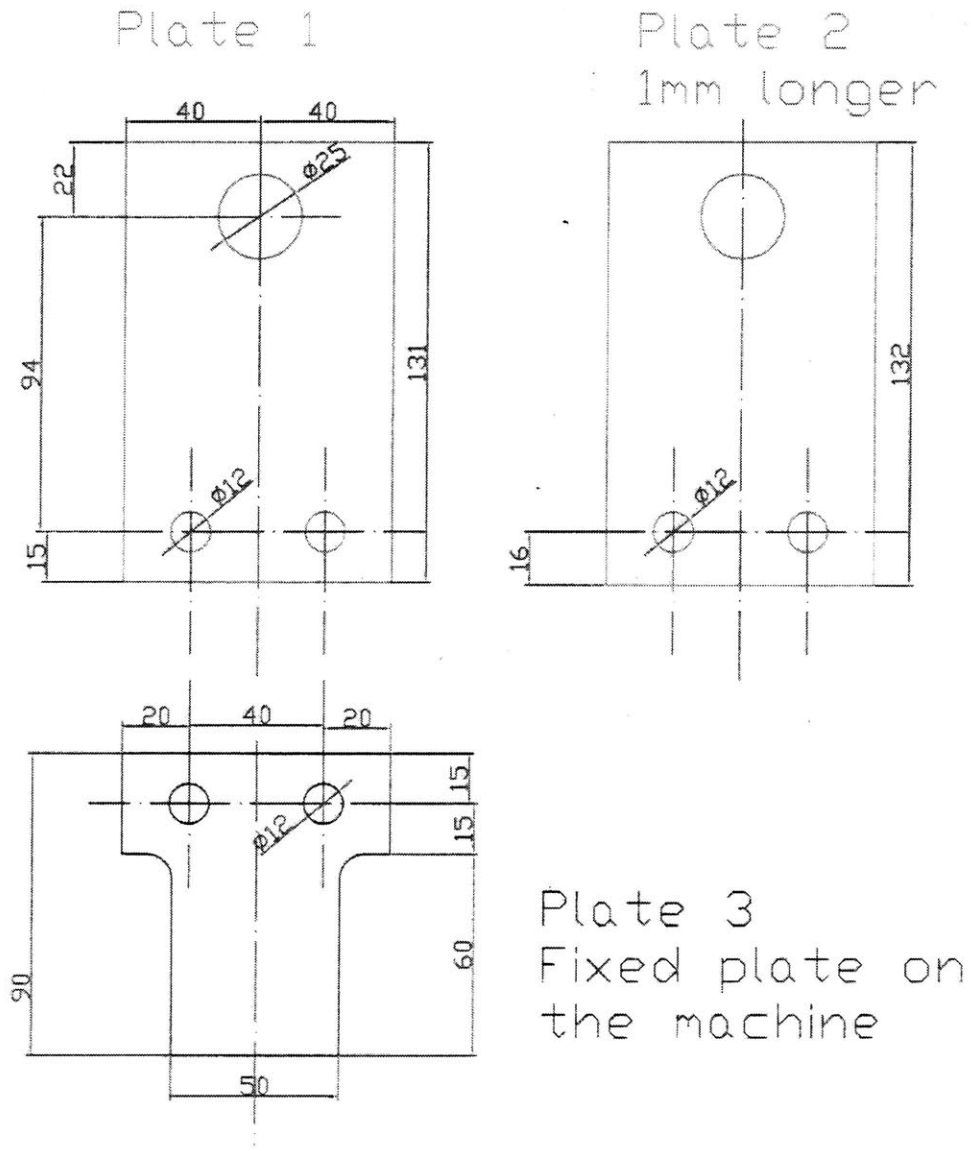

Figure B-1: Geometric characteristics of the fixture designed for the Compact Tension specimens experiments

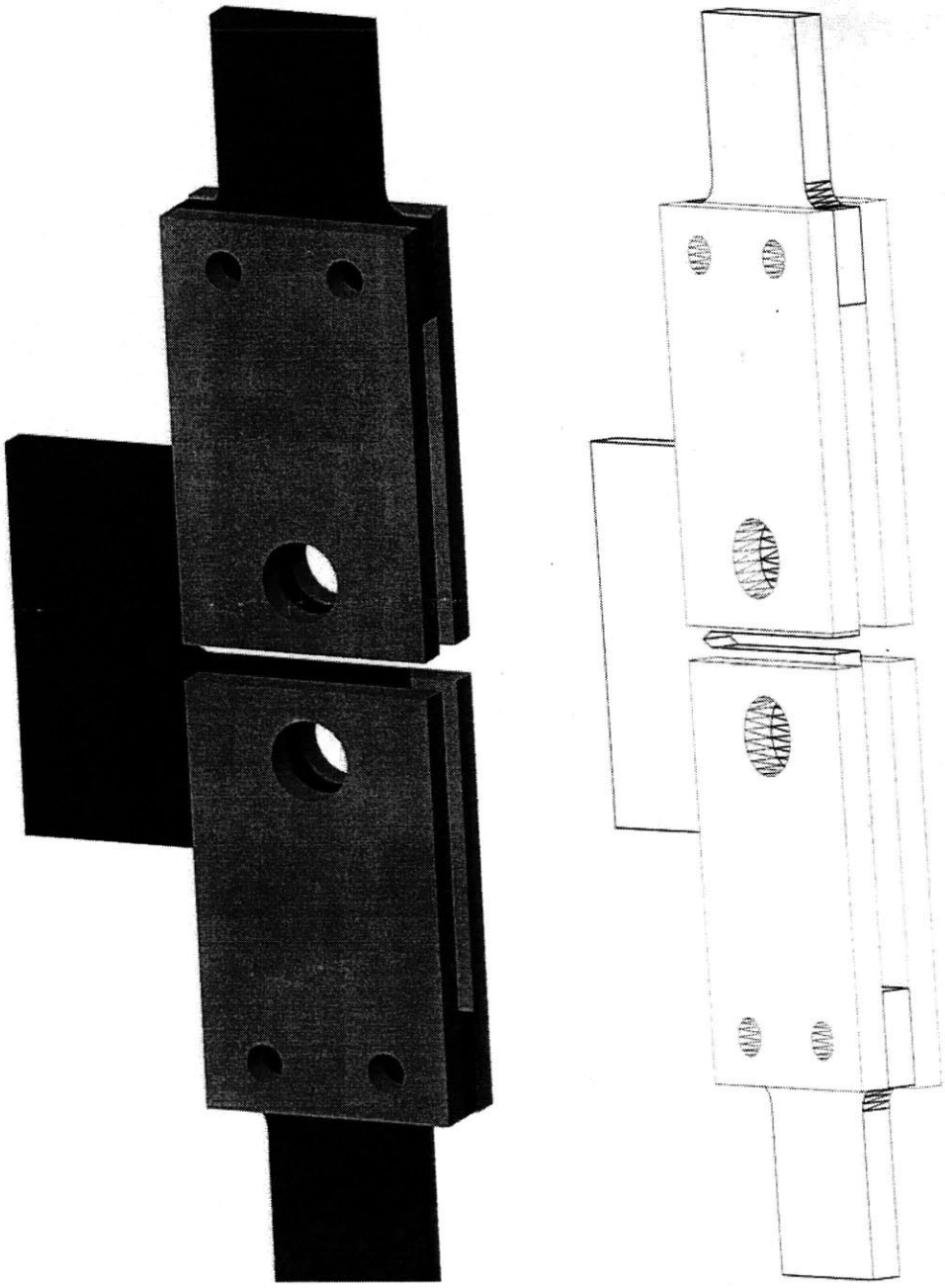

Figure B-2: Schematics of the fixture and the CT specimen

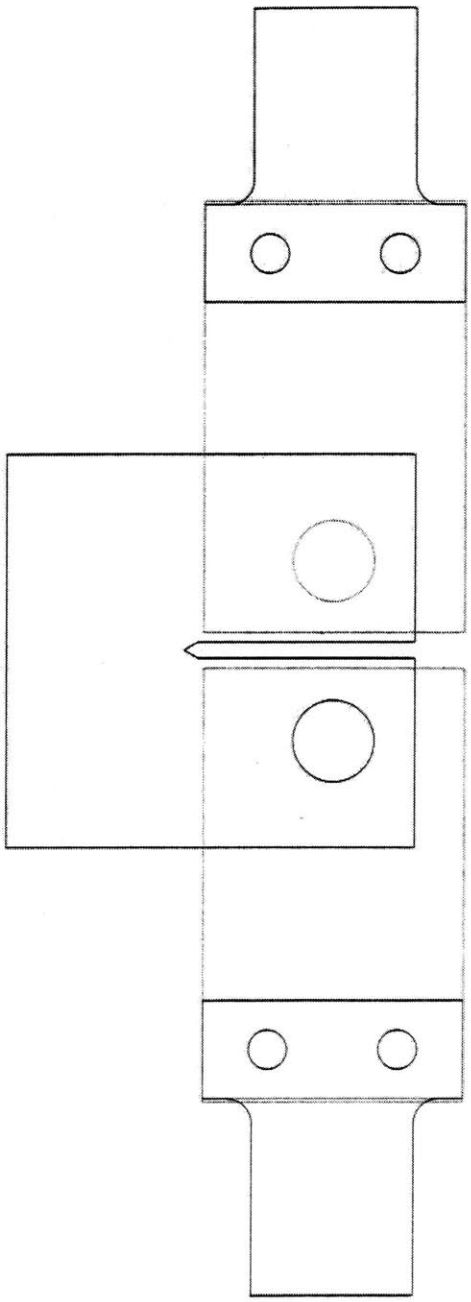

Figure B-3: Mounting of the CT specimen on the fixture

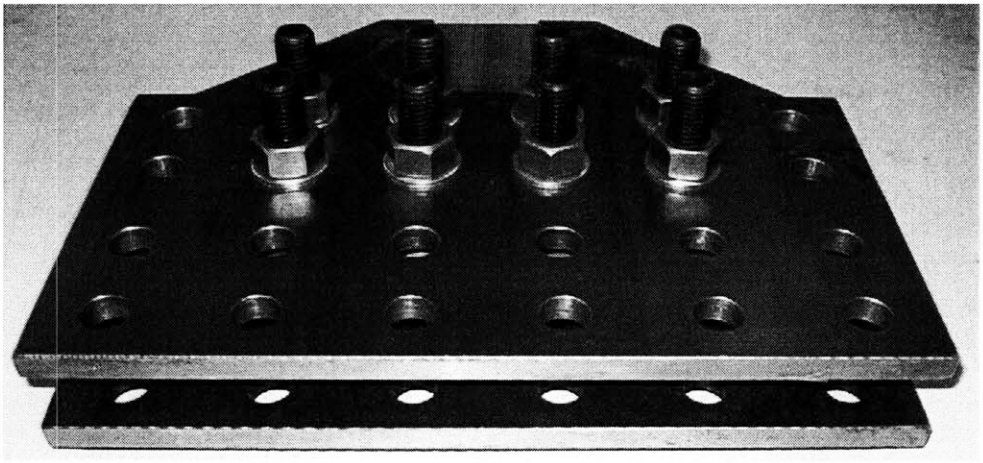

Figure B-4: Photograph of the fixture designed for the intermediate-scale tests

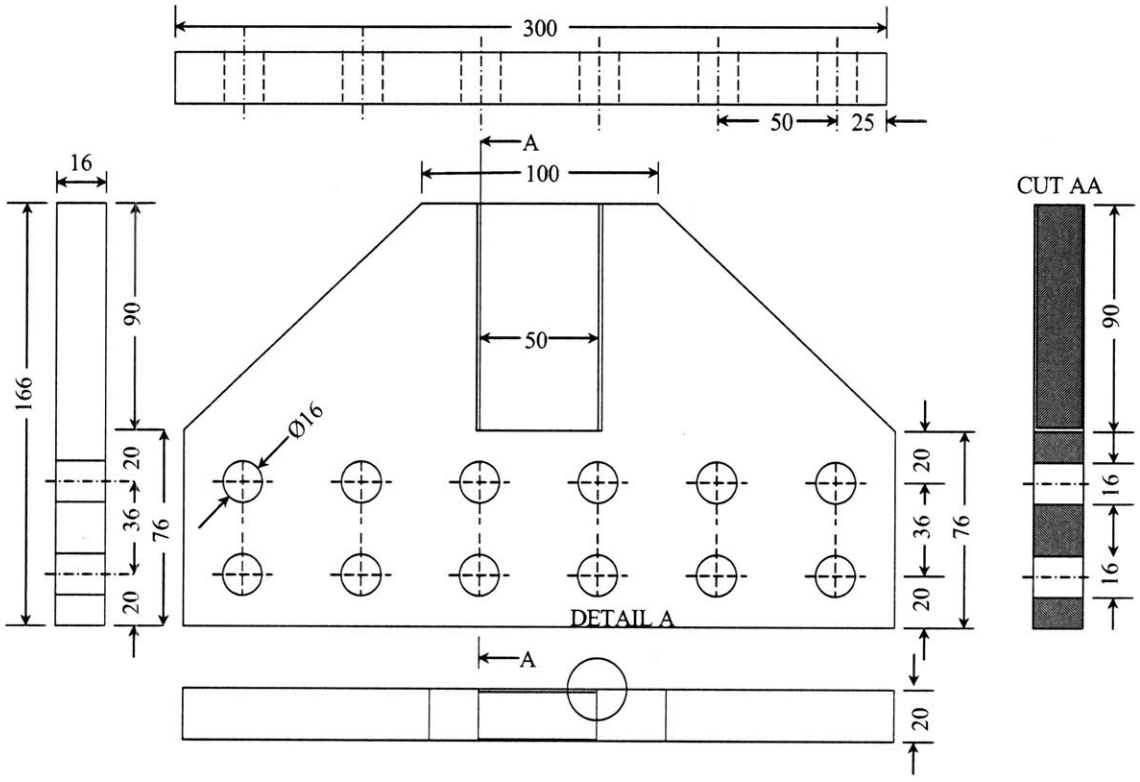

Figure B-5: Schematic of the fixture design (dimensions in mm)